THE
PHYSICAL REVIEW
A journal of experimental and theoretical physics established by E. L. Nichols in 1893

VOL. 61, NOS. 5 AND 6 MARCH 1 AND 15, 1942 SECOND SERIES

The Mesotron Component of Cosmic Rays

HENRI D. RATHGEBER
4 Beach Road, Hampton S7, Victoria, Australia
(Received December 8, 1941)

From experimental and theoretical results a complete qualitative picture of the mesotron component is evolved. The intensity, the production, the decay-coefficient of the mesotrons in the whole atmosphere as well as the origin of the mesotrons at sea level are obtained in the form of curves. It is further shown that this picture gives a satisfactory interpretation of the anomalous absorption, the atmospheric effects and the latitude effect at sea level.

INTRODUCTION

THE cascade theory of electron showers which is based on relativistic quantum mechanics has been successfully applied to the results of cosmic-ray experiments. The observed intensity of cosmic rays in the high atmosphere as well as the latitude effect at high altitudes have been explained by the same primary energy spectrum.

The cascade theory, however, cannot give an interpretation of cosmic-ray intensity at sea level consistent with the latitude effect at the same height. It is known that nearly all the cosmic-ray particles at sea level are not electrons but particles of higher penetrating power which must, at least partly, be of secondary origin on account of their decay.[1,2]

Although all the measurements of the absorption of the mesotron component give a real radioactive decay, they are not in quantitative agreement. In the present paper it is attempted to give an explanation of these differences as well as a consistent picture of the formation and decay of the mesotrons in the whole atmosphere.

THE MESOTRON INTENSITY IN THE ATMOSPHERE

The total number of cosmic particles which travel in a vertical direction has been known for some time from sea level to a height of 30 km[3] (curve 1, Fig. 1). Recently the number of particles penetrating 4 to 18 cm of lead has been measured.[4–7] At sea level this number is about 80 percent of the total intensity[8] (point *A*). The relative intensity of the hard component in the whole atmosphere (curve 2) is obtained by tracing the curve of the penetrating particles through this point. Thus an upper limit for the mesotron intensity which itself is assumed identical with the penetrating particles only up to a height of 8 km is found. This assumption might not be completely correct even at low

[1] H. Euler and W. Heisenberg, Erg. der exak. Naturwiss. **17**, 1 (1938).
[2] B. Rossi, Rev. Mod. Phys. **11**, 296 (1939).
[3] G. Pfotzer, Zeits. f. Physik **102**, 23 (1936).
[4] E. G. Dymont, Nature **144**, 782 (1939).
[5] A. Ehmert, Zeits. f. Physik **115**, 326 (1940).
[6] M. Schein, W. P. Jesse, and E. O. Wollan, Phys. Rev. **57**, 847 (1940).
[7] M. Schein, W. P. Jesse, and E. O. Wollan, Phys. Rev. **59**, 615 (1941).
[8] P. Auger, J. de phys. et rad. **6**, 226 (1935).

altitudes as shown by the relative occurrence of slow mesotron and proton tracks at 4300-m altitude which contain about 70 percent mesotrons and 30 percent protons.[9]

Further the number of mesotrons at the limit of the atmosphere must be zero on account of their decay. A third value for the construction of the mesotron curve is the position of its maximum which must be below the height of the maximum production of mesotrons. As is found later the difference in height of the two maxima should be small because of the high decay-coefficient at that height which is independent of the mesotron intensity within wide limits. The precise shape of the curve (curve 3) found in this way is not important for the present purpose.

THE PRODUCTION OF MESOTRONS IN THE ATMOSPHERE

The production of mesotrons in a block of 2-cm lead has been measured between pressures of 30 and 5 cm Hg.[6] In order to extrapolate the results to the whole atmosphere the following assumptions are made:

(1) The mesotrons are produced in pairs by photons which must have at least an energy of twice the rest mass of a mesotron. The minimum energy is set at 4×10^8 ev.[4] The number of these photons is proportional to that of the electrons of the same energy.

(2) The production of mesotrons is independent of the energy of the photon provided it is above the minimum.

A curve representing the number of electrons in the atmosphere with an energy $>4\times10^8$ ev is calculated by making use of the cascade theory[10] and the primary energy spectrum.[11] A curve (curve 4) parallel to this is traced through the measured points *B*, *C*, *D*, *E* the position of which is given by the experiment[6] in relation to the intensity of the penetrating particles (curve 2). The good fit of the points and the curve is a justification of the assumptions. The second of these is not necessarily correct because the relative energy spectrum of the mesotron producing rays does not change considerably below the maximum of the total intensity at 8 cm Hg. A further point lies considerably below the curve, but as it has been measured in a thicker block (5 cm Pb), the producing radiation is absorbed in it to a greater extent. The original point lies, when expressed in radiation units, at a depth $l=17$. The additional absorber is $l=2/0.4=5$ which brings the total depth to 22

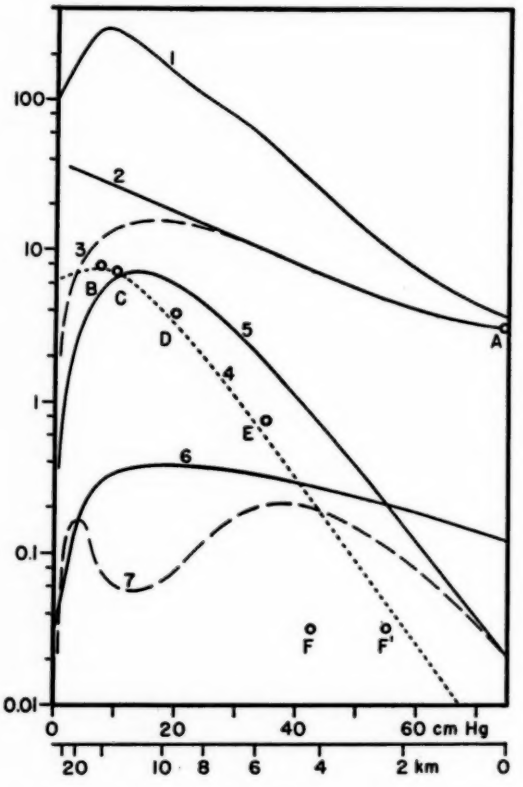

FIG. 1. Curve 1: Total number of cosmic-ray particles at latitude 50° North; curve 2: number of penetrating particles; curve 3: number of mesotrons; curve 4: number of mesotrons produced in 2-cm lead; curve 5: number of mesotrons produced in a column of air 1 km high; curve 6: decay coefficient per km of mesotrons; curve 7: contribution of layers 1 km thick to number of mesotrons at sea level.

and the point to position *F'*. Thus the agreement becomes satisfactory.

A transformation from lead to air is necessary for obtaining the production in the atmosphere itself. In the absence of an adequate theory this transformation is assumed to be proportional to the number of protons and neutrons in a nucleus or to the mass. Thus multiplying the production per gram and per cm² with the air mass in a

[9] W. M. Powell, Phys. Rev. **59**, 471 (1941).
[10] H. J. Bhabha and W. Heitler, Proc. Roy. Soc. **A159**, 432 (1937).
[11] W. Heitler, Proc. Roy. Soc. **A161**, 261 (1937).

column of 1-km height and of 1-cm² section one obtains the production of mesotrons per km (curve 5).

Because of the decrease of the production of mesotrons and the increase of the density of air with increasing pressure, the production in air goes through a maximum at a height of 12 km (15 cm Hg), i.e., considerably below the maximum of total intensity.

THE DECAY OF THE MESOTRONS

In certain radioactive decay experiments the production of the radioactive elements continues during the measurement of the decay rate. Similar conditions apply to the present problem for which the decay equation is:

$$(\alpha+\beta)N=(dN/dH)+P.$$

In this α is the absorption coefficient, β the decay coefficient, N the number of particles, H the height above sea level, P the production of mesotrons, and dN/dH the differential of the intensity-height curve (curve 3). With the exception of the decay coefficient all other quantities are known either from experiments or from the present paper. Thus it is possible to calculate β for the whole atmosphere (curve 6).

As the average momentum of the mesotrons is proportional to its decay path L or inversely proportional to β

$$L=1/\beta=p\tau_M/\mu_M$$

(τ_M and μ_M decay time and mass of mesotron at rest), this curve gives the average energy of the mesotrons as a function of altitude.

This fact together with the cascade theory of electron and photon absorption explains the shape of the curve A. At the top of the atmosphere the average energy of the mesotrons will be equal, on account of their production in pairs, to half the average energy of the photons, which in turn equals that of the primary particles. This latter is estimated[12] at about 5×10^9 ev at the latitude under consideration. Comparing this with $L=13$ km for $E=1.5\times10^9$ ev, one finds that the decay-coefficient becomes $\beta=0.025$/km. This value agrees well with the present results which give $\beta=0.03$/km.

With increasing depth of the atmosphere the energy of the mesotron producing rays decreases rapidly through the mechanism of shower production; i.e. the decay coefficient increases.

At still greater depths of the atmosphere (below 10 km) the production of mesotrons in air falls off. As the mesotrons of the lower energy ranges disappear preferentially through decay and absorption the mean energy increases and consequently the decay coefficient decreases. The same difference in the energy spectra of the mesotrons at sea level and at 6 km has also been directly observed.[13] A further check is found in the coinciding of the maximum decay, which is equal to βN and takes place at a pressure of 20–30 cm Hg, and of the hump in the absorption curve which is due to the decay electrons.

The decay time at sea level which is calculated by taking the different values of mean energy at sea level as well as of the mesotron rest mass, lies between 1 and 3 μsec.

THE ORIGIN OF THE MESOTRONS AT SEA LEVEL

A fraction $e^{-(\alpha+\beta)H}$ of the mesotrons which originate in a layer H km high will reach sea level. The contribution to the intensity at sea level of the different layers is obtained by multiplying the number of mesotrons formed in each layer by the above factor.

Down to sea level the production of mesotrons per decay path is of the same order as their intensity. Therefore the decay coefficient of all mesotrons (curve 6) at the height H can be taken as that of the mesotrons produced at the same height.

If this approximation is sufficient, the sum of all contributions which were calculated in the described way (curve 7) must be equal to the number of mesotrons found at sea level, which is approximately the case.

The important result is that the mesotrons at sea level come in about equal parts from two definite layers; the first has a maximum at 6 km and the second at 22 km. The mesotrons from the stratosphere are of higher energy than those

[12] I. S. Bowen, R. A. Millikan, and H. V. Neher, Phys. Rev. **53**, 217 (1938).

[13] M. Schein, E. O. Wollan, and G. Groetzinger, Phys. Rev. **58**, 1027 (1940).

from the troposphere. It is not possible to decide whether the difference in their mean energy is sufficient to identify them with components found in absorption experiments at sea level.[14] It is further to be noticed that practically nothing is contributed from layers between 10 and 15 km.

THE ANOMALOUS ABSORPTION OF THE MESOTRONS

Even if in measurements of cosmic-ray absorption at altitudes of a few kilometers the air mass between this point and sea level is replaced by a much denser absorber of the same atomic weight, the intensity at the higher altitude is still greater than at sea level.

A density effect which was calculated recently[15] was found insufficient to account for this difference. The radioactive decay of the mesotrons however gives a decay path L of 6 to 10 km.[16,17] These results were calculated under the assumption that no mesotrons are produced below the highest measuring point.

Thus in comparing these values with the present results which give $L=8$ km at sea level, $L=5$ at 2 km and $L=4$ at 4 km, it must not be forgotten that mesotrons are produced below 4 km in sufficient quantity to account for the difference.

THE ATMOSPHERIC EFFECTS

Taking into account the results of the present paper one expects to find the cosmic-ray intensity at sea level I_{76}, which consists mainly of mesotrons, to be a function of the form:

$$I_{76}=G[F(E), T(H), P].$$

In the atmosphere the number of mesotrons produced at a certain pressure is only a function of the primary energy spectrum at the limit of the atmosphere $F(E)$. But the number reaching sea level is determined by the height of the layer in which they are produced. This height is a function of the pressure at sea level P and of the temperature distribution $T(H)$.

As all these quantities are functions of time, the intensity is a function of time also.

Simultaneous registration at stations distributed over the whole earth and correlation of series of observations extending over long periods enables one to separate three effects: variation of primary energy spectrum, barometric effect, and temperature effect. The latter, which is usually only correlated to ground-level temperature, varies of course with geographic situation and meteorologic conditions.[18]

It is known from balloon ascents that variations of atmospheric pressure at sea level are accompanied by such temperature changes in the stratosphere that the pressure at a fixed height in the upper stratosphere does not change. Thus the barometric effect as far as it is due to decay is only caused by changes in height of the lower mesotron contributing layer. In this case the decay coefficient obtained from the barometric effect[19,20] must be slightly smaller than the decay coefficient at sea level, because the high energy contribution does not vary with changes in barometric pressure. As the decay path calculated from the barometric effect under the assumption of adiabatic pressure changes is $L=4$ km or about half the true $L_{76}=1/\beta=8$ km, the changes in height of the contributing lower layer must be about twice those for an adiabatic pressure change. In fact a factor 3.5 is found by comparing the observed pressure change at a height of 9 km δP_9, which is equal to 1.5 times the pressure change δP_S at sea level,[21] with the calculated adiabatic change $\delta P_{9A}=0.42\delta P_S$.[22] In consideration of the large possible error in all values, the agreement is satisfactory.

In other experiments, which confirm also the present deductions, the cosmic-ray variations have been measured at a depth of 40 m of water.[23] All the mesotrons from the lower layer are absorbed in the water and in fact no barometric effect has been observed. The remaining half-diurnal period of 0.2 percent amplitude whose maxima coincide with those of the half-diurnal

[14] E. Regener, Physik. Zeits. **34**, 880 (1933).
[15] E. Fermi, Phys. Rev. **57**, 485 (1940).
[16] B. Rossi and D. B. Hall, Phys. Rev. **59**, 223 (1941).
[17] W. M. Nielson, C. M. Ryerson, and L. W. Nordheim, Phys. Rev. **59**, 547 (1941).
[18] A. Duperrier, Proc. Roy. Soc. **A177**, 204 (1941).
[19] H. D. Rathgeber, Naturwiss. **26**, 842 (1938).
[20] W. Kolhörster and I. Matthes, Physik. Zeits. **40**, 142 (1939).
[21] W. H. Dynes, M. O. Geophysical Memoirs No. 2 (1912).
[22] B. Haurwitz, Ver. Geophys. Inst. Leipzig [2] **3** (No. 5).
[23] E. Regener and W. Rau, Naturwiss. **27**, 803 (1939).

pressure oscillation of the atmosphere, must be due to effects taking place in the upper layer.

An observed seasonal effect has been attributed to changes in the mean air temperature and has given a decay path $L=32$ km.[24] The seasonal changes in temperature extend through the whole atmosphere, but in summer the temperature in the stratosphere is much lower than in winter and probably causes a descent of the high mesotron contributing layer. Thus the decrease in mesotron intensity due to a rise in the lower layer is partially compensated by an increase due to the upper contributing layer and explains the high value found.

The intensity variations which remain after barometric correction, on passage of warm or cold air fronts, are obviously due to changes in the normal temperature distribution.[25]

Further it is to be expected that changes in the primary energy spectrum which for example are caused by magnetic storms, should be accompanied not only by intensity variations but also by changes in the coefficient of the barometric effect.

THE LATITUDE EFFECT AT SEA LEVEL

Any acceptable picture of the mesotron component must give a satisfactory interpretation of the latitude effect at sea level. The present results combined with the cascade theory are able to give this in a qualitative manner.

Below a height of 8 km (in radiation units $l=10$) the number of secondary electrons produced by electrons with energy $<y=4$ falls off rapidly. Therefore primary electrons $<4\times10^8$ ev $\times e^y=2\times10^{10}$ ev (the critical energy for mesotron production is assumed to be 4×10^8 ev) cannot produce mesotrons below that height. As electrons of an energy superior to 2×10^{10} ev are not influenced by the earth's magnetic field, the contribution from the lower mesotron producing layer is not subjected to the latitude effect.

Thus the latitude effect for the upper layer is twice the observed effect, i.e., 30 percent. Because only the mesotrons produced by the higher energy electrons in the upper layer will reach sea level it is possible to estimate the latitude effect of this layer to be inferior to 50 percent.

SUMMARY

A possible curve of the mesotron intensity in the whole atmosphere has been obtained.

The mean decay coefficient of these mesotrons rises from 0.03/km at the limit of the atmosphere to a maximum of 0.4/km at a height of 10 to 12 km and falls off again to 0.1/km at sea level. The corresponding average mesotron energies are: 3×10^9, 2×10^8 and 1×10^9 ev.

The mesotrons which reach sea level originate in about equal parts in two distinct layers, one around a height of 6 km and the other above 17 km. The latter is composed of mesotrons of high energy and the former of mesotrons of lower energy.

Further it is shown that these results explain the differences in the experimental determinations of the decay path and give a consistent qualitative picture of the mesotron component.

[24] P. M. S. Blackett, Phys. Rev. **54**, 973 (1938).
[25] D. H. Loughridge and P. Gast, Phys. Rev. **58**, 662 (1940).

The Intensities of the Hard and Soft Components of Cosmic Rays as Functions of Altitude and Zenith Angle

KENNETH GREISEN
Cornell University, Ithaca, New York
(Received January 14, 1942)

The intensities of the hard and of the soft component of cosmic rays have been recorded by a coincidence method as a function of zenith angle, at the four elevations 259, 1616, 3240, and 4300 meters, and the errors which may occur in the measurements have been studied. The absolute directional intensities have been calculated, as well as the integrated intensities at the various elevations. A comparison has been made between the variation of the hard component and the variation of the soft component with depth. The nature of the variation of the hard component with zenith angle and altitude suggests that there may be appreciable production of mesotrons at low altitude.

INTRODUCTION

IN view of the discussions and hypotheses which have been presented recently concerning the nature and origin of the soft and hard components of cosmic rays,[1-9] it seems to be of importance to determine unambiguously the intensities of these components as functions of altitude and zenith angle. During the last summer, therefore, measurements were carried out at Ithaca, New York (elevation 259 m), and at Denver, Echo Lake, and Mt. Evans, Colorado (elevations 1616, 3240, and 4300 m, respectively), with a counter telescope directed at various zenith angles, in an effort to obtain both the directional and total intensities at each elevation.

The directional intensities were calculated on the assumption that all of the multiple coincidences obtained were due to the passage of single particles through the counters, although an effort was also made to ascertain the errors which are involved in such an assumption. No attempt was made to distinguish sharply between mesotrons and electrons, but rather the distinction was between particles capable of penetrating only the counter walls and those capable of penetrating also a certain thickness of lead.

DESCRIPTION OF THE APPARATUS

The apparatus used consisted of six identical Geiger-Müller counters, supported in a straight line by a light wooden frame (see Fig. 1) which could be tipped at any desired zenith angle. The separation between the axes of the extreme counters was 36.4 cm. The counters were made of brass, and were of the self-quenching type, containing 9 percent alcohol and 91 percent argon with a total pressure of 11 cm. The internal diameter was 4.24 cm, the length of the collecting wire was 20 cm, and the thickness of the counter walls was 1 mm. Between the counters were light, removable wooden shelves on which 2 cm of lead could be placed, while above the top counter was a similar shelf on which 3 cm of lead could be placed. The lead absorber was cut so that it had the same width as the counters, in order to reduce the coincidences due to scattering of particles into the beam.

The apparatus was housed in a station wagon, the roof of which was composed mostly of wooden slats approximately $\frac{1}{4}$ inch thick. Care was taken that no dense part of the station wagon or of nearby buildings or mountains should be in the solid angle of the counter telescope at any of the zenith angles used. The four zenith angles at which measurements were made were 0°, 29°, 46°, and 56° to the south, the axes of the counters being always in the

[1] W. Heisenberg and H. Euler, Naturwiss. **17**, 1 (1938).
[2] B. Rossi, Phys. Rev. **57**, 469 (1940).
[3] E. Nelson, Phys. Rev. **58**, 771 (1940).
[4] G. Bernardini, B. N. Cacciapuoti, B. Ferretti, O. Piccioni, and G. C. Wick, Phys. Rev. **58**, 1017 (1940).
[5] L. W. Nordheim, Phys. Rev. **59**, 554 (1941).
[6] M. Schein, W. P. Jesse, and E. O. Wollan, Phys. Rev. **59**, 614 (1941).
[7] J. F. Carlson and M. Schein, Phys. Rev. **59**, 840 (1941).
[8] G. Cocconi, Phys. Rev. **60**, 532 (1941).
[9] B. Rossi and K. Greisen, Phys. Rev. **60**, 121 (1942).

east-west direction. The starting potentials of the counters were checked daily and all counters were operated at exactly the same voltage above the starting potential.

The recording circuit contained a coincidence-anticoincidence arrangement which was not of an unusual type and will not be described.

PRESENTATION OF DATA

With the apparatus described above, the following measurements were made:

(a) Sixfold coincidences with all lead absorber in place. The rate at which such coincidences occur will be denoted by N. The total absorber thickness in this condition, including both the lead, the counter walls, and the wood between and above the counters, was equivalent to 167 g/cm² of lead. Since there are very few

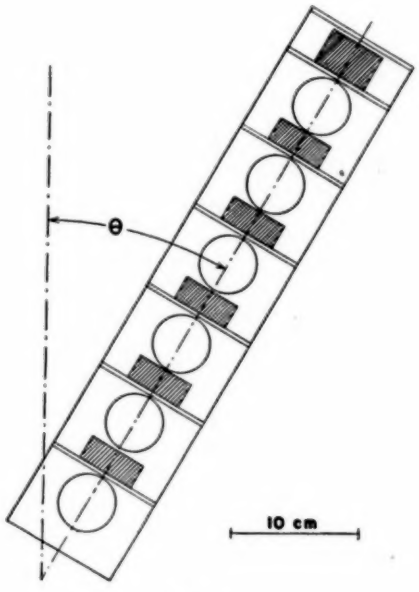

FIG. 1.

electrons capable of penetrating this thickness of lead, N is proportional to the number of mesotrons with momentum above 3.0×10^8 ev/c which arrive in the solid angle of the counter telescope.[10]

TABLE I. Intensities of soft and hard components as functions of altitude and zenith angle.

Altitude (meters)	Depth in g/cm²	Zenith angle 0°	29°	46°	56°
259	1007	$N+n=2.86\pm0.021$	2.10 ± 0.026	1.24 ± 0.020	0.73 ± 0.015
		$N=2.27\pm0.021$	1.67 ± 0.024	1.08 ± 0.020	0.65 ± 0.015
		$n=0.59\pm0.030$	0.43 ± 0.035	0.16 ± 0.028	0.08 ± 0.021
		$n'=0.55\pm0.034$		0.42 ± 0.038	
		$n+n'=1.14\pm0.045$		0.58 ± 0.047	
1616	857	$N+n=3.94\pm0.024$	2.89 ± 0.066	1.74 ± 0.044	1.04 ± 0.032
		$N=2.85\pm0.067$	2.25 ± 0.056	1.33 ± 0.036	0.85 ± 0.027
		$n=1.09\pm0.071$	0.64 ± 0.087	0.41 ± 0.057	0.19 ± 0.042
		$n'=1.02\pm0.12$		0.53 ± 0.10	
		$n+n'=2.12\pm0.14$		0.94 ± 0.12	
3240	708	$N+n=6.53\pm0.075$	4.56 ± 0.057	2.56 ± 0.049	1.45 ± 0.030
		$N=4.13\pm0.062$	2.92 ± 0.048	1.97 ± 0.043	1.18 ± 0.028
		$n=2.40\pm0.10$	1.64 ± 0.075	0.59 ± 0.065	0.27 ± 0.041
		$n'=2.57\pm0.17$		1.02 ± 0.12	
		$n+n'=4.97\pm0.19$		1.62 ± 0.13	
4300	616	$N+n=9.18\pm0.093$	6.64 ± 0.079	3.79 ± 0.059	2.14 ± 0.044
		$N=5.19\pm0.068$	4.15 ± 0.061	2.54 ± 0.049	1.56 ± 0.038
		$n=3.98\pm0.11$	2.49 ± 0.10	1.25 ± 0.077	0.58 ± 0.058
		$n'=5.41\pm0.25$		2.18 ± 0.14	
		$n+n'=9.39\pm0.27$		3.43 ± 0.16	

(b) Sixfold coincidences with the lead absorber removed; this rate will be denoted by $N+n$. The difference n between the coincidence rates with and without the lead absorber is proportional to the number of particles with sufficient energy to penetrate the counter walls and the wooden shelves (12 g/cm² brass plus 1.7 g/cm² wood) but with insufficient energy to penetrate 167 g/cm² of lead. This number includes electrons with energy above approximately 2×10^7 ev, and also those mesotrons which are stopped by 167 g/cm² of lead ("slow" mesotrons).

(c) Twofold coincidences between the extreme counters, with the same absorber as in the measurement of $N+n$.

(d) Twofold coincidences between the extreme counters, with the inactive counters and the shelves removed. In both of the measurements (c) and (d) the number of showers and chance coincidences recorded is the same. Therefore the difference between the counting rates (d) and (c) represents the number of particles capable of penetrating two counter walls (2.3 g/cm² of brass) but not capable of penetrating

[10] Because of the finite dimensions of the counters, not all particles traverse the counters perpendicularly to the axes of the counters; therefore the effective absorber thickness is larger than 167 g/cm². By a treatment very similar to that used below in calculating the directional intensities (page 216), one can show that the average absorber thickness is given by

$$\bar{x}=x_0\frac{\int_0^{\tan^{-1}a/l}(a-l\tan\varphi)\cos^3\varphi d\varphi}{\int_0^{\tan^{-1}a/l}(a-l\tan\varphi)\cos^4\varphi d\varphi},$$

where x_0 is the thickness perpendicular to the counter axes, a is the effective length of the counters, and l is the separation between the axes of the extreme counters. For $a=20$ cm, $l=36.4$ cm, we find that $\bar{x}=1.023x_0$. This correction is therefore negligible.

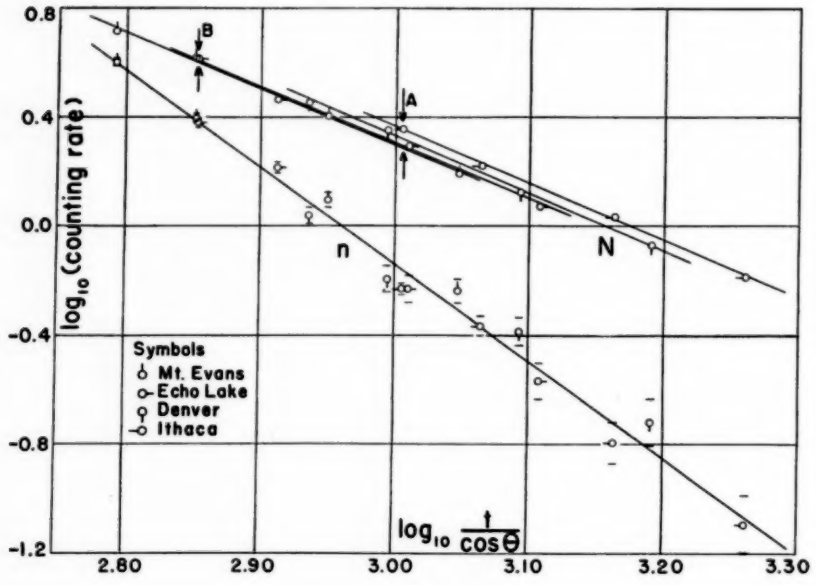

FIG. 2.

12 g/cm² of brass plus 1.7 g/cm² of wood. This number will be denoted by n', and may be considered as the intensity of "slow" electrons (energy roughly between 4×10^6 ev and 2×10^7 ev). We find at all elevations that n' is of approximately the same magnitude as n. The zenith angle variation of n' is not as significant as the zenith angle dependence of N or n, because of the large amount of scattering which the slow electrons undergo in the air.

In Table I we present, corresponding to the various altitudes and zenith angles at which they were measured, the rates $N+n$, N, and n', and the deduced values of n and $n+n'$, all expressed in coincidences per minute. The errors listed are the statistical (root mean square) errors. The column labeled "depth" indicates the atmospheric depth in g/cm², as calculated from the average barometric pressures.

The values for the intensities of the hard component in the vertical direction may be compared with similar measurements of Rossi, Hilberry, and Hoag,[11] with those of Rossi and Hall,[12] and with some recent measurements of Rossi and collaborators (unpublished). In the first of these experiments, triple coincidences were counted, while in the second and third the rates given are quadruple coincidence rates. The absorber thicknesses were 160, 196, and 196 g/cm² of lead, respectively. In all three experiments the number of side showers recorded was reduced by shielding the counters on the side with 10 or 11 cm of lead. In Table II we present the ratios of the intensities of the hard component at the other elevations to the intensity at Denver, as obtained in the present experiment and in the three experiments quoted.

The only values in this table which show a disagreement appreciably greater than the statistical errors are the ratios at Mt. Evans, and the discrepancy is in such a direction as to indicate that in the present experiment a few percent of the coincidences at Mt. Evans were due to air showers, which were not recorded in the experiment of Rossi, Hilberry and Hoag because of the shielding of the counters with lead.

TABLE II. Ratio of intensities of the hard component in the vertical direction to the intensity at Denver.

Location and elevation	Rossi, Hilberry, and Hoag	Rossi and Hall	Rossi and collaborators	Greisen
Mt. Evans 4300 meters	1.72 ±0.014			1.82 ±0.046
Echo Lake 3240	1.41 ±0.011	1.38±0.014	1.42±0.010	1.45 ±0.040
Denver 1616	1.00 ±0.00	1.00±0.00	1.00±0.00	1.00 ±0.00
Chicago 180	0.766±0.007			
Ithaca 259				0.795±0.021

[11] B. Rossi, N. Hilberry, and J. B. Hoag, Phys. Rev. 57, 461 (1940).
[12] B. Rossi and D. B. Hall, Phys. Rev. 59, 223 (1941).

CALCULATION OF THE DIRECTIONAL INTENSITIES

In Fig. 2 we have plotted the values of log N and of log n against the corresponding values of log $(t/\cos\theta)$; i.e., against the logarithm of the distance in g/cm² to the top of the atmosphere. The statistical errors are indicated where possible, but for the values of N they are too small to appear outside the dots. The "semaphor" signs indicate the elevations at which the measurements were made. The "soft" electrons n' have not been included in the figure because the variation of n' with zenith angle is strongly affected by scattering of the low energy particles in air.

The graph will be discussed in greater detail below, but here we wish to stress the nature of the variation of the coincidence rates with zenith angle. It appears that at any elevation the intensity of the hard component and also (within the rather large errors) that of the soft component can be expressed by a power of $\cos\theta$,[13] and that the exponent does not change appreciably with elevation in the range from 259 m to 4300 m. It will be shown that under a single, mild, simplifying assumption, this experimental fact leads to the conclusion that the *directional intensities are strictly proportional to the counting rates*, although the proportionality constants may be slightly different for the soft and hard components.

Consider the counter telescope tipped so that the axes of the counters are horizontal and the line joining the centers of the counters (the "principal axis") makes an angle θ_0 with the vertical direction, as indicated in Fig. 3, where only the extreme counters are shown. Let θ be the angle between the vertical direction and any line passing through the axes of the counters, and φ the angle between this line and the principal axis. We wish to calculate the relation between the coincidence rate $N(\theta_0)$ and the cosmic-ray intensity along the principal axis, $I(\theta_0)$.

The single simplifying assumption is that over the small range of angle subtended by the diameters of the counters, $I(\theta)$ varies linearly with θ, so that integration over the diameter becomes unnecessary, and one may use as the average intensity over the diameter the intensity along a line passing through the axes of the counters.[14] Over the range of θ included by the variation of φ, the accurate expression

$$I(\theta)=I(\theta_0)(\cos^n\theta/\cos^n\theta_0)=I(\theta_0)\cos^n\varphi$$

will be used, where n is the exponent indicated by the slope of the lines in Fig. 2. The relation between $N(\theta_0)$ and $I(\theta_0)$ is (see Fig. 3):

$$N(\theta_0)=\int\int I(\theta)f(\varphi,x)d\varphi dx$$

$$=I(\theta_0)\int\int\cos^n\varphi f(\varphi,x)d\varphi dx,$$

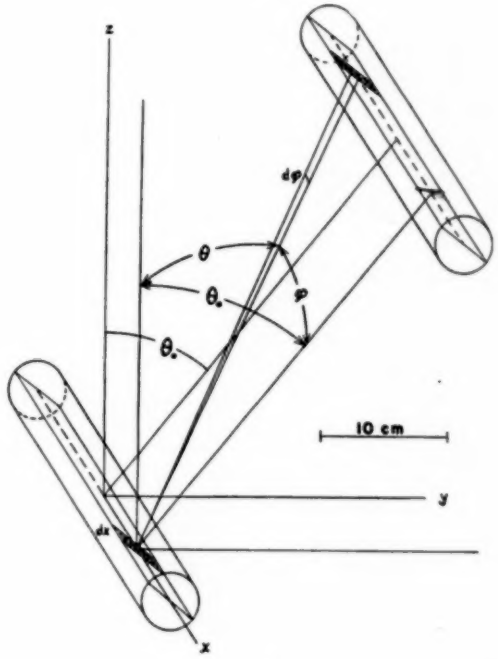

FIG. 3.

[13] The close resemblance of the zenith angle dependence of the total intensity to a $\cos^2\theta$ law has been pointed out by Johnson [T. H. Johnson, Phys. Rev. **43**, 307 (1933)], by Skobelzyn [D. Skobelzyn, Comptes rendus **194**, 118 (1932)], and by others.

[14] The error thus introduced can easily be evaluated and shown to be small. If $I(\theta)$ varies as $\cos^2\theta$, the ratio between the correct average intensity over the diameter, and the assumed average intensity, is given by

$$1+\frac{1}{6}\left(\frac{b}{l}\right)^2(\tan^2\theta_0-1)$$

where b is the diameter of a counter, and l is the separation between extreme counters. Using the dimensions of our counter array, we find the above ratio is less than 1 by 0.23 percent at $\theta_0=0°$, increases to exactly 1 at $\theta_0=45°$, and is greater than 1 by 0.24 percent at $\theta_0=55°$. Thus over the range of angle we used, the error is not greater than ¼ percent. The percent error increases rapidly as one approaches 90°, and is 3 percent for $\theta_0=75°$; however, for such large zenith angles the percent errors involved in the measurements are so large that one is still justified in using the assumption.

where f is a function of the angle φ and of the dimensions of the apparatus, and the limits of integration are functions only of the dimensions of the apparatus. Therefore

$$N(\theta_0)=\text{const.}\times I(\theta_0),$$

where the constant depends only on the dimensions of the counter array and on the exponent n.[15]

Thus the graph in Fig. 2 may be used as a logarithmic graph of *intensity* of the hard and soft components against atmospheric depth in the direction of motion. The logarithms of the absolute intensities differ only by a constant from the logarithms of the counting rates, although the constant may have slightly different values for the hard and soft components.

In order to determine the proportionality constant, let us first consider the counters as *rectangular* sensitive areas, of length a and width b. b is equal to the inside diameter of the counters,[16] and a is equal to the length of the fine collecting wire (this is true for counters such as ours, in which contact is made by a thick rod to a fine collecting wire, and the outer cylinder extends several cm beyond the wire at both ends). If l represents the separation of the axes of the extreme counters, we then obtain (see Fig. 3):

$$N(\theta_0)=\int\int\frac{b^2}{l}I(\theta)\cos^2\varphi d\varphi dx$$

$$=I(\theta_0)\cdot\frac{2b^2}{l}\int_0^{\tan^{-1}a/l}(a-l\tan\varphi)\cos^{n+2}\varphi d\varphi.$$

TABLE III. Absolute intensity in the vertical direction $I(0)$; the number of particles per cm² per minute per unit solid angle.

Alt. (M)	Depth (g/cm²)	N	n	$n+n'$
259	1007	0.443±0.004	0.115±0.006	0.222±0.009
1616	857	0.557±0.013	0.213±0.014	0.41 ±0.03
3240	708	0.806±0.012	0.47 ±0.020	0.97 ±0.04
4300	616	1.014±0.014	0.78 ±0.022	1.83 ±0.05

[15] Similar calculations have been carried out by Johnson[13] and by Froman and Stearns [D. K. Froman and J. C. Stearns, Can. J. Research **A16**, 29 (1938)], under slightly different assumptions, so that the proportionality between $N(\theta_0)$ and $I(\theta_0)$ was not brought to light.

[16] J. C. Street and R. H. Woodward, Phys. Rev. **46**, 1029 (1934).

For the case $n=2(I(\theta)\propto\cos^2\theta)$, this becomes

$$\frac{N(\theta_0)}{I(\theta_0)}=\frac{b^2}{4}\left(\frac{a}{3l}-\tan^{-1}\frac{a}{l}+\frac{a^2}{l^2+a^2}\right)=4.77$$

and for the case $n=3(I(\theta)\propto\cos^3\theta)$, we obtain

$$\frac{N(\theta_0)}{I(\theta_0)}=\frac{2b^2}{5}\left\{\frac{1}{l(a^2+l^2)^{\frac{1}{2}}}\times\left(l^2+3a^2-\frac{1}{3}\frac{a^4}{l^2+a^2}\right)-1\right\}=4.67.$$

The numbers 4.77 and 4.67 are calculated from

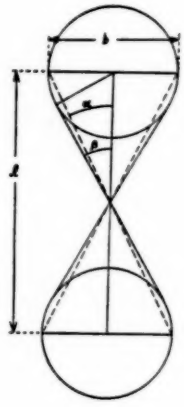

FIG. 4.

the following dimensions of our counter array: $a=20$ cm, $l=36.4$ cm, and $b=4.24$ cm.

In treating the counters as rectangular sensitive areas, we underestimate the angle subtended by the counters, both along the width and along the length of the counters, if we assume the counters are really sensitive *cylinders*. The error along the length of the counter arises because of the solid angle subtended by the circular ends of the cylinders, half of which angle extends beyond the solid angle subtended by the rectangular areas. If one regards the intensity as constant over the small additional solid angle, one obtains for the correction due to all four semicircular areas:

$$\Delta N(\theta_0)=I(\theta_0)\frac{\pi b^3}{2l}\int_0^{\tan^{-1}a/l}\cos^n\varphi\sin\varphi\cos\varphi d\varphi$$

$$=I(\theta_0)\frac{\pi b^3}{2l}\cdot\frac{1}{n+2}\left[1-\left(\frac{l^2}{l^2+a^2}\right)^{(n+2)/2}\right].$$

For the dimensions of our counter array, $\Delta N(\theta_0)=0.338I(\theta_0)$ if we take a $\cos^2\theta$ dependence, and $\Delta N(\theta_0)=0.323I(\theta_0)$ for the $\cos^3\theta$ dependence.

The error along the width of the counter is shown in Fig. 4, where the situation is exaggerated for the sake of clarity. The maximum angular divergence of the particles is really given by angle β rather than by α, where

$$\sin\beta=\tan\alpha=b/l.$$

Under our assumption that the intensity varies linearly along the diameters of the counters, the correction therefore to be applied to the factors calculated above is simply to multiply them by the ratio β/α, which in our case amounts to increasing the factors by 0.67 percent.

Finally, therefore, we have the results

$$N(\theta_0)=5.14I(\theta_0), \quad \text{if} \quad I(\theta)\propto\cos^2\theta,$$

$$N(\theta_0)=5.03I(\theta_0), \quad \text{if} \quad I(\theta)\propto\cos^3\theta.$$

TABLE IV. Integrated intensity J_1, the number of particles per minute which cross an area of 1 cm² placed horizontally. $J_1=2\pi\int_0^{\frac{1}{2}\pi}\sin\theta\cos\theta I(\theta)d\theta$.

Alt. (M)	Depth (g/cm²)	N	$N+n$	$N+n+n'$	n	$n+n'$
259	1007	0.68	0.81	1.04	0.14	0.37
1616	857	0.86	1.13	1.46	0.27	0.60
3240	708	1.21	1.74	2.47	0.52	1.26
4300	616	1.62	2.53	4.00	0.91	2.38

TABLE V. Integrated intensity J_2, the number of particles per minute which cross a sphere of 1 cm² cross section. $J_2=2\pi\int_0^{\frac{1}{2}\pi}\sin\theta I(\theta)d\theta$.

Alt. (M)	Depth (g/cm²)	N	$N+n$	$N+n+n'$	n	$n+n'$
259	1007	0.90	1.06	1.40	0.16	0.50
1616	857	1.14	1.47	1.92	0.33	0.78
3240	708	1.62	2.26	3.20	0.64	1.58
4300	616	2.17	3.28	5.13	1.11	2.96

The exponent n indicated by the lines in Fig. 2 is actually 2.1 for the hard component, and 3.6 for the soft component. If the "very soft" component n' were plotted, the slope for this component would be somewhat less than 3 (because of the scattering). However, the variation in the proportionality factor is only 2 percent as the exponent changes from 2 to 3. In the next section we have for the sake of ease in extrapolation and graphical integration always dealt with the total intensities N, $N+n$ and $N+n+n'$; for these, the indicated exponent is between 2 and 3, and we have taken the proportionality factor as 5.12 throughout. This is accurate for the hard component, and may be in error by about 1 percent for the intensities which include the soft component.

In Table III we present the absolute intensities (particles per cm² per minute, per unit solid angle) in the vertical direction, obtained simply by dividing the corresponding coincidence rates (see Table I) by 5.12. Since the statistical error for the soft component is in all cases more than 2 percent, the error made by using the factor 5.12 for the soft component as well as for the hard component is negligible.

INTEGRATED INTENSITIES

The intensity J_1 may be defined as the number of particles per minute which cross, at any angle, a unit area placed horizontally. J_1 can be calculated as follows:

$$J_1=\int_0^{\frac{1}{2}\pi}2\pi\sin\theta\cos\theta I(\theta)d\theta$$

$$=\frac{\pi}{5.12}\int_{\cos^2\theta=0}^{\cos^2\theta=1}N(\theta)d(\cos^2\theta)$$

$$=(\pi/5.12)\times(\text{Area under graph of } N(\theta) \text{ against } \cos^2\theta).$$

The evaluation of the integral becomes particularly simple in the case of the hard component, because the intensity of this component is almost exactly proportional to $\cos^2\theta$. In the graphs of the intensities which include the soft component ($N+n$ or $N+n+n'$), the curvature is so small that the extrapolation to $\theta=\frac{1}{2}\pi$ is

TABLE VI. $I(0)$, J_1, and J_2, as obtained by other experimenters. The intensities include both hard and soft components.

Authors	Alt. (M)	$I(0)$	J_1	J_2
T. H. Johnson (reference 13)	189	0.70	0.96	
	1915	0.99	1.44	
J. C. Street and R. H. Woodward (reference 16)	0	0.80±0.028		1.48±0.055
D. K. Froman and J. C. Stearns (reference 15)	37	0.973±0.032	1.31±0.042	1.82±0.06
	4300	3.80±0.25	5.1±0.37	7.1±0.5

very easy in all cases. The intensities J_1 thus calculated are given in Table IV for the "fast" mesotrons N, for all particles capable of traversing the six counters $N+n$, and for all particles capable of traversing 2.3 g/cm² of brass (two counter walls) $N+n+n'$. The last columns give the differences n and $n+n'$.

The intensity J_2 may be defined as the number of particles per minute which cross a sphere of unit cross section. J_2 is directly related to the ionization per minute per unit volume observed in an ionization chamber, and is given by

$$J_2=\int_0^{\frac{1}{2}\pi} 2\pi \sin\theta I(\theta)d\theta$$

$$=\frac{2\pi}{5.12}\int_{\cos\theta=0}^{\cos\theta=1} N(\theta)d(\cos\theta)$$

$$=(2\pi/5.12)\times(\text{Area under graph of } N(\theta) \text{ against } \cos\theta).$$

The intensities J_2 thus calculated are listed in Table V.

In the evaluation of J_2, the contribution in the angular range between $\theta=55°$ and $\theta=90°$ is larger than in the evaluation of J_1; moreover, the slope of the graph of N against $\cos\theta$ changes more rapidly than does the slope of the graph of N against $\cos^2\theta$. Hence the results for J_2 cannot be considered as accurate as the results for J_1.

The numbers in Tables III, IV and V may be compared with the similar results of Johnson,[13] Street and Woodward,[16] and Froman and Stearns,[15] which are summarized in Table VI. The intensities listed in this table were obtained with no absorber except the walls of the counters and a thin roof, and hence include both soft and hard components. A comparison of the results in Tables III to V for $N+n$ and $N+n+n'$ demonstrates the critical dependence of the observed total intensities on the absorption which takes place in the counter walls. This alone may be sufficient to explain the differences in the results.[17]

[17] It seems likely that the high values obtained by Froman and Stearns at 4300-m elevation may be due to an over-correction for the inefficiency of their counters.

INTERPRETATION OF THE VARIATION WITH DEPTH

It is immediately obvious from the graphs in Fig. 2 that the decrease of n with depth is much more rapid than the decrease of N. In fact, the values of n are consistent with a straight line on the logarithmic graph, having a slope of -3.6. If one connects (as is done in the figure) the values of N obtained at *one elevation* and different zenith angles, one obtains for each elevation a straight line of slope -2.1; and if one connects the values of N obtained at *one zenith angle* and different elevations, one obtains curves showing a still less rapid decrease. The difference between the variation with depth of the soft and of the hard component has been observed by Rossi and Benedetti,[18] by Regener and Ehmert,[19] and by Bernardini and collaborators.[4] The implications, regarding the origin of the soft component, have been discussed by Rossi and Greisen.[9]

Let t represent the depth in g/cm² in the vertical direction and $y=t/\cos\theta$ represent the atmospheric depth in the direction of motion of the observed particles. The graph in Fig. 2 indicates definitely that N is not a function only of the depth y, since the values of N at two equal depths $y_1=t_1/\cos\theta_1$ and $y_2=t_2/\cos\theta_2$ are not equal unless $t_1=t_2$. This is especially true for the points obtained in Denver and in Ithaca, for which the possible effect of showers or other systematic errors is small and the differences are many times the statistical errors.

A reason for the differences is well known; they are the effect of spontaneous decay of the mesotrons, which causes the intensity to be a function not only of the depth in g/cm² but also of the geometrical distance from the place of production of the mesotrons. The differences could also be explained if the directional intensity of the primary rays were not isotropic, but since the zenith angle θ in our experiment was toward the south, and the latitudes were well above the knee of the latitude effect, there should be no differences due to magnetic effects. There is, in addition to the decay, another density effect,[20,21] which influences the energy

[18] B. Rossi and S. De Benedetti, Ricerca Scientifica **5** (2), 119 (1934).
[19] E. Regener and A. Ehmert, Zeits. f. Physik **111**, 501 (1938).
[20] E. Fermi, Phys. Rev. **57**, 485 (1940).
[21] O. Halpern and H. Hall, Phys. Rev. **57**, 459 (1940).

TABLE VII. Predicted values of $\log_{10}(N_3/N_2)$, where N_3 and N_2 are observed at equal depths y but at different vertical depths t and different inclinations. t and y are expressed in g/cm². p_2 is the momentum at the depth y, in ev/c. The values are calculated on the assumption that $\tau_0/\mu = 9\times10^{-4}$ and that the mesotrons are produced at a depth $y = 103$ g/cm². The last row gives the observed values of $\log_{10}(N_3/N_2)$.

p_2(ev/c)	$y=t_3=1007$g/cm² $t_2=857$	$t_2=708$	$t_2=616$	$y=t_3=708$g/cm² $t_2=616$
3×10^8	0.129	0.31	0.47	0.128
8×10^8	0.085	0.20	0.31	0.078
2×10^9	0.050	0.12	0.18	0.042
Observed, for $p_2>3\times10^8$	0.04±0.01	0.06±0.01	0.07±0.01	0.005±0.01

loss by collision of the mesotrons; but in air this effect is negligible except for extremely high energies.

In order to compare the differences between values of N obtained at equal depths y with the predicted differences due to decay, one needs to know the place of production of the mesotrons, the angular distribution at the place of production, and the momentum spectrum. This information is not available. For a qualitative comparison, however, we may calculate the effect for mesotrons of certain momenta, taking a reasonable value for the depth of production and assuming that the mesotrons have the same direction as the primaries by which they are produced.

At two different vertical depths t_2 and t_3, let the zenith angles θ_2 and θ_3 be so chosen that $y = t_2/\cos\theta_2 = t_3/\cos\theta_3$. Let N_2 represent the number of mesotrons of momentum p_2 observed at t_2 in the direction θ_2, and let N_3 represent the number of mesotrons of the same momentum observed at t_3 in the direction θ_3. Let us denote by L_2 and L_3 the corresponding distances from the place of production of the mesotrons (depth y_1) to the place of observation. If we assume that the momentum loss of the mesotrons is a constant given by a ev/c per g/cm² of air, we obtain the relation (see Euler and Heisenberg,[1] Rossi[22])

$$\log\frac{N_3}{N_2} = \frac{\mu}{\tau_0}(L_2-L_3)\cdot\frac{1}{P},$$

where

$$P=\frac{p_2+ay}{1+\log(p_1/p_2)/\log(y/y_1)}.$$

$p_1 = p_2 + a(y-y_1)$ is the momentum of the mesotrons at the place of production, τ_0 is the proper lifetime and μ is the rest-mass. We take for τ_0/μ the value 9×10^{-4} (cm-c/ev),[23] and we assume for y_1 the value 103 g/cm² (1/10 of the atmosphere). The lengths L may be evaluated with the aid of the relation $z = z_0\log(t_0/t)$ between altitude z and vertical depth t, in which (according to our barometer readings) $z_0 = 84\times10^4$ cm and $t_0 = 1036$ g/cm².

Thus we have calculated the differences $(\log_{10}N_3 - \log_{10}N_2)$ which are given in Table VII. The calculations have been made for three different values of the momentum p_2: 3×10^8, 8×10^8, and 2×10^9 ev/c. In the first three columns of the table, N_3 represents the number of mesotrons in the vertical direction at Ithaca ($t_3 = 1007$ g/cm², $\theta_3 = 0$), and N_2 represents the number of mesotrons in an inclined direction at one of the other stations (Denver, Echo Lake, and Mt. Evans, respectively, for columns one, two, and three), the inclinations being so chosen that the depth in the direction of observation is the same at all four stations. If the mesotrons were monoenergetic, and all had at the depth of observation a momentum equal to one of the values chosen for p_2, the numbers in the row corresponding to that momentum should represent the separations in Fig. 2 between the topmost line and the three lower lines, respectively, at the depth indicated by arrow A. In the last column of the table, N_3 represents the number of mesotrons in the vertical direction at Echo Lake ($t_3 = 708$ g/cm², $\theta_3 = 0$), and N_2 represents the number of mesotrons in an inclined direction at Mt. Evans, so chosen that the depth in the direction of observation is the same at both stations. If the mesotrons were monoenergetic, and had one of the momenta for which the effect has been calculated, the number in the last column corresponding to that momentum should represent the separation

[22] B. Rossi, Rev. Mod. Phys. **11**, 296 (1939).

[23] See Rossi and Hall, reference 12. This result has been confirmed recently in another experiment by Rossi and collaborators, an account of which is to be published shortly.

between the two lines in Fig. 2 at the depth indicated by arrow B.

In the last row of Table VII, we have given the observed differences $(\log_{10} N_3 - \log_{10} N_2)$, which are taken directly from Fig. 2 at the depths indicated by arrows A and B. It may be noted that the observed difference between Denver and Ithaca (0.04 ± 0.01) is in agreement with the predicted separation for $p_2 = 2 \times 10^9$ ev/c (0.050), which is a reasonable estimate of the effective momentum at sea level. All of the other observed differences are much lower than those predicted. In particular, the predicted effect between the higher elevations (which is given at depth B by the last column in the table, and at depth A by the difference between the figures in the second and third columns) is of the same order of magnitude as the predicted effect between the lower elevations (given by the first column); whereas the observed effect between the higher elevations is practically zero. This discrepancy remains, even if the calculations are repeated using different values for the lifetime or for the depth of production of the mesotrons.

The discrepancy might be accounted for if many side showers were recorded at the high elevations, since these might reduce the apparent decrease in intensity with increasing zenith angle, and since the number of showers increases with altitude faster than the number of mesotrons. However, auxiliary experiments described below show that the number of such showers recorded with six counters in coincidence is at most a very small fraction of the number of mesotrons, while the discrepancy is very large.

The discrepancy may be satisfactorily explained, however, if one takes into account that mesotron production takes place at *all* depths below the top of the atmosphere, and if one makes two assumptions: (1) that mesotron production is still an important process at depths corresponding to the elevation of Mt. Evans (4300 meters), and (2) that mesotrons produced with small momentum have a large angular divergence from the direction of the primaries by which they are produced. Under these two assumptions, many of the mesotrons which are observed at the higher elevations in an inclined direction have been produced *near the place of observation* by primaries which have traversed the atmosphere in nearly vertical directions. These mesotrons have not been appreciably reduced in number by decay. Looking at the phenomenon from another point of view, we may say that the effective depth of observation for these mesotrons lies between t and $t/\cos\theta$. Near sea level, however, mesotron production is rare, so that most of the observed mesotrons are produced far from the place of observation. The mesotrons observed at sea level must therefore have been created with such large momentum that their divergence from the direction of the primaries is small. For *these* mesotrons, the effective depth of observation is very nearly $t/\cos\theta$, as is assumed in the calculations presented above.

This explanation might account for the difference $(\log N_3 - \log N_2)$ being small when one compares intensities observed at the higher altitudes, and for the differences being roughly as predicted by the theory when one compares intensities observed near sea level. We consider, therefore, that the results of this experiment on the intensity of the hard component as a function of altitude and of zenith angle are an indication of the production of mesotrons at fairly low altitudes.

SYSTEMATIC ERRORS IN THE MEASUREMENTS

(1) Inefficiency

Auxiliary experiments performed with the counters used in this experiment[24] indicate that the inefficiency of the counters due to the "dead-time" following each pulse is 0.2 percent or less at 259-m elevation. This implies an error in the measurements with six counters which is about 1 percent in Ithaca and increases to about 2.5 percent at the highest elevation.

Other types of inefficiency, i.e., that due to time lags and that due to occasional failure of the particles to produce ions in a counter, have been shown by our auxiliary experiments to be smaller than 0.5 percent per counter, and are a constant fraction of the counting rate. Therefore they have no influence on the relative rates, and introduce an error less than 3 percent in the absolute rates.

[24] We expect to publish a detailed account of these experiments in the near future.

(2) Chance Coincidences

An experiment performed with the same apparatus in Ithaca, in which the counting rates were increased by a radium source, indicates that the resolving time of the circuit is about 6 or 7 microseconds, and that the number of sixfold chance coincidences is completely negligible.

(3) Scattering

The decrease in the number of coincidences, due to scattering of particles out of the beam, has been neglected.

(4) Showers

Occasionally two or more electrons which are members of the same shower may simultaneously traverse all of the counters and be recorded as only one particle. This effect tends to reduce slightly the number of electrons recorded. No effect at all of this type is expected for mesotrons.

A more serious error, which affects the counting rates with lead as well as those without lead between the counters, is caused by *side showers* which discharge all the counters simultaneously. This effect tends to increase all of the counting rates.

The error caused by showers is the most difficult to eliminate or evaluate. If one wishes to record only mesotrons of high energy, one may reduce the number of side showers recorded by shielding the counters on the sides (as well as above the counters) with a large thickness of lead. If one wishes to record electrons, however, the presence of lead alongside and near the counters distorts the results because of the showers which originate in the lead itself. Likewise one cannot use the device of placing alongside the coincidence counters additional counters, which are so connected that a coincidence is recorded only when the side counters are not simultaneously discharged. Such a device would discriminate against true coincidences caused by electrons, since all observed electrons are members of more or less dense air showers. This device also reduces the coincidences recorded for mesotrons by several percent,[25] because the side counters are sometimes discharged by knock-on electrons accompanying the mesotrons.

It has been suggested that one may correct for the showers recorded, by measuring the coincidence rate with one of the counters slightly out of line, and subtracting this rate from the coincidence rates with all the counters in line. The correction thus obtained, however, is much too large, both because of the knock-on electrons which discharge the counter out of line when a particle goes through the other counters, and because of the shower particles accompanying the electrons which traverse the counter array.

In our experiment, the number of side showers recorded was reduced by using a large number (six) of counters in coincidence. Auxiliary experiments were performed in which one of the middle counters (in line) was so connected that a coincidence between the other counters was only recorded when this counter was not simultaneously discharged. Such measurements were taken with varying numbers of the other counters in coincidence, from the two extreme counters alone to all of the five remaining counters. The results are not conclusive enough to be entirely satisfactory, but indicate that the number of showers recorded is quite large when only two counters are in coincidence, and decreases rapidly as the number of counters in coincidence is increased. With six counters in coincidence, the number of showers recorded seems to be not more than a few percent of the coincidence rates at the highest elevation, and negligible at the lowest elevation.

The error in the measurements due to the recording of side showers is in a direction opposite to that of the other errors, which also increase somewhat with altitude and partially compensate for the error due to showers. The exact corrections for all the errors are not known, but we know that the corrections are small, of the order of magnitude of the statistical errors. Hence we have not applied to the data any corrections for the systematic errors discussed above.

The writer wishes to express his thanks to Professor Bruno Rossi for suggesting this experiment, and for assistance in carrying out the measurements and evaluating the results.

[25] See Rossi, Hilberry and Hoag (reference 11), Schwegler [A. Schwegler, Zeits. f. Physik **96**, 62 (1935)]. This result is substantiated by similar experiments now in progress.

The Angular Distribution of Positron Annihilation Radiation

ROBERT BERINGER* AND C. G. MONTGOMERY
Sloane Physics Laboratory, Yale University, New Haven, Connecticut
(Received January 7, 1942)

The angular distribution of the two quanta which are emitted in the annihilation of a positron and an electron was observed with coincidence counters of high resolving powers both in time and angle. The direct observations are consistent with the hypothesis that the two quanta are emitted in exactly opposite directions to within at least one degree. A comparison of the counter efficiency obtained from this angular distribution curve with a direct and independent measurement of the counter efficiency for annihilation radiation shows that the half-width of a possible distribution of deviations from strict collinearity is zero to within 15 minutes of angle. It may be concluded that the momentum balance is accurately maintained by the quanta alone, and that, in general, a positron stops before it is annihilated in accord with the theoretical estimates.

INTRODUCTION

BEFORE the discovery of the positron, Dirac[1] predicted the existence of electron states of negative total energy. For free electrons, momentum considerations demanded that when such states were filled by transition from states of positive energy, two gamma-ray quanta must be simultaneously emitted. Later calculations[2] of the probability of this process of positron annihilation gave the result that positrons passing through matter would, in general, stop before being annihilated and the two quanta, each having an energy of mc^2, would be emitted in directly opposite directions. These two simultaneous quanta were first detected by Klemperer.[3] He measured coincidences between two Geiger counters placed close to the source of annihilation radiation so that the solid angle subtended by one counter at the source was nearly 2π. Better angular resolution was obtained by Alichanian, Alichanow, and Arzimovitch,[4] in whose experiments the solid angle subtended by one counter was about 0.7 steradian. From a knowledge of the angular relation between the two quanta, we can determine whether or not the positron is annihilated while in motion or whether a third body, such as a nucleus, is involved in the process. The experiments reported here were undertaken to determine this angular relation more precisely by using counters subtending a solid angle of only 0.015 steradian.

THE COINCIDENCE EXPERIMENTS

Two counters, each with an electrostatic shield and an amplifying tube, were mounted upon arms which permitted rotation about an axis parallel to the counter wires. The counters[5] had cathodes three centimeters long of seamless copper tubing 1.05 cm in diameter, sealed in a glass envelope. They were filled with a mixture of 94 percent argon plus 6 percent oxygen, to a pressure of 9 cm of mercury. A source of annihilation radiation was placed at the axis of rotation. Coincidences from the simultaneously emitted gamma-rays were recorded with a Rossi type adding and a hard tube recording circuit. The arrangement is shown schematically in Fig. 1. The coincidence circuit had a resolving time

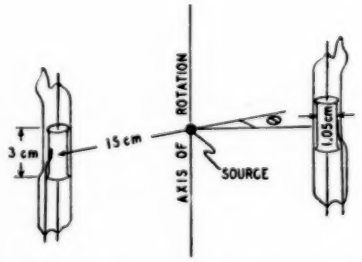

FIG. 1. Schematic arrangement of counters for observing coincidences from annihilation radiation.

* Junior Sterling Fellow, 1941–1942.
[1] P. A. M. Dirac, Proc. Roy. Soc. **A126**, 360 (1930).
[2] P. A. M. Dirac, Proc. Camb. Phil. Soc. **26**, 361 (1930); H. A. Bethe, Proc. Roy. Soc. **A150**, 129 (1935).
[3] O. Klemperer, Proc. Camb. Phil. Soc. **30**, 347 (1934).
[4] A. I. Alichanian, A. I. Alichanow, and L. A. Arzimovitch, Nature **137**, 703 (1936), and C. R. (Doklady) **1**, 287 (1936).
[5] C. G. Montgomery and D. D. Montgomery, J. Frank. Inst. **231**, 447–467, 509–545 (1941).

of 3×10^{-6} second as determined by the accidental counts registered with the counters separated by several meters, each near a radium source. A vacuum-tube pulse generator[6] was also used for this determination and gave results in substantial agreement.

Foils of Cu^{64} activated by about 10-μa hours bombardment in the 3.7-Mev deuteron beam of the Yale cyclotron were used as positron sources. They were pressed into small pellets and covered with 0.32 g/cm^2 of Pb, sufficient to stop the positrons. With such a source of annihilation radiation at the point of intersection of the axis and the perpendicular plane bisecting the counter cathodes, the ratios of coincidence to single counting rates were determined for various angular deviations of one counter from the line through the center of the source and the second counter. These deviations were measured with an optical lever. In all, ten sources were used from which about 800 coincidence counts were recorded. Corrections were applied to the data for all spurious coincidences. In no case was the measured natural coincidence background owing to cosmic rays and accidental counts from other sources higher than 5 percent of the observed annihilation coincidence rate, while that caused by accidental counts from the annihilation quanta themselves as calculated from the resolving time of the circuit did not exceed 10 percent.

Figure 2 shows these observations. The vertical lines attached to the points represent the probable errors of the ratios as computed from the number of counts involved in each determination. It is apparent from this figure without further consideration that the two annihilation quanta are emitted in very nearly opposite directions. We shall now proceed to discuss this more precisely.

THE COUNTER EFFICIENCY

It is evident that if the annihilation quanta are all emitted in exactly opposite directions, the ratio of the coincidence rate to the counting rate of a single counter at $\theta=0$ is equal to the efficiency of the counter for gamma-radiation of this energy, since if n quanta per second are passing through each counter, the single counting rate is ϵn, where ϵ is the efficiency, and the coincidence rate is $\epsilon^2 n$. Thus a determination of counter efficiency by an independent experiment will allow us to draw more precise conclusions. Knowing the number of positrons emitted per sec. from a Cu^{64} source, we can easily determine the efficiency for the annihilation radiation by observation of the single counting rate when the source has been wrapped with enough material to stop all positrons. One assumes that all positrons are annihilated with the emission of two quanta, which is very nearly the case[2] for Cu^{64} positrons; and that the whole counter cathode area is sensitive.

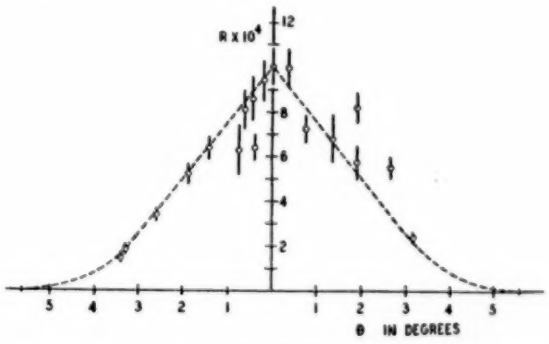

FIG. 2. Observations of coincidences from annihilation radiation. The ordinates are the ratios of the coincidence counting rates to the counting rates of a single counter at angles given by the abscissae. The broken lines represent what is expected if the two quanta are emitted in exactly opposite directions.

An activated Cu foil was fastened to the central electrode of a small ionization chamber which could be evacuated. The current between the source and the thick brass shell of the chamber was measured with a vacuum-tube electrometer. By taking the ratio of the number of electrons to positrons from Cu^{64} as 1.6,[7] the number of positrons emitted per sec. may be calculated when correction has been made for those positrons which do not escape from the Cu foil but nevertheless give rise to annihilation quanta. This correction was made by graphical integration of the electron and positron spectra given by Townsend.[8] The mean value of three determinations of the efficiency was $(10\pm1)\times10^{-4}$. The probable error has been estimated in

[6] C. G. Montgomery, W. E. Ramsey, D. B. Cowie, and D. D. Montgomery, Phys. Rev. **56**, 635 (1939).

[7] S. N. Van Voorhis, Phys. Rev. **50**, 895 (1936); C. V. Strain, Phys. Rev. **54**, 1021 (1938).

[8] A. A. Townsend, Proc. Roy. Soc. **A177**, 357 (1941).

TABLE I. Calculated value of the maximum counting rate ratio as a function of the half-width of $D(\varphi)$.

Half-width, $1/b$	0	1	10′	20′	1°
R at $\theta=0$	ϵ	0.98ϵ	0.89ϵ	0.81ϵ	0.61ϵ

such a way as to allow for uncertainties in the positron-electron ratio and in the energy spectra of the particles. This value is in good agreement with other measurements of the efficiency of similar counters for 0.5-Mev gamma-rays.[9]

DISCUSSION

We are now in a position to evaluate more precisely the results of the coincidence experiment. If the two quanta are emitted exactly collinearly, the cone described by one counter at a point source limits the region in which the second counter may register coincidences between collinear quanta. For this case, the variation of the counting ratio R with the angle θ measured from the second counter to the in-line position of source and counters is given by $R=\epsilon(1-\theta/2\alpha)$, where ϵ is the counter efficiency for the quanta and 2α the cone angle measured about the axis. Plotting the counting ratio *vs.* θ, one gets two straight lines having a common intercept on the R axis at the efficiency and cutting the θ axis at $\pm\alpha$, which for counters of 1.05 cm sensitive width 15 cm from the axis is 4.0°.

For the sources used, which were roughly spherical and 4 mm in diameter, the expected variation of counting ratio with θ for collinear quanta is given by a much more complicated expression but is not markedly different from that of the ideal point source. The broken line in Fig. 2 is calculated for a plane source of 4-mm extension with a uniform surface density of isotropic collinear quantum pair emitters. The behavior of this function is almost that for the point source model for values of θ where the whole source contributes coincidences. The tails start beyond $\theta=2.5°$ where this condition is no longer satisfied. Furthermore, the ordinate at $\theta=0$ is 0.996ϵ as compared with ϵ for the point source case. The agreement with the observations is excellent and we may conclude that within limits of, say, one degree, the two quanta are emitted in exactly opposite directions.

We may determine these limits more precisely by a simple consideration. Let us suppose that directions of emission of the two quanta make an angle $(\pi-\varphi)$, the frequency of occurrence of a given φ being represented by some distribution function such as

$$D(\varphi)=\frac{b/\pi}{1+b^2\varphi^2}.$$

This function has a maximum at $\varphi=0$, falls to half this maximum value at $\varphi=\pm 1/b$, and is normalized to have a unit area. The calculated value of the counting rate ratio R at $\theta=0$ is a very sensitive function of the half-width $1/b$. Table I shows several of the calculated values.

If we say that the maximum value of R from Fig. 2 is $(10\pm 1)\times 10^{-4}$, and use the measured value of the counter efficiency we get $R/\epsilon=1.0\pm 0.14$ and $1/b=0\pm 15'$. The half-width is, of course, essentially positive, and we may conclude from these arguments that the two quanta are on the average collinear to within 15 minutes of angle.

Any lack of collinearity in the two quanta must be explained either as a scattering of the gamma-rays after their emission or must represent some momentum other than that of the quanta. This monentum may be either the momentum of the positron or the electron before annihilation or the momentum gained by a third body, an atomic nucleus for example, during the annihilation process. The experiments described above show, however, that this momentum is extremely small. If the deviation from collinearity is as much as 1°, the corresponding momentum is only that of a 9-kev electron, a deviation of 15′ corresponds to the momentum of an electron of less than 1-kev energy.

[9] J. V. Dunworth, Rev. Sci. Inst. **11**, 167 (1940); F. Norling, Phys. Rev. **58**, 277 (1940); N. Feather and J. V. Dunworth, Proc. Roy. Soc. **A168**, 566 (1938).

X-Ray *L*-Series Satellite Lines

L. PINCHERLE
King's College, London, England
(Received October 6, 1941)

A theoretical treatment is given of the $L\alpha$ and $L\beta$ x-ray satellite lines. The satellites are assumed to arise from doubly-ionized atoms, and calculations of wave-length positions and of relative intensities are made on the method of the self-consistent field. Comparison of computed and observed satellite profile structure is made. A classification of reported experimental component lines is proposed in terms of theoretical transitions.

I. INTRODUCTION

A THEORETICAL attempt is made to classify the satellites of the x-ray line $L\alpha_1$ recently studied experimentally by C. A. Randall and L. G. Parratt[1] in the atomic number range $Z=42$ to $Z=56$. The earlier experimental results of F. K. Richtmyer and R. D. Richtmyer[2] are also discussed, and the tentative classification is extended to the $L\beta$ lines studied by these authors.

As stated by the experimenters,[1] we have in reality a sort of continuous spectrum of satellites, with maxima of intensity, and the component resolution is somewhat arbitrary. But, as these satellites are known as "lines," we shall keep this denomination, which, for some of the lines, is also theoretically justified.

The satellites are here supposed to arise from doubly ionized atoms. The theoretical calculation of the expected structure is by the usual method which has been previously explained in similar calculations.[3] Because most of the considered satellites show the particular increase in intensity due to the Auger effect investigated by D. Coster and R. de L. Kronig,[4] we assume that the additional vacancy is in the M_{IV} or M_V shell, i.e., the $3d$ shell. A complete calculation of the satellite structure is made only for this additional vacancy, and only a rough estimate is made of the position of the satellites due to the ionization of other shells.

II. OUTLINE OF THE CALCULATION

The electrostatic integrals which determine the separation of the satellites have been calculated for 37 Rb and 55 Cs. For these elements, tables of eigenfunctions evaluated with the method of the self-consistent field[5] are available. The approximation given by these eigenfunctions in the present calculations is made worse by the fact that the additional vacancy modifies the atomic field; but these eigenfunctions seem better than the Slater eigenfunctions which have been used for similar calculations. The magnetic parameters have been deduced from the experimental separations of the parent-lines. $j-j$ coupling has been assumed, and it is shown that calculations in intermediate coupling give only slightly different results.

The separation from $L\alpha_1$ of the $L\alpha_1$ satellites for other values of Z have been interpolated from the corresponding values for $Z=37$ and $Z=55$ according to a linear law. This may seem strange, because it is generally assumed that $\Delta\nu$, being the difference of two quadratic functions of Z, is itself a quadratic function of Z; and accordingly Moseley diagrams are plotted in which $(\Delta\nu)^{\frac{1}{2}}$ is a linear function of Z.[6] But in $j-j$ coupling $\Delta\nu$ is determined by the difference of the electrostatic integrals of the two missing electrons in the initial and in the final state, and these integrals are linear functions of Z, so that $\Delta\nu$ is also such a function.

A rough way of estimating this function for the center of gravity of the satellites is the following: Consider the $L\alpha$ satellites due to an

[1] C. A. Randall and L. G. Parratt, Phys. Rev. **57**, 786 (1940), later referred to as R-P.
[2] F. K. Richtmyer and R. D. Richtmyer, Phys. Rev. **34**, 574 (1929), later referred to as R-R.
[3] See F. K. Richtmyer, Rev. Mod. Phys. **9**, 391 (1937) and references; F. K. Richtmyer and E. G. Ramberg, Phys. Rev. **51**, 925 (1937); R. D. Richtmyer, Phys. Rev. **56**, 146 (1939); L. Pincherle, Atti Ist. Ven. **96**, 287 (1937).
[4] D. Coster and R. de L. Kronig, Physica **2**, 15 (1935).
[5] D. R. Hartree, Proc. Roy. Soc. **A143**, 506 (1933); **151**, 96 (1935).
[6] These diagrams were introduced by F. K. Richtmyer, Phil. Mag. **6**, 64 (1928).

additional vacancy in 3d, then

$$h\Delta\nu = \text{Energy}\,(L_{III}+M_V) - \text{Energy}\,(2M_V) - \text{Energy}\,(L_{III}) + \text{Energy}\,(M_V),$$

and expressing both $\Delta\nu$ and the energies in Rydbergs,

$$\Delta\nu = (Z_L^2/4)+[(Z_M+1)^2/9] - 2[(Z_M+\epsilon)^2/9] - (Z_L^2/4) + (Z_M^2/9),$$

Z_L, Z_M being the effective nuclear charges acting on the L_{III} and M_V electrons, respectively. If we now take Slater's[7] value, $\epsilon=0.3$, and use the empirical formula

$$Z_M = 0.72Z - 18.2,$$

we obtain the relation

$$\Delta\nu = 0.064Z - 1.52,$$

which gives the right order of magnitude of $\Delta\nu$ for every Z. The fact that the experimental values seem to fit in a Moseley diagram is mainly due to the narrow range of values of Z for which these diagrams have been plotted; actually the experimental points can be made to lie on a straight line as well when $(\Delta\nu)^{\frac{1}{2}}$ as when $\Delta\nu$ is plotted against Z.

This linear interpolation does certainly not introduce more important errors than the other approximations. In this connection we note that the available Hartree eigenfunctions refer to monovalent metals, and this fact makes the interpolation somewhat less reliable. The interpolated values of the electrostatic integrals for $Z=47$ are in good agreement with the values calculated by R. D. Richtmyer.[8]

The fact that for the various lines the coefficient of Z is not the same causes the aspect of the whole structure to change when Z varies, but not significantly in the range of value of Z here considered. The real cause for the observed changing is examined in Section III.

We may note that, if any electrostatic integral is supposed to vary with Z according to a linear law

$$F = a + bZ,$$

we can reasonably assume that b is very near to the value of F calculated with hydrogen eigenfunctions. We have then a very simple way of effecting extrapolation to near elements when the value of F is known for a given Z. This is shown by Table I which gives the values of b (in Rydberg units) for several electrostatic integrals (a) calculated with hydrogen eigenfunctions, and (b) deduced from the values for $Z=37$ and $Z=55$ (calculated with Hartree eigenfunctions).

TABLE I. Values of b in the relation $F=a+bZ$.

Integral*	Value calc. with hydr. eigenf.	Value from $F(37)$ and $F(55)$
$F^0(2s, sp)$	0.32	0.32
$F^0(2p, 2p)$	0.36	0.36
$F^2(2p, 2p)$	0.18	0.17
$F^0(2s, 3d)$	0.21	0.21
$F^0(2p, 3p)$	0.19	0.18
$F^2(2p, 3p)$	0.05	0.05
$G^0(2p, 3p)$	0.02	0.02
$G^2(2p, 3p)$	0.02	0.02
$F^0(2p, 3s)$	0.17	0.17
$F^0(2p, 3d)$	0.21	0.22
$F^2(2p, 3d)$	0.07	0.07
$G^1(2p, 3d)$	0.07	0.07
$G^3(2p, 3d)$	0.04	0.04
$F^0(3p, 3d)$	0.15	0.15
$F^0(3d, 3d)$	0.17	0.17
$F^2(3d, 3d)$	0.09	0.09
$F^4(3d, 3d)$	0.06	0.06

* Notations as in Condon and Shortley, *The Theory of Atomic Spectra* (Cambridge, 1935).

III. SATELLITES OF $L\alpha_2$

The linear interpolation cannot be carried out at once for all $L\alpha$ satellites. Some lines are satellites not of $L\alpha_1$, but of $L\alpha_2$. In the case of an $L\alpha_2$ satellite, the jumping electron passes to L_{III} from M_{IV}, so that, if we want the separation from $L\alpha_1$, we must subtract from the difference of the electrostatic integrals in the initial and final states the separation $(5/2)z_{3d}(Z)$ between the M_{IV} and M_V levels. For these lines we must add the corresponding $(5/2)z_{3d}$ to the calculated value for $Z=37$ and $Z=55$, then carry out the linear interpolation, and subtract, for every Z, $(5/2)z_{3d}(Z)$ from the obtained value.

As z_{3d} increases with Z^4, the satellites of $L\alpha_2$ for $Z=37$ are practically superimposed on the satellites of $L\alpha_1$, are gradually separated from them with increasing Z and shift towards the parent line. For $Z=56$ the separation is almost complete and most of the $L\alpha_2$ satellites are unobservable because they are superimposed on $L\alpha_1$ itself. For higher values of Z these satellites are included between $L\alpha_1$ and $L\alpha_2$.

[7] J. C. Slater, Phys. Rev. **36**, 57 (1930).

[8] R. D. Richtmyer, Phys. Rev. **56**, 146 (1939).

TABLE II. Separations of the satellites of $L\alpha_1$ and $L\alpha_2$ from $L\alpha_1$. (Rydberg units.)

Line		$Z=$	37 Int. c.	37 jj-c.	42	47	51	56	Int.
		$(5/2)z_{3d}=$	0.15		0.28	0.49	0.72	1.12	
		$\delta\nu=$	0.17		0.20	0.25	0.30	0.38	
Satellites of $L\alpha_1$ M_V ionized	$L_{III}M_V4\rightarrow M_VM_V$	4	1.17	1.10	1.24	1.39	1.50	1.65	33.3
		3	1.36	1.43	1.72	2.00	2.23	2.52	(100.0)
		3	1.19	1.23	1.45	1.67	1.85	2.07	8.9
		2	1.05	1.03	1.16	1.30	1.40	1.54	44.4
		1	1.53	1.42	1.70	1.99	2.21	2.50	20.7
		1	1.24	0.93	1.09	1.25	1.38	1.54	14.8
Satellites of $L\alpha_1$ M_{IV} ionized	$L_{III}M_{IV}3\rightarrow M_VM_{IV}$	4	1.19	1.14	1.33	1.52	1.67	1.86	66.7
		3	1.59	1.48	1.76	2.05	2.27	2.56	10.4
		3	1.39	1.24	1.46	1.69	1.87	2.09	0.7
		2	1.37	1.31	1.54	1.77	1.95	2.18	41.5
		2	1.17	1.07	1.24	1.41	1.54	1.71	13.0
		2	1.04	0.98	1.12	1.26	1.38	1.52	1.1
		1	1.25	1.24	1.47	1.70	1.88	2.11	23.3
		1	1.12	1.15	1.35	1.55	1.71	1.91	10.0
		0	1.17	1.17	1.37	1.56	1.72	1.92	11.1
Satellites of $L\alpha_2$ M_V ionized	$L_{III}M_V4\rightarrow M_{IV}M_V$	4	0.64	0.70	0.64	0.50	0.33	0.00	50.0
		4	1.04	1.04	1.07	1.03	0.94	0.70	16.7
		3	0.83	1.02	1.11	1.11	1.06	0.87	16.7
		3	1.23	1.36	1.54	1.64	1.66	1.57	14.1
		3	1.03	1.12	1.24	1.29	1.26	1.11	21.1
		2	1.09	1.16	1.25	1.26	1.21	1.03	21.1
		2	0.89	0.92	0.95	0.91	0.81	0.57	0.4
		2	0.76	0.83	0.84	0.76	0.64	0.38	15.6
		1	1.37	1.31	1.49	1.60	1.62	1.53	15.6
		1	1.24	1.22	1.38	1.45	1.45	1.34	6.7
Satellites of $L\alpha_2$ M_{IV} ionized	$L_{III}M_{IV}3\rightarrow M_{IV}M_{IV}$	2	1.23	1.24	1.37	1.42	1.39	1.25	20.7
		2	1.01	1.07	1.14	1.14	1.07	0.87	29.6
		1	1.09	1.24	1.37	1.42	1.40	1.26	23.7
		1	0.39	0.71	0.69	0.60	0.46	0.17	14.8

As a result of this shifting of the $L\alpha_2$ satellites, the aspect of the whole satellite structure changes from element to element, and some of the observed irregularities in the varying of the experimental separations with Z are thus explained. Other irregularities may be due to alterations in the atomic field, such as those produced by the completion of an electronic shell. Others may be traced to a difference in the relative probability of the M_{IV} and M_V levels being ionized through the Coster-Kronig process; such a difference would alter the ratio between the intensities of the $L\alpha_2$ and $L\alpha_1$ satellites.

IV. RESULTS: $L\alpha$ SATELLITES

Table II gives, for every $L\alpha$ satellite due to a $3d$ ionization, the theoretical separation from $L\alpha_1$ for $Z=37$, 42, 47, 51, 56, and the intensity, calculated in $j-j$ coupling, under the hypothesis that M_{IV} and M_V have the same probability of being ionized, and referred to that of the most intense line taken as 100. For every Z the experimental value of $(5/2)z_{3d}$ and the assumed natural width of the theoretical lines are given. For $Z=37$ the separations calculated in intermediate coupling are also given. For some lines the correction is large, but the main features are the same as in $j-j$ coupling. For increasing values of Z the $j-j$ coupling becomes an increasingly better approximation.

The natural width (full width at half maximum) has been assumed the same for all theoretical transitions and has been interpolated from the fairly well established values 0.25 (Rydberg units) for $Z=47$,[9] and 1.18 for $Z=79$,[10] according to the law:[11]

$$\delta\nu=m+nZ^4.$$

We note that the ratio between the natural width $\delta\nu$ of the satellites under consideration and their separation $\Delta\nu$, which ratio may give an idea

[9] L. G. Parratt, Phys. Rev. **54**, 99 (1938).
[10] F. K. Richtmyer, S. W. Barnes, and E. G. Ramberg, Phys. Rev. **46**, 843 (1934).
[11] L. Pincherle, Rend. Acc. Lincei **20**, 29 (1934).

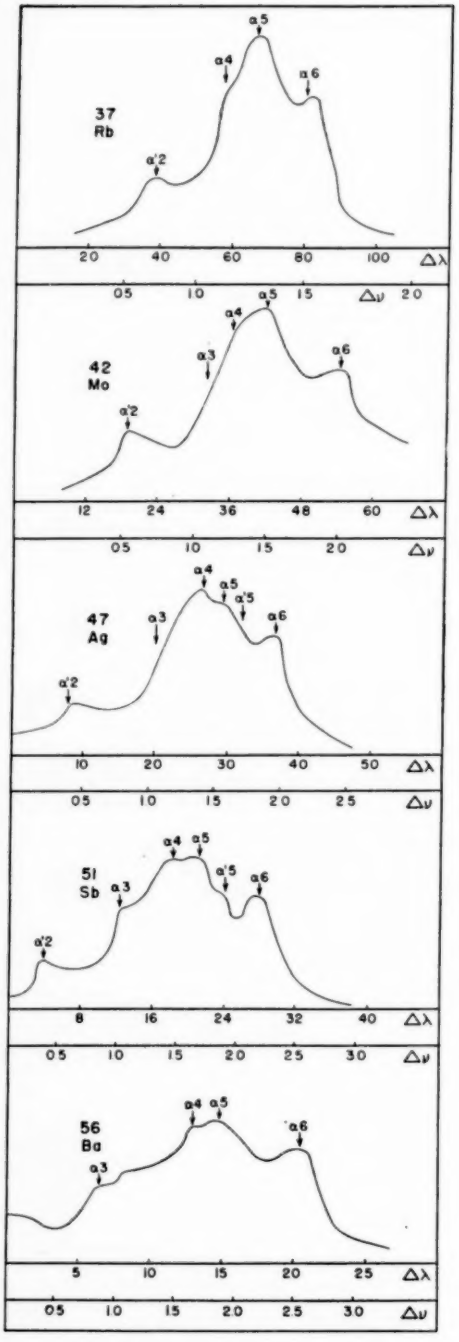

FIG. 1. Theoretical contours of $L\alpha$ satellites.

of their sharpness, is given by a formula

$$\delta\nu/\Delta\nu=\delta\lambda/\Delta\lambda=(m+nZ^4)/(a+bZ)$$

(a, b, m, n, constant). As n is very small, for small Z the ratio decreases when Z increases, then reaches a minimum, and afterwards increases. For the satellites under consideration the minimum is in the neighborhood of $Z=40$, so that this is the best region in which to observe them.

Extrapolating the values given by Table II, up to $Z=79$, we obtain values in good agreement with the values given by Richtmyer and Ramberg.[12] The extrapolated values are systematically about 0.1 Rydberg lower than the values of the above said authors; this may be due either to the wide range over which the extrapolation has been carried out, or to the different kinds of eigenfunctions used in the two cases.

The theoretical satellite profile is obtained if we assume that every theoretical line is shaped according to the formula

$$J_\nu/J_0=1/(1+(2\nu/\delta\nu)^2$$

where J_ν is the intensity at the distance ν from the center of the line, and $\delta\nu$ is the full width at half maximum. For every frequency we add up the contributions of all the lines. The result is shown in Fig. 1, which gives the profile of the $L\alpha$ theoretical satellites for $Z=37$, 42, 47, 51, 56. In abscissa both $\Delta\nu/R$ and $\Delta\lambda$ (X. U.) measured from the parent line are plotted to enable a comparison with the experimental results which are summed up in R-P Fig. 2. The ordinate scale of each curve of Fig. 1 is in arbitrary units.

Inspection of Fig. 1 shows that, in general aspect, the four to six overlapping "lines" are not dissimilar from the experimental contours. There are three maxima: The first, α_2', corresponds to the transition $L_{III}M_V4\rightarrow M_{IV}M_V4$, the most intense $L\alpha_2$ satellite (its gradual shifting towards the parent line is clearly visible). The

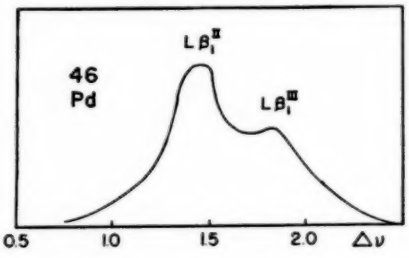

FIG. 2. Theoretical contours of $L\beta_1$ satellites.

[12] F. K. Richtmyer and E. G. Ramberg, Phys. Rev. **51**, 925 (1937).

TABLE III. Experimental separations from $L\alpha_1$ of the $L\alpha$ satellites ($\Delta\nu/R$).

	Randall and Parratt*										Richtmyer and Richtmyer							
Z		α'_2	α_2	α_4	α_5	α'_5	α_6	α_7	α_8	α_9	α'_9	α^{I}	α^{II}	α^{III}	α^{IV}	α^{V}	α^{VI}	α^{VII}	α^{VIII}
37												0.37	0.49	0.68	0.87	1.05			
38												0.40	0.52	0.65	0.92	1.07			
40												0.43	0.58	0.73	1.00	1.18			
41												0.45	0.61	0.75	1.10	1.24	1.41		
42	0.19	0.37	0.47	0.63	0.75		1.01					0.46	0.64	0.80	1.09	1.35	1.60	1.82	2.22
44		0.33	0.50	0.70	0.87		1.21	1.48				0.49	0.69	0.89	1.22	1.51	1.84		
45		0.36	0.54	0.72	0.92		1.25	1.56	1.77	1.94		0.51	0.72	0.93	1.25	1.57			
46		0.42	0.55	0.76	0.98	1.14	1.31	1.68	1.88	2.20		0.54	0.74	1.01	1.33	1.67	2.06		
47		0.47	0.58	0.77	1.01	1.17	1.38	1.79	2.03			0.57	0.80	1.08	1.41	1.78			
48		0.47	0.62	0.82	1.07	1.25	1.47	1.78	1.98	2.23		0.58	0.81	1.10	1.50	1.88			
49			0.65	0.85	1.24	1.28	1.57	2.06	2.52	2.81		0.60	0.83	1.13	1.54	1.98			
50			0.55	0.89	1.16	1.48	1.85	2.17	2.46										
51				0.95	1.22		1.76	2.31	2.69	3.02	3.50								
52				0.95	1.22		1.82	2.51	2.86	3.37	4.06								
53				0.86	1.18		1.69	2.34	3.07	3.97									
56					1.39		1.73	3.17	4.01	4.98	6.03								

* For $Z=42$ some lines are classified here differently than in R–P.

second, the principal maximum, very wide and perhaps at least three overlapping lines, is generally found to correspond to the transition $L_{III}M_V2\rightarrow M_VM_V2$. An inflection (which for some elements takes the aspect of a second maximum) on the side of greater ν corresponds to $L_{III}M_{IV}3\rightarrow M_VM_{IV}4$. This inflection or maximum is followed by a less marked inflection corresponding to $L_{III}M_{IV}2\rightarrow M_VM_{IV}3$. Then a broad line is suggested on the side of the small ν, which is the superimposition of several faint satellites, both of $L\alpha_1$ and of $L\alpha_2$. The third and last general maximum is the sharpest and corresponds almost exactly to $L_{III}M_V3\rightarrow M_VM_V4$, the most intense single satellite of $L\alpha_1$.

Table III gives the experimental lines. R-R α^1 corresponds to R-P α_3, α^{II} to α_4, and so on. No R-R line corresponds to α_2' or α_5'. The satellite α_4 is the most intense, then comes α_5; the satellites, α_3 and α_6, have about the same intensity; α_5', when it appears, has also this intensity: α_7 is the faintest one. The agreement with the experimental separations is rather poor, as was to be expected owing to the poor approximation given by this kind of calculations; the reasons that the theoretical separations are generally larger than the experimental values have been discussed by Richtmyer and Ramberg.[13]

In spite of the quantitative disagreements, some interesting conclusions can be drawn. The lines which can be assigned to the configuration under consideration are α_3 to α_7, because they show the intensity anomaly due to the Coster-Kronig effect. It is most likely that the most intense experimental line, namely $L\alpha_1$, corresponds to the maximum of the theoretical curve, and it must then be classified, at least for $Z>42$, as the superimposition of several faint theoretical transitions, $L_{III}M_V2\rightarrow M_VM_V2$ being the most important. Then α_5 corresponds mainly to $L_{III}M_{IV}3\rightarrow M_VM_{IV}4$ and probably α_5' to $L_{III}M_{IV}2\rightarrow M_VM_{IV}3$ though for some elements it may be a_5' which corresponds to $L_{III}M_{IV}3\rightarrow M_VM_{IV}4$. The change in the aspect of these three lines from element to element is brought about by the shifting of two satellites of $L\alpha_2$, namely $L_{III}M_{IV}3\rightarrow M_{IV}M_{IV}2$ and $L_{III}M_{IV}1\rightarrow M_{IV}M_{IV}2$, which lie in the considered region; that is why the same experimental line, as classified by R-P or R-R, may correspond in different elements to different theoretical transitions. α_6 on the contrary can be assigned almost exactly to $L_{III}M_V3\rightarrow M_VM_V4$, the most intense satellite of $L\alpha_1$. As for α_7, the calculation in intermediate coupling shows that two weak lines, $L_{III}M_V1\rightarrow M_VM_V2$, and $L_{III}M_{IV}3\rightarrow M_VM_{IV}3$ are more widely separated from $L_{III}M_V3\rightarrow M_VM_V4$ than is found in $j-j$ coupling, so that α_7 may be the superimposition of these two lines. In this hypothesis the ratio of the intensities $\alpha_7:\alpha_6$ is 0.3, in agreement with experiment; but the fact that, when Z increases,

[13] F. K. Richtmyer and E. G. Ramberg, Phys. Rev. **51**, 925 (1937).

the separation between α_6 and α_7 increases rapidly cannot be accounted for by this explanation.

A classification in which α_7 is assigned to $L_{III}M_V3 \rightarrow M_VM_V4$ and α_5, α_5' and α_6 to the principal maximum of the theoretical curve would not account for the intensity of α_4.

$L\alpha_3$ corresponds to several faint lines, most $L\alpha_2$ satellites, $L_{III}M_{IV}2 \rightarrow M_{IV}M_{IV}2$ being the most important, and, if its intensity allowed its

TABLE IV. Theoretical separations from $L\alpha_1$ of the satellites due to single ionization.

Ionized shell	$L\alpha_1$ satellites		$L\alpha_2$ satellites	
	$Z=37$	$Z=55$	$Z=37$	$Z=55$
$1s$	11.1	12.5	11.0	11.5
$2s$	6.0	7.9	5.8	6.9
$2p$	7.0	9.5	6.9	8.5
$3s$	1.1	1.5	1.0	0.5
$3p$	1.2	1.7	1.0	0.7
$3d$	1.2	1.9	1.0	0.9
$4s$	0.1	0.3	0.0	−0.7
$4p$	0.1	0.3	−0.1	−0.8
$4d$		0.3		−0.8

being observed for $Z>50$, it should be found to move towards the parent line. α_2' is almost exclusively $L_{III}M_V4 \rightarrow M_{IV}M_V4$, the most intense $L\alpha_2$ satellite, and its not being observed for $Z>48$ is due to the fact that it gets too near to the parent line. It was suggested however by R-P that α_2' does not show the intensity anomaly shown by lines due to a $3d$ ionization, so that it should be assigned to another vacancy, probably in the N shell; then α_3 would correspond to $L_{III}M_V4 \rightarrow M_{IV}M_V4$. But the measure of the intensity of α_2' is difficult as it lies in the strong background of the parent-line, so it seems that the first classification is preferable.

The arrows in Fig. 1 indicate the positions at which the experimental lines are fitted by the proposed classification. For instance for $Z=47$ the following components fit more or less the theoretical curve: α_2' at $\Delta\nu=0.5$, intensity 32; α_3, $\Delta\nu=1.1$, intensity 40; α_4, $\Delta\nu=1.3$, intensity 100; α_5, $\Delta\nu=1.55$, intensity $=52$; α_5' $\Delta\nu=1.75$ intensity 44; α_6, $\Delta\nu=2.0$, intensity 65.

To try to classify the other satellites observed by R-P, the separations of the centers of gravity of the satellites due to a single additional vacancy in any other shell nl have been calculated. They are given by:

$\Delta\nu = F_0(2p, ml) - F_0(3d, nl)$ for the $L\alpha_1$ satellites,
$\Delta\nu = F_0(2p, nl) - F_0(3d, nl) - (5/2)z_{3d}$ for the $L\alpha_2$ satellites.

Table IV gives the results for $Z=37$ and $Z=55$. The interpolation to other values of Z is linear for the satellites of $L\alpha_1$, and must be carried out as explained in Section III for the satellites of $L\alpha_2$. The values of $\Delta\nu$ for an N ionization are uncertain, because the ionization in $2p$ alters the N eigenfunctions in a more considerable way than it alters those of inner electrons; and they are certainly lower than the real values, as follows from the fact that the additional ionization places the N electrons, on the average, nearer to the nucleus and so increases $F_0(2p, 4l)$ more than $F_0(3d, 4l)$.

The satellites due to a vacancy in the N shell cannot probably be observed because they are too near to $L\alpha_1$. The N vacancy however may easily be double, either because of the rather high probability of the N shell being ionized, or, more likely, as a result of an Auger effect in which an initial $L-M$ ionization is transformed into a $L-N-N$ one. The resultant of the many

TABLE V. Separations of the $L\beta_1$ satellites (Rydberg units).

	Line		$Z=$ 37		56	
			$\delta\nu=$ 0.17		0.38	
			Int. coup.;	*jj*-coup.		Int.
	$L_{II}M_V3 \rightarrow M_{IV}M_V$	4	1.08	1.12	1.84	(100)
	3	3	1.48	1.46	2.55	43.2
M_V	3	2	1.28	1.22	2.07	12.3
ionized	2	3	1.34	1.40	2.39	34.6
	2	2	1.14	1.16	1.92	43.2
	2	1	1.01	1.07	1.73	33.3
M_V	$L_{II}M_{IV}2 \rightarrow M_{IV}M_{IV}2$	1.12	1.29	2.13	27.8	
ionized	1	2	1.36	1.47	2.61	27.8
	1	0	0.66	0.94	1.52	11.1

lines arising from such an ionization could then be α_2', as previously stated, or superimposed on it. If for $Z=42$ the lines observed by R-P are classified as in the present paper, then the line with a separation of 0.19 Rydberg from $L\alpha_1$ is most likely to be the one under consideration.

The satellites due to a $3s$ or $3p$ ionization should be superimposed on those due to a $3d$ ionization, but these satellites must be extremely faint, because, if $3s$ or $3p$ happen to be excited, they

have a great chance of being destroyed through an Auger effect (in which a $3d$ electron fills the vacancy and an N electron is ejected) before the emission of the line $L\alpha$ has taken place. Such an Auger effect will then leave the atom with a $L-M-N$ ionization, the vacancy in the M shell being in M_{IV} or M_V.

The satellites which arise from an additional L vacancy have a very large separation. They have been observed by Burbank[14] for $Z=47$ at the position foretold by the theory, but, strangely have not been observed for $Z=42$ by Veith and Kirkpatrick[15]—the new line found by these authors is probably a satellite of $L\beta_3$.

We see then that the other satellites observed by R-P, namely α_8, α_9, α_9' cannot be explained as due to atoms with a single additional vacancy and must then be assigned to atoms ionized three times. Lines due to a double additional vacancy have been found for K satellites.[16] It is suggested here that the lines in question arise from the particular Auger effect by which the original vacancy in $3s$ or $3p$ is changed in a double vacancy, $3d+4l$. In first approximation the separation from the parent-line of a satellite due to a double additional vacancy is the sum of the separations which would be caused by the single vacancies. This gives about the right order of magnitude of the observed separations, particularly for α_8 and α_9, when we remember that the separation due to an N vacancy will be still increased when, besides $2p$, also $3d$ is ionized. The separation of α_9' seems too large to be explained with this cause; an $M-M$ ionization should be responsible.

The hypothesis that α_8, α_9, α_9' may be caused by a completely different mechanism, namely by a double transition with the emission of a single light quantum is disproved by earlier calculations of the author,[17] which show that, for $Z\sim 50$, the satellites due to double transitions have an intensity which is only 10^{-5} or 10^{-6} that of $L\alpha_1$, and are then unobservable. Moreover the intensity of these lines is proportional to Z^{-2}, so that they should be observed more easily for lighter elements, which is not the case.

[14] C. J. Burbank, Phys. Rev. **56**, 142 (1939).
[15] W. Veith and P. Kirkpatrick, Phys. Rev. **56**, 705 (1939).
[16] E. H. Kennard and E. Ramberg, Phys. Rev. **46**, 1040 (1934).
[17] L. Pincherle, Nuovo Cimento **14**, 185 (1937).

V. RESULTS: $L\beta$ SATELLITES

Table V, which is constructed exactly as Table II, gives the separations of the $L\beta_1$ satellites. As β_1 is not a component of a doublet, all the separations are linear functions of Z; so the values for $Z=37$ and $Z=56$ only are given, and the value of Z_{3d} is omitted. The natural width of these lines has been assumed to be the same as that of the $L\alpha$ satellites, as the natural width of the L_{II} and L_{III} levels are not much different. The profile of the group is shown in Fig. 2 which refers to $Z=46$, and it is very much the same for the other elements for which experimental data are available. It presents two maxima: the first, and more intense, corresponds to the most intense theoretical transition, $L_{II}M_V3\rightarrow M_{IV}M_V4$; the second is the superimposition of three lines, namely $L_{II}M_V3\rightarrow M_{IV}M_V3$; $L_{II}M_V2\rightarrow M_{IV}M_V3$; $L_{II}M_{IV}1\rightarrow M_{IV}M_{IV}2$.

TABLE VI. Separations from $L\beta_1$ of the maxima in the theoretical contours for the $L\beta_1$ satellites, and of the experimental lines.

	Maximum corresponding to the theoretical transition		Experimental lines (Richtmyer and Richtmyer)			
Z	$L_{II}M_V3\rightarrow M_{IV}M_V4$	$L_{II}M_V3\rightarrow M_{IV}M_V3$ and others	β_1^{I}	β_1^{II}	β_1^{III}	β_1^{IV}
41	1.27	1.66	0.42	0.85		
42	1.31	1.72	0.42	0.88	1.13	1.39
44	1.38	1.82	0.45	0.96	1.26	1.66
45	1.41	1.86	0.53	1.00	1.36	1.75
46	1.43	1.88	0.56	1.09	1.48	1.82
47	1.46	1.90	0.69	1.16	1.60	1.96
48	1.50	1.96	0.64	1.15	1.71	2.21
49	1.55	2.06	0.60	1.17	1.76	
50	1.60	2.16	0.65	1.31	1.82	

In Table VI the positions of the two maxima are compared, for every Z, with the experimental results of R-R. Of the experimental lines, β_2^{II} is the strongest, β_1^{I} and β_1^{III} have about the same intensity, and β_1^{II} is very weak. We see that in this case too the theoretical values are larger than the experimental ones. The most intense line $L\beta_1^{II}$ almost certainly corresponds to the most intense maximum of the theoretical curve and can then be classified as $L_{II}M_V3\rightarrow M_{IV}M_V4$, although some fainter theoretical lines are superimposed. $L\beta_1^{III}$ corresponds to the second maximum of the theoretical curve, and is the overlapping of three theoretical transitions. The

TABLE VII. Separations and intensities (in brackets) of $L\beta_2$ satellites for $Z=55$.

Final level	Initial level: $L_{III}M_{IV}3$	$L_{III}M_{IV}2$	$L_{III}M_{IV}1$	$L_{III}M_{IV}0$	$L_{III}M_V4$	$L_{III}M_V3$	$L_{III}M_V2$	$L_{III}M_V1$	
	M ionized				*M* ionized				
$M_{IV}N_{IV}3$	5.88 (51)	5.42 (13)							Satellites of $L\beta_{15}$ ($N_{IV}\rightarrow L_{III}$)
2	5.56 (13)	5.10 (18)	5.45 (14)						
1		5.43 (14)	5.78 (4)	5.76 (9)					
0			5.16 (9)						
$M_VN_{IV}4$					4.81 (61)	5.47 (21)			
3					4.94 (21)	5.60 (17)	5.19 (26)		
2						5.56 (26)	5.15 (1)	6.10 (19)	
1							5.05 (19)	6.00 (8)	
$M_{IV}N_V4$	5.76 (82)								Satellites of $L\beta_2$ ($N_V\rightarrow L_{III}$)
3	5.92 (13)	5.46 (51)							
2	5.83 (1)	5.37 (16)	5.72 (29)						
1		5.28 (1)	5.63 (12)	5.61 (14)					
M_VN_V5					5.17 (100)				
4					4.92 (21)	5.58 (61)			
3					5.25 (2)	5.90 (29)	5.49 (33)		
2						5.43 (5)	5.02 (27)	5.97 (13)	
1							5.40 (8)	6.35 (19)	
0								5.75 (9)	

separation $\beta_1^{II}-\beta_1^{III}$ is given fairly well by the theory.

It is proposed to classify $L\beta_1^{IV}$ in the same way as $L\alpha_8$, $L\alpha_9$, namely, as due to a double additional vacancy caused by an Auger effect in which an initial single $3s$ or $3p$ ionization is changed into a double one, M_{IV}(or M_V)$+N$.

It is more difficult to classify $L\beta_1^I$, and it seems that it can be explained only as due to a (probably double) N ionization, and in this case it should not present the Coster-Kronig intensity anomaly; in any case its great intensity is puzzling.

Finally, a few words for the $L\beta_2$ satellites. Their wave-length positions have been calculated for an additional $3d$ vacancy for $Z=55$ (for $Z=37$ the $4d$ shell is still unoccupied). Table VII gives their separations in intermediate coupling, and intensities in $j-j$ coupling (which is nearly reached). No experimental results are available for $Z=55$, but R-R results for $Z=53$ show that the theoretical values in the case of $L\beta_2$ are in less agreement with the experimental values than in the case of other lines. This is expected owing to the inadequateness of the $4d$ eigenfunction.

The theoretical contours of the $L\beta_2$ satellites (which have a larger natural width than the $L\beta_1$ satellites) are shown in Fig. 3. It suggests a doublet, the line on the side of shorter wave-length being the stronger. The experiments give two strong lines $L\beta_2^I$ and $L\beta_2^{II}$, and some fainter ones, as satellites due to a $3d$ ionization, but the two theoretical "lines" are a superimposition of so many theoretical transitions, that a classification is of academic value only.

We may note that a change in the aspect of the $L\beta_2$ satellites from element to element must be expected, as for $L\alpha$ satellites, when the satellites

of $L\beta_{15}(N_{IV}\rightarrow L_{III})$ gradually shift towards the parent line. These lines are almost completely separated from the $L\beta_2$ true satellites for $Z=79$.

As for the other experimental lines, that indicated by R-R as $L\beta_2(c)$ may be due to a double additional vacancy, as α_8 and α_9, and $L\beta_2(a)$, which does not show the Coster-Kronig intensity anomaly, is almost certainly the resultant of the many lines due to an additional N vacancy; the theoretical value for the separation of this line, namely $F_0(2p, 4d)-F_0(4d, 4d)$, is 0.9, in fair agreement with the experimental value. Also lines due to a double N ionization may of course contribute.

VI. CONCLUSIONS

(a) The separation of a satellite from the parent line is a linear function of the atomic number.

(b) If the parent line is a component of a doublet, the satellites of the other component may be superimposed; they move towards the parent line when Z increases, and produce a change in the aspect of the satellites from element to element.

(c) The following classification is proposed for the $L\alpha$ satellites:

$L\alpha_2'$ to $L\alpha_7$ are due to a $3d$ ionization;

α_2' is mainly the most intense satellite of $L\alpha_2$: $L_{III}M_V4\rightarrow M_{IV}M_V4$.

α_3 is the overlapping of several faint $L\alpha_2$ satellites.

Alternatively α_2' may be due to a (single or double) N ionization, and α_3 to $L_{III}M_V4\rightarrow M_{IV}M_V4$.

α_4 is the overlapping of several lines, $L_{III}M_V2\rightarrow M_VM_V2$ being the most important.

α_5 is mainly $L_{III}M_{IV}3\rightarrow M_VM_{IV}4$;

α_5' is probably mainly $L_{III}M_{IV}2\rightarrow M_VM_{IV}3$;

α_6 is almost exclusively $L_{III}M_V3\rightarrow M_VM_V4$, the most intense theoretical satellite of $L\alpha_1$.

α_7 remains unexplained, unless a more exact calculation shows that some weak theoretical line is beyond $L_{III}M_V3\rightarrow M_VM_V4$.

α_8, α_9, α_9' are due to ionized atoms; the double additional vacancy is $3d+4l$, and is brought about by an Auger effect from an initial state in which there is only one additional vacancy in $3s$ or $3p$.

(d) As for the $L\beta$ satellites:

$L\beta_1^{I}$ is probably the resultant of the many lines due to an additional single or double vacancy in the N shell.

B_1^{II} is mainly $L_{II}M_V3\rightarrow M_{IV}M_V4$.

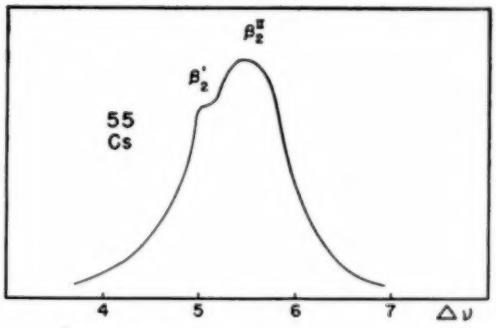

FIG. 3. Theoretical contours of $L\beta_2$ satellites.

B_1^{III} is the superimposition of $L_{II}M_V3\rightarrow M_{IV}M_V3$, $L_{II}M_V2\rightarrow M_{IV}M_V3$ and $L_{II}M_{IV}1\rightarrow M_{IV}M_{IV}2$.

β_1^{IV} is analogous to $L\alpha_8$, $L\alpha_9$.

$\beta_2(a)$ is due to an N ionization.

β_2^{I}, $\beta_2(b)$, β_2^{II}, which are known to be due to a $3d$ ionization, cannot be more precisely classified, being the overlapping of too many theoretical transitions.

$\beta_2(c)$ is analogous to $L\alpha_8$, $L\alpha_9$.

The Auger Effect in Relative Intensities and Widths of X-Ray Lines

JOHN N. COOPER*
Cornell University, Ithaca, New York
(Received December 22, 1941)

A systematic study of the widths and relative intensities of certain L lines in the atomic number range $70 \leq Z \leq 81$ has been made with a two-crystal spectrometer. It was found that in going from Ta (73) to Tl (81) the width of lines arising from L_{I} initial states increased in energy by approximately six electron volts, while the widths of lines arising from L_{II} and L_{III} initial states increased by only approximately one electron volt. Further, the intensities of L_{I} lines relative to the intensities of L_{II} and L_{III} lines showed a marked decrease with atomic number. Both of these variations can be attributed to the rapid increase with atomic number of the probabilities of the Auger transitions $L_{\mathrm{I}} \rightarrow L_{\mathrm{III}} M_{\mathrm{IV}}$ and $L_{\mathrm{I}} \rightarrow L_{\mathrm{III}} M_{\mathrm{V}}$. The results on line widths are in accord with the theory of Weisskopf and Wigner. All the data recorded indicate that Auger transitions are of prime importance in determining the relative intensities and widths of certain x-ray lines.

I. INTRODUCTION

THAT the Auger effect plays an important part in determining both the relative intensities and the widths of x-ray lines was first recognized by Coster and Kronig.[1] Auger transitions, otherwise known as radiationless transitions, increase the widths of lines since they decrease the lifetime of the states; secondly, they decrease the relative intensities of diagram lines since Auger transitions allow an atom to leave a state without emitting a quantum; thirdly, they increase the relative intensities of "second-order" lines, otherwise known as "satellite" lines, since the final states of many Auger transitions are the initial states for satellite emission.

The importance of Auger transitions in x-ray spectroscopy is increased by the fact that their probabilities often vary rapidly from one element to the next. Accordingly, the Auger effect provides exactly the sort of mechanism required to explain the puzzling variations that have been observed in line widths and in relative intensities. Indeed, this rapid variation of Auger probabilities with atomic number makes it possible to distinguish the results of Auger transitions from the effects of other processes.

The present paper reports systematic measurements of the widths and relative intensities of certain L-series lines for elements of atomic number between 73 and 81. In this region it is known that the probabilities of the Auger transitions from an L_{I} initial state to the final states of double ionization $L_{\mathrm{III}} M_{\mathrm{IV}}$ and $L_{\mathrm{III}} M_{\mathrm{V}}$ are rapidly changing with atomic number. Therefore, one may expect appreciable changes in relative intensities and widths of lines arising from L_{I} transitions. The expected variations are clearly shown by the data reported here.

II. THEORY OF SHAPES AND WIDTHS OF X-RAY LINES

On the assumptions of the Dirac radiation theory Weisskopf and Wigner[2] found that the frequency distribution of a line arising from transitions between the states A and B was given by

$$J(\nu)\Delta\nu = \frac{(\Gamma^A+\Gamma^B)\Delta\nu}{[(\Gamma^A+\Gamma^B)/2]^2+4\pi^2(\nu-\nu_{B^A})^2}.$$

Here Γ^A and Γ^B are, respectively, the reciprocals of the mean life[3] of atoms in states A and B, and $\nu_{B^A}=(E_A-E_B)/h$ where E_A and E_B are the most probable energies of states A and B. The full width at half maximum of this distribution is $\Delta\nu=(\Gamma^A+\Gamma^B)/2\pi$ in frequency units, or $\Delta E=\hbar(\Gamma^A+\Gamma^B)$ in ergs.

The width of a line is seen to be proportional to the sum of the reciprocals of the mean lifetimes

* Now at the University of Southern California.
[1] Coster and Kronig, Physica 2, 14 (1935).
[2] Weisskopf and Wigner, Zeits. f. Physik **63**, 54 (1930).
[3] The mean life of atoms in the state A is here defined as the time required for N atoms in that state at time $t=0$ to be reduced to $1/e$ of N (e is the Naperian base).

of the initial and final states. It is convenient to interpret $h\Gamma^A$ and $h\Gamma^B$ as the energy widths of states A and B, respectively. Speaking in these terms, one may say that the width of a line is equal to the sum of the widths of the initial and final states.

The reciprocal of the mean life of a state Γ^A is equal to the sum of the probabilities of all spontaneous transitions from state A to any other state, so one may write

$$\Gamma^A = \sum_B \gamma_B{}^A,$$

where $\gamma_B{}^A$ is the probability for the transition $A \rightarrow B$, and the sum extends over all possible transitions. Taking account of both radiative and Auger processes, one may rewrite the above in the form

$$\Gamma^A = \sum_R \gamma_R{}^A + \sum_S \gamma_S{}^A,$$

where $\gamma_R{}^A$ is the transition probability for the radiative transition $A \rightarrow R$ and $\gamma_S{}^A$ is the probability for the Auger transition $A \rightarrow S$.

Several investigators have made calculations on the relative importance of radiative and Auger transitions in determining the widths of energy levels. Ramberg and Richtmyer[4] have computed both $\sum_R \gamma_R{}^A$ and $\sum_S \gamma_S{}^A$ for the K, $L_{\rm I}$, $M_{\rm I}$, $M_{\rm II}$, $M_{\rm III}$, and $N_{\rm I}$ levels for Au (79). They found that the radiative process accounts for almost all the transitions from the K shell, but that for all other levels investigated, the Auger contribution to the level width was dominant. For the $L_{\rm I}$ level of gold they found the ratio of Auger transition probabilities to radiative transition probabilities to be six to one. Pincherle,[5] working on gold but using hydrogenic wave functions, also found this ratio to be roughly six to one, although his calculated value of the width was less than half that of Ramberg and Richtmyer. Such data as are available on fluorescence yields confirm the idea that Auger transitions are often far more probable than radiative ones.

Further, an Auger transition may be highly probable for one element, and forbidden for an element adjacent in the periodic table.[6] Any abrupt change in the probability of a given Auger transition should result in a corresponding change in the width of the initial state and hence in a variation of the widths of all x-ray lines associated with that state. Thus, for a series of elements, one may study the changes in the probability of an Auger transition through observations of the variation in the widths of selected x-ray lines.

III. THE AUGER TRANSITIONS $L_{\rm I} \rightarrow L_{\rm III} M_{\rm IV,V}$

The two Auger transitions that are the primary concern of this paper have a common $L_{\rm I}$ initial state and their final states (of double ionization) are $L_{\rm III}M_{\rm IV}$ and $L_{\rm III}M_{\rm V}$. These radiationless transitions are possible whenever the energy of the $L_{\rm I}$ state is greater than the energies of the states $L_{\rm III}M_{\rm IV}$ and $L_{\rm III}M_{\rm V}$, respectively. In Fig. 1 the difference in the ν/R values of the $L_{\rm I}$ and $L_{\rm III}$ states is plotted as a function of atomic number; on the same graph, the ν/R values for the $M_{\rm IV}$ and $M_{\rm V}$ states of element $Z+1$ are also plotted. It is clear from the figure that the Auger transition $L_{\rm I} \rightarrow L_{\rm III}M_{\rm V}$ can take place for elements of atomic number below 50 and above 73, while the transition $L_{\rm I} \rightarrow L_{\rm III}M_{\rm IV}$ is confined to elements of atomic numbers below 50 or above 77.

If the probabilities $\gamma^{L_{\rm I}}_{L_{\rm III}M_{\rm IV}}$ and $\gamma^{L_{\rm I}}_{L_{\rm III}M_{\rm V}}$ become sufficiently large, they may constitute the principal factor in fixing the width of the $L_{\rm I}$ level. Calculations of Ramberg and Richtmyer[4] indicate that these two transitions alone contribute 62 percent of the width of the $L_{\rm I}$ level for gold. For elements of atomic number between 50 and 72 these transitions are forbidden and so contribute inappreciably. On the basis of these considerations one should expect a large change in the width of the $L_{\rm I}$ level for elements between 72 and 79.

Data on the satellites of the $L\alpha$ doublet confirm the importance and high probabilities of the Auger transitions $L_{\rm I} \rightarrow L_{\rm III}M_{\rm IV,V}$. The $L\alpha$ satellites, according to Druyvestyn[7] and others, arise from transitions from the states of double ioniza-

[4] Ramberg and Richtmyer, Phys. Rev. **51**, 913 (1937).
[5] L. Pincherle, Nuovo Cimento (N.S.) **81**, 162 (1935).
[6] This is true because such a transition is possible only when the energy of the initial state is greater than that of the final state (of double ionization) and is most probable when this energy difference is not too great. When the energy difference is very large, the probability of the Auger transition is small, since the wave function describing the ejected electron oscillates too rapidly to make the transition probability integral large.
[7] M. J. Druyvestyn, Zeits. f. Physik **43**, 707 (1927).

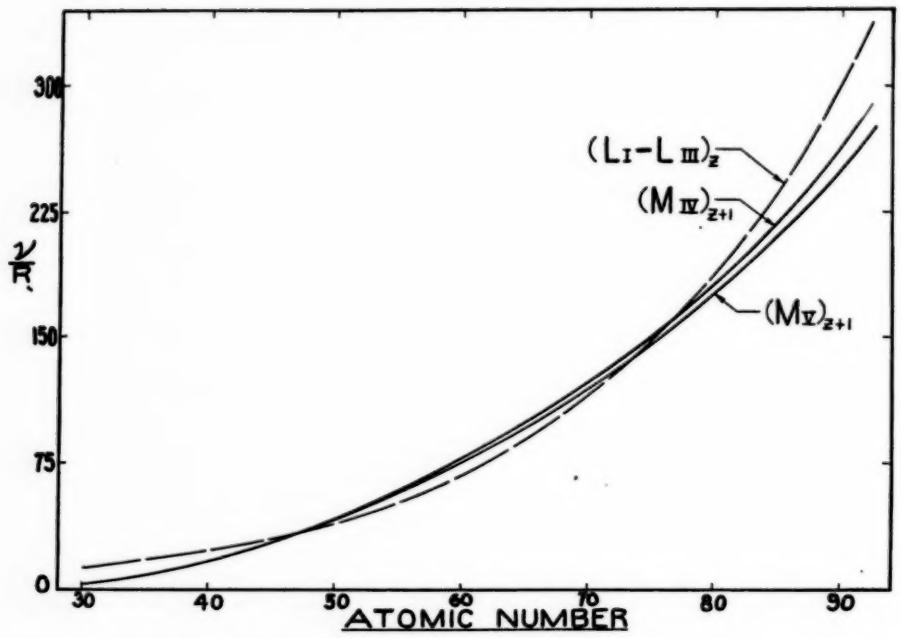

FIG. 1. Coster-Kronig diagram. The Auger transition $L_I \rightarrow L_{III}M_{IV}$ ($L_I \rightarrow L_{III}M_V$) is possible for an element of atomic number Z if the energy difference $L_I - L_{III}$ is greater than the energy of the $M_{IV}(M_V)$ level of element $Z+1$.

tion $L_{III}M_{IV}$ and $L_{III}M_V$. Early observations of these satellites showed that they were intense relative to the $L\alpha$ doublet for elements of atomic number above 73 and below 50, while they were very weak for elements in the atomic number range $50 \leq Z \leq 73$. The explanation of this intensity anomaly was proposed by Coster and Kronig[1] who suggested that the high probability of the Auger transitions $L_I \rightarrow L_{III}M_{IV,V}$ for elements below 50 and above 73 should result in a great increase in the number of atoms which reach the initial state for $L\alpha$ satellite production. Hirsh[8] measured photographically the relative intensities of the $L\alpha$ satellites in the atomic number range $40 \leq Z \leq 52$. His data confirmed the prediction of Coster and Kronig, as have subsequent measurements on the $L\alpha$ satellites by Randall and Parratt,[9] who used a two-crystal spectrometer.

Shrader,[10] also using a two-crystal spectrometer, has determined the relative intensities of the $L\alpha$ satellites for elements of atomic number between 73 and 92. His results are shown in Fig. 2. The curve fitting his data is arbitrarily resolved into two components, one assigned to each of the transitions $L_I \rightarrow L_{III}M_V$ and $L_I \rightarrow L_{III}M_{IV}$ which are possible for elements of atomic number greater than 72 and 76, respectively.

If one assumes that the sum of the probabilities of the Auger transitions $L_I \rightarrow L_{III}M_{IV,V}$ is roughly proportional to the relative intensity of the $L\alpha$ satellites, it is apparent that the sum $\gamma^{L_I}_{L_{III}M_{IV}} + \gamma^{L_I}_{L_{III}M_V}$ should increase rapidly with atomic number for $73 \leq Z \leq 81$. As a consequence, *the width of the L_I level should increase with atomic number in this range. Data presented in the present paper confirm this assumption and prediction.*

Any increase in the probabilities of Auger transitions from the L_I state should result in a decrease in the intensities of L_I lines relative to the intensities of L_{II} and L_{III} lines, provided (1) there exists no corresponding abnormal behavior in Auger transitions from the L_{II} and L_{III} states, and (2) the ratio of the numbers of atoms reaching the L_I, L_{II}, and L_{III} states is constant. This prediction is based on the obvious fact that the relative number of atoms leaving the L_I level by radiative transitions must decrease as

[8] F. R. Hirsh, Phys. Rev. **48**, 722 (1935).
[9] Randall and Parratt, Phys. Rev. **57**, 786 (1940).
[10] R. E. Shrader, unpublished work. The author is grateful to Dr. Shrader for the use of his unpublished curve.

the Auger probabilities increase. Coster and De Langen[11] have shown that the intensities of the L_I lines, $L\beta_3$ and $L\beta_4$, are smaller relative to the intensity of the L_{II} line $L\beta_1$ for Ag (47) than for Sn (50) and Sb (51). The probabilities of the Auger transitions $L_I \rightarrow L_{III}M_{IV,V}$ are much greater for silver than for tin and antimony, so their data are in agreement with expectations. *Data presented in this paper reveal a marked decrease with atomic number in the intensity of the L_I lines relative to the L_{II} and L_{III} lines from* Ta (*73*) *to* Tl (*81*).

IV. EXPERIMENTAL

The direct-reading two-crystal spectrometer used in the present work has been described by Richtmyer and Barnes.[12]

The ionization chamber, 10 inches long, was filled with argon to a pressure of three atmospheres. At one angstrom the chamber absorbed 99 percent of the incident intensity. Special provision was made to collect ions produced near the entrance window before re-combination. The ionization currents were amplified in a Brown-DuBridge circuit, with an FP-54 electrometer tube mounted adjacent to the ionization chamber. Either of two input resistors, of the order of 10^{10} and 10^{11} ohms, respectively, could be placed in the control-grid circuit.

The x-ray tube was of the Coolidge type with demountable filament and target assemblies. Because the target was not shielded from the filament, the maximum ordinate was checked after recording each spectral curve to make certain that no appreciable tungsten layer had been deposited on the target. The focal spot was roughly 10×5 mm. The x-rays made an angle of thirty degrees with the target face; the cathode electrons, sixty degrees. The tube window was a disk of beryllium which transmitted 84 percent of the incident intensity at 1.274A (Au $L\alpha_1$).

The targets used were prepared as follows: Yt (70) and Lu (71) powdered samples, reported to be "alloyed" with aluminum, were pressed into a thin layer of lead (82) which had been melted onto copper and silver, respectively. There were definite x-ray spectral indications that other rare earths were also present in the samples. These targets were not entirely satisfactory and the power dissipation had to be limited to approximately 300 watts in each case. The Ta (73), W (74), and Pt (78) targets were made by hard soldering a strip of each to copper. Crushed metallic bits of Rh (75), Os (76), and Ir (77) were forced into silver with a hydraulic press. A thin foil of Au (79) was hard-soldered to 25-ml silver. These targets were entirely satisfactory for powers up to one kilowatt. The Th (81) target was made by evaporating thallium in vacuum and allowing it to condense on a sheet of 10-ml copper which had been previously soft soldered to the target carriage. The evaporation was carried out in a tube designed to hold the entire target carriage, so that it would not be necessary to heat the thallium once it had been deposited. It was necessary to limit the x-ray tube power to 500 watts to prevent the re-evaporation (or sputtering) of the thallium.

The data for all lines of a given element were recorded at the same x-ray tube voltage. For every element except thallium, this voltage was approximately three times the excitation potential of the L_I state. With the thallium target the tube was often unstable at this potential (46 kv) so all thallium data were taken at 42 kv. Tube currents varied from one to thirty milliamperes. Both the tube voltage and current were maintained con-

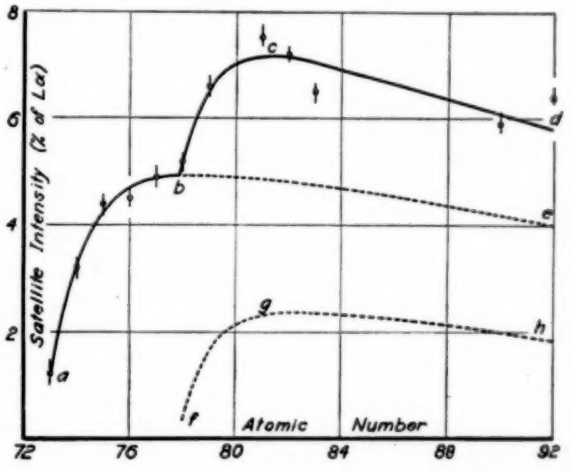

FIG. 2. The intensity of the $L\alpha$ satellites relative to the $L\alpha$ doublet as a function of atomic number. The curve *abe* represents the contribution of the Auger transition $L_I \rightarrow L_{III}M_V$, while the curve *fgh* is attributed to the transition $L_I \rightarrow L_{III}M_{IV}$. (Data taken by Dr. R. E. Shrader.)

[11] Coster and De Langen, Physica **3**, 282 (1936).
[12] Richtmyer and Barnes, Rev. Sci. Inst. **5**, 351 (1934).

stant within 1.5 percent by manual control throughout the recording of each spectral curve.

V. CRYSTALS

The observed widths of x-ray lines should be corrected for the finite resolving power of the spectrometer. For a two-crystal spectrometer the resolving power depends on (1) the geometrical divergence of the x-ray beam and (2) the diffraction patterns of the crystals. Parratt[13] and others have shown that with slits properly arranged the resolving power of the spectrometer is limited by the crystal diffraction patterns. For the data presented here the geometrical resolving power was 250,000. This is approximately 25 times as great as the physical resolving power of the instrument, as determined by the diffraction patterns of the crystals.

The correction to the observed width of a line may be a function of the width and shape of the line in question, as well as of the diffraction patterns of the crystals. Several correction formulae have been proposed and used for correcting widths reported in the literature, but as a general formula each is open to question.

On the approximations (a) that the diffraction patterns of the crystals in both the (1, +1) and (1, −1) positions are identical, and (b) that their shapes and the true x-ray line shape may each be represented by a Gaussian error function, it has been shown that

$$W_T^2 = W_0^2 - W_c^2,$$

where W_T is the true width of the line, and W_0 and W_c are the observed widths in the (1, +1) and (1, −1) positions, respectively. Since W_0 for L-series lines is considerably greater than W_c, one may write

$$W_T = W_0[1-(W_c/W_0)^2]^{\frac{1}{2}}, \\ \leqq W_0-(W_c^2/2W_0).$$

Thus for Gaussian error shapes the correction is proportional to the square of the (1, −1) width and inversely proportional to the width of the observed (1, +1) curve.

If one assumes the shapes to be given by the classical dispersion function, the correction formula may be written in the simple form:

$$W_T = W_0 - W_c.$$

Here the correction is simply the width of the (1, −1) curve and is independent of the observed width of the line. The correction for the classical dispersion shapes is always greater than that for the Gaussian error shapes.

There is much experimental evidence that the (1, −1) shapes of most lines in the wave-length region $0.5\text{A} \leq \lambda \leq 3.0\text{A}$ lie somewhere between the classical dispersion and the Gaussian error shapes. Parratt and Miller[14] have shown that the square of the classical dispersion curve gives a reasonably good fit for a large number of observed (1, −1) shapes in this wave-length region. The fact that the shapes of observed (1, −1) curves lay between the Gaussian error and classical dispersion shapes led Richtmyer, Barnes, and Ramberg[15] to propose the correction formula

$$W_T = W_0 - \tfrac{1}{2}W_c,$$

which gave more consistent values for W_T of certain lines than did either of the formulae above.

In the search for a better established correction formula Parratt[16] made extensive measurements on the widths of certain $K\alpha$ doublets in various parallel and anti-parallel positions for 16 pairs of crystals. He found that for several pairs of crystals one could write $W_T = W_0 - 29W_c^{1.7}$ where W_T is the true width, W_c the $(n, -n)$ width, and

TABLE I. Data on condition of calcite crystals.

Date	Observer	Radiation	(1, +1) full width x.u.	(1, −1) full width x.u.	Percent reflection
Dec. 1938	Shrader	Cu$K\alpha$ 1.54A	—	0.15	61
Apr. 1939	Parratt	Mo$K\alpha$ 0.71A	0.38	0.087	48.5
Oct. 1939	Cooper*	Mo$K\alpha$ 0.71A	0.36	0.088	56.5
June 1940	Cooper	Mo$K\alpha$ 0.71A	0.365	0.090	55
June 1940	Cooper	Cu$K\alpha$ 1.54A	0.57	0.152	60.5

* Between the measurements of Parratt and those of Cooper the crystals were ground and etched several times, following the method of Manning [Rev. Sci. Inst. 5, 316 (1934)]. The increase in the widths of the (1, +1) and (1, −1) curves and the decrease of the percent reflection from October, 1939 to June, 1940 is probably due to general deterioration of the crystal faces, although the differences are all of the order of the uncertainties involved in the measurements.

[13] L. G. Parratt, Phys. Rev. **46**, 749 (1934).

[14] Parratt and Miller, Phys. Rev. **49**, 280 (1935).

[15] Richtmyer, Barnes, and Ramberg, Phys. Rev. **46**, 843 (1934).

[16] L. G. Parratt, Rev. Sci. Inst. **6**, 387 (1935).

TABLE II. Widths of L-series lines.

Line	Transition	λ (x.u.)	Δλ obs. (x.u.)	Δλ cor. (x.u.)	ΔV cor. ev	Estimated Error in Δλ obs.
Ytterbium (70)						
$L\beta_3$	$L_{\mathrm{I}}M_{\mathrm{III}}$	1449.4	2.32	2.21	12.9	0.08
$L\beta_4$	M_{II}	1488.2	2.63	2.51	13.9	0.08
$L\gamma_3$	N_{III}	1219.8	1.34	1.23	10.2	0.05
$L\beta_1$	$L_{\mathrm{II}}M_{\mathrm{IV}}$	1472.5	1.41	1.30	7.4	0.03
Lutecium (71)						
$L\beta_3$	$L_{\mathrm{I}}M_{\mathrm{III}}$	1398.2	2.15	2.04	12.8	0.15
$L\beta_1$	$L_{\mathrm{II}}M_{\mathrm{IV}}$	1420.7	1.21	1.10	6.7	0.03
$L\beta_2$	$L_{\mathrm{III}}N_{\mathrm{V}}$	1367.2	1.65	1.54	10.1	0.05
Tantalum (73)						
$L\beta_3$	$L_{\mathrm{I}}M_{\mathrm{III}}$	1304.1	1.73	1.62	11.7	0.03
$L\beta_4$	M_{II}	1343.1	2.18	2.07	14.1	0.04
$L\gamma_2$	N_{II}	1103.0	1.26	1.15	11.6	0.03
$L\gamma_3$	N_{III}	1097.1	1.09	0.98	10.0	0.03
$L\beta_1$	$L_{\mathrm{II}}M_{\mathrm{IV}}$	1324.2	1.05	0.94	6.6	0.02
$L\gamma_1$	N_{IV}	1135.6	1.11	1.00	9.5	0.03
$L\gamma_6$	O_{IV}	1111.5	0.70	0.59	7.3	0.04
$L\beta_2$	$L_{\mathrm{III}}N_{\mathrm{V}}$	1281.9	1.42	1.31	9.8	0.03
Tungsten (74)						
$L\beta_3$	$L_{\mathrm{I}}M_{\mathrm{III}}$	1259.9	1.70	1.59	12.3	0.03
$L\beta_4$	M_{II}	1298.8	2.18	2.07	15.1	0.04
$L\gamma_2$	N_{II}	1065.9	1.23	1.12	12.1	0.03
$L\gamma_3$	N_{III}	1059.9	1.11	1.00	11.0	0.03
$L\beta_1$	$L_{\mathrm{II}}M_{\mathrm{IV}}$	1279.2	0.97	0.86	6.5	0.02
$L\gamma_1$	N_{IV}	1096.3	1.02	0.91	9.3	0.02
$L\gamma_6$	O_{IV}	1072.1	0.64	0.53	5.7	0.04
$L\beta_2$	$L_{\mathrm{III}}N_{\mathrm{V}}$	1242.0	1.34	1.23	9.8	0.03
Rhenium (75)						
$L\beta_3$	$L_{\mathrm{I}}M_{\mathrm{III}}$	1217.6	1.75	1.64	13.6	0.03
$L\beta_4$	M_{II}	1256.3	2.22	2.11	16.4	0.04
$L\gamma_2$	N_{II}	1029.9	1.25	1.14	13.2	0.03
$L\gamma_3$	N_{III}	1023.6	1.13	1.02	12.0	0.03
$L\beta_1$	$L_{\mathrm{II}}M_{\mathrm{IV}}$	1236.0	0.92	0.81	6.5	0.02
$L\gamma_1$	N_{IV}	1058.7	0.98	0.87	9.5	0.02
$L\gamma_6$	O_{IV}	1034.4	0.69	0.58	6.7	0.05
$L\beta_2$	$L_{\mathrm{III}}N_{\mathrm{V}}$	1204.1	1.27	1.16	9.8	0.03
Osmium (76)						
$L\beta_3$	$L_{\mathrm{I}}M_{\mathrm{III}}$	1176.8	1.77	1.66	14.7	0.03
$L\beta_4$	M_{II}	1215.8	2.17	2.06	17.1	0.05
$L\gamma_2$	N_{II}	995.9	1.24	1.13	14.0	0.04
Osmium (76).—*Continued*						
$L\gamma_3$	N_{III}	989.8	1.11	1.00	12.6	0.03
$L\beta_1$	$L_{\mathrm{II}}M_{\mathrm{IV}}$	1194.5	0.88	0.77	6.6	0.02
$L\gamma_1$	N_{IV}	1022.8	0.91	0.80	9.4	0.02
$L\gamma_6$	O_{IV}	998.8	0.76	0.65	6.5	0.05
$L\beta_2$	$L_{\mathrm{III}}N_{\mathrm{V}}$	1166.9	1.21	1.10	9.9	0.03
Iridium (77)						
$L\beta_3$	$L_{\mathrm{I}}M_{\mathrm{III}}$	1138.5	1.68	1.57	14.9	0.04
$L\beta_4$	M_{II}	1177.2	2.10	1.99	17.7	0.06
$L\gamma_2$	N_{II}	963.3	1.20	1.10	14.6	0.04
$L\gamma_3$	N_{III}	957.1	1.09	0.99	13.3	0.03
$L\beta_1$	$L_{\mathrm{II}}M_{\mathrm{IV}}$	1155.4	0.85	0.74	6.8	0.02
$L\gamma_1$	N_{IV}	988.8	0.87	0.76	9.6	0.02
$L\gamma_6$	O_{IV}	964.9	0.70	0.59	7.8	0.05
$L\beta_2$	$L_{\mathrm{III}}N_{\mathrm{V}}$	1133.0	1.12	1.01	9.7	0.03
Platinum (78)						
$L\beta_3$	$L_{\mathrm{I}}M_{\mathrm{III}}$	1101.7	1.70	1.59	16.1	0.17
$L\beta_4$	M_{II}	1139.9	2.05	1.94	18.4	0.09
$L\gamma_3$	N_{III}	926.0	1.09	0.98	14.1	0.03
$L\beta_1$	$L_{\mathrm{II}}M_{\mathrm{IV}}$	1117.6	0.84	0.73	7.2	0.02
$L\gamma_1$	N_{IV}	956.0	0.85	0.75	10.1	0.02
$L\beta_2$	$L_{\mathrm{III}}N_{\mathrm{V}}$	1099.7	1.10	0.99	10.1	0.04
Gold (79)						
$L\beta_3$	$L_{\mathrm{I}}M_{\mathrm{III}}$	1065.5	1.70	1.59	17.2	0.15
$L\beta_4$	M_{II}	1104.2	2.05	1.94	19.6	0.09
$L\gamma_2$	N_{II}	902.5	1.20	1.10	16.6	0.05
$L\gamma_3$	N_{III}	895.8	1.07	0.97	14.9	0.03
$L\beta_1$	$L_{\mathrm{II}}M_{\mathrm{IV}}$	1081.3	0.81	0.70	7.4	0.02
$L\gamma_1$	N_{IV}	924.6	0.80	0.70	10.1	0.02
$L\gamma_6$	O_{IV}	901.0	0.60	0.50	7.6	0.04
$L\beta_2$	$L_{\mathrm{III}}N_{\mathrm{V}}$	1068.0	1.04	0.93	10.1	0.04
Thallium (81)						
$L\beta_3$	$L_{\mathrm{I}}M_{\mathrm{III}}$	998.5	1.60	1.49	18.4	0.06
$L\beta_4$	M_{II}	1037.0	1.89	1.78	20.4	0.05
$L\gamma_2$	N_{II}	845.7	1.12	1.02	17.5	0.04
$L\gamma_3$	N_{III}	839.3	1.02	0.92	16.1	0.04
$L\beta_1$	$L_{\mathrm{II}}M_{\mathrm{IV}}$	1013.0	0.75	0.64	7.7	0.02
$L\gamma_1$	N_{IV}	865.7	0.71	0.61	10.0	0.02
$L\gamma_6$	O_{IV}	842.3	0.47	0.37	6.4	0.04
$L\beta_2$	$L_{\mathrm{III}}N_{\mathrm{V}}$	1008.2	0.95	0.84	10.2	0.03

W_0 the $(n, +n)$ width (all widths in x.u.). Crystals satisfying this relation are said to be of Class I; those which do not are grouped in class II.

Data on the crystals in the present work (3A and 3B, used by Richtmyer, Barnes, and Ramberg,[15] and by Shrader[10]) are recorded in Table I. Comparing these data with those of Parratt, one sees that the crystals are rather poor at Mo $K\alpha$ (0.71A) and good at Cu $K\alpha$ (1.54A). The crystals do not fall into class I. Consequently the correction formula proposed by Parratt for crystals of class I is not applicable and one must resort to some other scheme for correcting the observed widths. The corrections applied to the observed widths reported here were determined as follows: Parratt's values of the true widths of the Mo $K\alpha$ and the Cu $K\alpha$ lines were accepted as standards. Then the corrections for Mo $K\alpha$ was 0.10 x.u. and for Cu $K\alpha$ 0.12 x.u. It was then assumed (a) that the correction was a linear function of the wave-length in the range from 0.71A to 1.54A and (b) that the correction is a function of wave-length alone. The first assumption cannot introduce appreciable error, but the second is open to question. It was made only because it is not yet known how the correction should be influenced by the width.

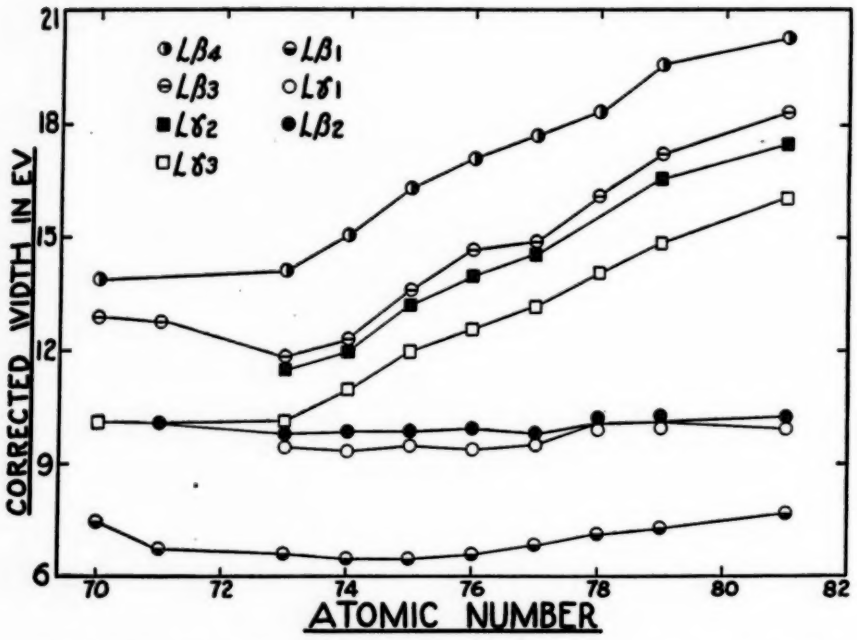

FIG. 3. Widths of L-series lines in electron volts as a function of atomic number. The lines $L\beta_3$, $L\beta_4$, $L\gamma_2$, and $L\gamma_3$ arise from L_I initial states; $L\beta_1$ and $L\gamma_1$ are L_{II} lines, and $L\beta_2$ has an L_{III} initial state.

VI. WIDTH DATA

Data on the width of certain L lines of ten elements are presented in Table II. The observed widths in x.u. were those measured after correction for zero drift of the amplifying circuit, for the background of continuous radiations, and for overlapping of neighboring lines. The "corrected" widths were obtained by subtracting a correction for the diffraction patterns of the crystals. In the last column of Table II are the estimated errors in the observed widths. Lines with large errors were either very weak or badly overlapped by neighboring lines.

In Fig. 3 the corrected widths, in electron volts, of seven L lines are plotted as a function of atomic number. Of these seven lines, $L\beta_3$, $L\beta_4$, $L\gamma_2$, and $L\gamma_3$ arise from transitions from an L_I initial state, while $L\beta_1$ and $L\gamma_1$ have an L_{II} initial state, and $L\beta_2$ arises from a transition from the L_{III} state. For elements 73 to 81, the lines arising from the L_I initial state show increases in widths of approximately six electron volts while the lines arising from L_{II} and L_{III} initial states have changes in width of the order of one electron volt. *Thus, as predicted by consideration of the Auger effect, the L_I lines show rapid increases in widths for elements 73 to 81, while L_{II} and L_{III} lines show but small changes.*

Since each of the L_I lines has so nearly the same increment in width, it seems conclusive that an

TABLE III. Comparison of present width data with that of other observers.

Element	Line	Cooper	Williams*	R. B. R.[13]
W(74)	$L\beta_1$	0.97	0.94	
	$L\beta_2$	1.34	1.38	
	$L\gamma_1$	1.02	1.01	
Ir(77)	$L\beta_1$	0.85	0.82	
	$L\beta_2$	1.12	1.17	
	$L\gamma_1$	0.87	0.92	
Pt(78)	$L\beta_1$	0.84	0.80	
	$L\beta_2$	1.10	1.14	
	$L\gamma_1$	0.85	0.84	
Au(79)	$L\beta_1$	0.81	0.79	0.81
	$L\beta_2$	1.04	1.06	1.04
	$L\beta_3$	1.70		2.00
	$L\beta_4$	2.05		2.00
	$L\gamma_1$	0.80	0.79	0.82
	$L\gamma_2$	1.20		1.20
	$L\gamma_3$	1.07		1.06
	$L\gamma_6$	0.60		0.60
Tl(81)	$L\beta_1$	0.75	0.74	
	$L\beta_2$	0.95	1.00	
	$L\gamma_1$	0.71	0.74	

* J. H. Williams, Phys. Rev. **45**, 71 (1934).

increase in the width of the L_I state is responsible for the major part of this variation. It is true that some small portion of the width changes may be attributed to changes in the breadths of the final states, and indeed, several other factors may have some influence on the line widths. Nevertheless, the conclusion stands that the observed variations are due primarily to the change in the width of the L_I level and that all other factors are of secondary importance.

A few of the lines measured by the author have also been measured by other observers. A comparison of the widths reported in this paper with those of the other observers is given in Table III. The observations agree within the experimental error for every line except Au $L\beta_3$. This line overlaps Au $L\beta_2$ so badly that an arbitrary graphical resolution must be carried out. Richtmyer, Barnes, and Ramberg[15] used only classical dispersion curves for $L\beta_2$ and $L\beta_3$ and neglected the "residuals," whereas the author adjusted the shapes of the two lines to fit the observed contour.

VII. RELATIVE INTENSITIES

The relative intensities are assumed to be proportional to the product of the energy width and the relative maximum ordinate of each spectral curve. Since all the lines compared had approximately the same (classical dispersion) shape, and nearly the same wave-length, the uncertainty introduced by this approximation is believed to be less than that involved in the comparison of maximum ordinates. None of the numerous and troublesome corrections required for the most precise comparisons of relative intensities has been made.

TABLE IV. Relative intensities of L-series lines.

	Relative to $L\beta_1$ ($L\beta_1=100$)			Relative to L ($L\gamma_1=100$)		
	$L\beta_2$	$L\beta_3$	$L\beta_4$	$L\gamma_2$	$L\gamma_3$	$L\gamma_6$
Yt(70)	—	(14.8–?)	(13.0–?)	—	—	—
Lu(71)	44.4	(15.7–?)	—	—	—	—
Ta(73)	46.1	18.5	13.4	17.3	25.1	2.0
W(74)	46.2	16.2	13.8	14.1	20.4	2.8
Rh(75)	44.5	15.2	11.4	13.3	18.5	4.7
Os(76)	45.8	13.9	11.1	11.5	17.0	6.2
Ir(77)	45.7	14.2	10.7	12.4	15.5	7.3
Pt(78)	43.7	14.1	9.9	—	—	—
Au(79)	45.0	13.0	10.1	10.5	14.1	11.3
Tl(81)	45.1	9.4	8.8	11.0	13.1	12.3

Two methods for comparing maximum ordinates were used. First, the spectrometer was set on the peak of each line in succession with the power in the x-ray tube and the sensitivity of the recorder kept constant. After subtracting the background of continuous radiation and the contribution of overlapping lines, the relative maximum ordinates were measured. Second, the maximum deflection produced by each of the lines was made approximately full scale and the relative maximum ordinate for each was computed by the use of the known ratios of amplifier sensitivities and of the measured x-ray tube currents. An average of the relative maximum ordinate given by these two methods was used in computing the relative intensities.

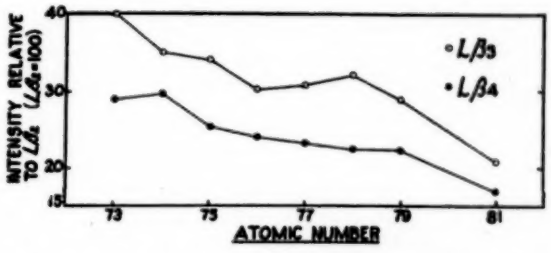

FIG. 4. The intensities of $L\beta_3$ and $L\beta_4$ relative to $L\beta_2$. $L\beta_3$ and $L\beta_4$ arise from L_I initial states while $L\beta_2$ has the initial state L_{III}.

In Table IV the areas (products of maximum ordinate and width) of $L\beta_2$, $L\beta_3$ and $L\beta_4$ relative to the area of $L\beta_1$ ($L\beta_1=100$) are recorded. The greatest wave-length separation of any of these lines from $L\beta_1$ is 53.5 x.u. It is estimated that the values reported are accurate to within two percent of the area of $L\beta_1$. In Fig. 4 the intensities of $L\beta_3$ and $L\beta_4$ are plotted relative to $L\beta_2$ which is an L_{III} line. *These data show that the intensities of the two L_I lines are decreasing relative both to the L_{II} line and to the L_{III} line in the atomic number range $73 \leq Z \leq 81$.*

The intensities of $L\gamma_2$, $L\gamma_3$, and $L\gamma_6$ relative to $L\gamma_1$ are also recorded in Table IV. The maximum wave-length separation from $L\gamma_1$ is 38.5 x.u. and the estimated error is approximately two percent of the intensity of $L\gamma_1$. [The line $L\gamma_6$ ($L_{II}O_{IV}$) is not observed for elements of atomic number below 70, but rapidly increases in relative intensity from Ta (73) to Tl (81). Its behavior is quite extraneous to the topic being discussed.]

Once again, it is clear that the lines arising from L_I transitions ($L\gamma_2$ and $L\gamma_3$) are decreasing in intensity relative to a line ($L\gamma_1$) which has an L_{II} initial state.

VIII. CONCLUSIONS

The widths of lines arising from L_I transitions increase strikingly with atomic number in the range $73 \leq Z \leq 81$. At the same time the intensities of these lines relative to lines arising from L_{II} and L_{III} transitions show corresponding decreases. These observations are accounted for qualitatively by the role of the Auger effect. Only two Auger transitions are considered in the present discussion. Although beyond doubt these two are the principle ones involved in the topics of the present paper, there are certainly many more Auger transitions some of them with similar dramatic changes in probability from element to element. It is highly probable that many of the anomalies in x-ray line widths and relative intensities in other atomic number ranges will soon be shown to be due to Auger transitions.

The author wishes to express his gratitude to Professor L. G. Parratt for his helpful suggestions and for his enlightening discussions.

MARCH 1 AND 15, 1942 PHYSICAL REVIEW VOLUME 61

Radiations from Radioactive Gold, Tungsten, and Dysprosium*

ARNOLD F. CLARK†
Department of Physics, Indiana University, Bloomington, Indiana

(Received December 4, 1941)

Level schemes are deduced for gold and tungsten from the measurement of beta-gamma and gamma-gamma coincidences, together with a knowledge of the energies of the various radiations emitted. The beta-ray spectrum of Au^{198} is simple with an end-point of 0.78 Mev. The residual nucleus emits two gamma-rays in cascade. W^{187} has a complex beta-ray spectrum. The high energy group has a maximum energy of 1.4 Mev while the one of lower energy has an end-point of 0.5 Mev and is followed by a 0.9 Mev gamma-ray and some other gamma-rays which give gamma-gamma coincidences. The dysprosium beta-ray end-point is 1.2 Mev and the maximum energy gamma-ray is 1.1 Mev.

IN order to obtain energy level schemes for radioactive nuclei, it is necesssry to know the energies and intensities of all gamma-rays emitted during the process, the energy distribution of all beta-rays emitted, and also any correlations between beta-rays emitted by the parent nucleus and the gamma-rays produced by the product. Up to the present our knowledge of all these factors, for any radioactive species, has been quite limited. In general one has available, or can determine with ease, data on the maximum energy of the electrons emitted during the process. In some cases the shape of the beta-ray spectrum is also known and information is available as to whether the spectrum is simple or complex. In those cases in which the spectrum is complex the value of the inner end point has not been determined with any great accuracy. Frequently gamma-rays have been found and the energies and intensities of these have been determined in a few instances.

Norling,[1] Mitchell, Langer and McDaniel,[2] and Dunworth[3] have applied coincidence counting methods to the latter problem and have been able to derive reasonable energy level schemes for several radioactive transformations. In particular, level schemes for the disintegration of Mn^{56} (2.5 hours), In^{116} (54 min.), Sb^{124} (60 days), and others have been determined. It is the pur-

* Thesis submitted to the Graduate Faculty of Indiana University in partial fulfillment of the requirements for the degree of Doctor of Philosophy.

† Now at the Radiation Laboratory, University of California.

[1] F. Norling, Zeits. f. Physik **111**, 158 (1938).

[2] A. C. G. Mitchell, L. M. Langer, and P. W. McDaniel, Phys. Rev. **57**, 1107 (1940), also **56**, 380 (1939).

[3] J. V. Dunworth, Rev. Sci. Inst. **11**, 167 (1940).

pose of the present experiments to apply these methods to the investigation of radioactive gold (2.7 days), tungsten (24 hours), and dysprosium (2.5 hours).

APPARATUS

Counters were used singly to determine, by the method of absorption of beta-rays in aluminum, the beta-ray end-point. Two counters, in a coincidence circuit, were used to determine the energy of gamma-rays by measuring the range of Compton electrons ejected by them from aluminum. Coincidences between two or more gamma-rays and coincidences between beta- and gamma-rays were also measured.

Two types of counters were used in most of the experiments. Glass-walled counters of conventional design, having a brass cathode 0.0025 cm thick, were filled with argon to a pressure of 8.5 cm Hg, and 1 cm Hg of petrolic ether to aid in quenching the discharge. The sensitive region is about 7.5 cm long and 2.7 cm in diameter. The glass wall and brass cathode stop electrons with energies less than 300 kev.

In order to count electrons of energy less than this, especially designed counters having thin windows were made. These counters have a thick brass envelope and are fitted with thin aluminum windows. The windows are each 0.0025 cm thick which will absorb electrons of energy less than 70 kev and are supported on grids with transmitting areas of 1 cm^2. These counters were filled with argon at a pressure of 5 cm Hg and 1 cm of petrolic ether.

Because of the thin aluminum windows, the counters could not be baked out and were accordingly unstable. This defect was cured by a long period of evacuation and by passing a discharge through them to free the gas from the walls. After this treatment the counter thresholds increased only slightly in a period of four months.

The counters, source and absorbers were supported on two brass rods in a large copper-lined box. The apparatus could be so arranged that it could be used to measure beta-gamma and gamma-gamma coincidences on the one hand, or the energy of Compton recoil electrons from gamma-rays on the other. In either case the two counters were placed in a horizontal plane with their centers a known distance apart. If the energy of Compton recoils was to be measured, the radioactive source was placed on one side of the counters and an aluminum radiator, thick enough to stop all beta-rays, was interposed between the source and the counters. Sheets of aluminum of varying thickness were then placed between the two counters, and the number of coincidences per minute was measured as a function of the thickness of the aluminum. The energy of the gamma-ray was then obtained from the maximum range of the Compton electrons with the help of a curve published by Curran, Dee, and Petrzilka.[4]

In the cases in which beta-gamma or gamma-gamma coincidences were to be measured, the source was mounted on an aluminum block between the two counters. The block was of such a thickness that no beta-rays from the source could pass through it and at the same time it served as a radiator for Compton electrons from the gamma-rays of the source. In those cases in which coincidences between two or more gamma-rays were to be measured, a similar piece of aluminum was placed between the source and the other counter.

If coincidences between beta- and gamma-rays were to be measured the thick aluminum block between the source and one of the counters (hereafter called the beta-counter) was removed and arrangements made to place thin sheets of aluminum between this source and the counter so that only electrons with ranges greater than a certain specified amount would be detected. In this manner beta-gamma coincidences could be determined as a function of the energy of the beta-rays being recorded in the beta-counter.

In all cases the number of single counts in each counter was measured before and after each run. With the help of this information and the known resolving time of the circuit the chance coincidence rate could be calculated and subtracted from the total coincidence rate. The resolving time of the coincidence circuit was obtained in the usual manner by placing a separate source over each counter, measuring the counting rate of each counter singly and of the two in coincidence. If N_1, N_2, and N_c, are the single counting rate in each counter and the coincidence

[4] S. C. Curran, P. I. Dee, and D. Petrzilka, Proc. Roy. Soc. **169**, 269 (1938).

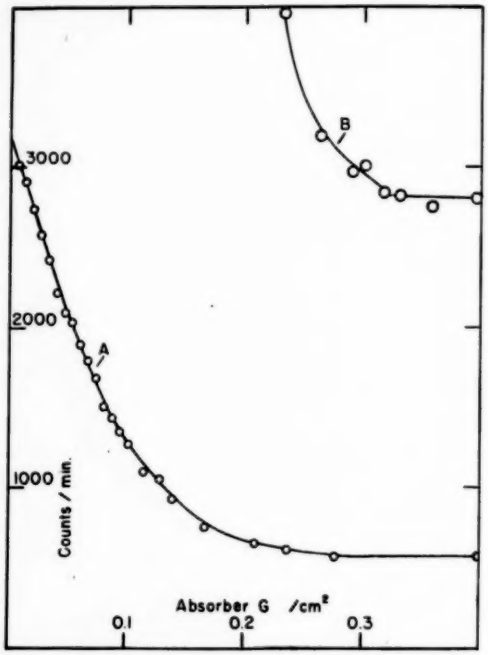

FIG. 1. Absorption of beta-rays from gold. Curve B, showing end-point, taken with stronger source than curve A.

counting rate, respectively, then

$$N_c = 2\tau N_1 \times N_2, \quad (1)$$

where τ is the resolving time in question. In the experiments the value of 2τ varied between 9×10^{-8} min. and 7.5×10^{-8} min. depending on the counters used.

In addition, the coincidence rate due to cosmic rays was measured for every arrangement used and also subtracted from the total coincidence rate in any experiment. The cosmic-ray rate amounted to approximately 0.2 min.$^{-1}$.

The voltage source, amplifiers, and recording mechanism were those described by Mitchell, Langer, and McDaniel.[2] The apparatus could count at a rate of 30,000 per minute in each counter.

EXPERIMENTS AND RESULTS

Gold

Gold was bombarded with slow neutrons from the Indiana University cyclotron and experiments were performed on the radioactive species Au^{198} of half-life 2.7 days.

Using the method of absorption in aluminum, McMillan, Kamen, and Ruben[5] obtained a beta-ray end-point of 0.78 Mev. Richardson[6] examined the spectrum in a cloud chamber, and obtained 0.83 Mev as a maximum energy of the beta-rays. In addition, he found an internal conversion line at 0.44 Mev.

The gamma-rays have been investigated by Richardson,[6] who measured the energy of the Compton electrons and photoelectrons produced by suitable radiators in a cloud chamber. He found two lines with energies of 0.44 and 0.28 Mev of intensities 1.2 to 1, respectively. In addition, he suggested that there was a weak line at 0.7 Mev. Sizoo and Eijkman[7] obtained some evidence for a weak gamma-ray of 2.5 Mev by analyzing the absorption curve of the radiation in lead.

Absorption curves of the beta-rays were taken under various conditions. The two curves shown in Fig. 1 were taken with very different source strengths as is indicated by the disparity in intensity of the gamma-ray backgrounds. The background in Curve B was determined with the aid of other points at greater absorber thickness, not shown on the graph, and is therefore more accurate than it appears to be. The range of the beta-rays determined from this curve is 0.31 ± 0.01 g/cm^2 which is in good agreement with McMillan, Kamen, and Ruben. Using Feather's old rule,[8]

$$R = 0.511E - 0.091, \quad (2)$$

which appears to be more accurate than the more

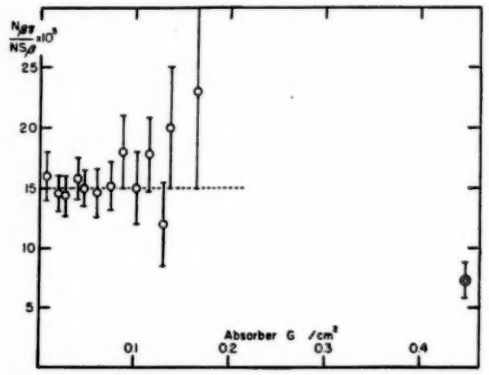

FIG. 2. Beta-gamma coincidences in gold. Double circle shows $N_{\gamma\gamma}/N_\gamma S_\gamma$.

[5] E. McMillan, M. Kamen, S. Ruben, Phys. Rev. **52**, 375 (1937).
[6] J. R. Richardson, Phys. Rev. **55**, 609 (1939).
[7] Sizoo and Eijkman, Physica **6**, 332 (1939).
[8] N. Feather, Phys. Rev. **35**, 1559 (1930).

recent one in the low energy region, one obtains an end-point energy of 0.78 Mev.

Experiments on beta-gamma and gamma-gamma coincidences were performed with both the thin aluminum-walled counters and the counters with glass envelopes. The number of gamma-gamma coincidences per recorded gamma-ray was found to be $(0.073\pm0.015)\times10^{-3}$.

The number of beta-gamma coincidences per recorded beta-ray taken with the thin-walled counters is shown as a function of the absorber thickness in Fig. 2. The vertical lines through the points indicated are calculated from the mean statistical errors, including the errors due to the background. It will be seen from the figure that the number of beta-gamma coincidences per recorded beta-ray is a constant independent of the energy of the beta-rays. Beta-gamma coincidences taken at larger absorber thickness than shown, but using the thick-walled counters, indicate that the coincidence rate per recorded beta-particle does not decrease at higher energies, but remains approximately constant all the way to the end point. From a curve of this type one would be led to suppose that the beta-ray spectrum of gold is simple, and that the disintegration of Au^{198} always leads to the same excited state of Hg^{198}, from which the gamma-rays follow. The average number of beta-gamma coincidences per recorded beta-particle can be taken from the curve and yields a value of $(0.15\pm0.01)\times10^{-3}$.

In order to calculate the number of gamma-ray quanta emitted per disintegration one employs the following considerations. Let there be N disintegrations per second and let K be the average number of gamma-quanta per disintegration. If S_β and S_γ are the sensitivities, including solid angle factor of the counters to beta- and gamma-rays, respectively, and if S_γ is supposed to be essentially constant in the region of gamma-ray energies involved, then the number of beta-gamma coincidences is given by

$$N_{\beta\gamma}=NS_\beta\cdot KS_\gamma \tag{3}$$

and the number per recorded beta-ray, by

$$N_{\beta\gamma}/NS_\beta=KS_\gamma. \tag{4}$$

Similarly the number of gamma-gamma coincidences is given by

$$N_{\gamma\gamma}=NS_\gamma{}^2K(K-1) \tag{5}$$

and the number per recorded gamma-ray by

$$N_{\gamma\gamma}/NKS_\gamma=S_\gamma(K-1). \tag{6}$$

The ratio of these quantities is

$$R=\frac{N_{\gamma\gamma}/NKS_\gamma}{N_{\beta\gamma}/NS_\beta}=\frac{K-1}{K}. \tag{7}$$

From these equations and the data given above

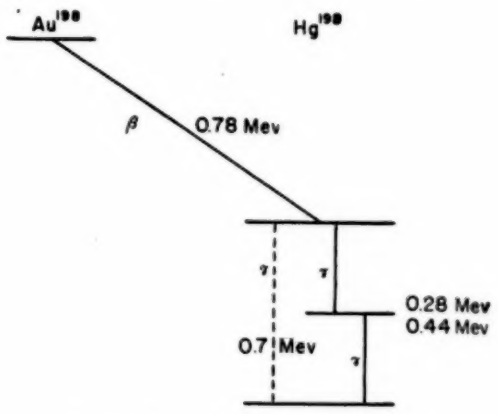

FIG. 3. Energy level scheme for gold.

one can determine a value of K, the number of gamma-quanta per disintegration. If, as a first approximation, one takes the efficiency of the counters for the various gamma-rays as equal, one obtains a value of $K=1.9$. This value of $K\approx2$ fits well with the level scheme proposed by Richardson, who assumed that the 0.28 Mev and 0.44 Mev gamma-rays are in cascade.

If, on the other hand, one assumes the level scheme of Richardson with $K=2$, one can calculate the gamma-ray efficiencies of the counters for the two gamma-rays in question.

Using formulas similar to Eqs. (3) and (5), one obtains for this apparatus

$$S_\gamma(0.44)=0.09\times10^{-3},\quad S_\gamma(0.28)=0.06\times10^{-3}.$$

An estimate of the solid angle of the gamma-counter allows one to solve for the absolute efficiencies of the gamma-rays. The results were in agreement with Norling's curve[9] to within the experimental errors.

[9] F. Norling, Phys. Rev. **58**, 277 (1940).

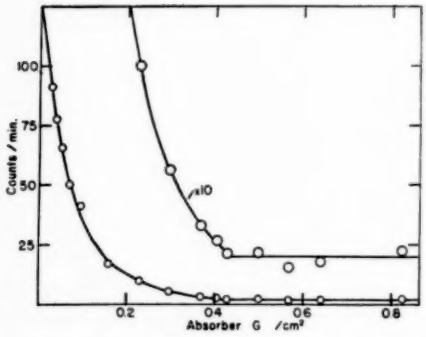

FIG. 4. Coincidence absorption of Compton electrons from tungsten gamma-rays.

The level scheme proposed by Richardson is shown diagrammatically in Fig. 3. Since no evidence has been found indicating the presence of a low energy group of electrons, it is supposed that Au^{198} goes to an excited state of Hg^{198} from which the two gamma-rays of energy 0.44 or 0.28 Mev are emitted in cascade. The weak 0.7 Mev gamma-ray may be placed hypothetically as a parallel mode in competition with the other gamma-rays in cascade. It will not affect the value of K within errors common to this type of experiment since it is relatively weak in intensity.

In view of the fact that, for ranges of electrons less than 0.1 g/cm², both internal conversion electrons and disintegration electrons are counted by the beta-ray counter, we tried to see if internal conversion electrons would have any effect on the number of beta-gamma coincidences per recorded beta-ray. One would expect a slight decrease in the number of beta-gamma coincidences per recorded gamma-ray for electrons of range less than 0.1 g/cm². Unfortunately the statistical errors could not be kept small enough to detect this effect, which should be about 5 percent. It is of interest, in this connection, to note that Norling,[10] found coincidences between internal conversion electrons and disintegration electrons in gold.

At the conclusion of these experiments, a recent paper of Norling[11] came to our attention in which he failed to find gamma-gamma coincidences in gold. The gamma-ray counters he used had walls of lead 1 mm thick which probably absorbed the 0.28 Mev gamma-ray to such an extent that no coincidences were observed. He did observe beta-gamma coincidences for two absorber thicknesses and the number of these per recorded beta-ray was independent of the energy.

Tungsten

The tungsten activity was induced with both slow and fast neutrons by Minakawa[12] who obtained 24.0±0.1 hours for the half-life. He found 1.1 Mev for the maximum energy of the beta-ray spectrum by absorption in aluminum, Fajans and Sullivan[13] analyzed the spectrum in a cloud chamber and also by absorption in aluminum, obtaining 1.40±0.05 and 1.40 to 1.44 Mev by the respective methods. In addition they measured a gamma-ray by the lead absorption method and gave 0.87 Mev for its energy. According to their experiments the activity is to be attributed to the isotope W^{187}. Since negative electrons are emitted, the resulting isotope is Re^{187}.

In the present experiments, a tungsten strip 0.025 cm thick was bombarded on a probe

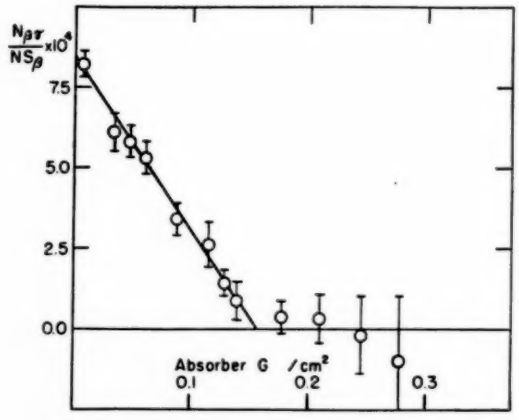

FIG. 5. Beta-gamma coincidences in tungsten.

inserted into the deuteron beam in the cyclotron. Tungsten bombarded by deuterons give several radioactivities.[13] These possible contaminations include three rhenium periods with half-lives of 20 minutes, 90 hours, and 52 days, and a tungsten activity of 74.5 days. The short half-life had decayed before the observations started.

[10] F. Norling, Naturwiss. **27**, 593 (1939).
[11] F. Norling, Arkiv f. Mat. Astr. och Fysik **B27**(3), 9 (1941).
[12] O. Minakawa, Phys. Rev. **57**, 1189 (1940).
[13] K. Fajans and W. H. Sullivan, Phys. Rev. **58**, 276 (1940).

The measurements were made without chemical separation. However, the activity followed the chemistry of tungsten and the residue had no gamma-activity. The final check on the contamination was an examination of the decay curves. The curves showed that there was a negligible amount of the 20-minute, 52-day, and 75-day activities present during the time coincidence runs were being taken. The rate of decay indicated that about six percent of the initial beta-singles was due to the 90-hour rhenium activity. Since this activity has no gamma-rays associated with it,[14] the only effect it would have is to increase the number of beta-counts and decrease the ratio $N_{\beta\gamma}/NS_\beta$. A correction was made for this contamination at various absorber thicknesses, by assuming that the shape of the beta-spectrum for rhenium is the same as for tungsten. The corrections were twelve percent or less, and have no effect on the inner end point.

No satisfactory beta-ray end-point was obtained because of the high gamma-ray background, but a rough determination giving 1.3 ± 0.1 Mev was sufficient to identify the spectrum.

The absorption of Compton electrons, determined with the thin-walled counters, is shown in Fig. 4. It will be seen that the range of the Compton electrons is 0.42 ± 0.03 g/cm². With the curve of Curran, Dee, and Petrzilka this corresponds to 0.90 Mev.

The results of experiments on beta-gamma coincidences with thin-walled counters are shown in Fig. 5. It is clear that the type of curve obtained here is entirely different from that shown in Fig. 2 for gold. The increase in beta-gamma coincidences in tungsten for low energy beta-particles shows that the beta-ray spectrum is complex. The absence of coincidences with thick absorbers indicates that there are no gamma-rays associated with high energy electrons. Points at still higher absorber thickness were reached with the help of thick-walled counters, and also indicated no beta-gamma coincidences. The straight line extrapolation of the beta-gamma coincidences per recorded beta-ray gives an end-point of 0.155 ± 0.015 g/cm². From Feather's old rule, the energy is 0.49 Mev of the lower energy group. Using values for the beta-ray end-point (1.4 Mev), the end-point of the lower energy group (0.5 Mev) and the energy of the gamma-ray (0.9 Mev), one can obtain a satisfactory level scheme for the disintegration of W^{187}. The level scheme is given in Fig. 6. The scheme is complicated, however, by the fact that we have observed gamma-gamma coincidences which suggest that there are other low energy gamma-rays in parallel with the 0.9 Mev gamma-transition.

To help in an attempt to obtain a value for K, the number of gamma-rays accompanying the low energy beta-group, as well as to get some idea of the relative intensity of the two groups, one may proceed as follows: the number of gamma-gamma coincidences per recorded gamma-ray was found to be

$$N_{\gamma\gamma}/(NKS_\gamma)_\beta=(K-1)S_\gamma=1.5\pm0.1\times10^{-3}. \quad (8)$$

The number of beta-gamma coincidences per recorded beta-particle at this absorber thickness

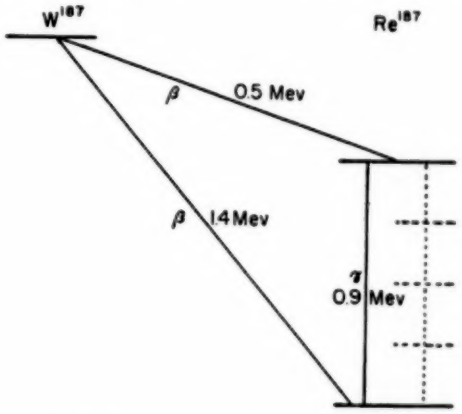

FIG. 6. Proposed energy level scheme for the disintegration of tungsten.

was

$$N_{\beta\gamma}/NS_\beta=\alpha KS_\gamma=0.84\pm0.05\times10^{-3}, \quad (9)$$

where α is the fraction of the total number of disintegrations belonging to the low energy group. If two groups are present, Eq. (7) is replaced by

$$R=(N_{\gamma\gamma}/NKS_\gamma)/(N_{\beta\gamma}/NS_\beta)_0$$
$$=(K-1)/\alpha K=1.79. \quad (10)$$

A rough value for the branching ratio α may be estimated from the slope of $N_{\beta\gamma}/NS_\beta$ as a

[14] G. T. Seaborg, Chem. Rev. **27**, 1 (1940).

function of absorber thickness to be expected if one assumes that the two beta-ray distributions have a shape to be expected from theory. Comparison of the calculated with the experimental slope led to the estimate $\alpha=0.4\pm0.2$, which gives $K\approx4$.

An independent estimate for K may be obtained by assuming a reasonable value for the average gamma-ray sensitivity. The dimensions of the experimental arrangement gave roughly 0.15 for the solid angle of the gamma-counter divided by 4π. Assuming an average absolute gamma-ray efficiency of 0.3×10^{-2}, one finds that S_γ becomes 0.5×10^{-3}. Then from Eq. (8), K is 4. These rough estimates seem to show that the data are consistent.

Dysprosium

The 2.5-hour activity induced by slow neutrons is probably due to Dy^{165}, since there is only one stable isotope of holmium (165) to which the dysprosium decays (emitting negative electrons), and since otherwise the isotope would be isomeric with a stable isotope of dysprosium.

Meitner[15] and Hevesy and H. Levy[16] agree on a beta-ray energy of 1.4 Mev. Mitchell, Langer, and McDaniel[2] suggested the existence of a gamma-ray. Meitner obtained the gamma-ray energy by rough absorption measurements in lead and found the energy to be of the order of magnitude of 0.6 Mev. This would be an estimate of the average gamma-ray energy.

A small amount of dysprosium oxide held on to an aluminum backing in a paraffin base was bombarded with slow neutrons from the cyclotron, to produce the source for this experiment.

The range of the beta-rays was measured with the thin-walled counters, and was found to be 0.49 ± 0.02 g/cm². This corresponds to an end-point of 1.20 Mev.

Compton recoils were measured to obtain the maximum energy gamma-ray. The glass-walled brass cathode counters gave a range of 0.5 ± 0.1 g/cm² which corresponds to a gamma-ray energy of 1.1 Mev.

Beta-gamma coincidences were found with the thin-walled counters with no absorber in front of the beta-counter. There were so many beta-rays per recorded gamma-ray that with a usable beta-rate there were too few gamma-rays to get an adequate number of coincidences for accurate work.

Gamma-gamma coincidences were also detected, indicating that the gamma-spectrum is probably complex.

The writer wishes to express his thanks to Professor Allan C. G. Mitchell, who suggested the problem, for his advice and interest in the work, and also to Professor E. J. Konopinski for many helpful suggestions concerning the correlation of the results. The author also is indebted to Professor J. M. Cork of the University of Michigan for irradiating the first samples used in the experiment, and to his colleagues at Indiana University for running the cyclotron and checking calculations.

APPENDIX

Errors

One would like to find criteria for a minimum relative error in beta-gamma coincidence experiments. On this basis Dunworth[3] has developed a formula for the maximum useful source strength for a given geometry:

$$N\approx1/2\tau,$$

where N is the source strength and τ is the resolving time of the coincidence circuit.

Under certain conditions it may be better to use still weaker source strengths because the usable counting rate of a tube counter is limited at high rates by missing, and multiple pulses. If the source strength is too high one must sacrifice solid angle, to which the error is more sensitive than to the source strength. According to Dunworth's formula for f, the relative error due to statistical fluctuations in the total coincidence rate, this quantity depends on the source strength N approximately as $N^{-\frac{1}{2}}$. It depends on the solid angles subtended by the two counters, which are proportional to his ϵ_1 and ϵ_2, as $(\epsilon_1\epsilon_2)^{-\frac{1}{2}}$. It is evident that the best arrangement would be to have the counters as close as possible to increase ϵ_1 and ϵ_2 by increasing the solid angle and then to use such a source strength as to produce the maximum usable counting rate.

[15] L. Meitner, Arkiv. f. Mat. Astr. och Fysik **A27**(3), 17 (1941).
[16] G. Hevesy and H. Levy, Kgl. Dansk. Vid. Sels. **14**, 5 (1936).

On the Theoretical Half-Lives of β-Activities

CHARLES L. CRITCHFIELD
Research Laboratories of Physics, Harvard University, Cambridge, Massachusetts
(Received December 5, 1941)

The theoretical half-lives of forbidden beta-transitions are determined as a function of the maximum energy and the nuclear charge. This is done for the usual five types of interaction which may be assumed in Fermi's theory of beta-decay. It is also assumed that the nuclear charge is very small compared with 137. It is found that the half-lives in most first forbidden and some second forbidden transitions may be expected to manifest the same dependence on energy as those in allowed transitions, i.e., approximately proportional to the inverse fifth power of the maximum energy. In general, however, first forbidden transitions may obey an inverse seventh power law and second forbidden an inverse seventh or ninth power law.

I

KONOPINSKI and Uhlenbeck[1] have determined the theoretical energy distribution of electrons emitted in forbidden beta-transitions for the five distinct types of interaction between the nuclear and the emitted particles. They also point out that the half-lives of forbidden transitions in light nuclei will depend upon a number of factors and that in general a simple correlation between half-life and energy cannot be expected. One difference between light and heavy nuclei in this respect is that the light nuclei probably have stationary states which belong to a rather definite multiplet;[2] and rapid beta-transitions can take place only between levels which are components of the same multiplet.[3] Thus beta-transitions in light nuclei may have abnormally long lives even though the change in angular momentum entailed is "allowed."

A further complication to be expected in light nuclei arises from the approximate equality of the absolute value of the Coulomb energy of the ejected electron and its maximum energy. In order to be able to estimate more closely the relative effect of Coulomb and kinetic energy in determining the half-life the distribution curves of reference 1 have been integrated for all interactions.

The decay constant which characterizes the beta-transition according to Fermi's theory[4] may be written as the product of two factors

$$\lambda = GI(w, Z). \tag{1}$$

Z is the charge number of the product nucleus and w is the maximum energy (including rest energy) of the electron or positron in units of mc^2. For electron emission Z is taken to be positive; for positron emission, negative. In allowed spectra $I_0(w, Z)$ is the integral over all electron energies of the "Fermi-distribution." A subscript 0 will be put on $I(w, Z)$ if it applies to allowed transitions.

We shall consider only the limiting case of small Z. In this limit the effect of the Coulomb field on the probability of emission of an electron with energy E, $1 \leq E \leq w$, is an extremely slowly varying function of E, at least for the great majority of possible values of E. The effect of the Coulomb field will accordingly be disregarded entirely in integrating the allowed spectra and will be expanded in a series of powers of αZ for the forbidden spectra. As soon as a definite form of interaction between light and heavy particles is established an integration $I(w, Z)$ which would apply to forbidden spectra of heavy elements would be useful in studying the matrix elements of large nuclei. Nordheim and Yost[5] have presented a formula for the decay constants of allowed spectra which is valid for all Z and large enough w.

In the limit of small Z, $I_0(w, Z)$ is practically independent of Z and is given by the well-known

[1] E. J. Konopinski and G. E. Uhlenbeck, Phys. Rev. **60**, 308 (1941).
[2] E. Wigner, Phys. Rev. **51**, 106, 947 (1937).
[3] E. Wigner, Phys. Rev. **56**, 519 (1939).
[4] E. Fermi, Zeits. f. Physik **88**, 161 (1934).
[5] L. W. Nordheim and F. L. Yost, Phys. Rev. **51**, 942 (1937).

formula

$$I_0(w)=\frac{(w^2-1)^{\frac{1}{2}}}{60}(2w^4-9w^2-8)+\tfrac{1}{4}w\ln(w+(w^2-1)^{\frac{1}{2}}). \quad (2)$$

Two unknown factors are included in G of Eq. (1). One of them is the "Fermi constant" g which in general is five constants giving the amount of scalar, vector, tensor, axial vector, and pseudoscalar interaction which exists. The other is the square of the matrix element of the interaction, $|M(Q)|^2$. The operator Q acts on the waves of the nuclear particles changing proton into neutron in positron emission and neutron into proton in electron emission. In addition Q may contain other operators as factors. If Q be simply proportional to the spin operator we shall denote Q by $\boldsymbol{\sigma}$: similarly Q will be denoted by $\mathbf{r}$, ρ_2, 1, etc., if it is proportional to these operators.

Allowed beta-spectra can have Q proportional to 1 giving the Fermi selection rules[4] or to $\boldsymbol{\sigma}$ giving Gamow-Teller[6] selection rules or to a linear combination of these operators. If allowed transitions are between known levels of the same multiplet the value of G for each kind of interaction can be determined. A complete discussion and table of results for allowed spectra is given by Wigner in reference 3.

It is the purpose of this paper to present the integrals $I_1(w, Z)$ and $I_2(w, Z)$ which obtain in first and second forbidden transitions, respectively. Estimates of the ratios of matrix elements which appear in forbidden spectra to those which appear in allowed spectra are also made.

II

A beta-transition will be called *first forbidden* if the wave functions of initial and final nuclei differ in parity but do not differ in angular momentum by more than two units. The decay constant of a first forbidden transition involves an integral over one of the energy distributions found in reference 1. A few minor departures from the method of Konopinski and Uhlenbeck will be introduced here and these are as follows:

(a) It is at once evident that the above definition of first forbidden transitions includes the "allowed pseudoscalar" transitions of reference 1;

(b) the nuclear wave functions will be assumed to be real so that the cross product terms in reference 1 will not be included in our results;[7]

(c) the Dirac notation with ρ's and σ's will be used.[8] A scalar operator on the four spin indices is represented by ρ_3, a polar vector by $(\rho_1\boldsymbol{\sigma}, 1)$ a tensor by $(\rho_3\boldsymbol{\sigma}, \rho_2\boldsymbol{\sigma})$, an axial vector by $(\boldsymbol{\sigma}, \rho_1)$ and the pseudoscalar by ρ_2; there was found[1] to be no distinction between ρ_1 and ρ_2 so far as the shapes of forbidden spectra are concerned but the two lead to different values of the matrix element and it is important to keep them separated in estimating decay constants;

(d) instead of B_{ij}, T_{ij}, and S_{ijk} (the irreducible symmetric tensors) of reference 1 we shall use the "normalized" equivalents denoted by square brackets in Eq. (3):

$$\begin{aligned}[\boldsymbol{\sigma}\mathbf{r}]_{ij}&=\tfrac{1}{2}B_{ij},\\ [\mathbf{r}\mathbf{r}]_{ij}&=R_{ij},\\ [\mathbf{r}\boldsymbol{\sigma}\times\mathbf{r}]_{ij}&=\tfrac{1}{2}T_{ij},\\ [\boldsymbol{\sigma}\mathbf{r}\mathbf{r}]_{ijk}&=\tfrac{1}{6}S_{ijk}.\end{aligned} \quad (3)$$

Estimates of the magnitude of $M(Q)$ will be made on the basis of the expected magnitude of the factors which appear in Q. For example if $Q=[\boldsymbol{\sigma}\mathbf{r}\mathbf{r}]$ the magnitude of $M([\boldsymbol{\sigma}\mathbf{r}\mathbf{r}])$ is expressed as

$$M([\boldsymbol{\sigma}\mathbf{r}\mathbf{r}])\cong R^2M(\boldsymbol{\sigma}). \quad (4)$$

In Eq. (4) R is the nuclear radius in units of h/mc. The well-known empirical relation between R and the atomic weight A is closely given by the equation

$$2R=\alpha A^{\frac{1}{3}} \quad (\alpha=1/137). \quad (5)$$

A factor ρ_3 in Q is equivalent to a factor unity but if ρ_1 or ρ_2 appears the appropriate factor depends upon the velocities of the nuclear particles. An approximate value of the average velocity of nuclear particles can be derived from the doublet separations of Li^7 and related nuclei assuming a Hartree model and Thomas forces or from the expected kinetic energy in nuclei. Such estimates necessarily involve arbitrary factors but a fair average of the results for the velocity, β, is about $\frac{1}{6}$ (light velocity is unity) and this value will be adopted in the following calculations.

[6] G. Gamow and E. Teller, Phys. Rev. **49**, 895 (1936).

[7] For the implications of the assumption of real wave functions see E. Wigner, *Goett. Nachrichten* (1932), p. 546.

[8] P. A. M. Dirac, *The Principles of Quantum Mechanics* (Oxford 1935).

In order to get some idea of the effect of ρ_1 and ρ_2 on the value of matrix elements which contain them we assume a proton to be in a four-component s wave

$$\psi_P = (A,\ 0,\ -B\cos\theta,\ B\sin\theta e^{i\phi}),$$

where A depends upon $\mathbf{r}$, is positive and of the magnitude of unity; B is positive and of the order of β_P, the velocity of the proton. Since ρ_1 and ρ_2 induce a change of parity let it be supposed that the proton is changed into a neutron in a p wave

$$\psi_N = (A'\cos\theta,\ -A'\sin\theta e^{i\phi},\ B',\ 0)$$

with A' positive and $B' \cong |\beta_N|$. The contribution of ρ_1 to the matrix element is then approximately $\int\psi^*_N\rho_1\psi_P d\tau / \int\psi^*_N\psi_P d\tau \cong |\beta_N| - |\beta_P|$ and that of ρ_2 is $\int\psi^*_N\rho_2\psi_P d\tau / \int\psi^*_N\psi_P d\tau \cong i\{|\beta_N| + |\beta_P|\} \cong i/3$. Even if the entire difference in energy of initial and final nuclei, w, were supplied by the kinetic energy of the transformed nuclear particle the occurrence of ρ_1 in Q should give rise to a factor $w/M\beta \cong w/300$ in the matrix element. The dependence of matrix elements proportional to ρ_1 on differences in velocities of nuclear particles has been pointed out before by Marshak.[9]

First forbidden transitions which depend upon ρ_1 or ρ_2 do not depend upon $\mathbf{r}$ and so the radiation may be called monopole radiation. Since a change of parity is effected by the operators ρ_1 and ρ_2, however, the radiation may more properly be called *pseudo-monopole*, a term which serves also to distinguish between first forbidden and allowed monopole emission. Both types of monopole transitions give rise to the Fermi distribution in energy.[1] It follows that the decay constant for first forbidden transitions of the pseudo-monopole variety is determined by Eqs. (1) and (2) with the appropriate values of G and w. In Table I the possible Q which lead to pseudo-monopole transitions are shown together with the estimated value of G_1/G_0, the ratio of G for first forbidden to G for allowed transitions under the same interaction. In the last column of Table I and also of the following tables the possible changes of nuclear angular momentum, Δi, which are of interest are given. If more than one Δi is possible for a certain Q the sum of angular momenta (absolute values) of initial and final nuclei must be at least as large as the largest Δi for that Q. Primes are put on the smaller numbers to indicate this restriction. Henceforth the interactions will be designated by X as shown in Table I.

TABLE I. Pseudo-monopole.

Interaction	X	Q	$G_1/G_0 \sim$	Δi
Scalar	S	0	0	—
Vector	V	$\rho_1\boldsymbol{\sigma}$	$10^{-5}w^2$	0′, 1
Tensor	T	$\rho_2\boldsymbol{\sigma}$	0.1	0′, 1
Axial Vector	A	ρ_1	$10^{-5}w^2$	0
Pseudoscalar*	P	ρ_2	0.1*	0

* Since P leads to no allowed transitions this value has a meaning only if P occurs in combination with another operator.

In (beta) dipole radiations the energy distribution is different for different interactions X. Furthermore the tensor and axial vector interactions each have three possible Q. The decay constant which obtains for a particular X will be written $\lambda(X)$ and for those interactions which contain more than one matrix element $\lambda(X)$ represents a sum over the Q. It is found by integrating the results of reference 1 that $\lambda(X)$ for all dipole transitions may be written

$$\lambda(X) = \sum_Q G_1(Q, X)\Big\{a'_{QX}y_a(w) + b'_{QX}y_b(w) + \frac{\alpha Z}{2R}(b'_{QX}+c'_{QX})y_c(w) + c'_{QX}\left(\frac{\alpha Z}{2R}\right)^2 I_0(w)\Big\}, \quad (6)$$

$$y_a(w) = \frac{(w^2-1)^{\frac{1}{2}}}{15120}(16w^6-118w^4-407w^2-16) + \frac{4w^3+w}{144}\ln\,(w+(w^2-1)^{\frac{1}{2}}),$$

$$y_b(w) = \frac{(w^2-1)^{\frac{1}{2}}}{2520}(4w^6-40w^4-247w^2-32) + \frac{2w^3+w}{24}\ln\,(w+(w^2-1)^{\frac{1}{2}}),$$

$$y_c(w) = \frac{(w^2-1)^{\frac{1}{2}}}{360}(4w^5-28w^3-81w) + \frac{6w^2+1}{24}\ln\,(w+(w^2-1)^{\frac{1}{2}}).$$

[9] R. E. Marshak, Phys. Rev. **59**, 937(A) (1941).

TABLE II. Dipole.

X	Q	$G_1/G_0\sim$	a'_{QX}	b'_{QX}	c'_{QX}	Δi
S	$\rho_2 r$	R^2	6	-1	1	0
V	$\mathbf{r}$	R^2	6	1	1	0′, 1
T	$\rho_3(\sigma, \mathbf{r})$	R^2	2	-1	1	0
	$\rho_3(\sigma\times\mathbf{r})$	R^2	3	1	1	0′, 1
	$\rho_3[\sigma\mathbf{r}]$	R^2	6	0	0	0′, 1′, 2
A	$(\sigma, \mathbf{r})$	R^2	2	1	1	0
	$(\sigma\times\mathbf{r})$	R^2	3	-1	1	0′, 1
	$[\sigma\mathbf{r}]$	R^2	6	0	0	0′, 1′, 2
P	0	0	0	0	0	—

TABLE III. Pseudo-dipole.

X	Q	$G_2/G_0\sim$	a'_{QX}	b'_{QX}	c'_{QX}	Δi
S	0	0	0	0	0	0
V	$\rho_1[\sigma\mathbf{r}]$	$10^{-5}R^2w^2$	6	0	0	1′, 2
	$\rho_1\sigma\times\mathbf{r}$	$10^{-5}R^2w^2$	3	-1	1	1
T	$\rho_2[\sigma\mathbf{r}]$	$0.1R^2$	6	0	0	1′, 2
	$\rho_2(\sigma, \mathbf{r})$	$0.1R^2$	2	-1	1	0→0
A	0	0	0	0	0	0
P	$\rho_2 r$	$0.1R^2$	6	-1	1	1

$I_0(w)$ is the same as in Eq. (2) and the values of a'_{QX}, b'_{QX}, c'_{QX} are given in Table II.

It is interesting to note that in most of the possibilities for dipole radiation $b'_{QX}=-c'_{QX}$ and according to Eq. (6) the same half-life will be predicted for electron and positron emission for the same w and Z. Terms proportional to $Z^2(c'_{QX}=1)$ appear in most of the dipole transitions and for the usual energies, $w\sim 5$ or 6, the Z^2 terms are by far the largest in Eq. (6). This, together with the fact that the strongest pseudo-monopole transitions are independent of w (except for $I_0(w)$ as a factor), would indicate that, whatever the true interaction may be, the chances are good that the first-forbidden half-lives are simply proportional to w^{-5} the same as for allowed spectra. Evidence in the experimental material for a fifth power dependence for the majority of activities is presented in a paper by Itoh.[10]

III

Second forbidden transitions will be defined as those in which the angular momentum of the nucleus changes by not more than three units and in which there is no change in parity; it is assumed that no matrix elements vanish accidentally and thus only the changes in angular momentum which are not allowed need be considered in the second forbidden. By extending the classification introduced for first forbidden transitions there are found two classes of second forbidden transitions: pseudo-dipole, for which the matrix elements are proportional to the first power of $\mathbf{r}$ and to ρ_1 or ρ_2, and (beta) quadrupole, quadratic in $\mathbf{r}$.

The decay constant in pseudo-dipole transitions is given by Eq. (6) with values of a'_{QX}, b'_{QX}, c'_{QX} given in Table III.

Quadrupole transitions have decay constants which are determined by Eq. (7)

$$\lambda(X)=\sum_Q G_2(Q,X)\Big\{a''_{QX}Y_a(w)+b''_{QX}Y_b(w)+\frac{\alpha Z}{2R}(b''_{QX}+c''_{QX})Y_c(w)+\Big(\frac{\alpha Z}{2R}\Big)^2 c''_{QX}Y_d(w)\Big\}, \quad (7)$$

$$Y_a(w)=\frac{(w^2-1)^{\frac{1}{2}}}{340200}(50w^8-515w^6-3417w^4-536w^2+8)+\frac{9w^5+5w^3}{1080}\ln\,(w+(w^2-1)^{\frac{1}{2}}),$$

$$Y_b(w)=\frac{(w^2-1)^{\frac{1}{2}}}{113400}(20w^8-260w^6-2553w^4-704w^2+32)+\frac{6w^5+5w^3}{360}\ln\,(w+(w^2-1)^{\frac{1}{2}}),$$

$$Y_c(w)=\frac{(w^2-1)^{\frac{1}{2}}}{40320}(48w^7-536w^5-4322w^3-1175w)+\frac{32w^4+24w^2+1}{384}\ln\,(w+(w^2-1)^{\frac{1}{2}}),$$

$$Y_d(w)=\frac{(w^2-1)^{\frac{1}{2}}}{10080}(40w^6-358w^4-1889w^2-208)+\frac{16w^2+7w}{96}\ln\,(w+(w^2-1)^{\frac{1}{2}}).$$

[10] J. Itoh, Proc. Phys. Math. Soc. Japan 22, 531 (1940).

The coefficients a''_{QX}, b''_{QX}, c''_{QX} are found in Table IV.

IV

Of the above results only those on the pseudo-monopole radiation apply strictly to linear combinations of interactions as well as to single interactions. In general, a linear combination will introduce cross products of matrix elements which give the same change in angular momentum and the radiations could not be classified as simply as it has been done. On the other hand cross products of matrix elements which are of different size can usually be neglected in comparison with the square of the larger one. The transition probabilities obtained above may thus be applied to more general interactions than single choices of S, V, T, A, or P. In fact it has been assumed throughout that P does not occur alone and only under this assumption is it logically consistent to imply that P gives rise to no allowed transitions.

The terms of Eqs. (2), (6), and (7) which contain w to the highest power afford asymptotic expressions for the integrals $I_0(w)$, $I_1(w, Z)$ and $I_2(w, Z)$, respectively. The approximate forms of I_1 and I_2, however, do not approach the exact value as rapidly as for I_0 with increasing w. But assuming that I_0 has been calculated exactly one finds the ratios of I_1 and I_2 to I_0 are given by the asymptotic expression to 10 percent and better for $w=4$ and larger. For dipole transitions, therefore

$$I_1(w, Z)/I_0(w) \cong \frac{w^2}{63}(2a'_{QX}+3b'_{QX}) + \frac{w}{3}\left(\frac{\alpha Z}{2R}\right)(b'_{QX}+c'_{QX})+c'_{QX}\left(\frac{\alpha Z}{2R}\right)^2. \quad (8)$$

By using Eq. (5) and $A=2Z$ it is evident that the decay constant will depend upon energy essentially in the same way as for allowed transitions whenever

$$w^2 < 40Z^{4/3}c'_{QX}/(2a'_{QX}+3b'_{QX}). \quad (9)$$

Only those pseudo-monopole radiations which contain w^2 in G_1/G_0 and dipole radiations for which w^2 is larger than the right-hand side of (9) manifest a seventh power dependence of decay constant on lifetime as far as first forbidden transitions are concerned.

A similar expression of the results on second forbidden transitions may also be useful. Of course the conclusions that have been drawn for dipole radiations apply directly to the pseudo-dipole. If the inequality (9) holds even second forbidden transitions will obey the fifth power law although the decay constants are very much smaller than for allowed transitions. For quadrupole transitions the relation (10) holds to 15 percent and better for $w=5$ and larger.

$$I_2(w, Z)_{\text{quad}}/I_0(w) \cong \frac{w^4}{1134}(5a''_{QX}+6b''_{QX}) + \frac{w^3}{28}\frac{\alpha Z}{2R}(b''_{QX}+c''_{QX})+\frac{5w^2}{42}\left(\frac{\alpha Z}{2R}\right)^2 c''_{QX}. \quad (10)$$

The relation between w and Z for which a seventh power law may be expected for quadrupole transitions is practically the same as (9) with double primed quantities in place of the single primed ones. If the inequality is reversed a ninth power law should hold.

The Coulomb fields of light nuclei exercise a small effect on the transition probability and may be taken into account through approximate formulae as given, for example, in reference 5. As mentioned above, however, the Coulomb effect is practically the same for all electron energies and thus does not influence the integrals appreciably. It is only for very slow electrons that a noticeable variation is to be expected.

It appears within the range of possibility that $I_0(w)$ governs the dependence of half-lives on energy for most of the light radioactive nuclei

TABLE IV. Quadrupole.

X	O	$G_2/G_0\sim$	a''_{QX}	b''_{QX}	c''_{QX}	Δi
S	$\rho_3[\mathbf{rr}]$	R^4	3	−1	1	1′, 2
V	$[\mathbf{rr}]$	R^4	3	1	1	1′, 2
T	$\rho_3[\boldsymbol{\sigma}\mathbf{rr}]$	R^4	3	0	0	2′, 3
	$\rho_3[\mathbf{r}\boldsymbol{\sigma}\times\mathbf{r}]$	R^4	2	1	1	2
A	$[\boldsymbol{\sigma}\mathbf{rr}]$	R^4	3	0	0	2′, 3
	$[\mathbf{r}\boldsymbol{\sigma}\times\mathbf{r}]$	R^4	2	−1	1	2
P	0	0	0	0	0	—

both in allowed and in forbidden transitions. If this were true it would indicate that either the tensor interaction or the pseudoscalar is important to the beta-process. It would be desirable, however, to find some light nuclei which obey the seventh or ninth power laws. According to the results of reference 1 it is such nuclei that would produce spectra which differ in shape significantly from the allowed spectra.

I am indebted to Professor Eugene Paul Wigner of Princeton University and Dr. Henry S. Sommers, Jr., of Harvard for many interesting discussions related to the subject matter of this paper.

MARCH 1 AND 15, 1942 PHYSICAL REVIEW VOLUME 61

The Multiple Scattering of Fast Electrons

L. A. KULCHITSKY AND G. D. LATYSHEV
Physical-Technical Institute of the Academy of Science of the Ukrainian S. S. R., Kharkow

(Received October 31, 1941)

The method and apparatus are described which were developed for the investigation of the multiple scattering of fast electrons. The scattering of electrons with an energy of 2.25 Mev is studied in the foils of aluminum, copper, iron, molybdenum, silver, tin, tantalum, gold, and lead. The results obtained are compared with the theory of multiple scattering. For elements from Al ($Z=13$) to Sn ($Z=50$) the experimental values for the multiple scattering coincide with those theoretically predicted. For heavy elements Ta ($Z=73$), Au ($Z=79$), Pb ($Z=82$) the experimental values are 10 to 13 percent lower than calculated.

I. INTRODUCTION

THE nuclear scattering of fast electrons has been investigated in many experimental researches. In the majority of cases, the singular or elementary nuclear scattering was investigated. All these investigations showed a close agreement between the experimental values and those calculated according to Mott's theory.

The multiple scattering of electrons was studied chiefly by Sheppard and Fowler,[1] and Fowler.[2] They investigated the scattering of electrons with a mean energy of approximately 10 Mev. The spectral composition of the energy of the electrons was spread between 2 and 17 Mev. The scattering was investigated in thin lead, aluminum, and carbon plates placed in the center of a Wilson chamber. The results obtained were compared with Williams'[3] theory. This author found that the angular distribution of the scattered electrons coincides approximately with the Gauss curve, while the mean angle for the scattering is in close agreement with those theoretically predicted for light elements (Al, C). For lead, the value of the mean angle of scattering is approximately twice as small as that theoretically calculated.

M. Slawsky and H. Crane[4] (Wilson chamber method) investigated the multiple scattering of electrons with energies near 0.9 Mev. The most probable angle of scattering in these experiments was so large, that the application of the theory of multiple scattering is not warranted as the scattering was diffuse.

For scattering in Al only, Slawsky and Crane compare their experimental values with the theory of Bethe, Rose, and Smith.[5] In this case the most probable angle coincided with that theoretically calculated.

Oleson, Chao, Halpern, and Crane[6] investigated the multiple scattering of electrons with

[1] C. W. Sheppard and W. A. Fowler, Phys. Rev. **56**, 849 (1939); **57**, 273 (1940).
[2] W. A. Fowler, Phys. Rev. **54**, 773 (1938).
[3] E. J. Williams, Proc. Roy. Soc. **169**, 531 (1939); Phys. Rev. **58**, 292 (1940).
[4] M. M. Slawsky and H. R. Crane, Phys. Rev. **56**, 1203 (1939).
[5] H. A. Bethe, M. E. Rose, and L. P. Smith, Proc. Am. Phys. Soc. **78**, 573 (1938).
[6] N. L. Oleson, K. T. Chao, J. Halpern, and H. R. Crane, Phys. Rev. **56**, 482, 1171 (1939).

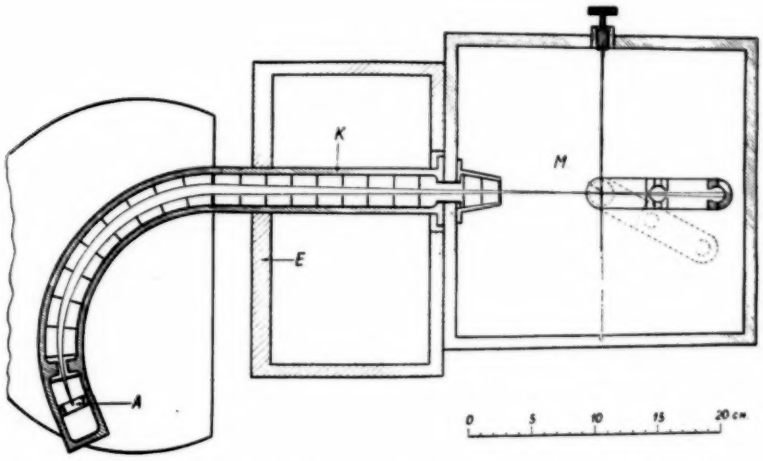

FIG. 1. General lay-out of the apparatus. Section in horizontal plane. *A*, the source; *M*, the target; *K* the spectrograph chamber; *E*, magnetic shield.

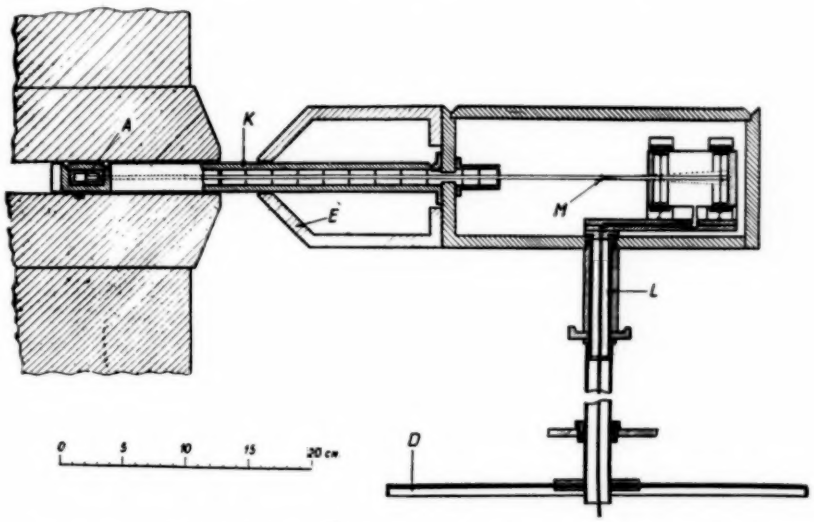

FIG. 2. General lay-out of the apparatus. Vertical section. *A*, source of electrons; *M*, target; *E*, magnetic shield; *L*, the glass-ground joint with leads to the counters and a tube to the vacuum pump; *O*, circular dial divided in degrees.

an energy of between 2 and 8 Mev in thin plates of lead and carbon, placed in the center of a Wilson chamber. In the comparison of experiments these authors came to the same conclusion as Fowler and Sheppard, and Fowler.

As can be seen, the multiple scattering of electrons has been investigated only by the Wilson chamber method with small statistical accuracy, and with considerable averaging of energy of the scattered electrons.

The purpose of this investigation is a detailed study of the multiple scattering of electrons under precise and definite experimental conditions.

II. THE EXPERIMENTAL METHOD

The source of fast electrons was a thin-walled glass tube containing radium emanation, placed between the poles of an electromagnet at a point *A* (Fig. 1). By means of a magnetic field, and a system of diaphragms shown in Figs. 1 and 2 a homogeneous, narrow and almost parallel pencil of electrons was obtained. As can be seen from Figs. 1 and 2, this electronic beam, after passing the system of diaphragms, entered a large metal chamber. In the center of this chamber far from the walls, the investigated substance was placed in the form of a thin plate

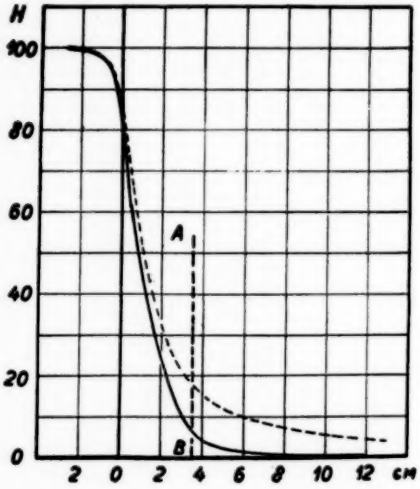

FIG. 3. Variation with distance of the stray magnetic field on the edges of the pole shoes. The dotted line—without magnetic shield; the solid line—with the shield. *AB*, position of the magnetic shield.

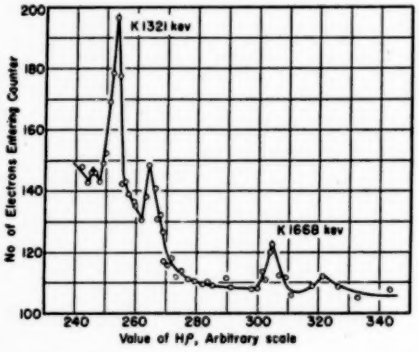

FIG. 4. Part of the natural spectrum of RaC.

(the target). The electronic beam was focused on this target and scattered by it.

The scattered electrons were registered by two G–M counters in coincident arrangement and the counters were placed in the same metal chamber, evacuated to a pressure of 10^{-2} mm Hg. The geometrical arrangement of the counters can be seen in Figs. 1 and 2.

By means of a special arrangement, the two counters could be rotated round the axis through the scattering target.

As the scattering plate was in the center of the chamber and the counters sufficiently far from one another, the electrons which could pass both counters could be emitted from a very small volume containing the scattering target. Electrons scattered by the walls of the chamber, and the other parts of the apparatus, could not

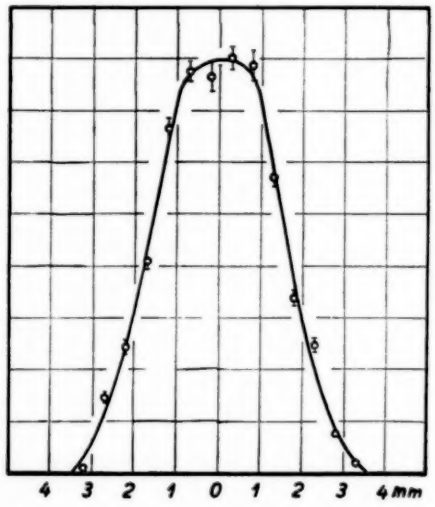

FIG. 5. Form of the electronic beam in the horizontal plane at a distance of 151 mm from the exit diaphragm.

pass simultaneously both counters, and therefore were not registered.

The scattering plate was mounted on an aluminum frame, and by rotating it through 90°, the target could be placed near the upper lid of the chamber; this was done to measure the background of the counters. This measurement was very small indeed and contributed only a small part of the measured effect; the correction for the background counts had to be made only when the scattering at large angles (30–40°) was investigated.

It was impossible to measure the background counts with the raised target when investigating the scattering at small angles (0–5°); in this case the primary beam could pass unhindered into the counters, but in scattering at small angles, the background was too small in comparison with the measured effect, and its influence could be ignored.

In all investigations of the scattering of electrons, the geometry of the electronic beam, its cross section, divergence homogeneity and the influence of the edges of the diaphragms, etc., are of primary importance. Because of this, a great deal of time was spent in obtaining a well-defined electronic beam and for measuring its geometry. This part of the work is described in Section V.

The axis around which the counters could be rotated was connected with a large circular

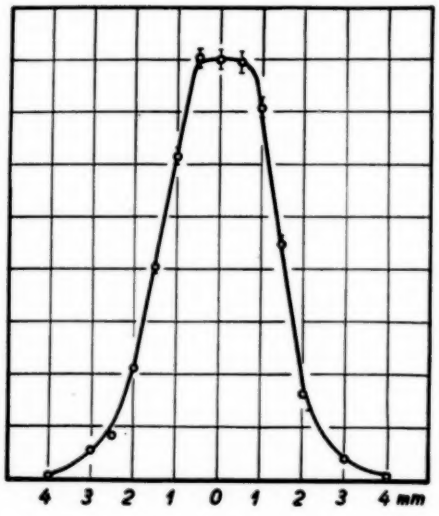

FIG. 6. Form of the electronic beam in the vertical plane at a distance of 151 mm from the exit diaphragm.

graduated dial, by means of which the angle of rotation of the counters could be ascertained.

III. APPARATUS

1. The Magnet

The cross section of the pole-shoes of the electromagnet was a segment of a circle (see Fig. 1). The gap between the pole-shoes was 23 mm. To diminish the fringing flux, a magnetic shield was placed at a distance of 35 mm from the pole-shoes, exactly at the point where the electronic beam leaves the region of the magnetic field.

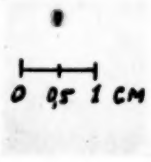

FIG. 7. Photogram of the electronic beam spot in the plane of the target.

The distribution of the magnetic field near the pole-shoes without the magnetic shield is given in Fig. 3 (dashed curve). The solid curve shows the distribution of the magnetic field with the shield. The current for the electromagnet was taken from a storage battery. The strength of the magnetic field was determined by the usual method, with a search coil and a ballistic galvanometer.

2. The Electronic Beam. Diaphragms

The geometrical shape of the electronic beam was determined by several diaphragms placed inside the apparatus. The height of all the diaphragms was 2.5 mm. In the region of the magnetic field the electrons described an arc of 115°, the radius of this arc being equal to 121 mm. The holes in the diaphragms arranged on the surface perpendicular to the direction of the magnetic field, subtended an angle of 2.1° from the axial line of the beam.

After leaving the region of the magnetic field, the electronic beam was focused on the scattering substance (target) placed at a distance of 225 mm from the magnet.

Along the calculated geometrical path of the electronic beam, several diaphragms were placed (see Figs. 1 and 2). All diaphragms were made of aluminum to diminish the scattering. All the inside walls were lined with aluminum for the same purpose. There were three defining diaphragms. The first formed an electronic source, the second was placed at the boundary of the region of the magnetic field, where the path of the electron is transformed from the arc of a circle into a straight line. The size of the third and last diaphragm was 1.5×2.5 mm^2. These three diaphragms were made accurately according to the calculated form of the electronic beam; other diaphragms were a little wider.

FIG. 8. Microphotograms of the electron beam spot: (a) in the horizontal plane, (b) in the vertical plane.

3. The Target

The substance used as a target is in the form of a thin plate. It was fastened to an aluminum frame by two silk threads, and by rotating at 90° could be raised to the upper lid of the apparatus. The target was 73 mm from the last

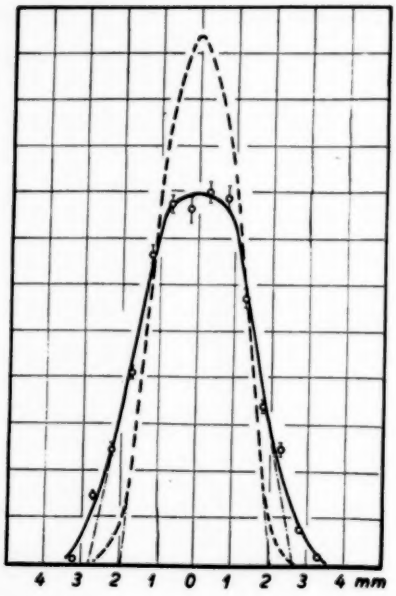

FIG. 9. Normalized curves of the electron beam in the horizontal plane measured by the G-M counter and by microphotogram method. The dash-point curve gives the extrapolation of the linear parts of the curves.

diaphragm and 37.5 mm from the entrance window of the first counter. The area of the targets was 20×20 mm². The thickness was chosen in such a way, that a half-width of the Gauss curve for scattering electrons was approximately equal to 10° for all elements.

4. The Counters

The diameter and the length of the cylindrical parts of the G–M counters were, respectively, equal to 13 mm and 45 mm. The distance between the axes of the counters was 47.5 mm. The first counter had two windows, the second only one, the size of the windows being 3.6×4.5, 5.3×6.7, and 8.6×10.5 mm consecutively; the first figure gives the width, and the second the height.

The first window was covered by a silvered celluloid film; the next two by aluminum foil 10 micron thick.

The central wires of the counters were made of steel wire 0.2 mm in diameter.

The G–M counters were placed inside a metal chamber evacuated to 10^{-2} mm Hg, and could be rotated round the target by means of a glass-ground joint, the same ground joint being used also for evacuation of the counters (13 cm Hg). All the wire belts from the counters to the amplifier passed through the same ground joint.

The potential of the counters was 2000 volts. A metal dial 458 mm in diameter and divided into 360 degrees was fastened to the ground joint.

5. The Amplifier

The amplifier was built according to the scheme developed by M. S. Kosodaev and G. D. Latyshev.[7] A description is given elsewhere.

6. The Glass-Ampoules

The glass tubes filled with radon (the ampoules) were 0.5–0.7 mm in diameter and 5–7 mm in height; the wall-thickness equalled 0.1 mm and the strength of the radon source was between 100–200 mC.

7. The Apparatus. Focusing the Electric Beam

A general scheme of the apparatus is given in Figs. 1 and 2. The apparatus, as a whole, could be shifted by means of micrometrical screws, and in this way the path of the electrons between the pole-shoes could be changed.

The source of electrons (a point "*A*" in Fig. 1) could also be shifted along the path of the electrons. By means of these two movements the electronic beam could be focused on the surface of the target; after the beam was well-focused the apparatus was securely fixed and lagged from outside with lead for shielding the counters from γ-rays.

Experience showed that the focusing was not spoiled during the changing of the radon sources. By means of a special screw, the distance between the pole-shoes could be increased and point "*A*" brought outside. After changing the radon sources the pole-shoes could be screwed to exactly the same position.

IV. THE MEASUREMENTS OF THE ENERGY OF ELECTRONS

Under the conditions in our experiments the most precise determination of the energy of electrons was procured by the investigation of the natural β-spectrum of RaC. A part of the

[7] A. I. Alikhanov, G. D. Latyschev, J. Exper. Theor. Phys. **10**, 9–10 (1940).

energy distribution of the electrons of natural β-spectrum of RaC is given in Fig. 4. On this curve the abscissae represent the deflections of the ballistic galvanometer proportional to the $H\rho$. The ordinates represent the number of electrons entering the counter in the unit-time at different values of $H\rho$. The curve in Fig. 4 is given without the recalculation for equal intervals of $H\rho$.

In these investigations of the natural β-spectrum, the counters were oriented at zero-angle in the direction of the electronic beam; the target was raised to the lid of the apparatus. Because of this, the electronic beam entered the windows of both counters. The energy of the entering electrons was changed by the variation of the magnetic field. The maximum on Fig. 4 designated by K 1321 kev represents the transition of the conversion of electrons of K shell of RaC′ from the excited level of the nucleus RaC′ equal to 1414 kev; the maximum 1399 kev represents the transition of the conversion of electrons of K shell produced by the x-rays of energy 1761 kev.

It is easy to see that the position of these maxima given on Fig. 4 does not coincide precisely with the values of the energy (or $H\rho$) written near each maximum. The electrons loose some energy inside the walls of the glass ampoules in which the radon is encased and because of this, all the maxima must be more or less displaced to the region of smaller energies.

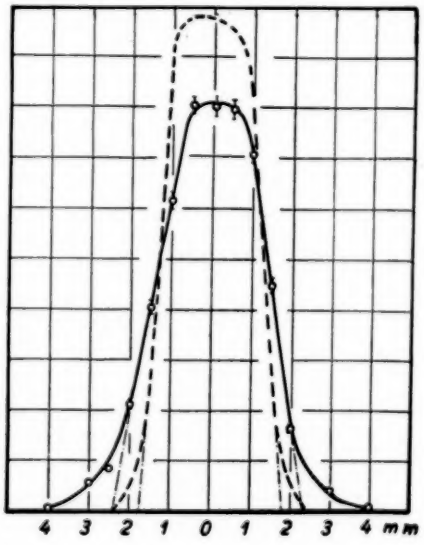

FIG. 10. Normalized curves of the electron beam in the vertical plane measured by the G-M counter and by microphotogram method. The dash-point curve gives the extrapolation of the linear parts of the curves.

The energy of conversion electrons (K 1321 and L 1399 kev) from the K and L shells of the atoms of RaC′, differ only by 78 kev, i.e., only by 3 percent, and because of this the energy loss must be the same. The maxima are displaced by almost the same values. (In the region of the energies of electrons 1.5 Mev the energy loss of electrons changes very slowly with the energy.)

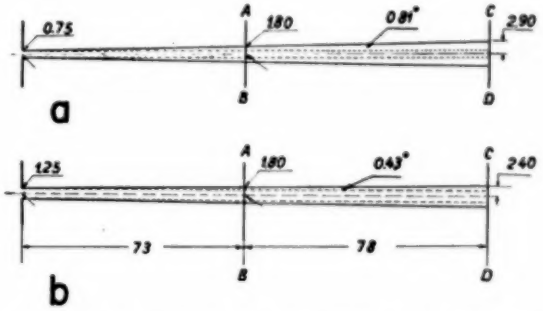

FIG. 11. The divergence of the electron beam. (a) In the horizontal plane. (b) In the vertical plane. The length scale is thrice diminished in comparison with the breadth. Dimensions are given in mm.

Therefore, knowing the difference H between the conversion electrons of the K and L shells of the RaC′ atom, from the excited energy level 1414 kev of the same atom, and knowing the difference in the deflections of the ballistic galvanometer, one can graduate it in H units.

In our experiments the energy of electrons which undergo the multiple scattering equals 2250 kev.

V. THE ELECTRONIC BEAM

We studied the electronic beam at two points: (1) at a distance of 151 mm from the point of emergence of the electrons from the last diaphragm, and (2) at the point where the target was placed at a distance of 73 mm from the last diaphragm.

At the first point, the beam was investigated by means of a G–M counter. A special counter was constructed which had a long narrow entrance slit, the width of which was 0.4 mm and its length 25 mm. By a special arrangement the counter could be shifted in a horizontal direction, the slit of the counter being vertical.

TABLE I. Scattering of electrons whose energy is 2.25 Mev. The angles are given in degrees. α_m is given according to Williams' theory. $\theta = \sqrt{\pi}\alpha_m$ is the half-width of the theoretical Gauss curve. θ_{th} is the half-width of the theoretical Gauss curve with the correction for the finite width of the beam. θ_{exp} is the half-width of the experimental Gauss curve. The last column shows the percent deviation of the experimental half-width value from the theoretical value.

Element	Z	A	$\sigma \frac{mg}{cm^2}$	δ	M	α_m	$\theta = \sqrt{\pi}\alpha_m$	θ_{th}	θ_{exp}	% deviation
I	II	III	IV	V	VI	VII	VIII	IX	X	XI
Al	13	26.97	26.6	2.00	60.2	5.36	9.5	9.85	9.50	− 3.7
Fe	26	55.84	15.4	2.10	41.4	5.39	9.55	9.90	9.60	− 3.0
Cu	29	63.57	17.15	2.31	46.8	6.05	10.7	11.05	10.40	− 3.0
Mo	42	96.00	12.4	2.31	36.6	5.87	10.4	10.75	10.25	− 4.6
Ag	47	107.88	11.55	2.34	35.1	5.90	10.45	10.80	10.20	− 3.7
Sn	50	118.7	17.40	2.37	34.2	5.96	10.55	10.90	10.65	− 2.3
Ta	73	181.4	8.9	2.45	28.7	6.02	10.65	11.00	9.85	−10.5
Au	79	197.2	8.9	2.54	29.4	6.72	11.10	11.40	9.20	−13.1
Pb	82	207.2	7.9	2.42	26.1	5.91	10.5	10.85	9.70	−10.6

The experimental results are given in Fig. 5. The abscissae represent the distances in mm from the middle of the beam, the ordinates, the number of electrons entering the counter in the unit time. This curve represents the distribution of the energy of electrons in the beam in the plane normal to the direction of the magnetic field.

By means of another arrangement the counter could be moved in a vertical direction, the slit of the counter being horizontal. The experimental results are given in Fig. 6. This curve gives the distribution of electrons in the plane parallel to the direction of the magnetic field and normal to the direction of the electronic beam.

At the second point, the electronic beam was investigated by the photographic method. Instead of the target a photographic plate was placed inside the apparatus. In Fig. 7 is shown a photographic tracing left by an electronic beam impinging on the photo-plate (target).

Figure 8 represents the microphotogram of this tracing. The abscissae give the distances from the center of the spot; the ordinates give the blackening of the plate, which in each point is proportional to the number of electrons impinging on this point.

Figure 8a gives the distribution of the intensity of the electronic beam in the horizontal plane; the same distribution for the vertical plane is given in Fig. 8b.

The small "tails" in the curves in Figs. 5, 6, 8a, and 8b are produced by the electrons scattered by the last diaphragm. From these curves the number of scattered electrons can be evaluated. Indeed by extrapolation of the linear parts of the curves, we can determine the area of the "tails." Dividing the sum of the areas of two "tails" (on the right and the left of the curve) by the whole area of the curve, we obtain the percent number of electrons scattered by the edges of the diaphragm. This calculation shows that in our experiments only 2–3 percent of all the electrons in the beam are scattered by the edges of the last diaphragm.

For the evaluation of the divergence of the electronic beam, the curves in Figs. 5 and 8a, which give the distribution of electrons in the horizontal plane, and Figs. 6 and 8b, which give the intensity distribution in the vertical plane, were normalized in pairs. These normalized pairs are given in Figs. 9 and 10.

By extrapolating the linear parts of the curves in Fig. 9 to the axis of the abscissae, we found that the breadth of the beam in the horizontal plane, at a distance of 151 mm from the last diaphragm, equalled 5.8 mm and 3.6 mm at a distance of 73 mm from the same diaphragm.

The breadth of the beam in the horizontal plane was 1.5 mm. The experimentally found shape of the beam in the horizontal plane is represented in Fig. 11a.

We can conclude, therefore, that the angle between the inclined path of the electrons and the horizontal axis of the beam does not exceed 0.8°. (The same angle was calculated by considering all the possible geometrical paths of electrons in the apparatus, limited by the given locations of the diaphragms, and was found to equal 0.9°.)

The height of the split of the last diaphragm in the vertical plane was 2.5 mm. From the data

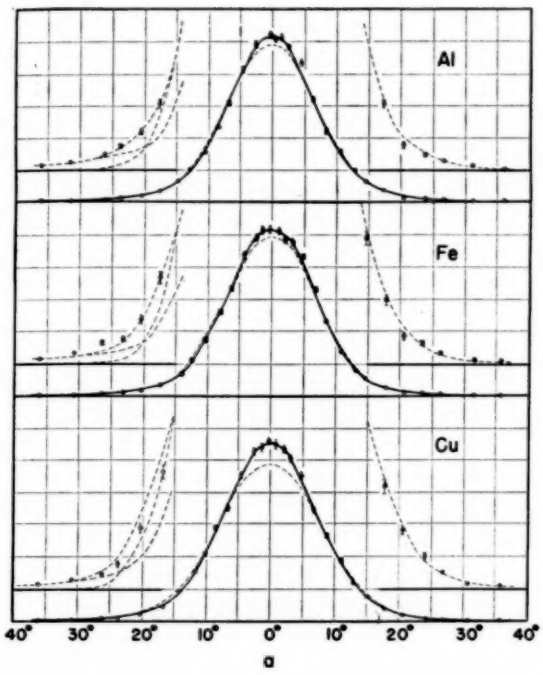

of Fig. 10, the height of the cross section of the electronic beam equals 4.8 mm at a distance of 151 mm from the diaphragm and 3.6 mm from the same diaphragm.

Figure 11b gives the shape of the beam in the vertical plane.

As previously, we can conclude that the divergence of the path of electrons from the horizontal axis in the vertical plane does not exceed 0.4° (the same angle calculated from consideration of all the possible paths limited by the given arrangement of diaphragms, was found equal to 0.32°).

From the distribution curve of the natural β-spectrum of RaC, given in Fig. 4, we can find the spectral composition of the beam impinging on the scattering foil. Indeed the breadth of the conversion maximum K 1321 kev, determined from Fig. 4, is equal to $\Delta H\rho = 5$ scale divisions of the deflection of the ballistic galvanometer, and is therefore equal to $5/251 \sim 2$ percent.

From this we can conclude that our electronic beam consists of electrons with an energy of 2250 ± 23 kev.

VI. THE EXPERIMENTAL RESULTS

We investigated the angular distribution of the scattered electrons with an energy of 2250

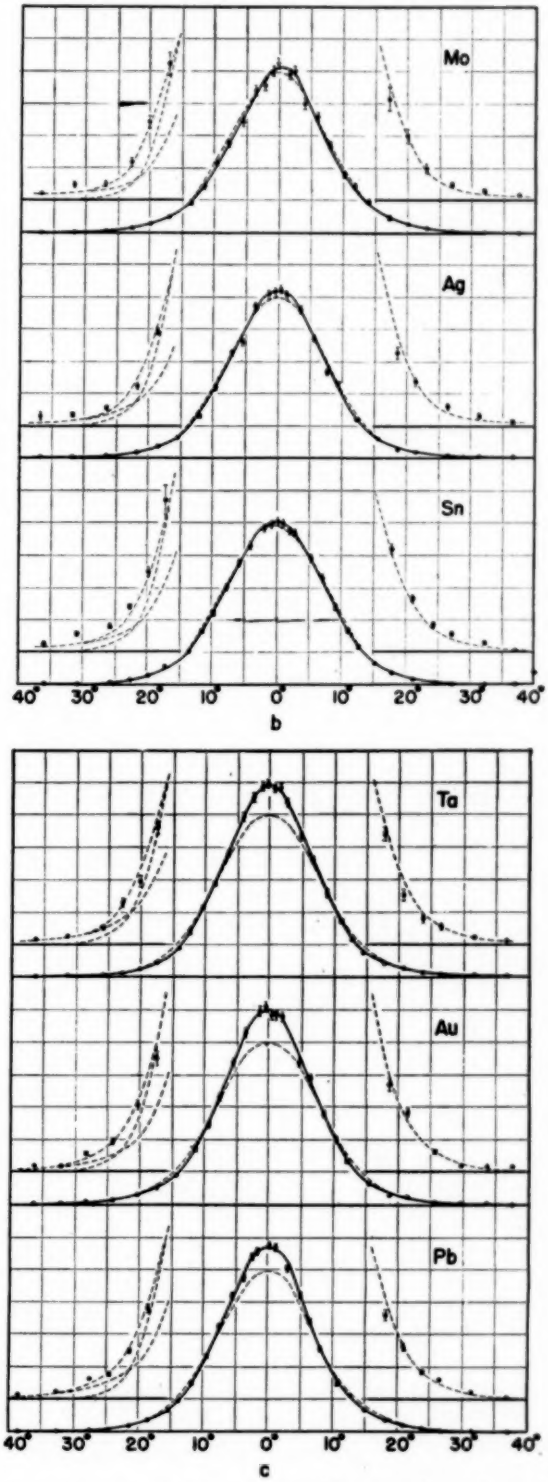

FIG. 12. a, b, c. Scattering of electrons in various elements. Experimental values are indicated by circles. The abscissae represent the angle of scattering, the ordinates the number of electrons scattered. The "tails" of the curves are magnified eight times in separate curves. Dotted curves represent theoretical values.

kev in the foils of Al, Fe, Cu, Mo, Ag, Sn, Ta, Au, and Pb. The thickness of the scattering foils (Table I) was chosen in such a way, that the half-width values of the Gauss curve would be equal for all the elements studied. The absolute value of the half-width was chosen to be equal to $\sim 10°$. The calculations show that at this value of the half-width, the theory of multiple scattering is applicable.

The experimental results are given in Fig. 12, the experimental values being designated by circles. The abscissae on these curves represent the angles of the scattering in degrees, the ordinates, the number of electrons. The experiments were carried on in a range of angles up to 35–40°. For angles larger than 40°, the number of electrons was too small.

The experimental points on the "tails" of the curves are given for clearness in the magnified scale (×8). The statistical fluctuations in the experimental values are represented in Fig. 12 by vertical dashes.

In our experiments the error in the determination of the half-width (the angle at which the intensity of the scattered electrons is diminished by "e" times) of the experimental curve does not exceed 3–4 percent.

VII. THE COMPARISON OF EXPERIMENTAL RESULTS WITH THE THEORY OF MULTIPLE SCATTERING

1. The Theoretical Formulae

The experimental results were compared with the theory of multiple scattering given by Williams.[3]

To date all the experiments carried out for the investigation of multiple scattering, were performed by the Wilson chamber method. In this method the projection of the path of the electron on the plane parallel to the bottom of the cloud chamber is usually measured. Because of this, all Williams' formulae are calculated for this case.

Williams' theory permits the calculation of the mean arithmetical value of the projection of the angle of deviation, and the angular distribution of the projections of the tracks of the scattered electrons.

According to Williams' theory of the multiple scattering in the foils, the angular distribution of the electrons scattered at small angles must be Gaussian. In the scattering at larger angles, the single scattering described by the Rutherford formula, predominates. In the intermediate region of the angles, these two distributions are superimposed.

The probability that the projection of the path of the electron lies between α and $\alpha+d\alpha$ is:

$$\rho(\alpha)d\alpha = g(\alpha)d\alpha + S(\alpha)d\alpha, \tag{1}$$

where $g(\alpha)$ is Gaussian, and $S(\alpha)$ is Rutherford's distribution of the scattered electrons.

Williams introduces two angles φ_2 and α_{mS}. When the electrons are scattered at angles less than φ_2, their distribution is purely Gaussian. When the scattering angles equal α_{mS}, the multiple scattering equals Rutherford's scattering. For angles larger than α_{mS}, the Gauss curve for the multiple scattering swiftly diminishes.

The Gauss distribution is given by:

$$g(\alpha) = \text{Const.} \exp\left[-\frac{\alpha^2}{\pi\bar{\alpha}_m{}^2}\right], \tag{2}$$

where $\bar{\alpha}_m$ is the mean arithmetical value of the projection of the angle of deviation, and equals

$$\bar{\alpha}_m = \left(\bar{\alpha} - \frac{\pi}{\varphi_2}\right) : \left(1 - \frac{\pi}{2\varphi_2{}^2}\right). \tag{3}$$

Here α is the mean arithmetical value for the projection of the angle of the deviation from the general distribution $P(\alpha)$ (Eq. (1))

$$\bar{\alpha} = 0.80(\log_e M)^{\frac{1}{2}} + 1.45, \tag{4}$$

where M is a value which characterizes the average number of collisions of electrons with the nuclei and equals

$$M = \frac{2\pi Z^{4/3}_{\text{eff}} N t h^2}{1.75^2 m_0{}^2 \beta^2 c^2} = 1850 Z^{4/3}_{\text{eff}} \frac{\sigma}{A}\frac{1}{\beta^2}, \tag{5}$$

in which A is the atomic weight of the substance, σ is the surface density in g/cm², and $Z_{\text{eff}} = (Z^2+Z)^{\frac{1}{2}}$ the value of the effective nuclear charge.

As a condition for the multiple scattering of the electrons we have $M \gg 1$.

The angle φ_2, which enters in (3) and the physical meaning of which was considered above,

equals:

$$\varphi_2 = 5.1(\log_e M)^{\frac{1}{2}} - 4.0. \quad (6)$$

The Rutherford distribution $S(\alpha)$ in Williams' theory has a form:

$$\begin{aligned} S(\alpha) &= 0 \quad \text{for} \quad \alpha < \varphi_2 \\ S(\alpha) &= \pi/\alpha^3 \quad \text{for} \quad \alpha > \varphi_2. \end{aligned} \quad (7)$$

The angle α_{mS} at which the value of the Gaussian distribution equals Rutherford's, is

$$\alpha_{mS} = 5.1\bar{\alpha}_m - 4.00. \quad (8)$$

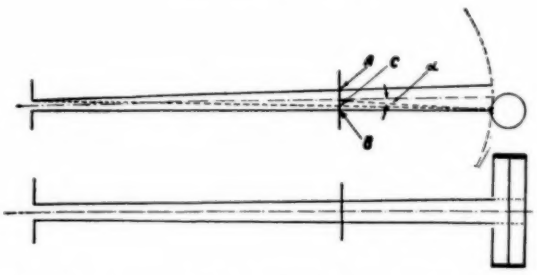

FIG. 13. Scheme of the electron beam investigation for calculating its finite breadth. AB—electron spot on the target. CB—section of the spot from which the electrons enter the slit of the counter, when turned at the angle α.

In all these formulae, the angles are in the units of δ. To convert into degrees, it is necessary to multiply them by δ.

$$\delta = 12.7\left(\frac{\sigma}{A}\right)^{\frac{1}{2}} \frac{Z_{eff}}{\beta^2 W}, \quad (9)$$

where W is the whole energy of the electron in Mev.

Contrary to the Wilson chamber experiments, where the experimentally found angular distribution is a projection of three-dimensional tracks on the bottom plane of the chamber, in our experiments a proper angular distribution of electrons in the space was investigated.

For the Gauss distribution, the half-widths of the distribution curve (the angle at which the intensity diminishes in "e" times) is the same for the distribution proper, and for its projection.

Because of this it was possible to compare theory with the values of the half-width of the experimentally found curves.

The half-width value for the Gauss curve equals

$$\theta = \pi^{\frac{1}{2}}\bar{\alpha}_m. \quad (10)$$

2. Correction for the Finite Dimensions of the Electronic Beam

All these formulae are valid if the beam impinging on the target is infinitesimally thin. In our experiments the beam was a definite thickness. Because of this a correction for the finite dimensions of the beam had to be made. For this, to the exit window of the counter a diaphragm was fastened with a narrow slit (0.3×4.5 mm). The intensity of the electronic beam was measured at different angular positions of the counter (which was changed by rotating the counter); the frame with the scattering target was raised. This investigation was done with the first counter only.

In this case a definite angular position of the counter is connected with a narrow region BC of the whole cross section of the beam AB impinging on the plate (see Fig. 13). The photograph of the spot left by the electronic beam is given in Fig. 7. The full height of the beam was caught by the counter.

It must be mentioned that the results of this experiment are given in Fig. 14. The abscissae are the angular positions of the counter, the ordinates, the number of electrons.

The whole area of this curve was divided into parts of 1° each, as is shown in Fig. 14. For each section a theoretical curve was constructed, normalized proportionally to the area of the section. The middle point of each section was shifted several degrees according to the position of the section in Fig. 14.

All the ordinates of this curve were added together. As a result a Gauss curve was found the half-width value of which was much larger than the previous one.

This correction for the finite dimensions of the beam did not exceed 3–4 percent in our experiments.

3. The Comparison of the Experimental Results with Williams' [3] Theory

The constructed theoretical curves were normalized with the experimental curves in Fig. 12, dashed lines represent the theoretical curves, and solid lines those found experimentally.

The values of half-width (i.e. the values of the angles at which the intensity of scattered

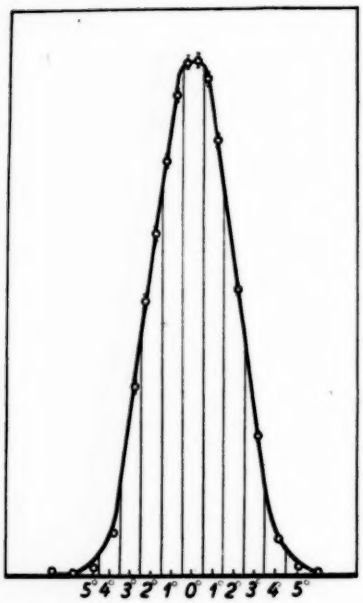

FIG. 14. Curve of the electron beam taken with the rotation of the counter round the target axis. On the axis of the abscissae the angle through which the counter turns are plotted; on the axis of the ordinates the number of electrons is plotted.

electrons is diminished by "e" times given in Table I columns IX and X) were found from the experimental and theoretical curves (Fig. 12).

The analysis of these results and the curves given in Fig. 12, show that the discrepancy between the experimental results and Williams' theory is not very great. The experimental value of the half-width is smaller than the theoretical value by only 3–5 percent.

As the atomic number of the scatterer is increased, this discrepancy also increases and for Ta, Au, and Pb reaches 10–13 percent.

The discrepancy has a systematical character which increases with the increase of the atomic number. This can be seen particularly clearly in Fig. 15, where the dependence of $\theta(\sigma/A)^{-\frac{1}{3}}$ on Z is given. Such graphical representation is possible in our case, because the thickness of the scattering foils was chosen so that the half-width of the scattering θ varies in all cases only between small limits (from 9.8 to 11.4 degrees) and the value "M" under the logarithm in Eq. (4) changes only slightly. The dashed curve in Fig. 15 gives the theoretical dependence of $\theta_B(\sigma/A)^{-\frac{1}{3}}$ from Z, and the circles and the solid curve give the experimentally found dependence.

As can be seen from these curves, there is a systematic deviation of the experimental values from the theoretical values, which lies outside possible experimental error. For light elements this deviation is of the order 4 percent, for the heavier elements it reaches 10–13 percent.

4. The Comparison with the Goudsmit and Saunderson[8] Theory

We compared our results with the theory of multiple scattering given by Goudsmit and Saunderson. As can be seen from columns IV and VII of Table II, our results are in perfect agreement with this theory for elements Al, Fe, Cu, Mo, Ag, and Sn. (The deviation does not exceed 1 percent; see Fig. 15.) For heavy elements the experimentally found scattering is smaller than that theoretically calculated by 10–13 percent. This discrepancy lies outside possible experimental errors.

5. Comparison with the Bethe, Rose, and Smith[5] Theory

In column VI of Table II are given the theoretical values of Gauss half-widths, calcu-

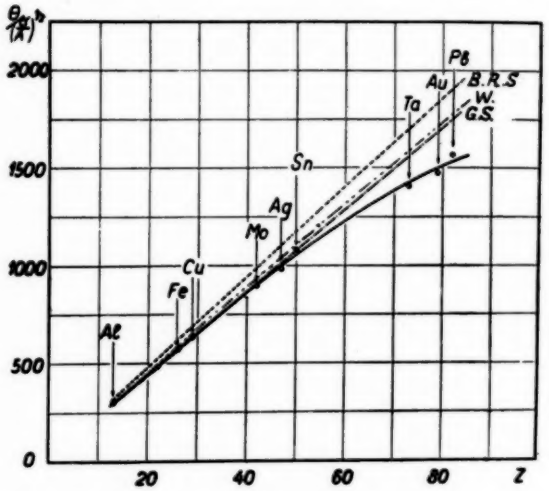

FIG. 15. On the axis of abscissae the atomic number Z is plotted; on the axis of the ordinates the values $\theta(\sigma/A)^{-\frac{1}{3}}$ are plotted. By the circles and solid line curve the experimental results are depicted. The dash-dotted curve is calculated according to the Goudsmit and Saunderson theory. The dot-dot-dashed curve is calculated according to Williams' theory. The dotted curve is calculated according to the theory of Bethe-Rose-Smith.

[8] S. Goudsmit and J. L. Saunderson, Phys. Rev. **58**, 37 (1940); **57**, 24 (1940).

TABLE II. Scattering of electrons whose energy is 2.25 Mev. The angles are given in degrees. θ_{exp} is the half-width value of the experimental Gauss curve. $\theta_{G.S.}$ is the half-width value according to the theory of Goudsmit-Saunderson. θ_{w} is the half-width of the Gauss curve according to Williams' theory. $\theta_{B.R.S.}$ is the half-width of the Gauss curve according to the theory of Bethe, Rose, and Smith.

Element	Z	θ_{exp}	$\theta_{G.S.}$	θ_{w}	$\theta_{B.R.S.}$	% deviation of θ_{exp} from $\theta_{G.S.}$	% deviation of θ_{exp} from θ_{w}	% deviation of θ_{exp} from $\theta_{B.R.S.}$
I	II	III	IV	V	VI	VII	VIII	IX
Al	13	9.50	9.40	9.85	9.95	+ 1.1	− 3.7	− 4.5
Fe	26	9.60	9.60	9.90	10.30	0.0	− 3.0	− 7.2
Cu	29	10.40	10.50	11.05	11.35	− 0.9	− 3.0	− 8.4
Mo	42	10.25	10.35	10.75	11.25	− 1.0	− 4.6	− 8.9
Ag	47	10.20	10.30	10.80	11.45	− 1.0	− 3.7	−10.9
Sn	50	10.65	10.65	10.90	11.55	0.0	− 2.3	− 7.8
Ta	73	9.85	10.95	11.00	11.85	−10.1	−10.5	−16.9
Au	79	9.90	11.35	11.40	12.25	−12.8	−13.1	−19.0
Pb	82	9.70	10.85	10.85	11.80	−10.6	−10.6	−17.8

lated according to the theory of Bethe, Rose, and Smith; in column III the experimental values. In column IX of the same table are given the percent deviations of the theoretical values from the experimental values. It can be clearly seen that the experimental values are always smaller than those theoretically calculated (see Fig. 15).

For aluminum, the half-width of the experimental curve of the scattering is 4.5 percent smaller than the theoretical value; as the atomic number increases, the deviation smoothly increases and for lead reaches 18 percent.

VIII. CONCLUSION

1. The apparatus and experimental method we developed was found exceedingly convenient for studying the multiple scattering of electrons in foils.

2. By this method the multiple scattering of electrons with an energy of 2.25 Mev, was investigated in Al, Fe, Cu, Mo, Ag, Sn, Ta, Au, and Pb foils.

3. From the experimental curves for the scattering, the half-width values of the Gauss curve were found with an accuracy of 3–4 percent.

4. The comparison of the experimental values of the half-width, with theory, showed that for elements from Al ($Z=13$) to Sn ($Z=50$) there is complete agreement with the Goudsmit-Saunderson theory, and the deviation does not exceed 1 percent; comparison with Williams' theory for the same elements shows that the experimental values are 3–4 percent smaller than in theory.

5. For heavy elements Ta ($Z=73$), Au ($Z=79$), Pb ($Z=82$) the experimental values for the half-width are smaller by 10–18 percent than those calculated by Williams and from the Goudsmit-Saunderson theory. This deviation is beyond all possible experimental errors.

6. The comparison of experimental results with the theory of Bethe, Rose, and Smith, shows that the experimentally found values for the half-width of the scattering curves are smaller than those calculated for all investigated elements. For aluminum this deviation is 4.5 percent, as the atomic number increases this deviation also increases and reaches 18 percent for lead.

In conclusion we would like to express our thanks to Dr. A. I. Alikhanov for consultation and to Dr. L. A. Artsimovitch for the discussion of results.

Mesotron Studies with Dual Telescope

F. A. Benedetto,* G. O. Altmann, and V. F. Hess
Department of Physics, Fordham University, New York, New York

(Received January 9, 1942)

A description of a large area dual telescope for mesotron studies is given. Continual check on operation is obtained by constant ratio of counts of upper to lower telescope within the natural statistical fluctuations. Correlations have been made between mesotron intensity and mass temperature of various fractions up to 0.2 of the daily atmosphere; air data being obtained by sounding balloon flights at Lakehurst, New Jersey. Thus, temperature coefficients from 0.37 to 0.46±0.03 percent per degree Centigrade were obtained. It is shown that the temperature coefficient varies as dz/dT when increasing fractions are taken, as expected. Correlations have also been made for the same mesotron intensities with change of height of two levels of the daily atmosphere. The assumption that mesotrons are produced throughout the atmosphere according to the distribution of the air mass leads to a mean rest lifetime rather smaller than that obtained by other methods.

IN a previous article[1] a preliminary analysis was made of mesotron intensity correlations with the temperature of various fractions of the *standard* atmosphere. It is the purpose of this article to present a description of the cosmic-ray telescope used in this investigation, and to submit further developments in the analysis of the data.

GENERAL DESCRIPTION OF THE TELESCOPE AND RECORDERS. TESTING

The telescope, devised by Professor W. F. G. Swann and one of us (V.F.H.), combines the features of large, well-defined sensitive area with moderately small solid angle. The complete assembly consists of six trays of Geiger counters arranged in vertical train; alternate trays are so connected for coincidence counting that in reality there are two independent but interposed telescopes of three trays each. The screening for vertical rays is provided by lead plates totaling ten centimeters between the first and second trays, and additional lead plates totaling twelve centimeters between the second and third trays of the telescopes. It is evident that by this arrangement in which both telescopes are subject to the same events a self-monitoring system is obtained; reliability of operation was guaranteed by the fact revealed by the tests that the two counters gave a constant ratio within the limits of statistical fluctuation. In each tray are 16 counters so disposed as to overlap one another and provide a continuous sensitive area. Arrangement of counters, trays and absorbers is illustrated in Fig. 1.

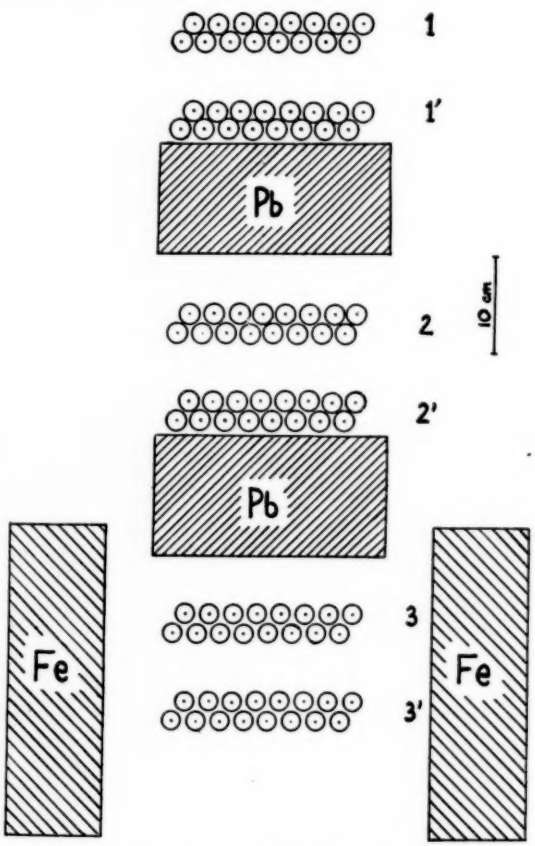

FIG. 1. Arrangement of counters, counter trays, and absorbers.

* Now at St. Mary's College, St. Marys, Kansas.
[1] V. F. Hess and F. A. Benedetto, Phys. Rev. **40**, 610 (1941).

TABLE I. r and α for temperature variations at indicated km levels and for $\bar{\theta}_{16}$.

	i vs. θ_0	i vs. θ_3	i vs. θ_6	i vs. θ_9	i vs. θ_{12}	i vs. $\bar{\theta}_{16}$	I vs. $\bar{\theta}_{16}$
$-r$	0.76±0.04	0.73±0.05	0.71±0.05	0.70±0.05	0.24±0.10	0.73±0.05	0.79±0.04
$-\alpha$	0.40±0.02	0.36±0.02	0.31±0.02	0.29±0.02	0.16±0.07	0.59±0.04	0.70±0.04

Note: The temperatures of the 0 km level ranged between 27 and −1°C, for 3 km between 13 and −21, for 6 km between −3 and −41, for 9 km between −24 and −52, for 12 km between −44 and −69 and the average temperature up to 16 km ranged between −18 and −37°C. α is given in percent per degree C.

TABLE II. r_f and α_f as functions of $T_f \cdot [\partial z/\partial T]_f$ and average $[\partial z/\partial T]_f$ for corresponding fractions.

	r_f	α_f	$[\partial z/\partial T]_f$ m/°C	Av. $[\partial z/\partial T]_f$ m/°C
I vs. $T_{1/5}$	−0.71±0.05	−0.37±0.03	13.3±2.2	17
I vs. $T_{2/5}$	−0.70±0.05	−0.40±0.03	21.8±1.8	18.5
I vs. $T_{3/5}$	−0.72±0.05	−0.41±0.03	29.7±0.5	20.5
I vs. $T_{4/5}$	−0.75±0.05	−0.46±0.03	49.3±0.9	24

The counters, 19.3 cm×2.0 cm, are of the glass envelope, copper cylinder, argon-oxygen type, and were constructed under the supervision of Mr. W. E. Ramsey of the Bartol Research Foundation. Anti-coincidence tubes are used across the ends of the counters of the top and bottom trays of each telescope to avoid difficulties due to slight changes in longitudinal sensitivity of the counters. The sensitive area thus defined is 321 cm². The distance between top and bottom trays is 65.7 cm, thus the solid angle subtended is 0.297 steradian or 4.7 percent of the total hemisphere. All amplifying tubes and connections are well shielded against stray electrical fields.

The lowest tray of each telescope is screened against side showers by an iron "wall" of four inches thickness. This "wall" weighs approximately one ton and is built on two L-shaped trucks mounted on rollers to facilitate periodic inspection of apparatus. Location of apparatus is in a basement laboratory beneath three floors and roof; with vertical rays screened by this and the 22-cm lead absorber of the apparatus the average rate of counts is ~10 counts/min.

The recorders are of a new type recently developed by Professor W. F. G. Swann. They consist essentially of a wheel on whose inside rim are milled a series of teeth; a magnetically operated plunger records a count by being pulled up against the sloping edge of a tooth and returning to its initial position against another sloped tooth, thereby rotating the wheel one division. Though in the special arrangement used by us the recorders are not to be considered *fast* they are certainly sufficiently fast for this type of counting. Their particular advantage is that overshooting is impossible, and reliability is insured by their sturdy construction.

In a device of this sort where many Geiger counters are employed, in this application 108 altogether, it is essential that operation be checked periodically since it is possible for failure of a single counter to go undetected for some time. A special test set was constructed by which it is possible to plug into a whole tray of 16 counters and test them simultaneously for paired coincidences. For routine checking however it is found that satisfactory results are obtained much more rapidly by checking each counter visually with an oscilloscope. Only four tubes have failed over a period of seven months operation.

CAMERA AND POWER SUPPLIES

Photos of recorder dials are taken at two-hour intervals by means of a small camera. Sufficient illumination is afforded by a No. 1 Photoflood lamp at about $\frac{1}{5}$-sec. exposure to give detailed records on Eastman Kodak "Insurance Bromide paper." A small Syncron motor takes up the paper continuously and controls the impulse commutator. At two-hour intervals an auxiliary motor (1 r.p.m.) is triggered by the impulse commutator; a cam device on this auxiliary motor operates two spring switches, one serving to keep the auxiliary motor running until the end of the cycle, the other allowing a momentary current to pass through the series connected photoflood lamp and magnetic device for the camera shutter.

The high voltage, −1012.5 v, is furnished by a set of B-batteries and is common to both tele-

scopes. Likewise all filaments are supplied from a storage battery which is on floating charge. Two separate power packs are used for the thyratron plate supplies and two neon stabilized packs furnish all bias potentials and plate current for the two telescopes, it being found necessary to have separate sources for the two telescopes to avoid electrical interaction.

OBSERVATIONS

Various Temperature Correlations

Most of our effort has been directed towards correlating ground mesotron intensity with temperature variations of different fractions of the atmosphere.[1] Data for 12-hr. (6 P.M.–6 A.M.) mean values of mesotron intensity observed between March 23 and July 31 (1941) are given in Table I. Mesotron data for the interval April 3 to August 21 were later recomputed according to 24-hr. means (6 P.M.–6 P.M.) and gave a more symmetrical distribution around the times of the Lakehurst sounding balloon flights, 4–6 A.M. For this latter analysis average *mass*[1] temperatures of the daily atmosphere were used; these latter results are given in Table II.

The following symbolism is used in Tables I and II:

i = 12-hr. mesotron mean values (6 P.M.–6 A.M.).
I = 24-hr. mesotron mean values.
θ = temperature *at* levels indicated by subscript (in km).
$\bar{\theta}_{16}$ = spatial average temperature up to 16 km.
T = *mass* temperature for fractions indicated by subscript $= [\int_{P_1}^{P_2}\theta dp]/[\int_{P_1}^{P_2}dp]$.
r = product-moment correlation coefficient.
α = temperature coefficient.

Table I indicates that there are increasingly good correlations as temperatures *at* levels approaching ground are used. The reason for this is principally meteorological: Temperature changes of the atmosphere occur primarily and more intensely near ground, particularly as far as changes from day to day are concerned. The temperature at the height of 12 km bears very little relation to day-to-day changes of the lower atmosphere, hence poor correlation with cosmic-ray intensity and a low temperature coefficient are obtained. From these values no preponderance of mesotron production at any specific level can be deduced.

The correlations in the last two columns of Table I are interesting for purposes of comparison with other authors but the spatial average temperatures as used there have no importance for the expected "air mass effect;" also total changes of temperature are diminished by the constancy of the temperature of the upper region which in turn makes the value of α unduly high.

When daily atmosphere values are used, α appears to be a slightly increasing function with increasing fractions of the atmosphere as in Table II. In all cases so far considered the fractions are taken from ground upward. The correlation coefficients for all these fractions are remarkably high and indicate that the values of α are fairly reliable. Increase of α with increasing fractions must be expected from the following consideration. By definition $\alpha = -[1/I][\partial I/\partial T]$, and if it is assumed that an increase of intensity is linearly proportional to a downward shift of air mass, α can be expressed $\alpha = [1/L][\partial z/\partial T]$ where L is a constant, corresponding to the average path length of the mesotrons from their points of origin until decay ("life range"). Thus average values of $[\partial I/\partial T]_f$ over certain fractions (f) of the atmosphere should be proportional to the corresponding *average*[2] $[\partial z/\partial T]_f$, as well as to α_f. Table II shows the values actually obtained. Some discrepancy from proportionality is to be expected as the number of data collected so far is rather small for this particular analysis.

CORRELATIONS WITH HEIGHT VARIATIONS OF ATMOSPHERIC CENTER OF GRAVITY

From the ordinary expression for the temperature coefficient

$$\alpha = -(1/I)(\partial I/\partial T) \equiv -(1/I)(\partial I/\partial z)(\partial z/\partial T) = (1/L)(\partial z/\partial T),$$

it follows that

$$L = -1/[(1/I)(\partial I/\partial z)] \equiv -1/\beta, \qquad (1)$$

where ∂z is the average variation in height of the region where mesotrons are produced. This region would be beneath the top of the atmosphere by some distance of matter traversed.

[2] *Average* $[\partial z/\partial T]_f$ values were obtained by plotting the actual values of $[\partial z/\partial T]_f$ for the upper boundary of f against the pressure and graphically integrating over the fraction in question.

However, since the barometer effect (total mass above the apparatus) probably affects both the distribution of production as well as that of absorption of mesotrons it was thought best to associate production levels with definite fractions of the prevailing atmosphere.

As a starting point, therefore, in our studies of mesotron variation as a function of changes of height of assumed mean production levels, the center of gravity of the daily atmosphere was first taken as the production level. Mesotron readings were the same 24-hour mean values as in the temperature correlation series; daily height variations of the center of gravity were taken from the height *vs.* pressure curves. It is seen from Eq. (1) that temperature does not enter into consideration in this correlation. Results for the level of the center of gravity gave:

$$r=-0.70\pm0.04$$

and

$$\beta=-17.5\pm0.9 \text{ percent/km.}$$

By taking a higher level, $p=400$ mb, we obtain the following

$$r'=-0.64\pm0.05$$

and

$$\beta'=-13.3\pm0.7 \text{ percent/km.}$$

To reduce β' to changes of height as they occur at the center of gravity, β' is multiplied by the inverse ratio of the mean heights of the two levels, so that

$$\beta'_{\text{red}}=(7.4/5.7)\beta'=-17.3 \text{ percent/km}$$

quite within the range of β, as given above.

The average path length L of the mesotrons can be computed from Eq. (1)

$$L=-1/\beta=5.7\pm0.4 \text{ km,}$$

provided that the average production level is not too far from the atmospheric center of gravity. For a mesotron spectrum of only 1 Bev mean energy, $\gamma=12.5$; and taking the above value for L we have $\tau_0\gamma=1.9\times10^{-5}$ sec. and $\tau_0=1.5\times10^{-6}$ sec. From $\partial z/\partial T=-\alpha/\beta$ we may also obtain an independent determination of the change of the height of the atmospheric center of gravity with the lower mass temperature. The value obtained, 22.5 meters/°C, checks with our study of the meteorological data which gave for the height variation of the center of gravity, $h_{cg}\backsimeq5.7$ km, a value of $\partial z/\partial T=23$ meters/°C.

CONCLUSION

Since it is rather probable that the mean energy of the mesotrons registered by this apparatus is considerably greater than 1 Bev, it would seem difficult to reconcile the above results with the heretofore accepted mean lifetime, $\sim2\times10^{-6}$ sec., of the mesotron at rest, unless one is willing to assume that the mesotrons are exclusively produced in the uppermost fifth of the atmosphere. That the production of mesotrons probably extends throughout the total atmosphere is indicated by our results as well as those of previous workers.[3-5]

ACKNOWLEDGMENTS

This investigation was made possible by the financial aid of the American Philosophical Society and the Carnegie Institution of Washington. We are especially indebted to Professor W. F. G. Swann for his design of the telescopes and recorders as well as for his allowing their construction in the shops of the Bartol Foundation. We wish also to thank Mr. Walter J. Moxom and Mr. Holzman of the La Guardia Airport Weather Bureau, and Mr. J. H. Kimball and Mr. D. R. Morris of the Weather Bureaus of New York for furnishing necessary meteorological data.

[3] M. Schein, E. O. Wollan, and G. Groetzinger, Phys. Rev. **58**, 1027 (1940).
[4] M. Schein, W. P. Jesse, and E. O. Wollan, Phys. Rev. **59**, 615 (1941).
[5] N. F. Beardsley, Phys. Rev. **59**, 402 (1941).

The Nuclear Spin and Magnetic Moment of K^{40}

J. R. ZACHARIAS
Columbia University and Hunter College, New York, New York*

(Received January 9, 1942)

The molecular beam magnetic resonance method has been employed to observe the nuclear spin and the h.f.s. $\Delta\nu$ of K^{40}. The apparatus and procedures of this experiment are different from those previously employed in the magnetic resonance method because of the small natural abundance of K^{40} and because both the nuclear spin and h.f.s. $\Delta\nu$ were previously unknown. The spin is shown to be 4 and the h.f.s. $\Delta\nu = 1285.70 \pm 0.1$ megacycles per second. The doublet is inverted. By comparison with the known nuclear moment of K^{39}, the nuclear moment of K^{40} is taken to be -1.290 nuclear magnetons.

BECAUSE of the abnormally long half-life of the beta-activity of potassium, it has long been suspected that the nuclear spin of K^{40} is large and integral. Even before Smythe and Hemmendinger[1] had shown that the radioactivity of potassium is undoubtedly due to K^{40}, it was indicated by Bethe and Bacher[2] that the long lifetime is not in contradiction with the Fermi beta-ray theory. The success of their argument depends on the assumption of a nuclear spin of 3 or 4, and since nuclear spins up to 9/2 were known, there was no particular objection to this. However, until the present experiment no successful attempt to observe the nuclear spin of K^{40} has been reported, although at least one serious attempt by Millman and Rabi† was made by the well-known molecular beam method of zero moments. All this is doubtless due to the small natural abundance of K^{40} given by Nier[3] as one part in 8600.

A preliminary report[4] of the results to be given in this paper has already been presented before the American Physical Society, and it was there given that the nuclear spin of K^{40} is indeed 4, and further that the nuclear magnetic moment is large (1.29 nuclear magnetons) and negative. The experimental method is a modification of the molecular beam magnetic resonance method which follows in many details the experiments described by Kusch, Millman, and Rabi[5] in a paper called "The Radiofrequency Spectra of Atoms," and hereinafter referred to as KMR. They report observations of the hyperfine structure for the atoms of Li^6, Li^7, K^{39}, and K^{41} and its Zeeman effect and Paschen-Back effect. In subsequent papers they have also studied Na, Rb, and Cs. Their observations are of two types, which can easily be understood by referring to Figs. 1 and 2, which represent the energy levels of an alkali atom in a magnetic field; Fig. 1 for a spin of $\frac{3}{2}$ and Fig. 2 for a spin of 4. These two figures should be enough to show the type of behavior for any spin.

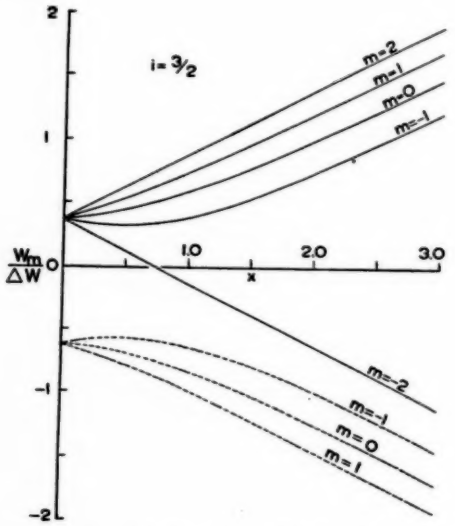

FIG. 1. Diagram of the energy levels of an atom with electronic angular momentum $J=\frac{1}{2}$ and nuclear spin $I=\frac{3}{2}$. The full curves are for the large $F=2$; the dotted curves are for $F=1$.

* Publication assisted by The Ernest Kempton Adams Fund for Physical Research of Columbia University.

[1] W. R. Smythe and A. Hemmendinger, Phys. Rev. **51**, 178 (1937).

[2] H. A. Bethe and R. F. Bacher, Rev. Mod. Phys. **8**, 82 (1936). See p. 196.

† Never published.

[3] A. O. Nier, Phys. Rev. **48**, 283 (1935).

[4] J. R. Zacharias, Phys. Rev. **60**, 168 (1941).

[5] P. Kusch, S. Millman, and I. I. Rabi, Phys. Rev. **57**, 765 (1940).

In Figs. 1 and 2 each energy state is specified by a value of $F=(I+\frac{1}{2})$ or $(I-\frac{1}{2})$ and the magnetic quantum number m. Those characteristic features of these curves which are the same for atoms with different nuclear spin or magnetic moment are:

(1) The number of states for either F is $2F+1$.

(2) In a magnetic field stronger than that given by $x=1$, all but one of the states with the larger F increase in energy with increasing field, and all of the states with the smaller F decrease in energy with increasing field. Thus the only possible transition between two adjacent states with the same F but with opposite sign for the atomic moment in high field is that between $m=-(I+\frac{1}{2})$ and $m=-(I-\frac{1}{2})$.

(3) In a given weak field the intervals between adjacent levels are all equal and equal to $(g_J-g_I)\mu_0 H/(I+\frac{1}{2})$. As will be indicated later the small term g_I provides a means of finding the sign of the nuclear moment.

(4) The diagrams are drawn for atoms with positive nuclear moment. For negative moment or inverted h.f.s. doublet the diagrams are inverted in the following respects: in weak field, states with the larger F have the smaller energy and the spacing about zero is inverted; item (2) above should read: in strong field, all states with smaller F increase in energy with increasing field, and all but one of the states with larger F decrease in energy with increasing field; the signs of all m's are reversed so that the adjacent pair of states with different sign of moment in high field are $m=(I+\frac{1}{2})$ and $m=(I-\frac{1}{2})$. All of the arguments of the present paper will be given with the notation for positive nuclear moment and with that diagram in mind.

One of the methods used by KMR[5] was to observe the frequencies associated with transitions between the two F levels of the h.f.s. doublet in very weak magnetic field. This yields a set of lines, the center of gravity of which is the h.f.s. $\Delta\nu$ itself and, if the magnetic field in which transitions occur is sufficiently weak, the spacing between adjacent members of the set of lines is $(g_J-g_I)\mu_0 H/h(I+\frac{1}{2})$. Their other procedure was to observe the frequencies associated with transitions in strong field of $m_F(\Delta m_F=\pm 1)$ with constant F. These lines occur at a frequency $\Delta\nu/(2I+1)$ if the field is sufficiently strong. Both of these methods of observation require some fore-knowledge of the h.f.s. $\Delta\nu$ in order to know in what part of the electromagnetic spectrum to search for transitions.

The present experiment differs from those of KMR on the other alkali atoms in that neither the nuclear spin nor the h.f.s. $\Delta\nu$ was known at all before starting the experiment. And also, since the natural abundance of K^{40} is so small, a gross search for radiofrequency spectral lines for K^{40} in the presence of those of K^{39} and K^{41} would be futile. However, there is little doubt that the nuclear spin of K^{40} with even atomic weight is integral and therefore different from the spin of K^{39} and K^{41} which is $\frac{3}{2}$. The following method was therefore devised.

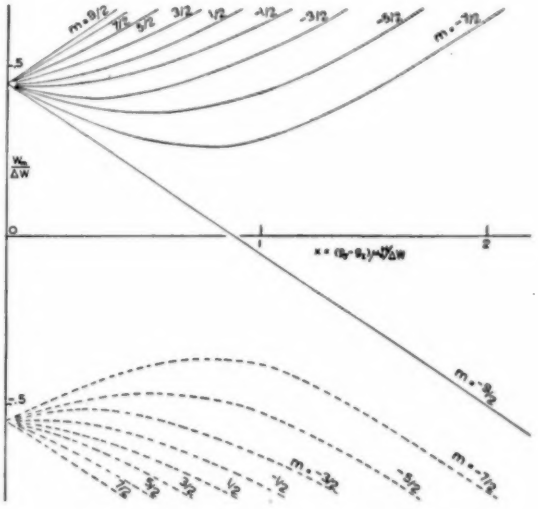

FIG. 2. Diagram of the energy levels of an atom with electronic angular momentum $J=\frac{1}{2}$ and nuclear spin $I=4$. The full curves are for the larger $F=9/2$; the dotted curves are for $F=7/2$.

The transition selected for use in this investigation is that between the two states $m_F=-(I-\frac{1}{2})$ and $m_F=-(I+\frac{1}{2})$ for $F=(I+\frac{1}{2})$ (see Fig. 1 or 2). The energy required for this transition in weak field is $(g_J-g_I)\mu_0 H/(I+\frac{1}{2})$ and except for the almost negligibly small term g_I is independent of the nuclear magnetic moment and of the h.f.s. $\Delta\nu$ to which it gives rise. That is, if the magnetic field is so weak that the coupling between the nucleus and the atomic electrons is not broken then the atom behaves as though its angular momentum is $(I+\frac{1}{2})$ and the tightness of the coupling makes no difference. Thus in a

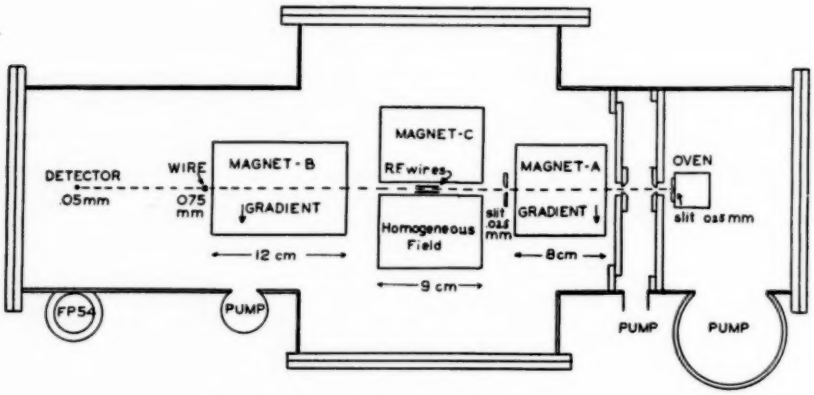

FIG. 3. Schematic diagram of apparatus.

sufficiently small magnetic field, transitions of the type referred to will occur at different frequencies for atoms with different nuclear spins, and at the same frequency for atoms with the same spin regardless of the $\Delta\nu$. And since the only other alkali nucleus with integral spin is Li^6, it is possible to isolate K^{40} in spite of its small natural abundance.

APPARATUS

Figure 3 is a schematic diagram of an apparatus constructed especially for experiments of this type. As in all molecular beam magnetic resonance experiments on alkali atoms, the molecular beam originates in an oven with a narrow slit covering its aperture. In this case the slit height is 1 cm and the width 0.025 mm so as to obtain a strong beam. The chamber in which the oven sits is pumped at 100 liters/sec., and is isolated from the main body of the apparatus by two slits which are adjustable for width and position by means of external screws. The beam is defined as usual by a collimating slit situated between magnets A and C and set at a width of 0.025 mm. The tungsten detecting filament (0.05-mm diameter) is altogether 50 cm from the oven. This is the shortest beam so far used for the magnetic resonance method and the total beam intensities are correspondingly very high (about 10^{-9} amp. at beam center).

The iron electromagnets A and B provide inhomogeneous fields with a ratio of gradient to field of about 1.2 over a beam height of 1 cm. This was obtained by suitable choice of circular milling cutters used to shape the pole pieces. These magnets are similar to those used by Millman, Rabi, and Zacharias[6] except that the dimensions were chosen to suit the peculiarities of this experiment. Thus, to reach the fields required, twenty turns of copper tubing were used instead of four. Magnet C has flat pole pieces 6 mm apart and provides a very uniform field over the beam height and that part of the path which is occupied by the radiofrequency transition field. The deflecting magnets A and B have their gradients in the same direction so that a beam of alkali atoms will be so strongly deflected that none strikes the detector. Scattering of the beam by the small amount of residual gas in the apparatus prevents reduction of the beam intensity below 0.1 percent. Even this requires placing a thin obstacle wire in the direct line of the beam to cut out any alkali molecules which would not be deflected by the magnets. If the radiofrequency field is set at a value for producing a transition accompanied by a change of the sign of the total atomic magnetic moment, then those atoms will be refocused by the magnet B and will detour around the obstacle wire and fall on the detector. Thus in this apparatus magnetic transitions appear as peaks of beam intensity.

The reason for this departure from the usual procedure of the molecular beam magnetic resonance method is obviously to be found in the small abundance of K^{40}. The transition selected for study is that between $m=-(I+\frac{1}{2})$ and $m=-(I-\frac{1}{2})$ for which the net atomic moments

[6] S. Millman, I. I. Rabi, and J. R. Zacharias, Phys. Rev. **53**, 384 (1938).

have opposite sign in the high magnetic fields used for deflecting and refocusing. Thus, it is just these states that can be made to detour about the obstacle wire and only with the aid of the obstacle wire to cut out the beam was it possible to make the background intensity sufficiently low so that a peak due to K^{40} would stand out above the fluctuations of the background.

The radiofrequency field is produced in the central portion of the homogeneous field magnet C by means of a loop of wire similar to that used in other magnetic resonance experiments. This experiment was conducted with two different loops, both of which were capable of producing the r-f field over the beam height of 1 cm. The first loop used was made of two strips, 3 cm long, of half-inch by sixteenth-inch copper spaced 1 mm apart. By slotting and soldering, these were made to be water cooled. The r-f current is fed in at one end of one strip and out the same end of the other strip. Thus the beam is in the r-f field for 3 cm. The other loop was made simply by bending a piece of half-inch by sixteenth-inch copper into the form of a vertical hairpin without water cooling. For this one the r-f field traversed by the beam is only one-half inch long.

PROCEDURE

A beam of atomic potassium is obtained and the slits are set in line having been made vertical previously by optical means. This is especially important because the obstacle wire cannot be very much broader than the beam but must block it completely. The obstacle wire was itself a plumb line of number 40 copper wire with a small amount of soft vacuum wax at the point of its support to provide the necessary damping. The obstacle wire can be accurately centered in the beam by adjusting its position until on moving the detector filament to either side of the beam center the same intensity is read. It is only after this procedure is carefully followed that the amount of residual beam at the central position is small enough to make the experiment possible.

The magnets A and B are then turned on and the beam intensity reading rises. This can occur for several reasons. First, atoms which are scattered in the oven chamber and which are not in the geometrical line of the beam can be deflected onto the detector by the magnets. Second, transitions of atomic magnetic moments could occur in the space between the magnets A and B because of collisions with other molecules (improbable), or because of sudden changes in value or directions of magnetic fields near the entrances to the various magnets. In fact, this last effect can be made extraordinarily large by reducing the magnetic field in the magnet C to some value near zero. With all of these effects, except the last, the beam still reads less than 0.1 percent of the original beam if the vacuum is good and the lineup is careful.

The radiofrequency oscillator is set at a convenient frequency, say, 4 megacycles and the current in magnet C is adjusted until a transition is observed by a sharp rise in the beam current. If this rise of intensity depends on the frequency of the r-f oscillator then since the nuclear spins are the same, the transition of m_F from -2 to -1 for both K^{39} and K^{41} is probably being observed. If the magnetic field were readily determined then this fact could be checked immediately. Because of hysteresis the magnet calibration against ampere turns is of no use at low fields and the following indirect method of checking is used. If the frequency of the r-f oscillator is raised, then the magnetic field must be correspondingly increased to observe transitions. If this process of increasing the field and frequency is continued, then the single observed transition becomes double, one large peak and one small peak. The large one is attributed to K^{39} and the small one to K^{41} since the nuclear spins are the same but the h.f.s. $\Delta\nu$'s are different. Since the h.f.s. $\Delta\nu$'s of both of these nuclei are known one of the peaks can be used to calculate the value of the field (by use of the Breit-Rabi formula) and the frequency for the other can be predicted. After this procedure was followed several times it became easy

TABLE I. Observed frequencies of peaks attributed to K^{40} with the corresponding frequencies for transitions of K^{39}. In the limit of small field the ratio ν_{40}/ν_{39} should approach 4/9. These observations were made with r-f field wires 4 cm long by 1 cm high.

ν_{39} Mc	ν_{40} Mc	ν_{40}/ν_{39}	ν_{39} Mc	ν_{40} Mc	ν_{40}/ν_{39}
3.924	1.72	0.442	11.40	4.87	0.427
3.88	1.714	0.442	16.18	6.775	0.419
5.92	2.575	0.441	17.007	7.096	0.418
7.896	3.405	0.432	32.034	12.87	0.402

to tell immediately that the observed peaks were due to the transitions mentioned above.

In searching for K^{40}, a procedure somewhat similar to the above was followed. First a magnetic field was set and determined by observing the transition (m_F from -2 to -1) for K^{39} at a frequency ν_{39}. If the field is weak then $H=2h\nu_{39}/\mu_0$. The field is held constant and the frequency of the r-f oscillator is changed to the value appropriate to K^{40} under the assumption that its spin is some integer 0, 1, 2, 3, 4, 5, or 6. These frequencies bear a simple relation to the frequency, ν_{39}, used for K^{39}, i.e., $\nu_{40}=\nu_{39}(I_{39}+\frac{1}{2})/(I_{40}+\frac{1}{2})$. We neglect g_I compared with g_J and the decoupling which shows itself in the curving of the state $m_F=-(I-\frac{1}{2})$. Thus assuming that the nuclear spin of K^{40} is 4, then for the same magnetic field we have $\nu_{40}=\nu_{39}4/9$.

RESULTS

The procedure outlined above was followed for assumed values of the spin of 0, 1, 2, 3, 4, 5, and 6. For none of these except 4 was there any sign of transition. For spin 4 the data are exhibited in Table I. The changes of beam intensity which occurred for the values of the frequencies ν_{40} were completely consistent with the known natural abundance but were not large enough to measure precisely nor to show resonance curves. The reason for this is as follows. Although the maximum possible amount of beam refocused for the observed transitions of K^{39} is 25 percent of original beam intensity, only 10 percent is observed because of the presence of the obstacle wire. That is, the gradients of the magnets were too small to force all atoms about the obstacle wire. For K^{40} with spin 4 the maximum possible amount to be expected is 11 percent of the total K^{40}-beam which is only 1/8600 of the beam. Thus only 5 parts in 10^6 of the main beam are expected to appear as a peak for K^{40} against a background of about 0.1 percent. This background therefore had to remain constant to 1 part in 200, just to allow a peak to be observed. It is possible to make observations by turning the r-f oscillator off and on and noting the galvanometer deflections. This procedure makes it important to have the FP54 detector (sensitivity 5×10^{-17} amp./mm) insensitive to the r-f oscillation. Very careful shielding and by-passing of leads made this possible at all but a few frequencies for which parts of the apparatus resonate to the r-f. Because of the wide frequency range this requirement was difficult to meet.

TABLE II. Observed frequencies of peaks attributed to K^{40} with the corresponding frequencies for transitions of K^{39}. These observations were made with r-f field 1 cm long by 1 cm high. The values of the magnetic field were calculated from the frequencies for K^{39} by means of the Breit-Rabi formula. The column labeled denominator of Eq. (1) is listed to indicate the precision of the calculated values of the h.f.s. $\Delta\nu$'s. They are all reliable to about ±0.01. Thus the precision of the calculated $\Delta\nu$ values is inversely proportional to these denominators.

ν_{39} Mc	ν_{40} Mc	Magnetic field calc. gauss.	denom. Eq. (1)	h.f.s. $\Delta\nu$ of K^{40} assumed positive	assumed negative
17.040	7.157	22.19	0.32	1226.	1260.
29.974	12.118	36.52	0.86	1254.	1276.
31.840	12.805	38.45	0.96	1260.	1280.
42.608	16.688	48.99	1.57	1269.	1283.
42.624	16.666	49.00	1.56	1274.	1288.
42.632	16.677	49.01	1.57	1268.	1282.
42.660	16.687	49.04	1.57	1269.	1284.
125.50	42.760	110.21	8.79	1280.0	1285.6
125.608	42.777	110.27	8.79	1281.9	1287.6
125.615	42.780	110.27	8.79	1281.7	1287.4
125.636	42.792	110.28	8.80	1281.0	1286.7
388.96	124.32	236.33	51.48	1284.6	1286.4
389.00	124.35	236.34	51.51	1284.2	1285.8
389.00	124.37	236.34	51.51	1284.2	1285.8
389.10	124.397	236.39	51.57	1284.0	1285.5
389.14	124.418	236.40	51.57	1283.9	1285.4
389.48	124.53	236.55	51.63	1284.1	1285.6
389.50	124.57	236.55	51.67	1283.5	1285.0
389.96	124.691	236.74	51.72	1284.9	1285.7
390.86	125.02	237.12	51.95	1283.9	1285.4

Table I shows that the observed ratio ν_{40}/ν_{39} does not remain quite constant as the field is increased. This arises because, for the fields used, decoupling of the nuclear spin and the atomic electrons is beginning for both K^{39} and K^{40}. One should be able to calculate the h.f.s. $\Delta\nu$ of K^{40} from this observed departure from constancy, but this set of data is not sufficiently good for the purpose for two reasons. First the chief cause of the departure is the h.f.s. decoupling of K^{39} and the second the data are not sufficiently accurate because they were taken with a length of r-f field for which the magnet was not sufficiently uniform. Consequently a smaller r-f region was used, by using smaller wires for the r-f and the data of Table II were taken. Table II is a summary of data taken to determine the h.f.s. $\Delta\nu$ of K^{40} and at the same time to demonstrate that the resonances observed are really consistent with the assumption of an atom with a nuclear spin of 4.

Table II contains values of the h.f.s. $\Delta\nu$ of K^{40} obtained when we assume that the nuclear moment is positive (tabulated in the fifth column) and negative (sixth column). These calculations are made with the use of the Breit-Rabi formula, which for these purposes can be put in the following convenient form:[7]

$$\Delta\nu=(\nu-g_I k)(g_J k-\nu)/\{(\nu-g_J k)-(g_J-g_I)k/9\}. \quad (1)$$

In this formula all symbols refer to K^{40} except k which is given by

$$k=\Delta\nu_{39}x_{39}/(g_J-g_I)_{39}$$

with

$$x_{39}=(g_J-g_I)\mu_0 H/\Delta\nu_{39}.$$

Since H is determined by observing the $(m_F=-2)\rightarrow(m_F=-1)$ transition for K_{39}, it is more convenient to eliminate it in terms of the observed quantity ν_{39} by writing

$$x_{39}=(\beta^2-1)/(2\beta-1),$$

where

$$\beta=1+2(\nu-g_I k)_{39}/\Delta\nu_{39}.$$

The actual procedure followed in applying this formula is first to use it without the small correction terms in g_I; then with this preliminary value of $\Delta\nu_{40}$ and the known values of g_I and $\Delta\nu_{39}$ for K^{39} to calculate a preliminary value of the g_I for K^{40}. This value of g_I is sufficiently accurate for the small terms but the sign of the correction terms is not known. The final calculations are made with both positive and negative sign. Thus inspection of columns 5 and 6 of Table II shows these results and that they are self-consistent for the nuclear moment taken negative (g_I positive) whereas they are inconsistent if it is taken positive (g_I negative). The weighted average of the values for the case of negative moment [weight proportional to the denominator of Eq. (1)] is 1285.65 Mc and the nuclear moment is taken to be negative.

Since the values of the $\Delta\nu$ obtained when a positive nuclear moment is assumed are inconsistent with each other by only a few times the possible errors of observation, it was decided to try to observe some other transition to obtain an independent value of the $\Delta\nu$ and if possible, a more precise one. The first obvious transition to try is that between the states $F=(I+\frac{1}{2})$; $m_F=(I-\frac{1}{2})$ and $F=(I-\frac{1}{2})$; $m_F=-(I-\frac{1}{2})$ at a field for which the jump is smallest for then the value of H need not be known well, and the determination of $\Delta\nu$ is as accurate as the observed transition frequencies. But this transition is one involving no change of m_F and if the radio-frequency field is perpendicular to the steady field, this transition would be highly improbable.[8] If K^{40} were an abundant isotope, this would be no great drawback, especially because the transition would occur at a not too difficult radiofrequency (obtainable with a 316-A oscillator) and with abundant isotopes transitions of this type are easily observed. In the present case it was decided to try the two transitions given by $m_F=-7/2$ to $m_F=-5/2$ for $\Delta F=\pm 1$. These states have maxima or minima for some value of the field and for a value of the magnetic field halfway between the maximum for one of the states and the minimum for the other the intervals mentioned above are independent of field and furthermore these are allowed transitions with the present type of r-f field and, in fact, were observed.

Through the kindness of Dr. Fay of the Bell Telephone Laboratories a 368-A oscillator tube was made available before they were generally obtainable and the required frequency near 950 Mc was obtained. On several occasions a pair of very small close peaks were observed. As previously described, observation of these peaks was made by noting galvanometer deflections as the oscillator was turned on and off. One of the chief difficulties with this experiment was associated with keeping the oscillator frequency sufficiently constant during an observation and making it come back to any desired frequency when turned back on. This is true because the theoretical half-width of the expected peaks is about 1/20,000, and it was not possible to obtain enough r-f current to make the half-width larger than that. However, once the reality of the peaks was established the precision of the calculated $\Delta\nu$ was then as good as the readings of the heterodyne wave meter. The separation between the peaks is very small (1 part in 10^4) and could not be

[7] S. Millman and P. Kusch, Phys. Rev. **58**, 438 (1940), Eq. (2).

[8] H. C. Torrey, Phys. Rev. **59**, 293 (1941). See Eq. (19).

observed well. However, as was expected it was possible to observe that the frequencies of these lines were not dependent, in first order, on the magnitude of the magnetic field. This fact substantiates the remark that the observed lines are associated with the transitions to which they are attributed. Also if this insensitivity to value of field were not true, then the lines would not be so sharp because the field is certainly not homogeneous to 0.01 percent. The average of three sets of data gives for the center of the pair 949.43 Mc which yields for the $\Delta\nu$ 1285.74 Mc. In this calculation the Breit-Rabi formula can be used directly and without any assumption of the magnitude or sign of the nuclear moment of K^{40}. Comparing this with the weighted average of the values given formerly 1285.65 Mc, it is easy to see that the negative nuclear moment is the proper one.

Averaging these two values, with no reason to give either one the greater weight, we write $\Delta\nu_{40}=1285.70\pm0.1$ Mc. To evaluate the nuclear moment of K^{40} from this value of the $\Delta\nu$, we make use of the experimental proof by Millman and Kusch[9] for the isotopic pairs Li^6, Li^7, Rb^{85}, Rb^{87}, that the ratios of the nuclear moments as observed by "molecular beam method" are equal to the h.f.s. $\Delta\nu$ ratios, due account being taken for the effect of nuclear spin. Thus we use $\Delta\nu_{39}=461.75$ Mc and $\mu_{39}=0.391$ nuclear magneton and obtain $\mu_{40}=-1.290$ nuclear magnetons, and 0.323 for the nuclear g.

Some discussion is necessary to show why it is believed that the substance giving rise to the peaks in this experiment is indeed K^{40}. First the observed intensity agrees as well as could be expected with the known abundance. Second the detecting filament will respond when cleaned of oxide coat only to elements with a lower ionization potential than sodium. There was no appreciable quantity of the known isotopes of Rb and Cs which have low enough ionization potential, but since they have known spins and moments they would be directly identifiable. Therefore a hitherto unknown isotope of either Rb or Cs could not be present in large enough quantity to have been observed. Third there was no dependence of the observed intensity of the small peaks to the temperature of the oven and it can be concluded that the substance has a vapor pressure of the same order of magnitude as that of potassium.

Although it was not surprising in view of the arguments from beta-ray theory that the spin of K^{40} is large and integral, some use has been made of the fact that the spin is 4 and not 3. Marshak[10] has shown that this spin adds support to the Gamow-Teller theory. On the other hand the large negative moment, as discussed recently by Inglis, does not seem to be readily understandable on a simple nuclear model. In view of the excellent self-consistency of the data for the assumption of negative moment there is little doubt about the correctness of this experimental result. It is of course natural to desire a determination of the sign of the nuclear moment such as was made by Kellogg, Rabi, and Zacharias[11] for H and D or that of Millman[12] by the magnetic resonance method which does not depend on a precise determination of the h.f.s. $\Delta\nu$. With the small abundance of K^{40} these methods do not at the moment seem feasible.

I wish to thank Professor I. I. Rabi, Dr. T. C. Hardy and the other members of the molecular beam laboratory for their assistance and encouragement during this experiment.

[9] S. Millman and P. Kusch, Phys. Rev. **60**, 91 (1941).

[10] R. E. Marshak, Phys. Rev. **59**, 957 (1941).

[11] J. M. B. Kellogg, I. I. Rabi, and J. R. Zacharias, Phys. Rev. **50**, 472 (1936).

[12] S. Millman, Phys. Rev. **55**, 628 (1939).

Nature of Electronic Levels in Ultraviolet Spectra of Hydrogen and Alkyl Halides

ROBERT S. MULLIKEN
Ryerson Physical Laboratory, University of Chicago, Chicago, Illinois
(Received December 3, 1941)

The nature of the excited electronic levels involved in the ultraviolet absorption spectra of the alkyl and hydrogen halides, also ICl, IBr, BrCl, is discussed. On the basis of band structures in the hydrogen halides, and other facts, it is concluded that the excited orbital is of σ type ($s\sigma$?) in the B, C bands, but of $p\pi$ type in the D, E bands. For the upper level of the B and C bands, the coupling changes from nearly J, j-like in the iodides to predominantly L, S-like in the chlorides. The tendency toward L, S-like coupling is greater in the hydrogen than in the alkyl halides. For the B, C "satellites" in HCl, a $4p\sigma$ excited orbital is indicated. The D, E bands show nearly J, j-like coupling for all halides. The natures of the excited orbitals in the various observed Rydberg series are also discussed. According to Price, two of the most prominent Rydberg series start with the A continuum and with the D, E bands, and so, according to the present study, should have σ and $p\pi$ excited orbitals, respectively. It is also concluded that the $np\pi$ "non-bonding" orbital in the normal states of the hydrogen halides and other diatomic hydrides probably is slightly bonding.

I. INTRODUCTION

THE hydrogen and alkyl halides show close analogies to one another in their ultraviolet absorption spectra. At longest wave-lengths (somewhat greater than λ2000 in most of these molecules) comes a continuous absorption region sometimes called A. At somewhat shorter wave-lengths (varying from near λ2000 in the alkyl iodides to near λ1300 in hydrogen chloride) are two strong narrow regions of absorption, not far apart, called B and C. Each of these consists of one or a few strong bands accompanied in the methyl halides by weaker bands. A further pair of regions, similar to B and C but at somewhat shorter wave-lengths, is found in the methyl halides and perhaps in other cases. The longer wave-length of these two regions is generally called D, and its shorter wave-length companion may be called E (Price calls both regions D in the case of the alkyl chlorides). Beginning at and including the D bands, several Rydberg series are observed. Additional fainter bands also are present.

The writer has shown[1] that the A region is explained by a transition from the normal electronic level N to an excited level Q, with MO (molecular orbital) electron configurations as follows:

$$N\colon\ \sigma^2\pi^4,\ {}^1\Sigma^+ \quad \text{or} \quad (\sigma a_1)^2(\pi e)^4,\ {}^1A_1$$
$$Q\colon\ \sigma^2\pi^3\sigma^*,\ {}^3\Pi,\ {}^1\Pi \quad \text{or} \quad (\sigma a_1)^2(\pi e)^3\ (\sigma^* a_1),\ {}^3E,\ {}^1E. \qquad (1)$$

The first set of symbols refers to the hydrogen halides. The second refers to the methyl halides, where the C_{3v} symmetry calls for the new symbols. However, since actually the effects of the changed symmetry on the forms of the orbitals in which we are interested are small, it will be convenient and will lead to no misunderstanding if only diatomic molecule symbols are used, and this will be done throughout the subsequent discussion (see following paper by E. Teller and the writer for critical comments). The orbitals in Eq. (1) are approximately of the forms:

$$\sigma = a(np\sigma_X) + b(1s_H \text{ or } \sigma_{Me});\quad \pi = np\pi_X;$$
$$\sigma^* = c(1s_H \text{ or } \sigma_{Me}) - d(np\sigma_X), \qquad (2)$$

where $np\sigma_X$ or $np\pi_X$ refers to a halogen atom AO (atomic orbital), σ_{Me} to an MO of the methyl group. The MO's σ, π, and σ^* are, respectively, bonding, non-bonding, and anti-bonding. Quantitative theoretical intensity calculations and comparison with observed intensities[1] confirmed that region A is explained in both hydrogen and alkyl halides by the Q, N transition.

II. NATURE OF EXCITED ORBITAL IN B, C BANDS

W. C. Price[2] was the first to study the hydrogen halide absorption spectra in the vacuum region, and discovered regions B, C analogous to those of the alkyl halides. (Similar regions are also found in ICl and similar molecules.) Some time ago[3] the writer concluded that regions B

[1] R. S. Mulliken, J. Chem. Phys. **8**, 382 (1940) and earlier references.

[2] W. C. Price, Proc. Roy. Soc. **A167**, 216 (1938).

[3] R. S. Mulliken, Phys. Rev. **47**, 413 (1935).

TABLE I. Term values in $cm^{-1} \times 10^3$ for halogen atom orbitals.*

Atom	Orbital† $(n+1)s$	$(n+1)p$	nd
Cl	32	20	(14)
Br	31	18	—
I	29	~19	18

* Estimated from data on atomic spectra [cf. R. F. Bacher and S. Goudsmit, *Atomic Energy States* (McGraw-Hill, 1932); also S. Murakawa, Zeits. f. Physik **109**, 162 (1938) on iodine]. For example, the configuration $(3p^4, {}^3P)4s$ of the Cl atom gives five levels (^4P and ^2P) covering a range from 71,934 cm^{-1} to 74,861 cm^{-1} above the $3p^5, {}^2P$ ground state. Subtracting a rough average of these figures from the energy of $3p^4, {}^3P$ of Cl^+ (105,000 cm^{-1} above the ground level of Cl) yields 32,000 cm^{-1}, as given above, as an approximate term value for the $4s$ orbital of chlorine. In the cases of nd of Cl and Br, the data in Bacher and Goudsmid give term values which are too small to be believed, and the estimate given above for Cl is based on data for argon.
† $n = 3$ for Cl, 4 for Br, 5 for I.

and C in methyl iodide both correspond to the excitation of a non-bonding π electron of state N to a non-bonding excited orbital, and suggested that the latter is of the C_{3v} species e, perhaps essentially a $5d\pi$ AO of iodine.[4] The upper levels of B and C would then correspond to:

$$B: (\sigma^2\pi^3, {}^2\Pi_{3/2})nd\pi; \quad C: (\sigma^2\pi^3, {}^2\Pi_{1/2})nd\pi. \quad (3)$$

The observed energy difference between B and C in CH_3I agrees closely with the energy difference between the $\sigma^2\pi^3$ levels $^2\Pi_{3/2}$ and $^2\Pi_{1/2}$ of the CH_3I^+ ion. The magnitude of this difference was predicted by the writer,[3] and then found by Price[5] from the limits of Rydberg series in the absorption spectrum of CH_3I. This agreement would be expected for J–j-like coupling between the $5d\pi$ electron and the CH_3I^+ core.

In his work on the hydrogen halides Price found that in every case the B and C bands consist of a P and R branch together with a strong Q branch. Price did not draw conclusions from this, but according to diatomic band spectrum theory, since state N is $^1\Sigma^+$, the presence of the Q branch shows that the upper levels of B and C must be $^1\Pi$ or $^3\Pi_1$ levels. This can only be explained if the excited orbital in Eq. (3) is *not* a π, but a σ or a δ orbital. Most probably we have

$$B: (\sigma^2\pi^3, {}^2\Pi_{3/2})nd\sigma; \quad C: (\sigma^2\pi^3, {}^2\Pi_{1/2})nd\sigma. \quad (4)$$

The possibility of a δ excited orbital is definitely excluded by the magnitudes of the orbital term values (cf. Table II). These are far too large for $nd\delta$, whose term value should be nearly the same in the halide molecules as that of nd in the halogen atoms (cf. Table I).

The identification given by Eq. (4) applies directly to the B and C bands of the hydrogen halides, but the indications that these are analogous to B and C of the alkyl halides are so strong[2] that it apparently must apply there also. This, however, involves a difficulty, namely that the main bands in the B region in methyl iodide appear to have a parallel-type structure,[6] which would not be possible for a σ but only for a π excited orbital. It was, in fact, this which led the writer to the suggestion of a $d\pi$ excited orbital in CH_3I. On the other hand, the writer had suggested a σ excited orbital for certain bands in ICl which appear also to be B, C bands.[3] The new and definite evidence from the hydrogen halides now raised the question whether the *apparent* parallel-type bands in methyl iodide could really be perpendicular-type bands in disguise; and it soon appeared that this is really very plausible. Further study (see following paper by E. Teller and the writer) has confirmed this idea. A consistent interpretation of the B and C bands of the hydrogen and alkyl halides, and of ICl and similar molecules, involving a σ excited orbital, therefore seems satisfactorily established.

TABLE II. Doublet interval $\Delta\nu_i(^2\Pi_{1/2} - {}^2\Pi_{3/2})$ in molecule-ions; intensity ratios I_C/I_B; wave-number intervals between B and C, and between D and E bands.

Molecule	$\Delta\nu_i = a$	$\nu_C - \nu_B$ (obs.)	X_{BC} (calc.)	I_C/I_B (calc.)	I_C/I_B (obs.)	$\nu_E - \nu_D$ (obs.)	I_E/I_D (obs.)
HCl	644	2345 2373*	2260	53	>10 >10*		
CH_3Cl	680	~1200	990			600 or 650†	~¾†
C_2H_5Cl						same†	~½†
HBr	2653	3457	2220	4.8	~2		
CH_3Br	2540	3070	1720	3.7		2660	
ClBr		2238					
HI		5570			~1		
CH_3I	5060	4915	[1700]‡	2.1	~5¼		
C_2H_5I	4700	~4650					
ClI		4713					
BrI		4668					

* "Satellites" of B and C bands.
† Based on photographs kindly sent the writer by Dr. W. C. Price.
‡ Estimated (see text).

[4] R. S. Mulliken, J. Chem. Phys. **3**, 513 (1935).
[5] W. C. Price, J. Chem. Phys. **4**, 539, 547 (1936).
[6] A. Henrici and H. Grieneisen, Zeits. f. physik. Chemie **B30**, 1 (1935), and earlier references given there.

III. TYPE OF COUPLING IN UPPER LEVEL OF *B*, *C*, AND *D*, *E* BANDS

It is now possible to proceed to a consideration of further points of interest about the *B* and *C* and other bands. The wave-number interval $\nu_C-\nu_B$ and the intensity ratio I_C/I_B are of especial interest. Table II gives experimental data on these, and also on the wave-number interval $\Delta\nu_i$ between the $^2\Pi_{3/2}$ and $^2\Pi_{1/2}$ levels of the molecule-ion (configuration $\sigma^2\pi^3$) as established from Rydberg series (Price, alkyl iodides) or from emission band spectra (HCl^+, HBr^+). For nearly ideal *J*, *j*-like coupling, assuming Eq. (4), states *B* and *C* should each be a narrow doublet. For Λ, *S* coupling, states *B* and *C* should be replaced by a $^3\Pi$ and a $^1\Pi$ state. For intermediate coupling, components $^3\Pi_2$ (lower) and $^3\Pi_1$ (upper) will correspond to the *B* doublet, and $^3\Pi_0$ (lower) and $^1\Pi$ (upper) to the *C* doublet. Selection rules permit transitions only to the $^3\Pi_1$, the $^3\Pi_{0^+}$ and the $^1\Pi$, with the intensity usually going mainly to the $^3\Pi_1$ and $^1\Pi$.[7] If transitions to the $^3\Pi_{0^+}$ may be neglected, there should then be one *B* transition and one *C* transition.

For ideal *J*, *j*-like coupling, $\nu_C-\nu_B$ should be practically equal to $\Delta\nu_i$, which is equal to the spin-orbit coupling coefficient *a* for π^3 of the molecule-ion, and I_C/I_B should be one. Exact formulas for $\nu_C-\nu_B$ and for I_C/I_B for intermediate coupling are known.[7] Qualitatively, the greater the departure from *J*, *j*-like toward Λ, *S* coupling, the larger $\nu_C-\nu_B$ and I_C/I_B should be. Table II thus indicates, for the *B*, *C* transitions, close approach to *J*, *j*-like coupling in the iodides and perhaps in ClBr, less close approach in CH_3Br, still less in HBr and CH_3Cl, and fairly good Λ, *S* coupling in HCl.

From the observed *a* and the observed $\nu_C-\nu_B$ values it is possible to compute[7] the coefficient *X* which measures the strength of coupling between the spin of the π^3 group and that of the excited σ electron. *X* is equal to the singlet-triplet separation which would be observed if *a* were zero (pure Λ, *S* coupling). Values of *X* calculated from the data for the *B*, *C* states are given for several of the molecules in Table II. In the cases of HCl and HBr, the calculated *X* values are plausible and indicate that *X* is nearly the same for Cl, Br, or I compounds. In the methyl halides, the calculated *X* values are erratic; the most reliable value is probably that for the bromide. In the chloride, the smaller calculated *X* may be real, although the data on $\nu_C-\nu_B$ are not very sure; in the iodide, the calculated *X*, which is imaginary, is of course impossible. One may perhaps estimate that *X* is about 1700 cm^{-1} in all the methyl halides, and attribute the discrepancies to disturbing effects of the methyl group.

TABLE III. Term values in $cm^{-1}\times10^3$ for halide molecule orbitals.*

Molecule	*A*	Excited Orbitals of *B*, *C*	*D*
CH_3Cl	~34	28.0	19.4
C_2H_5Cl		25.7	19.7
CH_3Br	~39	29.0	19.0
C_2H_5Br	~37	26.5	19.3
HI	~40	26.8	17.9?
CH_3I	~42	27.3	18.1
C_2H_5I	~40	25.5	18.1

* Obtained by subtracting wave numbers of observed bands (*B*, *C*, *D*) or of maximum of continuum (*A*) from wave numbers of ionization as obtained by Price from Rydberg series limits.

With *a* and *X* known, the intensity ratio I_C/I_B can be computed theoretically. The theoretical values are compared with observed values in Table II. Considering the extreme difficulties involved in estimating the observed absorption intensities from inspection of photographs in the Schumann region, the qualitative agreement found between theory and calculation may be considered satisfactory.

For the *D*, *E* transitions the data are scanty, but Table II indicates that the coupling is closely *J*−*j*-like even in the chlorides. The approximate equality of the intensities of the *D* and *E* bands in the chlorides is especially convincing. The *D* and *E* levels might then involve a σ excited orbital like the *B* and *C* levels, or might involve a π excited orbital; it can be shown that in *J*−*j*-like coupling two transitions separated by approximately $\Delta\nu_i$ are to be expected in either case. This is definitely observed in CH_3Cl, C_2H_5Cl, and CH_3Br; in CH_3I there is strong absorption where the *E* region should be but the observation of bands is obscured by strong predissociation. The fact that $I_E/I_D<1$ in the chlorides can be shown to indicate a π excited orbital (see below for further discussion).

[7] R. S. Mulliken, Phys. Rev. **57**, 500 (1940), Eqs. (9)–(10), putting $\mu=1$ in Eq. (9) since *X* here is relatively small.

IV. RYDBERG SERIES; IDENTIFICATION OF EXCITED ORBITALS

According to Price,[2,5] the two strongest Rydberg series in CH_3I, C_2H_5I, CH_3Br, HI (and perhaps others) may have their first members in the A absorption region, although of course the A region is continuous, while the higher series members become discrete. The fact that in methyl iodide the first member, after A, of the series is strongly predissociated, and the second somewhat so, is cited by Price as evidence for the allocation of A to the series. The σ^* excited MO of the Q state (upper level of the A region)—see Eq. (1)—could then be the first of a series of MO's whose higher members are definitely Rydberg MO's and so become AO-like, of type $md\sigma$, $ms\sigma$, or $mp\sigma$. The form of σ^* does not give much clue as to the choice among these possibilities, but $d\sigma$ seems rather probable, although the question must be left open. Some confirmation of the conclusion that the excited orbital is of σ type is given by the observed P, Q, R structure of the first member (after A) of this series in HI.

The inclusion of the A continuum in a Rydberg series seems not unreasonable. For example, among a number of Rydberg series in the He_2 emission spectrum,[8] there is one level with an abnormally large quantum defect; this can be understood if the level is the second of the $np\sigma$ series, whose first member $2p\sigma$ is represented only by an anti-bonding MO ($\sigma_u 1s$) with a large quantum defect referred to $n=2$, and analogous to the anti-bonding σ^* MO [cf. Eq. (2)] of the halides. In He_2, the configuration $2p\sigma^2$ occurs only in a repulsion state (normal state of He_2), while the level mentioned above, identified as $2p\sigma 3p\sigma$, gives a stable state somewhat above all other states of configuration $2p\sigma 2x\lambda$ but far below all states of configuration $2p\sigma 3x\lambda$. Similarly, it may be that σ^* in the halides, giving the repulsion state Q of Eq. (1), represents $nd\sigma$, but that when σ^* is replaced by $(n+1)d\sigma$ in the next member of the series, a stable state results.

The states B, C very probably form the first members of two Rydberg series of states of configuration $\sigma^2\pi^3 mb\sigma$ [cf. Eq. (4)]. If σ in the main Rydberg series just discussed above is $md\sigma$, then $mb\sigma$ is probably $ms\sigma$. This is supported by the fact that the term values of B, C agree somewhat closely with halogen atom $(n+1)s$ term values (see Tables I, III). No higher members of the B, C series have been found except probably in CH_3I and possibly HI, so it appears that the intensity of the series fades out unusually rapidly with increasing m. While this is rather difficult to understand, the factors governing intensities in molecular Rydberg series are more complicated than in atomic Rydberg series (see next paragraph), so that probably no great emphasis should be placed on such intensity relations. Moreover, the appearance of unresolved bands observed in absorption is extremely sensitive to the breadths of the band-lines, which can be increased by predissociation or auto-ionization so as to give great and irregularly located increases in *apparent* intensity.

For an atom, the only possible Rydberg series for excitation of an $np\pi$ electron would be those going to $ms\sigma$, $md\sigma$, $md\pi$, or $md\delta$ excited orbitals. Transitions to $mp\sigma$, $mp\pi$ and other orbitals would be forbidden. Thus only two series with a σ excited orbital would be possible. In the present molecular case, the restrictions are no longer so rigorous, since the molecular Rydberg orbitals are not pure s, p, or d. Deviations from pure s, p, and d should be greatest for the lowest members of a series; and for the inner or penetrating parts of the orbitals in higher members of a series. The *outer parts* of the MO's for the higher series members should, however, be practically pure s, p, or d. But for the intensity of a transition $np\pi \rightarrow mx\lambda$, it should usually be the inner part of the $mx\lambda$ orbital which is important, and it is to be expected from theory that this inner part remains fairly constant in form for any one series, at least for the higher members.

From the fact that the term value of the excited MO for the B, C bands (cf. Table III) changes considerably from methyl to ethyl to propyl halide, it may be concluded that the $b\sigma$ orbital is not entirely confined to the halogen atom but reaches out into the alkyl group.[5] This is also indicated by the fact that the main B, C bands in the methyl halides are accompanied by weaker bands involving excitation of deformation vibration in the methyl group, and the fact that the frequency of the latter is considerably

[8] W. Weizel, "Bandenspektren," *Handbuch der Experimentalphysik, Ergänzungswerk* (Leipzig, 1931), Vol. 1.

altered (lowered) as compared with molecules in their normal states.

Some excitation also of the carbon-halogen vibration, and a small decrease in the frequency of this vibration, occurs in methyl iodide, but not in the bromide or chloride. In the hydrogen halides too, some vibration, with a decrease in frequency, is excited, but only in the *C* bands—slightly in hydrogen iodide, more in the bromide, and considerably in the chloride. It is not at all clear why the effect should appear in the *C* and not in the *B* bands. On the whole, it appears that the change from $np\pi$ to $b\sigma$ in the *B*, *C* bands weakens the carbon-halogen or hydrogen-halogen bond slightly.

The data for HCl indicate that in the hydrogen halides this is due to the removal of the $np\pi$ rather than to the addition of the $b\sigma$, since the vibration frequency is considerably lower (2608 cm^{-1}) for $\sigma^2\pi^3$, $^2\Pi$ of HCl^+ than for $\sigma^2\pi^4$, $^1\Sigma^+$ of neutral HCl (2989 cm^{-1}). For the upper level *C*, the frequency is 2670 cm^{-1}.[2] These relations may be understood if π is not quite pure $np\pi_X$ as in Eq. (2), but is of the form

$$\pi = a(np\pi_X) + b(2p\pi_H), \qquad (5)$$

with $a \gg b$ yet with b not negligible—as seems entirely possible. In this way π would be slightly bonding in the hydrogen halides. Evidence from the spectra of several other molecules than HCl (CH, NH, OH, HBr and HBr^+) tends to support this conclusion. In the methyl halides, π is probably very nearly non-bonding.[9]

The states *D* and *E*, according to Price, form the lowest members of two of the weaker Rydberg series in CH_3I and CH_3Br, and of the only observed Rydberg series in CH_3Cl. For the *D*, *E* states, the closely $J-j$-like coupling deduced from Table II indicates a relatively non-penetrating orbit. The constancy of the term value in the methyl, ethyl, and propyl halides indicates that the excited orbital does not overlap the alkyl group. The fact[5] that the methyl group deformation frequency suffers almost no change from state *N* to the upper state of the *D* bands in the methyl halides points to the same conclusion. Observed slight excitation of the C—I frequency in the *D* bands of CH_3I may be attributed to a slight change in the strength of the C—I bond in excitation of the $5p\pi$ electron. In the absence of any facts requiring the assumption of a σ excited MO for the *D*, *E* bands, the foregoing facts can reasonably be explained if the excited orbital is of π type:

$$D\colon (\sigma^2\pi^3, {}^2\Pi_{3/2})c\pi; \quad E\colon (\sigma^2\pi^3, {}^2\Pi_{1/2})c\pi, \qquad (6)$$

since π orbitals are relatively non-bonding and non-penetrating.

If (6) is correct, the *D*, *E* bands of the methyl halides should be parallel bands (see the further discussion below). Since the moment of inertia is nearly unchanged in the transition, the bands under low resolution should appear as doublets plus a central *Q* branch like infra-red parallel bands. Judging from infra-red data,[10] the *Q* branch might be scarcely noticeable under very low resolution. For absorption at room temperature, the doublet width should be about 28, 24, or 20 cm^{-1} for the chloride, bromide, and iodide, respectively. Actually, Price reports that the *D* and *E* bands (vibrationless transitions) in CH_3Br, and likewise all members of the Rydberg series in CH_3I which begins with the *D* bands, are barely resolved doublets with $\Delta\nu$ about 40 cm^{-1}. According to an unpublished photograph kindly sent to the writer by Price, the *D* and *E* bands in CH_3Cl (also the following pair of bands forming the next member of the Rydberg series) are likewise barely resolved doublets. While the reported $\Delta\nu$'s are larger than they should be, they are very rough and it is probably safe to say that the observed doublets provide confirmation of (6).

In the hydrogen halides, *D* and *E* bands have not been identified by Price. If the excited orbital is of π type, they should be parallel bands and have *P*, *R* structure only (no *Q* branch).

[9] In the methyl halides, the "π" orbital must be of the general form $\pi \approx a[\Pi]_{H_3} + b(2p\pi)_C + c(5p\pi)_X$, where $[\Pi]$ refers to a quasi-π orbital which is a linear combination of 1*s* AO's of the three H atoms [cf. R. S. Mulliken, C. A. Rieke, and W. G. Brown, J. Am. Chem. Soc. **63**, 41, 1770 (1941)]. Recent unpublished computations by C. A. Rieke and R. S. Mulliken for methyl iodide indicate that b is practically zero, but that a may be as large as 0.2 (then $c=0.98$) or perhaps even 0.4 (then $c=0.92$). The coefficients are probably similar for the other methyl halides. The relation $b \approx 0$ means that the orbital is nearly non-bonding (both for C—I and C—H bonding) even if a is large. The only direct effect of a on bonding behavior should be to give a slight anti-bonding action among the three H atoms. It is evident that removal of an electron from the "π" orbital produces a positive charge of c^2 on the iodine atom, and of a^2 on the H_3 group. Another effect of $c<1$ is to reduce $\Delta\nu_i$ in proportion to c^2; this is pertinent if one attempts to interpret the empirical $\Delta\nu_i$ values of Table II.

[10] W. H. Bennett and C. F. Meyer, Phys. Rev. **32**, 888 (1935).

A weak band of this type given by Price at λ1515 in HI may reasonably be identified as a D band, since it gives almost exactly the same term value as one obtains from the main D band of CH_3I (cf. Table III). Identification of λ1515 in HI as a D band would exclude a possibility not yet mentioned, namely that the excited orbital of the D, E bands is $nd\delta$, which would be non-bonding and non-penetrating like $c\pi$ of Eq. (6) but would give PQR bands in HI.

The orbital $c\pi$ has not yet been identified. The most obvious identification would be $nd\pi$, since $np\pi \rightarrow nd\pi$ is expected (as in atoms) to give good intensity and $np\pi \rightarrow md\pi$ a good Rydberg series. There is one very serious difficulty, however, which also argues equally against $md\delta$. Namely, the term value of the excited orbital of the D, E states in the alkyl chlorides (whose only observed Rydberg series start with the D, E bands) is more than 19,000, as compared with an estimated 13,000–14,000 for $3d$ in the chlorine atom. In view of the evidence as to its non-bonding and non-penetrating character, it is difficult to see how the term value of $c\pi$ in the alkyl chlorides, if it is $3d\pi$, could be so much greater than that of $3d$ in chlorine. In the bromides, the difficulty is less serious, and in the iodides it disappears, since the term value of $c\pi$ there is equal to that of $5d$ of iodine; but the difficulty with the chlorides seems insuperable.

The only possible remaining interpretation for $c\pi$ is that it is $(n+1)p\pi$. In favor of this is the close agreement of the $c\pi$ term values with the $(n+1)p\pi$ term values of the halogen atoms (cf. Tables I and III). A $p\pi$ orbital might be even more nearly non-bonding than a $d\pi$. The only objection to $p\pi$ is that $np\pi \rightarrow mp\pi$ would presumably be weak, being forbidden in the atom. However, appreciable departures of $np\pi$ in the hydrogen halides [cf. Eq. (5)], and especially in the methyl halides,[9] from simple $np\pi_X$ may well account for the observed intensities of the Rydberg series. The fact that the D band in HI is much weaker than the B and C bands, while in CH_3I it is about as strong as the latter, may also be understood, since $np\pi$ is probably much purer $np\pi_X$ in HI than in CH_3I.

It is worth while to examine for a moment the energy levels to be expected for the configuration $(np\pi)^3(n+1)p\pi$ in pure $J-j$-like coupling, corresponding to (6). It is to be noted that the $(n+1)p\pi$ electron, like the $np\pi$, should have strong coupling between its orbital and spin angular momentum. From atomic theory and observations on atomic structure, it would be reasonable in the halides to expect a coupling coefficient a_{n+1} for $(n+1)p\pi$ of perhaps one-fifth as large a value as a_n of $np\pi$. In this event (neglecting disturbing influences of the methyl group in the case of the methyl halides), the core $np\pi^3$ and the excited electron $(n+1)p\pi$ would *each* have a quantum number ω with two possible values 1/2 and 3/2. The resulting states and their energies (neglecting the energy of the weak $J-j$-like coupling between $np\pi^3$ and $(n+1)p\pi$) would be: $D(3/2, 1/2)_{2,1}$, energy $-\frac{1}{2}(a_n+a_{n+1})$; $D(3/2, 3/2)_{3,0^+,0^-}$, energy $-\frac{1}{2}(a_n-a_{n+1})$; $E(1/2, 1/2)_{1,0^+,0^-}$, energy $+\frac{1}{2}(a_n-a_{n+1})$; $E(1/2, 3/2)_{2,1}$, energy $+\frac{1}{2}(a_n+a_{n+1})$. The numbers in parentheses refer to ω of $np\pi^3$ and of $(n+1)p\pi$, respectively, and the subscripts refer to the total Ω. The various Ω states are the analogues in case c ($J-j$-like) coupling of the components of the states $^3\Delta$, $^1\Delta$, $^3\Sigma^+$, $^1\Sigma^+$, $^3\Sigma^-$, $^1\Sigma^-$ which $\pi^3\pi$ would yield in Λ, S coupling. Transitions should occur in first approximation only to the two 0^+ states (in higher approximation also to the $\Omega=1$ states). These two 0^+ states correspond to mixtures of the $^3\Sigma^-$ (0^+ component only) and $^1\Sigma^+$ states of Λ, S coupling; in the latter, transitions only to the $^1\Sigma^+$ would occur. The two 0^+ states (one D and one E) should be separated by an interval a_n-a_{n+1} (see above). Thus the D and E bands in pure $J-j$-like coupling should be separated by somewhat *less* than $\Delta\nu_i$. There are indications that this is true in CH_3Cl (cf. Table II), but for CH_3Br the separation is slightly larger than $\Delta\nu_i$, which is rather unsatisfactory. On the other hand, the interesting fact (cf. Table II) that the D bands are somewhat stronger than the E bands in the alkyl chlorides is evidence in support of (6). For as Recknagel has shown,[11] in Λ, S coupling the $^1\Sigma^+$ is expected to be *lower* than the $^3\Sigma^-$ state for the configuration $\pi^3\pi$; and if there is a slight tendency toward Λ, S coupling in CH_3Cl, the 0^+ D state would then be the one which tends to become $^1\Sigma^+$ and gives the more intense transition. This agrees with the observations. This behavior is characteristic for $\pi^3\pi$. In

[11] A. Recknagel, Zeits. f. Physik **87**, 397 (1934).

the B, C bands, with configuration $\pi^3\sigma$, it is the higher frequency member C which gets stronger as one goes toward Λ, S coupling. Incidentally, this gives an additional argument against the configuration $\pi^3\pi$ for the B, C bands.

All but one or two of the weakest of the Rydberg series observed by Price have now been accounted for, but expected series ending in $md\pi$ and $md\delta$ have not yet been identified.

In HCl, no Rydberg series have yet been identified, but only the B, C bands. However, the latter are accompanied[2] by "satellites" B', C' which repeat all the characteristics of the B, C bands at very slightly higher frequencies and with much lower intensities. The frequency interval $\nu_{C'}-\nu_{B'}$ and the intensity ratio $\nu_{C'}/\nu_{B'}$ are nearly the same (cf. Table II) as the corresponding quantities for B and C. The C' level, like the C level, is accompanied by a considerable amount of vibrational excitation, with the C' state showing a somewhat lower vibration frequency than the C state (2564 instead of 2670). Band B', like B, is accompanied by no vibrational excitation. The B', C' bands have P, Q, R structure, indicating a σ or a δ excited orbital. The term value is too large for $3d\delta$. The B', C' bands cannot be explained by an isotope effect (neither by DCl nor by $HCl^{35,37}$). There seems to be no possibility but the following:

$$B'\colon (\sigma^2\pi^3, {}^2\Pi_{1\frac{1}{2}})c\sigma\,; \quad C'\colon (\sigma^2\pi^3, {}^2\Pi_{\frac{1}{2}})c\sigma, \qquad (7)$$

with $c\sigma$ identified as $4p\sigma$, which might perhaps help to account for the weakness of the bands. Since the bonding MO σ of Eqs. (1) and (2) may probably be considered for HCl as $3p\sigma$, $c\sigma$ may then be $4p\sigma$; this would explain why the $4p\sigma$ term value is larger (cf. Table I) than the $4p$ term value of the Cl atom.

MARCH 1 AND 15, 1942 PHYSICAL REVIEW VOLUME 61

Interpretation of the Methyl Iodide Absorption Bands Near λ2000

ROBERT S. MULLIKEN AND EDWARD TELLER
*Ryerson Physical Laboratory, University of Chicago, Chicago, Illinois and Columbia University, New York, New York**

(Received January 16, 1942)

The theory of the types and structures of bands in an electronic transition in an axially symmetrical molecule of symmetry C_{3v} is discussed. This is applied to the methyl iodide B band system near λ2000, and it is shown that the two types of bands observed (strong and weak bands of pseudo-parallel type, and weak bands looking like perpendicular bands but of abnormally wide spacing) can both be explained. The pseudo-parallel bands are really electronic-allowed perpendicular bands, the narrowness of their structure resulting from an electronic angular momentum ζ_e in the upper state which we find from the data to be equal to 1.0. This ζ_e is explained by the electronic structure of the upper state, which behaves nearly like a Π state of a linear molecule. The weak widely-spaced bands are another kind of perpendicular bands made allowed by an interaction of the degenerate electronic state with a degenerate (e-type) vibration; they are 1←0 and 0←1 bands of such a vibration, and of a second similar vibration. Their spacing is approximately $1+\zeta_e+\zeta_v$ (ζ_v is the magnitude of the angular momentum of the degenerate vibration which is excited), as contrasted with a spacing $1-\zeta_e$ for the pseudoparallel bands (which correspond to the excitation, at most, only of totally-symmetrical vibrational states). Several molecular constants for the ground and excited electronic states are determined from the observational data (cf. Table I). The moment of inertia for rotations around the symmetry axis is found to be about 6 percent greater in the excited state than in the ground state. The theory of the coupling of spin, orbital angular momentum, and molecular vibration for various strengths of spin-orbit coupling is discussed. The actual nearly J, j-like coupling causes the 0←1 band of the e vibration to appear with a relatively low intensity compared with the 1←0 band of the same vibration.

1. INTRODUCTION

THE ultraviolet absorption spectra of the methyl halides begin at long wave-lengths with a continuum (A), followed by two adjacent and similar regions (B, C) of more or less discrete bands. Apparently the proximity of the A

* E. T. on leave of absence from The George Washington University. The work was begun while E. T. was Visiting Professor at the University of Chicago. Publication assisted by the Ernest Kempton Adams Fund for Physical Research of Columbia University.

continuum causes predissociation in B and C, since these show the most details in methyl iodide, where A is farthest away.

In methyl iodide, two types of B bands have been found.[1] In one type the bands are unresolved and fairly narrow and look like parallel bands. These include the strongest B bands (B_1, B_2, B_3, B_4), involving excitation of 0, 1, 2, and 3 quanta of the totally symmetrical CH_3 deformation frequency.[1] There are also several weaker narrow bands involving totally symmetrical C – I vibrations. Some of the strong B bands are accompanied by one or two companions which may be transitions involving an extra quantum of one or another vibration in both upper and lower states. There are also some groups of bands, for example at 49,970–50,045 cm^{-1}, whose intensity decreases very rapidly with increasing temperature.[2] For this reason and because they cannot be explained by CH_3I vibrations, these bands may be ascribed to other molecules—perhaps to double CH_3I molecules, as mentioned by Henrici and Grieneisen and by Price.

The second type of B bands, including only broad weak bands, shows a series of roughly equidistant "lines" (mostly of about 20 cm^{-1} spacing), which may be interpreted as Q branches ($\Delta J=0$) of perpendicular bands ($\Delta K=\pm 1$, with a different K for each observed line). Every third line is stronger, as expected for rotation of the three hydrogen atoms of the methyl group around the symmetry axis with quantum number K. But a consistent interpretation of the whole B system presents difficulties.[1]

A comparative study of the hydrogen and alkyl halide spectra, however, points to rather definite conclusions as to the electron configurations involved.[3] It appears that the methyl halide B and C bands have normal (N) and excited (B, C) states which probably may best be described as follows (methyl group and halogen atom inner electrons are omitted):

$$N:(\sigma a_1)^2\pi^4,\ ^1A_1;\ B:\{[(\sigma a_1)^2\pi^3,\ ^2\Pi_{3/2}](\sigma^* a_1)\}_1;\quad C:\{[(\sigma a_1)^2\pi^3,\ ^2\Pi_{1/2}](\sigma^* a_1)\}_1. \tag{1}$$

The meaning of the symbols in (1) is as follows: σa_1 is a C – I bonding MO (molecular orbital) which is approximately of the axially symmetrical type σ characteristic of diatomic molecules, but more rigorously must be classified under the species a_1 of the symmetry C_{3v} characteristic of methyl iodide in its normal state. The symbol π refers to a nearly non-bonding orbital which probably differs little from a $5p\pi$ iodine AO;[4] strictly speaking this should be called πe corresponding to classification under the species e of C_{3v}. In states B and C one π electron has been excited to the large Rydberg orbital $\sigma^* a_1$. This orbital is perhaps predominantly $6s$ of iodine, but must extend into and considerably affect the CH_3 group, since only in that way[3] can we account for the considerable excitation of the CH_3 deformation and the decided lowering in the latter's frequency in the upper electronic state.

Because of the very strong spin-orbit coupling within the group π^3, the coupling between π^3 and $\sigma^* a_1$ is nearly J, j-like, so that there are essentially two states π^3, $^2\Pi_{3/2}$ and π^3, $^2\Pi_{1/2}$ of CH_3I^+, to either of which the $\sigma^* a_1$ electron is rather loosely coupled. The spin of the $\sigma^* a_1$ electron gives two levels with either of the core states $^2\Pi_{3/2}$ (levels with $\Omega=2$ and 1) and $^2\Pi_{1/2}$ (levels $\Omega=0^{\pm}$ and 1), but only the two levels with $\Omega=1$, one being the observed B and the other the observed C level, combine strongly with the ground state.[3] Ω here has the usual diatomic meaning; in the diatomic case one would speak of case c coupling. The wave functions of the two levels with $\Omega=1$ have the properties of mixtures of $^3\Pi_1$ and $^1\Pi$ functions. Combination of the B and C levels with N is due to the $^1\Pi$ part of the wave functions. From here on, we shall for the sake of simplicity think of both B and C upper levels as $^1\Pi$; this will lead to no error in the conclusions we shall reach in the earlier sections of the present paper. The effects of the mixed $^3\Pi_1$, $^1\Pi$ character of the B and C upper levels will be studied in the last section of this paper.

Strictly speaking, $^1\Pi$ is not a correct species label in the presence of C_{3v} symmetry, but ^1E should be used instead. Now Jahn and Teller

[1] For a review and references see H. Sponer and E. Teller, Rev. Mod. Phys. **13**, 76 (1941). This includes a tentative interpretation of the B bands as perpendicular bands.

[2] A. Henrici and H. Grieneisen, Zeits. f. physik. Chemie **B30**, 1 (1935).

[3] R. S. Mulliken, Phys. Rev. **61**, 277 (1942).

[4] See reference 2, footnote 9, in regard to the form of the π orbital of Eq. (1)

have shown[5] that orbitally degenerate electronic states (namely E states) of molecules of symmetry C_{3v} are not stable, but that, accompanied by distortion of the equilibrium configuration of the molecule, destroying the C_{3v} symmetry, such a state must split into two nondegenerate states. However, in CH_3I the H_3 group which is responsible for the C_{3v} symmetry and the ^1E classification is sufficiently remote from the iodine atom so that we may regard our $\pi^3\sigma^*$ state as a $^1\Pi$ perturbed by a weak C_{3v} external field. This perturbation and therefore also the Jahn-Teller splitting and accompanying distortion of the molecular configuration may then be minor effects.

If (1) is correct, the transitions from N to B and C are electronic-allowed transitions of perpendicular type, i.e., the electric moment of the electronic jump vibrates along a direction perpendicular to the C−I axis. The strongest of the observed bands, looking like parallel bands, must then be perpendicular bands. It will now be shown that the apparent parallel structure can be satisfactorily explained if the B and C electronic states behave like little-perturbed $^1\Pi$ states.

2. STRUCTURE OF THE PSEUDO-PARALLEL BANDS

We have to consider a prolate-symmetrical-top molecule, with the usual features plus an electronic angular momentum along the axis. It is easily seen that the rotational term (energy/hc) is given by

$$F(K, J) = B[J(J+1) - K^2] + AK_t^2 + \cdots$$
$$= B[J(J+1) - k^2] + A(k \mp \zeta_e)^2 + \cdots, \quad (2)$$

where K_t is the magnitude of the nuclear top angular momentum in units of $\hbar$, ζ_e is that of the electronic angular momentum in the same units, and A and B are the usual rotational constants inversely proportional, respectively, to the small (unique) and to the large moment of inertia. The − and + signs in Eq. (2) respectively correspond to ζ_e parallel (Π^+ state) or opposed (Π^- state) to the vector k of total angular momentum around the symmetry axis; k can take on all positive and negative integral values including zero. (*Throughout the discussion*, we shall use small k as a quantity having sign as well as magnitude, but large K as $|k|$. In some but not all places in the discussion one can write equally well K or k.) For a pure $^1\Pi$ (or $^3\Pi_1$) state, $\zeta_e = 1$, but by using the symbol ζ_e we can include the possibility that the magnitude of the electronic angular momentum has been somewhat reduced as a result of the C_{3v} symmetry. In the normal state of CH_3I, Eq. (2) holds with $\zeta_e = 0$.

In a perpendicular transition, the selection rules are $\Delta J = 0, \pm 1$ and Δk (or ΔK) $= \pm 1$. But if the transition is, as here, primarily an electron jump in which the quantum number k_e of the electronic angular momentum goes from zero to ± 1, the change in k is completely accounted for by the change in k_e and, if $\zeta_e = K_e = 1$ for the upper state, there is no change in k_t. That is, $\Delta k = \Delta k_e = \pm 1$, $\Delta k_t = 0$. Defining Δk as $k' - k''$, we have only $\Delta k = +1$ for the Π^+ upper state and $\Delta k = -1$ for the Π^- state. Transitions $\Delta k = -\Delta k_e = \pm 1$, giving $\Delta k_t = \mp 2$, are forbidden.

That the above rule is rigorous can be seen in the following way. A cyclic permutation of the three hydrogen nuclei must affect the wave functions of two combining states in the same way. Such a permutation may be carried out by rotating the molecule through the angle $2\pi/3$ around the figure axis, and then carrying out an opposite rotation (i.e., by $-2\pi/3$) on the electron wave function in the field of the fixed nuclei. The first operation multiplies the wave function by $e^{2k\pi i/3}$; the second operation leaves a $^1A_1$ electronic wave function unchanged, multiplies a $^1E^+$ function by $e^{-2\pi i/3}$ and a $^1E^-$ function by $e^{2\pi i/3}$. If the upper state is $^1E^+$ the permutation of the three protons will introduce the factor $e^{i(k'-1)2\pi/3}$ while in the $^1A_1$ lower state the factor $e^{ik''2\pi/3}$ appears. Equating the two exponentials and remembering that $|k' - k''| = 1$, we find that for a $^1E^+$ (or a $^1\Pi^+$) upper state $k' = k'' + 1$. But since Δk is $k' - k''$ we have $\Delta k = +1$ for a $^1E^+$ upper state. By a similar consideration one finds $\Delta k = -1$ for a $^1E^-$ upper state. For $\Delta k_e \approx \pm 1$ we find $\Delta k_t = \Delta k - \Delta k_e \approx 0$.

Since the K part of the band structure depends mainly on ΔK_t, as is seen from Eq. (2) neglecting $-BK^2$ (which is small since B/A is about 1/8 for CH_3I), the bands here should have the appearance which parallel bands ($\Delta K = 0$) have in the ordinary case where $\zeta_e = 0$ and $\Delta K_t \equiv \Delta K$. The frequencies of the lines should be

[5] H. A. Jahn and E. Teller, Proc. Roy. Soc. **A161**, 220 (1937); including spin, H. A. Jahn, Proc. Roy. Soc. **A164**, 117 (1938).

given by:

$$\Delta k=+1: \nu=\nu_0+\nu_J-B'(k+1)^2 +A_0'[(k+1)-\zeta_e']^2+B''k^2-A_0''k^2,$$

$$\Delta k=-1: \nu=\nu_0+\nu_J-B'(k-1)^2 +A_0'[(k-1)+\zeta_e']^2+B''k^2-A_0''k^2,$$

where ν_J represents the usual functions of J corresponding to P, Q, and R branches ($\Delta J=-1$, 0, $+1$), k refers always (in accordance with the usual convention) to the lower state in the transition, the primes and double primes refer in the usual way to upper and lower states, and the subscripts zero in A denote zero vibrational quantum numbers. The ν equations for both $\Delta k=+1$ and $\Delta k=-1$ can be reduced to the form

$$\nu=[\nu_0-B'+A_0'(1-\zeta_e')^2]+\nu_J \pm 2[A_0'(1-\zeta_e')-B']K+(A_0'-A_0'')K^2. \quad (3)$$

The + and − signs, respectively, correspond to an r branch ($K'-K''=+1$) and a p branch ($K'-K''=-1$).* If $\zeta_e'=1$, and B' is neglected compared with A_0', Eq. (3) becomes identical with the formula for ordinary parallel bands. So long as B' and $1-\zeta_e'$ are small, the appearance under incomplete resolution of bands corresponding to Eq. (3) should be similar to that of parallel bands. The methyl iodide B and C bands of the first type seem to be in harmony with this description.

3. THEORY AND STRUCTURE OF THE WIDELY SPACED BANDS

We turn now to the second type of B bands which look like widely-spaced but otherwise normal perpendicular bands. Assuming the strongest pseudo-parallel band (B_1) to be a vibrationless transition, we can interpret the weak, strongly temperature-dependent band at about 880 cm^{-1} toward the red as a 0←1 transition of an e-type (π-like) vibration superimposed upon the electronic transition. In fact, a perpendicular band has been observed at 885 cm^{-1} in the infra-red spectrum.[6] One can visualize the vibration of this frequency roughly as a bending vibration of the C−I bond with respect to the figure axis of the CH_3 group. Another ultraviolet band of perpendicular appearance shifted from B_1 toward *higher* frequencies by 780 cm^{-1} may be interpreted as the 1←0 transition of the same bending vibration superimposed upon the electronic transition.

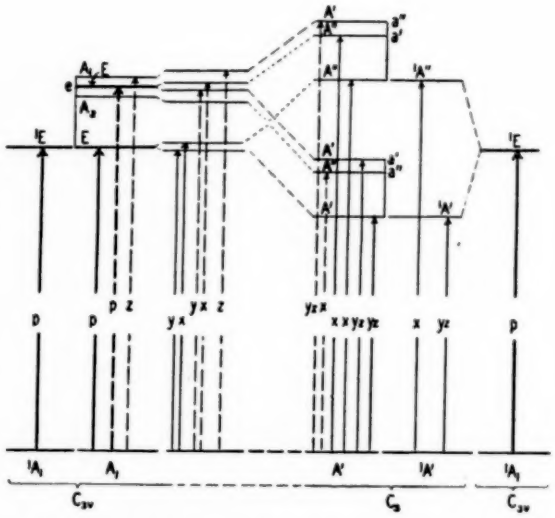

FIG. 1. *Left of diagram:* Allowed transitions for a CH_3I molecule with a $^1A_1$ lower and ^1E upper electronic state, with no vibration in the lower state and either no vibration or one quantum of e-type vibration in the upper state, assuming symmetry C_{3v} with z axis as symmetry axis. *Right of diagram:* Corresponding energy levels and transitions assuming symmetry C_s (one plane of symmetry passing through the C and I atoms and one hydrogen atom) for the upper electronic state, with yz plane as symmetry plane. *Middle of diagram:* Shows correlations between symmetry C_s and C_{3v}; at left of middle, distortion of C_{3v} symmetry only slight. Throughout the diagram, the symbols with left-hand superscript refer to electronic states, small-letter symbols refer to the vibration mode excited (if any), and the capital-letter symbols without left-hand superscript refer to vibronic states. Electronic-allowed transitions are shown by full vertical lines, vibronic-allowed transitions by dashed vertical lines; directions of polarization are indicated by letters x, y, z (p stands for x and y).

According to the simplest application of the Franck-Condon principle for polyatomic molecules, both bands described in the previous paragraph should be forbidden. For a degenerate upper electronic state of the E type in a molecule of the symmetry C_{3v}, however, the transitions become allowed. As we shall see, they can even become quite strong.

We consider first the 1←0 vibrational transition. In the lower electronic state the electronic wave function is of the $^1A_1$ type and the vibra-

* In the r branch, each K corresponds to a pair of k transitions of equal frequency, one a $\Delta k=+1$ transition with k positive, the other a $\Delta k=-1$ transition with k negative; and similarly for the p branch except that the signs of k are reversed. *Added in proof:* In Eqs. (3), (5), (6), (8), and (9), $(A_0'-A_0''-B'+B'')$ should appear instead of $(A_0'-A_0'')$; the B terms were omitted through an oversight.

[6] W. H. Bennett and C. F. Meyer, Phys. Rev. **32**, 888 (1928).

tional wave function (in the assumed absence of vibrational excitation) is likewise A_1. In the upper electronic state we may distinguish two sub-states E^+ and E^- both belonging to the degenerate approximately-$^1\Pi$ state. The E^+ and E^- states transform, respectively, like $e^{i\phi}$ and like $e^{-i\phi}$ under rotations of the molecule through the angles $\frac{1}{3}2\pi$ or $\frac{1}{3}4\pi$. The vibrational wave function in the excited state is similarly of the species E, and again we may distinguish two sub-states E^+ and E^-.

On combining the ^1E electronic with the E vibrational state, there must result,[1] according to group theory for symmetry C_{3v}, a $^1A_1$, a $^1A_2$, and a ^1E vibronic state (cf. Fig. 1). These three states are, respectively, analogous to the $^1\Sigma^+$, $^1\Sigma^-$, and $^1\Delta$ states which in a linear molecule would result from the interaction of a $^1\Pi$ electronic state and a Π vibrational state, for example a state with one quantum of a bending vibration. Combination with the vibrationless ground state (vibronic species $^1A_1$) is allowed, according to the vibronic selection rules, for both the $^1A_1$ and the ^1E upper vibronic states. The transition to the upper $^1A_1$ should give a weak parallel band. Such a vibronic-allowed electronic-forbidden transition draws its intensity from other electronic-allowed transitions of the same vibronic type.[1] In the present instance, this intensity should probably be taken mainly from the D bands, which lie at slightly higher frequencies than the B and C bands, are comparable to the latter in intensity, and are probably an electronic-allowed transition of the $^1A_1 \leftarrow {}^1A_1$ type.[3]

In detail, the $^1A_1$ and $^1A_2$ upper vibronic state wave functions are 50, 50 mixtures of wave functions E^+e^- and E^-e^+. (*Here and elsewhere in this paper we shall use large E for electronic and small e for vibrational E wave functions.*) On the other hand, the ^1E upper vibronic state is a degenerate state with components E^+e^+ and E^-e^- having transformation properties respectively like those of E^- and E^+ electronic states. This means that our initial pure E^+e^+ state becomes somewhat mixed with, among others, various vibrationless E^- electronic states (analogous to both $^1\Pi$ and $^1\Delta$ states of a linear molecule); simultaneously, E^-e^- is mixed with E^+. This permits a very weak vibronic-allowed combination with the ground level, in the form of a perpendicular band which should be approximately superimposed on the parallel band discussed in the preceding paragraph.

Actually the perpendicular band can be much stronger than the parallel band because of an effect similar but additional to the simple vibronic mixing just discussed. The effect consists in a mixing of the E^+e^+ state with the vibrationless electronic B state E^-, and similarly of E^-e^- with E^+. This is a result of the same mechanism which leads to the splitting of orbitally degenerate electronic states under the influence of non-totally-symmetrical deformations (in the present case e-type deformations) of the nuclear configuration. Such deformations cause changes in the electronic wave functions, and for small displacements one can calculate these with the help of perturbation theory. For an E electronic state the perturbing potential has non-diagonal matrix elements between the E^+ and E^- wave functions. These matrix elements give rise to a splitting of the degenerate electronic state, and as a general rule this splitting increases linearly with the nuclear displacement. Thus the symmetrical configuration no longer corresponds to a minimum of the energy. One finds, instead, new equilibrium positions. But if the e-type displacement gives rise only to *small* non-diagonal matrix elements, the distances of the new equilibrium positions from the symmetrical configuration may be smaller than the zero-point amplitudes of the e-type vibrations. In that case it is justifiable to consider non-diagonal matrix elements between vibronic states rather than non-diagonal matrix elements between electronic states. Then the E^+e^+ wave function will be mixed with the vibrationless E^- wave function of the same electronic state (i.e., the B state). Because of the close proximity of this particular E^- state to the E^+e^+ state, its effect is great. The selection rule forbidding transitions from the ground state to the e vibrational state of an upper electronic state would be completely removed if the distance of the actual equilibrium configuration from the symmetrical configuration should become equal to or should exceed the zero-point amplitude of the e vibration.

The way in which the $Ee \leftarrow A_1$ transition

becomes allowed as the influence of the e deformations on the E electronic state is increased is illustrated in Fig. 1. The right half of Fig. 1 indicates schematically how the energy levels corresponding to the vibrationless E and to the Ee states might be arranged if the influence of such deformations is so strong that the equilibrium configuration differs from the original C_{3v} configuration more strongly than would correspond to zero-point vibrational displacements. Both the electronic and the vibrational state are split; Fig. 1 shows a possible arrangement of the levels, and the allowed transitions, if the new equilibrium configurations have symmetry C_s. Transitions to both the vibrationless electronic states $^1A'$ and $^1A''$ resulting from the splitting of ^1E are about equally allowed, and further, for each of these a band corresponding to (half of) our 1←0 band is now strongly electronic-allowed, since one component of the split e vibrational state is now of the totally symmetrical species a' of the new symmetry. (In addition, two weak bands going to the other component a'' of the split e state are vibronic-allowed.)

If, on the other hand, the influence of the e-type deformations is much smaller, the arrangement of energy levels may be nearly the same as in the unperturbed C_{3v} case (cf. Fig. 1, left side of middle). This would correspond to a much smaller mixing between the E^+e^+ and E^- states and a much lower intensity of the 1←0 band. A relatively small amount of mixing is sufficient to account for the actually observed intensity in the methyl iodide 1←0 band.

The 0←1 transition can be explained by the same kind of mixing. Since the vibrationless E^+ electronic state is mixed to some extent with E^-e^-, a combination with the vibrating ground state A_1e^- becomes permitted. Similarly, the E^- upper state, through mixing with E^+e^+, is able to combine with A_1e^+.

To obtain the rotational structure of the 1←0 vibrational band of the B system, we consider the rotational energies of the E^+e^+ and E^-e^- states. These are

$$B'[J(J+1)-k^2]+A_1'[k\mp(\zeta_e'+\zeta_v')]^2+\cdots. \quad (4)$$

This is essentially the same as Eq. (2) for the vibrationless electronic state with the sole difference that here the quantity ζ_v' has been included.* This ζ_v' measures the magnitude of the average angular momentum of the one-quantum vibrational state e in the excited electronic state, in units of $\hbar$. In Eq. (4), the upper $(-)$ sign belongs to E^+e^+, the lower $(+)$ to E^-e^-.

In discussing the rotational structure of the (0←0) band we have seen that, in the $E^-\leftarrow A_1$ and $E^+\leftarrow A_1$ transitions, respectively, k decreases or increases by one unit. The same must be true for the $E^+e^+\leftarrow A_1$ and $E^-e^-\leftarrow A_1$ transitions, since these are made allowed only by the mixing of E^+e^+ with E^-, and of E^-e^- with E^+. Thus we have E^+e^+ giving only $\Delta k=-1$ here, and E^-e^- giving only $\Delta k=+1$. Hence the frequencies of the lines in the 1←0 band should be

$$\Delta k=-1:\ \nu=\nu_0+\nu_J-B'(k-1)^2 +A_1'[(k-1)-\zeta_e'-\zeta_v']^2+B''k^2-A_0''k^2,$$

$$\Delta k=+1:\ \nu=\nu_0+\nu_J-B'(k+1)^2 +A_1'[(k+1)+\zeta_e'+\zeta_v']^2+B''k^2-A_0''k^2.$$

Both equations can be reduced (cf. Eq. (3)) to the form

$$\nu=[\nu_0-B'+A_1'(1+\zeta_e'+\zeta_v')^2]+\nu_J \pm 2[A_1'(1+\zeta_e'+\zeta_v')-B']K+(A_1'-A_0'')K^2. \quad (5)$$

The $+$ and $-$ signs correspond to an r and a p branch, respectively.

The form of Eq. (5), i.e., $\nu=a+\nu_J\pm 2bK+cK^2$, is exactly the same as for ordinary perpendicular bands. If $B'-B''$ is negligible, as seems to be true for the B system of CH_3I, the term ν_J represents for each K value an intense line-like Q branch ($\Delta J=0$, $\nu_J=0$), together with spread-out P and R branches which with ordinary dispersion should appear merely as weak unresolved background. All this is the same as for an infra-red perpendicular band,[7] where for a 1←0 transition

$$\nu=[\nu_0+A_1''(1-\zeta_v'')^2-B']+\nu_J \pm 2[A_1''(1-\zeta_v'')-B']K+(A_1''-A_0'')K^2. \quad (6)$$

The only novel feature in Eq. (5) is the very large spacing of approximately $2[A'(1+\zeta_e'+\zeta_v')-B']$

* The identity in symbols between the *coefficient* A_1 and the *species* A_1 is purely accidental.

[7] See M. Johnston and D. M. Dennison, Phys. Rev. **48**, 868 (1935) for discussion of theory of ζ_v and determination of moments of inertia in the methyl halides.

between successive lines of the p or r branch. This is exactly what we need to explain the hitherto puzzling[1] fact that the observed 1←0 ultraviolet band has larger spacings than occur in any of the infra-red perpendicular bands of CH_3I, larger even than when ζ_v in Eq. (6) is negative (ζ_v in the methyl halides has values between the limits +1 and −1).[7] A quantitative study of the data on the 1←0 and 0←1 ultraviolet bands will be given below.

To obtain the predicted structure of the 0←1 band we consider the $E^+\leftarrow A_1e^-$ and the $E^-\leftarrow A_1e^+$ transitions. The rotational energy of the upper state is given by Eq. (2), that of the lower state by

$$B''[J(J+1)-k^2]+A_1''(k\mp\zeta_v'')^2+\cdots. \quad (7)$$

Since the transition draws its intensity from $E^+e^+\leftarrow A_1e^+$ and $E^-e^-\leftarrow A_1e^-$, Δk must be −1 for $E^+\leftarrow A_1e^-$ just as for $E^-e^-\leftarrow A_1e^-$, and similarly, +1 for $E^-\leftarrow A_1e^+$. Hence

$$\Delta k=-1:\ \nu=\nu_0+\nu_J-B'(k-1)^2 +A_0'[(k-1)-\zeta_e']^2+B''k^2-A_1''(k+\zeta_v'')^2,$$

$$\Delta k=+1:\ \nu=\nu_0+\nu_J-B'(k+1)^2 +A_0'[(k+1)+\zeta_e']^2+B''k^2-A_1''(k-\zeta_v'')^2,$$

which can both be reduced to

$$\nu=[\nu_0-B'+A_0'(1+\zeta_e')^2-A_1''\zeta_v''^2]+\nu_J \pm 2[A_0'(1+\zeta_e')+A_1''\zeta_v''-B']K +(A_0'-A_1'')K^2, \quad (8)$$

with the + and − signs for the r and p branches, respectively. Here again, in agreement with the observed 0←1 band, the structure is the same as that of infra-red perpendicular bands except for the very large spacing, which is predicted to be approximately $2[A_0'(1+\zeta_e')+A_1''\zeta_v''-B']$.

In connection with the study of the experimental data on the 0←0, 1←0, and 0←1 bands, it will be useful to know what is expected for the location and structure of the 1←1 band ($E^+e^+\leftarrow A_1e^+$ and $E^-e^-\leftarrow A_1e^-$). Using Eqs. (4) and (7) for the upper and lower states, respectively, one obtains

$$\nu=\{\nu_0-B'+A_1'[1-(\zeta_e'+\zeta_v')]^2-A_1''\zeta_v''^2\} +\nu_J\pm 2[A_1'(1-\zeta_e'-\zeta_v')+A_1''\zeta_v''-B']K +(A_1'-A_1'')K^2, \quad (9)$$

with the + and − signs for the r and p branches, respectively. If $\zeta_e'\approx 1$ and $\zeta_v'\approx\zeta_v''$, the coefficient of K is nearly zero, so that the band should be of pseudo-parallel type like the 0, 0 band.

4. ANALYSIS OF EXPERIMENTAL DATA ON 0→1 AND 1→0 BANDS

In this and the next section we seek to interpret the available data with particular reference to the 0←0, 1←0, and 0←1 B bands, and to obtain empirical values of various molecular constants and coefficients (ζ's and A's). In order better to understand the observed band structures, Fig. 2 has been constructed. This shows the K structures of the vibrationless and the 1-quantum e levels for the normal and the excited electronic state, together with the low-K lines of the p and r branches of the various bands which are possible (1←0 infra-red, 1←0, 0←0, 1←1, and 0←1 ultraviolet) for transitions among these levels. The J structure of the levels and bands is omitted. The positions of the various K levels in Fig. 2 have been drawn according to Eqs. (2), (4), (7), *with the schematic simplication that all coefficients A have been assumed equal.* Values of B/A, ζ_v'', ζ_v' and ζ_e' obtained from the analysis given below have been used.

Because of the presence of three equivalent hydrogen nuclei in CH_3I, every third K level has a doubled statistical weight corresponding to resultant nuclear spin 3/2 (weight 4) as compared with spin 1/2 with weight 2 for the remaining levels. The levels with doubled spin weight, and the corresponding transitions, which all have doubled intensity, have been determined[8] and are shown in Fig. 2 by heavy lines. The vertical lines representing the transitions in each band are arranged horizontally with spac-

[8] Cf. E. Bright Wilson, Jr., J. Chem. Phys. **3**, 283 (1935). Wilson's Table XII gives the *total* weight (nuclear spin weight, times number of levels of given K, times weight due to K-doubling) for each K value. Figure 2 here shows the distribution more in detail. For the ground state A_1 there is a single $K=0$ level with spin weight 4, and a set of levels $K>0$ with double weight because of $k=\pm K$ and in addition a spin weight two, or four in the case of levels where K is a multiple of three. For the states A_1e and E, the $K=0$ level is double (i.e. two $K=0$ levels probably very close together) and has a spin weight of two, or a total weight of four, as given by Wilson. Then there are *two* $K=1$ levels rather far apart, with a spin weight of four for one and two for the other, and each having a further double weight because of $k=\pm K$; thus the total weight of both $K=1$ levels together is 12, in agreement with Wilson. The Ee state is similar to A_1e and E, but the strongly weighted levels are differently distributed.

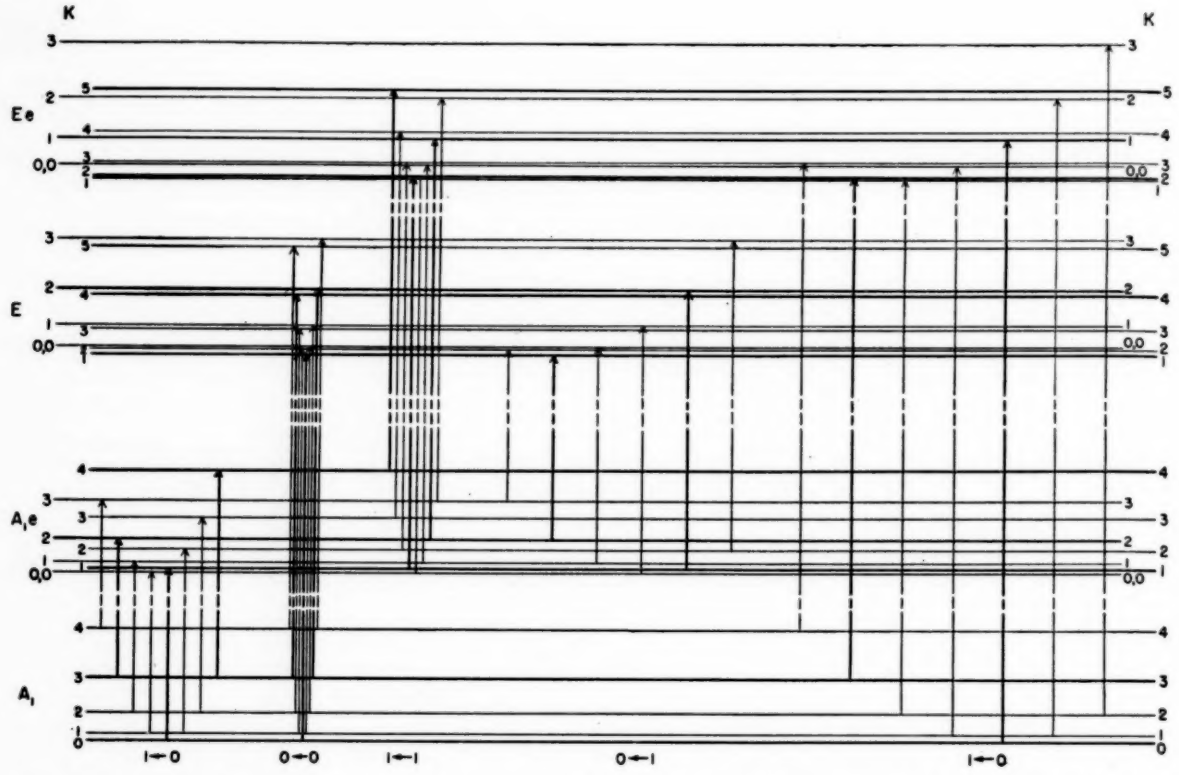

FIG. 2. Energy levels of the K rotation for the ground (A_1) and B excited (E) electronic states of CH_3I, with and without vibration of the type e; and allowed transitions among these levels. The changes in vibrational quantum number for the five possible bands are given at the bottom of the figure. Levels with double spin weight, and corresponding transitions, are shown by heavy lines. See second paragraph of Section 4 for further explanation.

ings proportional to those given by the appropriate equation for the band (cf. Section 3). Thus from the figure, keeping in mind that for thermal equilibrium the absorption intensities (aside from the effect of spin weight) should fall off with increasing K from a maximum at $K=0$, one can readily visualize the appearance of each band.

Referring now to the data of Henrici and Grieneisen[2] on the 0←1 ultraviolet band, and especially to their Fig. 1, one can immediately identify their strongest observed line at $\nu=48{,}878$ cm^{-1} with $r(1)$ of the 0←1 band of Fig. 2. With this identification, one can proceed to fit the set of ten observed lines in this band to an equation of the form of Eq. (8). Since the observed "lines" are Q branches ($\Delta J=0$), and if we assume $B'=B''$, the term ν_J in Eq. (8) drops out. [That $B'=B''$ is nearly true is indicated by the narrow symmetrical appearance[2] of the observed Q branches; also by the fact that the frequency of the totally-symmetrical C−I vibration does not differ much in the upper and lower electronic states.[2]] The following equation reproduces the data within an average deviation of less than ± 1 cm^{-1}:

$$\nu=48{,}858\pm 20.5K-(\tfrac{1}{3})K^2. \qquad (10)$$

According to Eq. (8), the coefficient of K in Eq. (10) should be equal to $2[A_0'(1+\zeta_e')+A_1''\zeta_v''-B']$, and the coefficient of K^2 to $(A_0'-A_1'')$.

With the help of infra-red data, we can now evaluate ζ_e'. Assuming $B'=B''$, B' can be obtained approximately from unresolved infra-red parallel bands; the value is 0.28 ± 0.02 cm^{-1}.[9] Then from the three infra-red perpendicular fundamental bands, $A_0''=5.08$ ($\pm$ about 0.3) cm^{-1} is obtained; unfortunately this is not very accurate.[9] Next we make use of the empirical

[9] The values of B_0'' and A_0'' are obtained from the moments of inertia $I_B=99\times 10^{-40}$ and $I_A=5.44\times 10^{-40}$ given in reference 7.

equation[6]

$$\nu = 885.15 + 7.70K + 0.032K^2 \qquad (11)$$

for the infra-red 1←0 perpendicular band of Fig. 2. The constants of Eq. (11) enable use to determine $A_1'' = 5.11$ (± about 0.3), then $\zeta_v'' = 0.19$, and finally $\nu_0 = 882.09$, for Eqs. (6), (11). Unfortunately the uncertainty in ζ_v'' is rather large (perhaps ±0.05).

Using the coefficient of K^2 in Eq. (10), we now obtain $A_0' = 4.78$ (± about 0.3). We can then evaluate ζ_e' and find the value 0.998, in excellent agreement with our original expectation that ζ_e' should be nearly 1. Unfortunately, however, there is an empirical probable uncertainty of about ±0.1 in our value; this goes back to the uncertainty in A_0''.

The value of ν_0 in Eqs. (8), (10) can now be determined as 48,839.3. Adding this to $\nu_0 = 882.1$ for the 1←0 infra-red band, we obtain 49,721.4 as a predicted ν_0 for the 0←0 ultraviolet transition. As we shall see below, this is in good agreement with what is obtained by a direct interpretation of the structure of that band. This agreement gives support to our interpretation of the 0←1 ultraviolet band, and also indicates that by good luck, the error in the value of A_0'' we have used, and so in the values of ζ_v'' and ζ_e', is well inside our estimates.

For the 1←0 ultraviolet band,[10] assuming that the strongest of the sixteen observed p and r transitions, with $\nu = 50{,}492$ cm^{-1}, has $K = 0$ as would be expected according to Fig. 2, we find

$$\nu = 50{,}492\tfrac{1}{3} \pm 21\tfrac{2}{3}K - \tfrac{1}{3}K^2. \qquad (12)$$

By comparison with the corresponding theoretical Eq. (5), and making use of the values of A_0'', B', and ζ_e' already determined, we find $A_1' = 4.75$ and $\zeta_v' = 0.34$, the latter a not unreasonable value. We further determine $\nu_0 = 50{,}466.6$.

The constants and coefficients so far determined are summarized in Table I. Two results of some interest are obvious. From the ν_0 values, the perpendicular frequency we have been discussing is seen to have the magnitude 882 cm^{-1} in the lower and 745 cm^{-1} in the upper state. The latter figure is considerably lower than the value 780 cm^{-1} obtained by Henrici and Grieneisen by subtracting ν of the 0←0 band from ν for $K = 0$ of the 1←0 band. The change is due to the large correction to ν_0 in the constant term in Eq. (5).

The second interesting result is the 6 percent decrease in A during excitation to the upper level of the ultraviolet bands. (Note that the *change* in A is accurately known.) This means a 6 percent increase in the moment of inertia around the symmetry axis and probably corresponds to a spreading out of the CH_3 umbrella. This is in harmony with the rather strong excitation of the CH_3 totally-symmetrical deformation vibration in the main series of bands B_1 to B_4, and with the 12 percent decrease in the frequency of this vibration in going to the upper state.

5. INTERPRETATION OF DATA ON 0←0, 1←1, AND OTHER BANDS

Putting the constants listed in Table I into Eqs. (3) and (9), it is possible to predict the exact structures of the 0←0 ($E \leftarrow A_1$) and the 1←1 ($Ee \leftarrow A_1e$) bands. If one assumes $B' = B''$ and $\Delta J = 0$, the equations are:

$$0\leftarrow 0 \text{ band}: \nu = 49721.1 \pm (-0.54)K - \tfrac{1}{3}K^2, \qquad (13)$$

$$1\leftarrow 1 \text{ band}: \nu = 49584.6 \pm (-1.84)K - 0.36K^2. \qquad (14)$$

The constant terms equal $\nu_0 - 0.28$ and $\nu_0 - 0.72$ in Eqs. (13) and (14), respectively. The + and −

TABLE I. Constants of CH_3I levels. A_1 refers to the ground electronic state, E to the excited state B; e refers to the degenerate vibration whose frequency is 885 cm^{-1} in the ground state.

State	ν	A	B	ζ_e	ζ_v
A_1	0.0	5.08	0.28	0.00	0.00
A_1e	882.1	5.11	0.28	0.00	0.19
E	49721.4	4.78		1.00	0.00
Ee	50466.6	4.75		1.00	0.34

[10] We have used the data of reference 2. It is possible that $K = 0$ is 50,554, which is nearly as strong as 50,492: cf. Figs. 1 and 2 of reference 2, also Table I and Fig. 3 of the paper of Scheibe, Povenz, and Linström [Zeits. f. physik. Chemie **B20**, 288 (1933)]. But most probably 50,492 has $K = 0$ and the relatively high apparent strength of 50,554 and the other rQ transitions as compared with corresponding pQ transitions can be explained by the effects of closer packing in the background of P and R branches in the r than in the p range. Some slight doubts as to the empirical correctness of our Eq. (12) are also raised by the fact that Scheibe, Povenz, and Linström, although generally agreeing fairly well with Henrici and Grieneisen, give ν values lower than those of the latter authors by amounts ranging from 25 to 38 cm^{-1} in the case of the 1←0 band.

signs correspond as usual to r and p branches, but the initial directions of these branches are reversed by the extra $-$ sign. A plot of Eq. (13) shows a head at the p line $K=1$ with $\nu=49721.3$, all the other K lines being at lower frequencies. All strong lines are crowded near this head, while weaker lines, with increasing spacing, tail off toward longer wave-lengths. These lines are of course all Q branches; for each Q branch there should be a P and an R branch covering at room temperature a range of perhaps ± 20 cm^{-1} on each side.[5] These P and R branches should form a weak penumbra extending (at room temperature) perhaps 15–20 cm^{-1} to higher frequencies outside the p, r head, and also a practically continuous background inside this head.

Henrici and Grieneisen describe the observed B_1 band at very low pressures as about 10 cm^{-1} wide with center at 49,715 cm^{-1}. Scheibe, Povenz, and Linström[10] speak of the band as having a head. In the case of some of the other pseudo-parallel bands, Henrici and Grieneisen also speak of a head. This is true of the 0←1 band of the CH_3 deformation frequency and of the 1←0 band of the C−I frequency, with heads at 48,478 cm^{-1} and 50,223 cm^{-1}, respectively. For the 1←0 (B_2) band of the CH_3 deformation frequency (at 50,805 cm^{-1} according to Henrici and Grieneisen), Scheibe, Povenz, and Linström record a head at 50,810 cm^{-1}. In all these cases, the head is on the ultraviolet side of the band. While the evidence is not wholly clear, it seems to agree within its own uncertainty with the predictions of Eq. (13). Further, Henrici and Grieneisen's observations to the effect that the B_1 band spreads toward both low and high (but especially toward low) frequencies with increase in pressure or temperature seem to be in harmony with expectation. The broadening toward high frequencies beyond the head may be attributed to the penumbra of R branches discussed above.

Accompanying the B_1 and B_2 bands are weaker bands on the long wave-length side. These become relatively stronger and more numerous at increased temperatures. Table II lists several such bands and our suggested identifications. There are two relatively strong bands (50,700 and 50,623) which we do not see how to explain.

On the high frequency side of B_2 there is a band of wide spacing with every third line strong, similar to those already discussed. This has already been identified[1,2] as a 1←0 band of a degenerate frequency of about 1250 cm^{-1} magnitude corresponding to the infra-red frequency of 1445 cm^{-1}. The seven observed Q frequencies in this band may be expressed by

$$\nu=50{,}942\pm 18K-\tfrac{1}{3}K^2, \qquad (15)$$

but this equation is less reliable than Eqs. (10) and (12). Proceeding as we did above in the case of Eq. (12), we find $\zeta_v'=-0.04$.

On the high frequency side of the band just mentioned, only low dispersion data are available. We shall not discuss these data here, since there is little we could add to existing interpretation. In the region of the lower frequency B bands, although we have discussed all the prominent features, there are some further weak bands, particularly at high temperatures. We shall not attempt to account for these here, since we believe that the nature of the B system is now in general satisfactorily established. The additional weak bands should be explainable by further vibrational transitions, or perhaps in part by vibronic-allowed true parallel transitions (cf. Section 3).

Some of them may arise from transitions to the $[(^2\Pi_{3/2})\sigma^*]_2$, i.e., $^3\Pi_2$ level, which should lie slightly below the $[(^2\Pi_{3/2})\sigma^*]_1$ level of Eq. (1). Such transitions, although forbidden in first approximation, could occur weakly as a result of spin-orbit coupling together with effects of the C_{3v} symmetry. Possibly the two unidentified bands of Table II belong to this category.

TABLE II. Bands satellite to B_1 and B_2.

ν	Identification
B_2: 50805	1←0 of CH_3 ∥ deformation vibration
772*	same plus 1←1 of C−I ∥ vibration
741*	same plus 2←2 of C−I ∥ vibration
700	no success in identifying this
B_1: 49721	0←0
687	1←1 of C−I ∥ vibration
652*	2←2 of C−I ∥ vibration
623	no success in identification
581–556 (double?)	581 fits 1←1 of Eq. (14); 560 or 568 fits 1←1 of CH_3 ∥ deformation vibration

* Appears only at high temperature, when also further bands appear at longer wave-lengths than those listed.

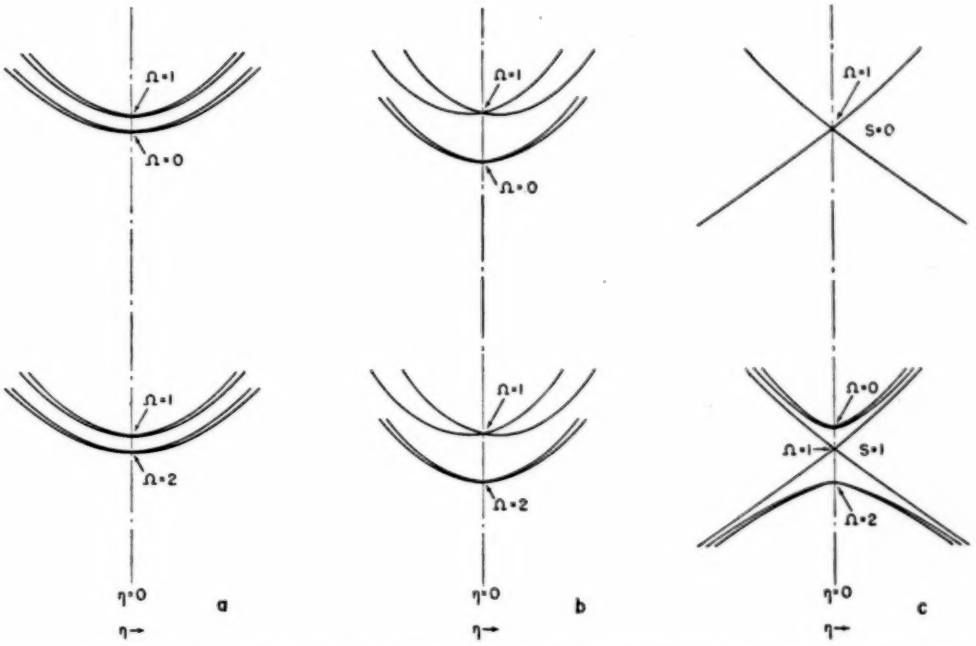

FIG. 3. Energy levels of the methyl iodide B and C states plotted against the displacement η of an e-type vibration. Figure 3a represents the energy levels for $J-j$-like coupling, Fig. 3c for $L-S$-like coupling and Fig. 3b for an intermediate case which corresponds approximately to the actual behavior of methyl iodide.

6. THE INFLUENCE OF SPIN

It has been mentioned in Section 3 that the upper electronic state of the B and C band systems, which is of E type, should be split by e type nuclear displacements, and that the equilibrium configuration should not have C_{3v} symmetry. The conclusions in Section 3 were based on the assumption that the splitting of the E level is sufficiently small to justify a perturbation treatment in which vibronic states of a model with C_{3v} symmetry serve as unperturbed functions. One important reason for the smallness of the splitting is that the degeneracy of the E electronic state is due to a π^3 configuration on the iodine atom and that this part of the molecule is not strongly affected by any e vibration. A second reason tending to make the splitting of the E level small is the $J-j$-like coupling between spins and orbits in the B and C states.

In the limiting case of pure $J-j$-like coupling an e vibration does not give rise to any linear splitting; i.e., the first-order perturbation energy for the electronic levels in question vanishes. This can be seen in the following way. For pure $J-j$-like coupling the electronic wave function can be written according to (1) as a product of a function characterizing the core ($^2\Pi_{3/2}$ for the B state and $^2\Pi_{1/2}$ for the C state) and a wave function of the outermost electron $\sigma^* a_1$. The core wave function contains the orbital degeneracy. But the number of electrons in the core is odd and the wave function of the core is only twofold degenerate; under these conditions no nuclear displacement can split the wave function of the core.[11] The same holds for the twofold degeneracy of the outermost electron. But for a product wave function the first-order perturbation vanishes if the perturbation is zero for the separate factors.

In Fig. 3a the electronic levels are plotted for $J-j$-like coupling as a function of an e-type displacement whose magnitude is measured by the abscissa η. For $\eta=0$ one obtains, as stated in Section 1, two twofold degenerate lower levels belonging to the $\Pi_{3/2}$ core; the Ω values of these levels are 2 and 1. In addition there appear two higher levels belonging to the $\Pi_{1/2}$ core, with

[11] For the proof, see H. A. Kramers, Proc. Acad. Sci. Amst. **33**, 595 (1930); E. Wigner, Nachr. Ges. Wiss. Göttingen (1932), p. 546; H. A. Jahn, Proc. Roy. Soc. **164**, 117 (1938).

$\Omega=0$ and $\Omega=1$; for $\Omega=0$ one actually finds two levels with a very small energy difference. The angular momentum Ω is composed of the orbital momentum* Λ, the component along the symmetry axis of the spin of the core, Σ_c, and that of the spin of the outer electron, Σ_e. In Table III all these momenta are shown for the various electronic states. The first column specifies the core wave function. The last column contains symbols to be used for the wave functions in the subsequent discussion. The splitting of the two $\Omega=0$ levels for $\eta=0$ is not taken into account in the table. If $\eta\neq 0$ the nuclear displacement gives rise to non-diagonal matrix elements between states which differ in the sign of Λ but which agree in the signs of Σ_c and Σ_e. Thus there are matrix elements between ψ_1 and ψ_{-3}, ψ_{-1} and ψ_3, ψ_2 and ψ_{-4} and finally between ψ_{-2} and ψ_4. In first approximation these matrix elements are proportional to η. It is seen that no matrix elements connect wave functions belonging to the same unperturbed energy. Therefore no splitting occurs which is proportional to the first power of the perturbing potential and therefore to the first power of η. The same result was obtained above by different reasoning. The non-diagonal matrix elements connecting states of different energies, however, give rise to second-order perturbations in the energy and it can be shown that all degenerate levels suffer a splitting proportional to η^2. This splitting is illustrated in Fig. 3a.

For extreme L, S-like coupling the influence of an e-type nuclear displacement is much more important. In Fig. 3c the behavior of the energy levels is illustrated for this case. At $\eta=0$ one finds a $^3\Pi$, with Ω values equal to ± 2, ± 1 and 0. Two levels with slightly different energies belong to the last value. In addition a $^1\Pi(\Omega=\Lambda=\pm 1)$ is found at a higher energy. If η is different from zero and is not very small, the main effect of the e-type displacement is a splitting of the $\Lambda=\pm 1$ degeneracy. One finds in the energy region of the original triplet three closely spaced levels whose energies increase linearly with η and three further levels whose energies decrease at the same rate with η. In the energy region of the original singlet one finds two energy levels, one increasing and the other decreasing linearly with η. The energy levels for small η values may be obtained by applying the method of perturbations. In the notation of Table III the triplet wave functions at $\eta=0$ may be written as follows: ψ_1 and ψ_{-1} for $\Omega=\pm 2$, $(1/\sqrt{2})(\psi_2+\psi_4)$ and $(1/\sqrt{2})(\psi_{-2}+\psi_{-4})$ for $\Omega=\pm 1$, ψ_3 and ψ_{-3} for $\Omega=0$. The singlet levels are $(1/\sqrt{2})(\psi_2-\psi_4)$ and $(1/\sqrt{2})(\psi_{-2}-\psi_{-4})$. The nuclear displacement gives rise to matrix elements between the degenerate pair of wave functions $(1/\sqrt{2})(\psi_2+\psi_4)$ and $(1/\sqrt{2})(\psi_{-2}+\psi_{-4})$ and also between the degenerate pair $(1/\sqrt{2})(\psi_2-\psi_4)$ and $(1/\sqrt{2})(\psi_{-2}-\psi_{-4})$. Therefore the first-order perturbation energy does not vanish for these pairs of levels, and these levels suffer a splitting which increases linearly with η. Further matrix elements occur between ψ_1 and ψ_{-3} and between ψ_{-1} and ψ_3. In this case the first-order perturbation vanishes but the small energy difference of the interacting levels brings about a large perturbation energy of the second order. For this reason the highest and lowest pair of potential energy curves of the triplet are sharply bent near $\eta=0$.

With increasing η the non-diagonal matrix elements between ψ_1 and ψ_{-3}, and between ψ_{-1} and ψ_3, become large compared with the splitting of the triplet at $\eta=0$. Then the highest and lowest potential curves of the triplet approach the middle curve. Figure 3c shows furthermore that the potential curves do not intersect anywhere except at $\eta=0$.

In Fig. 3b an intermediate case between pure

TABLE III. Angular momenta and symbols of wave functions for perfect J–j-like coupling.

	Ω	Λ	Σ_c	Σ_e	
$\Pi_{-1/2}$	-1	-1	$\frac{1}{2}$	$-\frac{1}{2}$	ψ_{-4}
$\Pi_{1/2}$	1	1	$-\frac{1}{2}$	$\frac{1}{2}$	ψ_4
$\Pi_{-1/2}$	0	-1	$\frac{1}{2}$	$\frac{1}{2}$	ψ_{-3}
$\Pi_{1/2}$	0	1	$-\frac{1}{2}$	$-\frac{1}{2}$	ψ_3
$\Pi_{-3/2}$	-1	-1	$-\frac{1}{2}$	$\frac{1}{2}$	ψ_{-2}
$\Pi_{3/2}$	1	1	$\frac{1}{2}$	$-\frac{1}{2}$	ψ_2
$\Pi_{-3/2}$	-2	-1	$-\frac{1}{2}$	$-\frac{1}{2}$	ψ_{-1}
$\Pi_{3/2}$	2	1	$\frac{1}{2}$	$\frac{1}{2}$	ψ_1

* On account of the C_{3v} symmetry, Ω and Λ do not have exactly integral values. In the following we shall consider the limiting case in which $\Lambda=1$ and $\Lambda=-1$ for the electronic functions E^+ and E^-. The argument would not lose its validity for non-integral values of Λ and Ω but in that case a somewhat more cumbersome notation would be necessary. Here and in the following discussion we shall attach *signs* to Λ and Ω, although as ordinarily defined these symbols refer to absolute values; we shall likewise use Σ with signs defined relative to the positive direction along the symmetry axis.

$L-S$-like and pure $J-j$-like coupling is represented. Corresponding to the actual properties of CH_3I the coupling shown in Fig. 3b is closer to the $J-j$-like than to the $L-S$-like coupling. For $\eta=0$ two pairs of levels occur with $\Omega=\pm2$, ±1 in the lower pair, and $\Omega=0$, ±1 in the upper pair. The wave functions belonging to $\Omega=\pm2$ and $\Omega=0$ for $\eta=0$ are the same for pure $L-S$-like coupling, pure $J-j$-like coupling, and for all intermediate couplings. In the wave functions of the lower $\Omega=\pm1$ levels in Fig. 3b ψ_2 and ψ_{-2} predominate, but a small admixture of ψ_4 and ψ_{-4} is present. The wave functions may be written in the form $\psi_2+\epsilon\psi_4$ and $\psi_{-2}+\epsilon\psi_{-4}$. Here ϵ is a number smaller than unity; the normalization factor has been omitted. In the upper levels with $\Omega=\pm1$ the main parts of the wave functions are ψ_4 and ψ_{-4}; the functions ψ_2 and ψ_{-2} appear with small negative coefficients. The wave functions are $\psi_4-\epsilon\psi_2$ and $\psi_{-4}-\epsilon\psi_{-2}$. For $\eta\neq0$ matrix elements exist between the $\Omega=\pm2$ and the $\Omega=0$ levels. This gives rise to quadratic perturbations in the energy. The perturbations are not very large, because of the relatively great distance between the levels concerned. At the same time, matrix elements appear between the lower $\Omega=1$ and the upper $\Omega=-1$ levels, and also between the lower $\Omega=-1$ and the upper $\Omega=1$ levels. These matrix elements cause quadratic perturbations similar to those affecting the $\Omega=\pm2$ and $\Omega=0$ levels. But because of the admixture of ψ_4 and ψ_{-4} functions in the lower $\Omega=\pm1$ level, smaller matrix elements appear between the lower $\Omega=1$ state and the $\Omega=-1$ belonging to the same energy. For small ϵ values, these matrix elements differ from the matrix elements mentioned above by a factor ϵ. As a consequence, a small first-order perturbation in the energy is obtained, and the splitting of the $\Omega=\pm1$ level varies linearly with η for small η values. The same holds for the upper $\Omega=\pm1$ level. Here the splitting is caused by the admixture of the ψ_2 and ψ_{-2} functions, which gives rise to small matrix elements between the upper $\Omega=1$ state and the $\Omega=-1$ state of the same energy. In Section 3 we had assumed a small linear splitting of the $\Omega=\pm1$ degenerate levels. Our present results justify that assumption.

The above discussion has a direct bearing on the intensity of the $1\leftarrow0$ and $0\leftarrow1$ transitions of an e-type vibration in the B band system. The $1\leftarrow0$ transition is made possible by admixture between the vibrationless electronic state E^- and the vibronic state E^+e^+ (and similarly by the admixture of E^+ with E^-e^-). Now the E^+e^+ state of the B system interacts with the vibrationless E^- state of the C system. This is due to the matrix element appearing for $\eta\neq0$, between the $\Omega=1$ state of the B system and the $\Omega=-1$ state of the C system. As a result the wave function $\psi_{-4}-\epsilon\psi_{-2}$ is admixed with the original function $\psi_2+\epsilon\psi_4$. The amount of this mixing is proportional to the matrix element and inversely proportional to the energy difference between the E^+e^+ level of the B system and the E^- level of the C system.

The E^+e^+ vibronic state of the B system also interacts with the E^- state of the same system. This interaction is due to the smaller matrix elements arising for $\eta\neq0$ between the $\Omega=1$ and $\Omega=-1$ states of the B system. As a result the wave function $\psi_{-2}+\epsilon\psi_{-4}$ is admixed with the original function $\psi_2+\epsilon\psi_4$. The amount of the mixing is proportional to the matrix element between the $\Omega=1$ and $\Omega=-1$ states of the B system: this matrix element is smaller than the one mentioned in the previous paragraph by roughly the factor ϵ. But the mixing is also inversely proportional to the energy difference between the E^+e^+ level and the E^- level of the B system. This energy difference is about five times smaller than the energy difference referred to in the last paragraph. Thus it is possible that the E^- states of the B system and the C system are admixed with the E^+e^+ state of the B system with coefficients of a similar magnitude.

The matrix element of the electric dipole causing the $1\leftarrow0$ transition of the B system is a sum of the dipole matrix elements due to the admixture of the E^- states of the B and C systems. The interference of these two dipole matrix elements must therefore be taken into account. The energy difference between E^+e^+ of the B system and E^- of the same system is positive. The energy difference between E^+e^+ of the B system and E^- of the C system is negative. This causes a difference in sign in the admixtures of the E^- function of the B system and the E^- function of the C system. On the other

hand, the dipole matrix elements leading from the ground state to the E^- states of the B and the C system differ in sign. Indeed the largest term in the E^- wave function of the B system is ψ_{-4} while that in the E^- wave function of the C system is ψ_{-2}. Now $\psi_{-4}+\psi_{-2}$ is the wave function of a pure triplet state which does not combine with the ground state. Therefore the dipole matrix elements leading to ψ_{-4} and to ψ_{-2} must differ by a factor -1. Since the matrix elements leading to the E^- states of the B and C system differ in sign and since these E^- states are admixed with opposite signs into the E^+e^+ state, it follows that a constructive interference exists between the contributions of the two E^- states to the intensity of the 1←0 transition.

The 0←1 transition of the 880 cm^{-1} vibration is made possible by the admixture of E^+e^+ states of the B and the C system with the vibrationless E^- state of the B system. Arguments similar to those given above can be used to find out whether the contributions of the two E^+e^+ states to the dipole matrix element tend to reinforce or to cancel each other. A difference from the previous reasoning arises in one point: while in the above discussion the E^+e^+ state lay between the two E^- states, in the present case the E^- state of the B system lies lower than either of the two E^+e^+ states. Consequently the two E^+e^+ states are admixed into the E^- state with the same sign. The dipole matrix elements leading from the vibrating electronic ground state to the two E^+e^+ states are of opposite signs. This is true for the same reason for which the matrix elements leading from the ground state of the molecule to the E^- states differ in sign. The result is that the interference between the two E^+e^+ states contributing to the dipole matrix element of the 0←1 transition is destructive.

The data published by Henrici and Grieneisen[2] contain indications that the 0←1 transition probability of the 880 cm^{-1} vibration is smaller than the 1←0 transition of the corresponding vibration. If one assumes that the intensities are roughly proportional to the vapor pressures at which the 0←1 and 1←0 bands appear, one finds that at 300°K the 0←1 band is 300 or 400 times less intense than the 1←0 band. If the intensity ratio were due to the Boltzmann factor arising from the thermal excitation of an 880 cm^{-1} quantum in the 0←1 transition, the ratio would be 65. The larger intensity ratio of 300 or 400 indicates that the 0←1 transition is weakened by the destructive interference discussed above. The same conclusion is reached from intensity measurements at 600°K. Here the 1←0 and 0←1 bands have the apparent intensity ratio of 60, which is to be compared with a Boltzmann factor of 8. But the existing intensity measurements in the B system of methyl iodide are not sufficiently accurate to justify a comparison between experiment and the quantitative consequences of the previous paragraphs. If accurate measurements were available, such a comparison could be utilized to obtain information about the quantity ϵ which measures the deviation from pure $J-j$-like coupling.

On the Triplets of Helium

D. R. INGLIS
The Johns Hopkins University, Baltimore, Maryland
(Received December 10, 1941)

It is well known that the inversion of the helium triplets and their deviation from interval rule are due to the spin-other-orbit and to the magnetic spin-spin interactions (respectively), which may be neglected in comparison with the spin-orbit interaction in treating the spectra of heavy elements. The preliminary calculation of Heisenberg is compared with the correct calculation of Breit for the lowest triplet. The extension to higher triplets, by Araki, is simplified and generalized, and the comparison with experiment is discussed.

I. THE LOW TRIPLET

THE part of the Hamiltonian of a two-electron atom which is attributed to the spins and spin magnetic moments of the electrons may be written[1]

$$\begin{aligned}H''=a\{&\tfrac{1}{2}Z[(\mathbf{s}_1\cdot\mathbf{l}_1)/r_1^3+(\mathbf{s}_2\cdot\mathbf{l}_2)/r_2^3]\\&-(m/h)[(\mathbf{s}_1+\mathbf{s}_2)\cdot(\mathbf{r}_2-\mathbf{r}_1)\times(\dot{\mathbf{r}}_2-\dot{\mathbf{r}}_1)\\&+\tfrac{1}{2}\mathbf{s}_1\cdot(\mathbf{r}_2-\mathbf{r}_1)\times\dot{\mathbf{r}}_1-\tfrac{1}{2}\mathbf{s}_2\cdot(\mathbf{r}_2-\mathbf{r}_1)\times\dot{\mathbf{r}}_2]/r_{12}^3\\&+[\mathbf{s}_1\cdot\mathbf{s}_2-3(\mathbf{s}_1\cdot\mathbf{r}_{12})(\mathbf{s}_2\cdot\mathbf{r}_{12})/r_{12}^2]/r_{12}^3\},\end{aligned}\tag{1}$$

where $a=(eh/mc)^2$. The first line is the part of the familiar "spin-orbit interaction" due to the field of the nucleus (including the "Thomas factor" $\frac{1}{2}$). The second line is the Larmor magnetic contribution to the screening part of the spin-orbit interaction and the spin-with-other-orbit interaction, and the third line contains the corresponding Thomas relativistic terms, which may be said to depend on the acceleration of each electron in the nuclear coordinate system caused by the Coulomb interaction with the other electron.[2] The fourth line is the magnetic spin-spin interaction.

Two prominent papers have treated the low triplet $1s2p\,^3P$ of helium in sufficient detail to include all terms of the interaction (1), and their results stand in some disagreement. Heisenberg's result for the relative energies of the states of the sp triplet, $^3P_2$, $^3P_1$, and $^3P_0$, respectively, is

$$a\langle(1/r^3)_p\rangle_{Av}\{\tfrac{1}{4}(Z-3)(1,-1,-2)+(1/16)(1,-5,10)\},\tag{2}$$

where the terms in $(Z-3)$ arise from the first three lines of (1) and the others from the last line. This result is based on neglect of exchange and on the approximation which considers the domain of the s electron as small, $r_s\to 0$. The later and more pretentious paper of Breit,[3] whose primary purpose was essentially a derivation of (1) and its consequences from relativistic reasoning analogous to that underlying the Dirac equation for one electron, leads to a triplet splitting given by the relative energies

$$C(0,-2,-3)-3d(0,-2,3),\tag{3}$$

where $C=\frac{1}{4}a\int u^*_1\{Z(\mathbf{l}_1/r_1^3+\mathbf{l}_2/r_2^3)-3h^{-1}(\mathbf{r}_2-\mathbf{r}_1)\times(\mathbf{p}_2-\mathbf{p}_1)/r_{12}^3\}_z u_1 d\tau$ and

$$d=-\tfrac{1}{4}a\int u^*_1\{(r_{12}^2-3z_{12}^2)/r_{12}^5\}u_1 d\tau.$$

Here $\mathbf{l}$ is the operator $\mathbf{r}\times\mathbf{p}/h$, $\mathbf{p}$ being linear momentum, and u_{ml} is a two-electron wave function of the configuration sp. A refined variational determination of these wave functions and the integrals containing them was carried out in Breit's paper, with quite satisfactory agreement with the observed triplet splitting in He, and presumably also in Li^+. For the sake of comparison of (2) with (3), we may specialize (3) to the simple case $r_s\to 0$, with neglect of exchange. In this case $r_{12}\to r_2$ and C reduces to $\frac{1}{4}a(Z-3)\times\langle(1/r^3)_p\rangle_{Av}$, so that the part of (3) involving it agrees with the corresponding part of the triplet splitting given by (2). The angular integration of d introduces a factor

$$\int(1-3\cos^2\theta)\sin^3\theta d\theta/\int\sin^3\theta d\theta=2/5,$$

making $d=-(1/10)a\langle(1/r^3)_p\rangle_{Av}$. We thus have

[1] W. Heisenberg, Zeits. f. Physik **39**, 499 (1926).
[2] L. H. Thomas, Phil. Mag. **3**, 1 (1926); J. Frenkel, Zeits. f. Physik **37**, 243 (1936); S. Dancoff and D. R. Inglis, Phys. Rev. **50**, 784 (1936).
[3] G. Breit, Phys. Rev. **36**, 383 (1939); **39**, 616 (1932). His integral D_0 is here denoted by $3d$. His integral D, arising from terms in e^4, need no longer concern us.

TABLE I. Diagonal elements of (4) and (5) by trace invariance.

m_l	m_{s_1}	m_{s_2}	(4)	(5)	J	(4)	(5)
1	+	+	1/10	1/16	2	1/10	1/16
0	+	+	−1/5	−1/8	1	−5/10	−5/16
1	+	−	−1/10	−1/16			
1	−	+	−1/10	−1/16			
1	−	−	1/10	1/16	0	10/10	10/16
−1	+	+	1/10	1/16			
0	+	−	1/5	1/8			
0	−	+	1/5	1/8			

the triplet energies

$$a\langle(1/r^3)_p\rangle_{Av}\{\tfrac{1}{4}(Z-3)(0,-2,-3)+(1/10)(0,-6,9)\} \quad (3')$$

and a separation ratio $({}^3P_2-{}^3P_1)/({}^3P_1-{}^3P_0)=-2/35$. The spin-spin terms of (2) are thus too small by a factor $\frac{5}{8}$. Since (2) has been rather widely quoted in the literature, it has some interest to point out the cause of the discrepancy. This lies in Heisenberg's *assumption* (reference 1, page 551) that the average value of

$$\{\mathbf{s}_1\cdot\mathbf{s}_2-3(\mathbf{s}_1\cdot\mathbf{r})(\mathbf{s}_2\cdot\mathbf{r})/r^2\}/r^3 \quad (4)$$

obtained by a classical treatment of the vector model, namely[4]

$$-\tfrac{1}{2}\{\mathbf{s}_1\cdot\mathbf{s}_2-3(\mathbf{s}_1\cdot\bar{\mathbf{l}})(\mathbf{s}_2\cdot\bar{\mathbf{l}})\}/r^3 \quad (5)$$

is valid also in quantum mechanics. His derivation from this point is somewhat indirect because of an appeal to Kronig's work on intensities, but his results may be derived very simply from (5) by use of trace invariance, and of the fact that the diagonal element of (5) for the singlet is zero, in the manner carried out in Table I. The corresponding correct calculation direct from (4), by use of the expression $m_{s_1}m_{s_2}(1-3\cos^2\theta)$ with $\cos^2\theta=1/5$ for $m_l=1$ and $3/5$ for $m_l=0$, is also carried out in the columns headed (4) in Table I, and the resulting contributions to the triplet splitting of course agree with (3′).

The calculation of Breit shows that the relative importance of the spin-spin term (the ratio d/C) is decreased by a factor $(0.21/0.2)/(0.91/0.5)=0.57$ when exchange and the s electron distribution in He are taken into account. This is so nearly equal to the factor $\frac{5}{8}$ which erroneously appeared in Heisenberg's calculation by neglecting these refinements that the error and neglect nearly annul one another and the results of the two calculations are very similar.

For the sake of a qualitative understanding of the distorted triplets it should be pointed out that the spin-orbit and spin-other-orbit couplings together would in helium make an inverted triplet obeying interval rule. This is manifest in the factor $(Z-3)$, which is negative for helium in the approximate formula (3′). It comes about because the magnitude of the spin-orbit coupling is determined by an effective nuclear charge $Z_{\text{eff}}=(Z-1)e=e$ and is further reduced by the "Thomas factor" $\frac{1}{2}$ because of the acceleration of the electron concerned, while the spin-other-orbit term arises primarily from the orbital motion of the p electron about the "spinning" s electron and its magnitude is determined by a charge $-e$, without any Thomas factor because the s electron is bound to the nucleus and not accelerated. The spin-spin interaction elevates the ${}^3P_0$ more than the ${}^3P_2$, while lowering the ${}^3P_1$, and in the approximation leading to (3′) it is responsible for the entire triplet splitting in Li^+, since there the spin-orbit and spin-other-orbit terms just annul one another.

Breit's evaluation of C and d takes into account both exchange and the finite domain of the s electron. The positive part of C, arising from the field of the bare nucleus, is thereby increased from $\frac{1}{2}C_0$ to $1.33C_0$, where $C_0=(R_H/\alpha^2)/24=m(e^4/\hbar c)^2/48$. (The value $\frac{1}{2}C_0$ is obtained by putting $\langle 1/r^3\rangle_{Av}=(me^2/\hbar^2)^3/[n^3l(l+\frac{1}{2})(l+1)]$ above.) The negative part of C, arising from the interaction of the electrons, is altered somewhat less, from $-1.5C_0$ to $-2.24C_0$. The increase in magnitude is in each case presumably caused mainly by a contraction of the scale of the p wave function, and a corresponding increase in density within and near the "s shell," due to the lowered potential within it. In the inter-electronic

[4] Here $\bar{\mathbf{l}}$ is the unit vector along l. A diagonal matrix element of $(\mathbf{s}_1\cdot\bar{\mathbf{l}})(s_2\cdot\bar{\mathbf{l}})$ may be obtained by multiplying by the operator l^2, so as to get rid of the unit vectors, taking the diagonal element, and then dividing by the proper value of l^2, which in our case is 2. In the m_l, m_{s_1}, m_{s_2}-representation of Table I, this leads to the evaluation of (5) as $\frac{1}{2}m_{s_1}m_{s_2}(1-3m_l^2/2)$. The mean value (5) may be derived from (4) by a classical treatment of the vector model in that representation thus:

$$\{\mathbf{s}_1\cdot\mathbf{s}_2-3(\mathbf{s}_1\cdot\mathbf{r})(\mathbf{s}_2\cdot\mathbf{r})/r^2\}_{Av}=s_{z_1}s_{z_2}\{1-3\langle z^2/r^2\rangle_{Av}\}$$
$$=s_{z_1}s_{z_2}\{1-(3/2)\sin^2(lz)\}$$
$$=s_{z_1}s_{z_2}\{-\tfrac{1}{2}+(3/2)\cos^2(lz)\}\rightarrow(5).$$

term, this increase is only partly compensated by the "incomplete screening," that is, by the fact that circulation of the p electron with an "s shell" is ineffective in the spin-other-orbit coupling. The net effect on C is an increase of 82 percent from $-\frac{1}{2}C_0$ to $-0.91C_0$, only about half of the change in $\langle 1/r^3\rangle_{Av}$. The effect on the spin-spin integral d is smaller, being a change from $-0.2C_0$ to $-0.21C_0$. The increased density near the s shell would alone make d considerably larger, but the finite spherical domain of the s electron has also a tendency to make d small because it distributes the s electron much more nearly isotropically about important positions of the p electron near the s shell, where $1/r_{12}^3$ may become very large—the integral is a maximum if both electrons are confined to the xy-plane, and is zero if they are isotropically distributed.

II. THE HIGHER TRIPLETS

The calculation of Breit for the low triplet has been repeated by Araki,[5] using slightly different wave functions which allow more polarization of the s distribution, and has also been extended by him to the higher triplets $1s3p\,^3P$ and $1snd\,^3D$. His results for the low triplet slightly improve the agreement with experiment but are not very significantly different from Breit's: the separation ratio $(^3P_2-{}^3P_1)/(^3P_1-{}^3P_0)$ equal to $1/14$ rather than $1/7$ implies an increase of the ratio d/C of only about 12 percent. With the approximations in the wave functions, probably neither calculation can claim an accuracy much greater than that. Among the higher triplets, Araki found both agreement and disagreement with the partially conflicting experimental data. In attempting to adjudge the seriousness of the disagreement, it is convenient to have at hand also a shorter calculation which is simplified in such a way as to present only those points which seem to be physically most important.

We neglect the interaction with the singlet, as did Breit, since it is small even in the high configurations where the singlet is nearby, and can only depress the central triplet level, decreasing the smaller separation slightly. There is so much less overlapping of the two single-electron wave functions in the configuration $1snd$ that we may treat the ^3D fairly well, and at the same time very simply, by neglecting exchange and the spatial extension of the s electron. So $r_s\to 0$, as above, and we have only one position vector. We construct Table II for $1snd\,^3D$, by use of (4) and the results of the angular integrations $\langle 1-3\cos^2\theta\rangle_{Av}=4/7, -2/7, -4/7$ for d states with $m_l=2, 1, 0$, respectively. The sixth column is obtained from the fourth by trace invariance as before. The spin-orbit and spin-other-orbit contributions are together listed in the seventh column. They alone form an inverted triplet obeying interval rule. The intervals are much distorted, but the inversion remains, when the spin-spin contributions are added (last column). It will be shown below that the ratios of the spin-spin contributions among themselves remain unaltered when one takes into account exchange and the extent of the s wave function. The only change is again a change of the scale of the spin-spin contributions, relative to the scale of the orbital contributions. The reasons for the change are essentially the same as in the ^3P case discussed above, and considerably less change is expected in $1s3d$ than in $1s2p$ because of the smaller overlapping of the single-electron wave functions. This leaves the $^3D_2$ very much nearer to the $^3D_3$ than to the $^3D_1$.

The agreement between the two sets of experimental data,[6,7] and their agreement with the theory, in the low triplet $1s2p\,^3P$ is gratifying. In the next triplet, $1s3p\,^3P$, the calculations of

TABLE II. Splitting of a ^3D in helium. Multiply by $\langle a/r^3\rangle_{Av}$ to obtain energies.

m_l	m_{s_1}	m_{s_2}	$m_{s_1}m_{s_2}(1-3\cos^2\theta)$	J	spin-spin	$\frac{1}{4}(Z-3)\dot{s}$	Sum
2	+	+	1/7	3	1/7	−1/2	−10/28
2	+	−	−1/7	2	−1/2	1/4	− 7/28
2	−	+	−1/7				
1	+	+	−1/14				
2	−	−	1/7	1	1/2	3/4	35/28
1	+	−	1/14				
1	−	+	1/14				
0	+	+	−1/7				

[5] G. Araki, Proc. Phys. Math. Soc. Japan **19**, 128 (1937).

[6] W. V. Houston, Proc. Nat. Acad. Sci. **13**, 91 (1927). Professor Houston has kindly pointed out the following misprints: In Fig. 1, the subscripts of $^3D_2$ and $^3D_3$ should be interchanged, as is obvious from the transitions drawn and from selection rules, and in the fifth line of Table I $^3P_0$ should read $^3P_1$, which combines with $^3D_{12}$.

[7] G. Hansen, Verh. d. deutsch phys. Ges. **10**, 5 (1929).

TABLE III. Triplet energies in strong and weak fields.

M_L	M_S	$H'''/(\mu_B H)$	H''	M_J	J	H''	$H'''/(\mu_B H)$
L	1	$L+2$	C_L+d_L	$L+1$	$L+1$	C_L+d_L	$L+2$
L	0	L	$-2d_L$	L	$L+1$	C_L+d_L	$(L+2)L/(L+1)$
$L-1$	1	$L+1$	$C_{L-1}+d_{L-1}$	L	L	$C_{L-1}-C_L+d_{L-1}-3d_L$	$(L^2+L+1)/(L+1)$
L	-1	$L-2$	$-C_L+d_L$	$L-1$	$L+1$	C_L+d_L	$(L+2)(L-1)/(L+1)$
$L-1$	0	$L-1$	$-2d_{L-1}$	$L-1$	L	$C_{L-1}-C_L+d_{L-1}-3d_L$	$(L^3-1)/(L^2+L)$
$L-2$	1	L	$C_{L-2}+d_{L-2}$	$L-1$	$L-1$	$C_{L-2}-C_{L-1}-C_L+d_{L-2}-3d_{L-1}+3d_L$	$(L-1)^2/L$

Araki yield a result intermediate between (3′) and the $1s2p\,^3P$ result, as one would expect by comparing the overlapping in the two configurations, and this disagrees sharply with the observed[8] separations $^3P_2-{}^3P_1=0.165$ cm^{-1}, $^3P_1-{}^3P_0=0.192$ cm^{-1}. Such a separation ratio, with one level almost midway between the other two, would require a ratio $d/C=1/12$, rather than over $\frac{1}{4}$ as calculated, and it is extremely unlikely that any of the approximations of the theory could introduce so large an error in this ratio. Configuration interaction seems to be excluded as a possible cause of the discrepancy, the nearest odd configuration being more than 5000 cm^{-1} distant. This seems to be the only measurement of this triplet available. Araki[5] and others[9] have quoted a supposedly experimental value of its separation ratio by Houston, although he measured only the over-all triplet width and stated what the separations would be if the ratio should be the same as in the lower triplet, a surmise based on Heisenberg's theoretical treatment. A repetition of the measurement would be of interest. In the $1s3d\,^3D$, the earlier analysis of Houston,[6] while apparently painstaking and legitimate, was made in spite of the difficulty that his experiments did not resolve this triplet, and his results may perhaps be said to have been superseded by the later measurements of Hansen,[7] who did succeed in resolving it into two lines, by use of liquid helium. The earlier results placed the $^3D_3$ nearer the $^3D_1$ than the $^3D_2$, a distortion which no plausible modification of the theory could give, while Hansen's separations are $^3D_3-{}^3D_2<0.01$ cm^{-1}, $^3D_2-{}^3D_1=0.04$ cm^{-1}, in accord with theory. In the high triplet $1s4d\,^3D$ no measurement of the separation ratio is available, although here again a surmise from reference 6 has been quoted as experimental.[5,9] The over-all separations of both the D triplets measured by Hansen agree with results of Araki.

III. DERIVATION FOR A GENERAL TRIPLET

We shall now derive an expression for the triplet splitting in terms of parameters C and d which is valid for any triplet. Other calculations have involved good, but still special, assumptions concerning the wave functions. In order to avoid specialization of the form of the wave function (beyond the properties of a triplet) and in order at the same time to avoid use of the theorems of group theory, we employ the method of comparing coefficients in the secular equations determined in two extreme representations.[10] This requires the calculation of only diagonal matrix elements. Because of the simplicity of the proper functions of the atom in a strong magnetic field (strong enough to make energies much larger than the triplet splitting, but much smaller than the singlet-triplet separation) we consider the secular equations of this Paschen-Back transition.

The wave functions of the triplet are

$$\psi_{M_L M_S}(r_1, r_2, \sigma_1, \sigma_2) = U_{M_L L}(r_1, r_2) S_{M_S}(\sigma_1, \sigma_2)$$

with

$$S_{\pm 1}=\delta(\pm\tfrac{1}{2}/\sigma_1)\delta(\pm\tfrac{1}{2}/\sigma_2);$$
$$S_0=\{\delta(\tfrac{1}{2}/\sigma_1)\delta(-\tfrac{1}{2}/\sigma_2)+\delta(\tfrac{1}{2}/\sigma_2)\delta(-\tfrac{1}{2}/\sigma_1)\}/\sqrt{2},$$

where the δ's are the Pauli single-electron spin functions. In this representation we first wish to reduce the diagonal elements of H'' to as few undetermined parameters as possible. The form

[8] R. C. Gibbs and P. G. Kruger, Phys. Rev. **37**, 1559 (1931).

[9] Bacher and Goudsmit, *Atomic Energy States* (McGraw-Hill, 1934).

[10] S. Goudsmit, Phys. Rev. **35**, 1925 (1930).

of the usual spin operations,

$$(s_x \pm i s_y)\delta(\pm\tfrac{1}{2}/\sigma) = 0,$$
$$(s_x \pm i s_y)\delta(\mp\tfrac{1}{2}/\sigma) = \delta(\pm\tfrac{1}{2}/\sigma),$$
$$s_z\delta(\pm\tfrac{1}{2}/\sigma) = \pm\tfrac{1}{2}\delta(\pm\tfrac{1}{2}/\sigma),$$

is such that only the z component of s_i contributes to a diagonal element of the first three lines of (1), which are linear in the $\mathbf{s}_i$ and may of course be factored in the familiar form $\mathbf{A}\cdot\mathbf{s} = \frac{1}{2}(A_x + iA_y) \times (s_x - is_y) + \frac{1}{2}(A_x - iA_y)(s_x + is_y) + A_z s_z$. Since the matrix element $(M_S | s_{iz} | M_S) = \frac{1}{2}M_S$ for $i = 1$ or 2, we may write the part of the matrix element $(M_L M_S | H'' | M_L M_S)$ which arises from the first three lines of (1) in the form

$$\tfrac{1}{2}aM_S(M_L | \{\tfrac{1}{2}Z(l_{1z}/r_1^3 + l_{2z}/r_2^3) - (m/\hbar) \times \tfrac{3}{2}[(\mathbf{r}_2 - \mathbf{r}_1)\times(\dot{\mathbf{r}}_2 - \dot{\mathbf{r}}_1)]_z / r_{12}^3\} | M_L) \equiv M_S C_{M_L}. \quad (6)$$

In the spin-spin terms, the proper value $\frac{1}{4}$ of $\mathbf{s}_1\cdot\mathbf{s}_2$ may be inserted directly, and the spin operations just listed may be used in the last term, to give the part of $(M_L M_S | H'' | M_L M_S)$ arising from the last line of (1) in the form

$$\tfrac{1}{4}a(M_L | \{1/r_{12}^3 - 3z_{12}^2/r_{12}^5\} | M_L) \equiv d_{M_L}$$
for $M_S = \pm 1$ and (7)
$$\tfrac{1}{4}a(M_L | \{1/r_{12}^3 - 3(1/r_{12}^3 - 2z_{12}^2/r_{12}^5)\} | M_L) = -2d_{M_L} \quad \text{for } M_S = 0.$$

These energies are listed in the fourth column of Table III for the states of the $M_L M_S$ representation (strong field). The values calculated from them for the JM_J representation, by use of trace invariance and the fact that these "internal" energies depend on J but not on M_J, are listed in the seventh column. In treating the Paschen-Back transition, we also introduce the perturbing energy of an external magnetic field H,

$$H''' = -\mu_B(\mathbf{L} + 2\mathbf{S})\cdot\mathbf{H},$$

and list its diagonal elements in Table III. Here μ_B is the Bohr magneton. (The fact, familiar from the vector model, that the Zeeman energies in the weak-field case are proportional to M_J for a given J, may be used together with trace invariance to obtain the last column of Table III from the strong-field case.) Table III gives the energies as one departs from either extreme of the Paschen-Back transition: in the strong-field case we have an expansion to the first order in the small quantity a/H and in the weak field case an expansion to the first order in the small quantity H/a. The intermediate transition of the two levels with $M = L$ is described by the roots E of a quadratic secular equation of the form

$$E^2 - (\alpha + \beta H)E + \gamma + \delta H + \epsilon H^2 = 0. \quad (8)$$

The sum of the last three terms, which do not contain E, is the product of the two roots. The central term δH is determined by the first-order expansion of the roots in either extreme case: using the strong-field energies listed in Table III, we find

$$\delta/\mu_B = L(C_{L-1} + d_{L-1}) - 2(L+1)d_L$$

and using the weak-field energies we find

$$\delta/\mu_B = \{L(L+2)(C_{L-1} + d_{L-1}) - (L-1)C_L - (2L^2 + 5L - 1)d_L\}/(L+1).$$

Since the C's are physically independent of the d's, this double determination of δ yields the two relations

$$C_{L-1} = [(L-1)/L]C_L$$
$$d_{L-1} = [(L-3)/L]d_L. \quad (9)$$

Similarly, the cubic equation for the three levels with $M = L - 1$ contains a coefficient of E which is equal to the sum of the products of the roots taken two at a time, and the double determination of the term which is linear in H furnishes two additional relations which, by use of (9), reduce to

$$C_{L-2} = [(L-2)/L]C_L$$
$$d_{L-2} = [(2L^2 - 13L + 12)/L(2L-1)]d_L. \quad (10)$$

By use of these relations the triplet energies in the seventh column of Table III may be written in terms of the two integrals C_L and d_L, which we now call simply C and d:

$$E_{L+1} = C + d$$
$$E_L = -(1/L)C - [(2L+3)/L]d \quad (11)$$
$$E_{L-1} = -[(L+1)/L]C + [(2L+3)(L+1)/L(2L-1)]d.$$

For $L = 1$, the separations of these levels are of course the same as Breit's result (3). For $L = 2$ they are compatible with Table II, and the ratios of the spin-spin terms are not affected by the greater generality. For any value of L, the

terms in C, which contain the spin-orbit and the spin-other-orbit contributions, imply the interval rule.

The Paschen-Back effect of a distorted ^3P has been treated by Green and Loring,[11] and their simple method may be extended to other triplets. They introduce the empirical zero-field energy differences. In order to obtain an entirely theoretical expression for the Paschen-Back energies, one may substitute the theoretical values of the energies relative to E_{L+1}, in their case $P_1=E_1-E_2$ and $P_0=E_0-E_2$, from (11). In practice, however, one would ordinarily evaluate the integrals C and d from these empirical separations, and the form of the equations in which the empirical values appear directly is the more convenient one.

Thanks are extended to Professors S. Goudsmit, W. V. Houston, and J. B. Green for helpful discussions.

[11] J. B. Green and R. A. Loring, Phys. Rev. **49**, 632 (1936). Their introductory neglect of the spin-spin term has no effect on their treatment of the Paschen-Back effect.

MARCH 1 AND 15, 1942 PHYSICAL REVIEW VOLUME 61

Term Formulae for the Configuration d^5

OTTO LAPORTE
University of Michigan, Ann Arbor, Michigan
(Received January 19, 1942)

Term formulae for a configuration of five equivalent d electrons have hitherto not been published. They are given below for the case of Russell-Saunders coupling. A surprising result is that although several terms appear more than once (two ^2G, two ^2F, three ^2D) and are therefore expected to depend irrationally upon the radial integrals, this is only so for two out of the three ^2D terms. For the other of the above terms the secular equation possesses roots linear in the radial integrals. The formulae obtained are able to represent satisfactorily the d^5 terms of Cr II.

FORMULAE representing the distances of the terms arising from a configuration of equivalent d electrons as a function of radial integrals are readily derived by diagonal sum methods as long as each term occurs only once. For d^2 such formulae were given by Slater[1] and for d^3 by Condon and Shortley[2] in which latter case only the sum of the energies of the two ^2D terms was obtained. The separate energies of these terms result without difficulty from a consideration of non-diagonal elements of the energy matrix; they were given by Ufford and Shortley[3] and by Serber,[4] using Van Vleck's[5] method. In the configuration d^4 the doubly occurring terms are more numerous than the others; the complete formulae were given by Ostrofsky.[6]

The energies of the configuration d^5 have hitherto never been published although they are of great importance to the experimental spectroscopist when investigating Cr II and its higher isoelectronic relatives. Also in Mg I and similar spectra can they be expected to be useful since they account for the d^5s^2 configuration as well. In spite of the greater number of magnetic levels (252 compared to 210 for d^4) the computations for d^5 are simpler because of the smaller number of multiply occurring terms (there are two ^2G, two ^2F, and three ^2D).

For these latter the method employed was that described by Condon and Shortley in Section 5[8] of their book.[7] Consider that space of eigenfunctions characterized by the maximum M_SM_L values for which the term pair in question occurs. In this space a complete set of orthonormal unit vectors is given, the unstabilized eigenfunctions $\Phi(m_s^1m_l^1m_s^2m_l^2\cdots)$. The proper linear com-

[1] J. C. Slater, Phys. Rev. **34**, 1293 (1929).
[2] E. U. Condon and G. H. Shortley, Phys. Rev. **37**, 1025 (1931).
[3] C. W. Ufford and G. H. Shortley, Phys. Rev. **42**, 167 (1932).
[4] R. Serber, Phys. Rev. **45**, 461 (1934).
[5] J. H. Van Vleck, Phys. Rev. **45**, 405 (1934).
[6] M. Ostrofsky, Phys. Rev. **46**, 604 (1934). For corrections see paper following this.

[7] E. U. Condon and G. H. Shortley, *Theory of Atomic Spectra*.

binations which represent the eigenfunctions Ψ of a term ^{2S+1}L in that space are known by the angular momentum operator method. It now becomes necessary to find two (or three) more linear combinations of the Φ perpendicular to the Ψ. This can immediately be done provided the $M_S M_L$ space does not have too many dimensions. However, the configurations d^4 and d^5 present cases where the space in question may have such high dimensionality that it may be quite difficult to find additional unit vectors by straightforward methods. In such cases the following procedure has been found useful.

Let the $M_S M_L$ space have n dimensions. In it n unstabilized eigenfunctions Φ_n are available which are orthonormal:

$$(\Phi_i \Phi_j) = \delta_{ij} \quad i, j = 1 \cdots n.$$

By the method of angular momentum operators m stabilized eigenfunctions Ψ_ν have been obtained as linear combinations

$$\Psi_\nu = \sum_{i=1}^{n} a_{\nu i} \Phi_i \quad \nu = 1 \cdots m,\ m < n,$$

where

$$(\Psi_\nu \Psi_{\nu'}) = \delta_{\nu\nu'}.$$

The problem is to find $n-m$ further Ψ functions completing the set. We now write:

$$\Psi_{m+1} = \sum_{\mu=1}^{m} b_\mu \Psi_\mu + c_1 \Phi_1.$$

Orthogonality with all previous Ψ_ν fixes b_μ:

$$b_\mu = -a_{\mu 1} c_1$$

and c_1 is determined by the normalization condition. To get the next unit vector Ψ_{m+2} a different Φ, say Φ_2 will have to be preferred by writing

$$\Psi_{m+2} = \sum_{\mu=1}^{m+1} b_\mu' \Psi_\mu + c_2 \Phi_2.$$

The determination of b_μ' and of c_2 is as before.

This method makes the construction of further unit vectors easy and straightforward. It was used on the 12-dimensional space $M_S = \frac{1}{2}$, $M_L = 2$ of d^5, in which 9 stabilized Ψ were known by the angular momentum operator method and three more had to be found. The secular determinant is only of order 3.

The final formulae are given below; they represent the energies of 16 terms as functions of three radial integrals F_0, F_2, F_4. These latter are, if we denote by $f(r)$ the radial part of the eigenfunctions

$$F_k = F^k / D_k \tag{1}$$

with

$$F^k = 2e^2 \int_0^\infty r^2 dr f^2 r^{-k-1} \int_0^r r'^2 dr' f^2 r'^k \tag{2}$$

and

$$D_0 = 1, \quad D_2 = 49, \quad D_4 = 441.$$

$$\begin{aligned}
^6S &= 10\,F_0 - 35\,F_2 - 315\,F_4, \\
^4G &= 10\,F_0 - 25\,F_2 - 190\,F_4, \\
^4F &= 10\,F_0 - 13\,F_2 - 180\,F_4, \\
^4D &= 10\,F_0 - 18\,F_2 - 225\,F_4, \\
^4P &= 10\,F_0 - 28\,F_2 - 105\,F_4, \\
^2I &= 10\,F_0 - 24\,F_2 - 90\,F_4, \\
^2H &= 10\,F_0 - 22\,F_2 - 30\,F_4, \\
(1)^2G &= 10\,F_0 - 13\,F_2 - 145\,F_4, \\
(2)^2G &= 10\,F_0 + 3\,F_2 - 155\,F_4, \\
(1)^2F &= 10\,F_0 - 25\,F_2 - 15\,F_4, \\
(2)^2F &= 10\,F_0 - 9\,F_2 - 165\,F_4, \\
(1)^2D &= 10\,F_0 - 4\,F_2 - 120\,F_4, \\
(2, 3)^2D &= 10\,F_0 - 3\,F_2 - 90\,F_4 \\
&\quad \pm (513\,F_2^2 - 4500\,F_2F_4 + 20700\,F_4^2)^{\frac{1}{2}}, \\
^2P &= 10\,F_0 + 20\,F_2 - 240\,F_4, \\
^2S &= 10\,F_0 - 3\,F_2 - 195\,F_4.
\end{aligned}$$

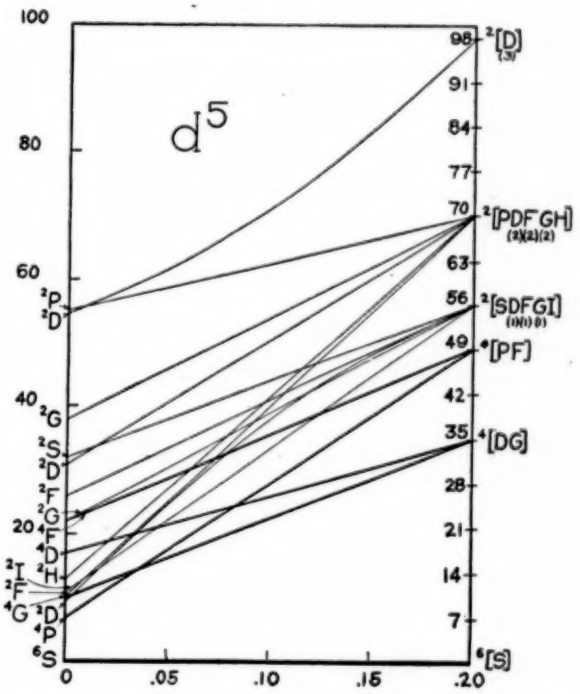

FIG. 1. Terms of configuration d^5 referred to ^6S as functions of F_4/F_2.

The number in parenthesis in front of a term symbol distinguishes the various terms of equal L and S values that occur. We should like to mention at this time that a standard notation should be provided for such multiply occurring terms, especially since they are so much more numerous in configurations of type f^2. It is evidently inadmissible to use letters a, b, c $\cdots$ here since they serve to label *any* sequence of

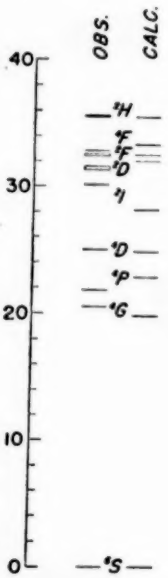

FIG. 2. Comparison with observed d^5 terms in the spectrum Cr II.

^{2S+1}L terms of equal parity regardless of whether they belong to the same configuration or not.

Since each element of the energy matrix is linear in the F_k it is to be expected that the energy of a singly occurring term is also linear in the F_k and that the energy of a term pair will contain the square root of a quadratic form in F_jF_k. Similarly a triple of terms is expected to contain the cube root of a form homogeneous of degree 3 in the F. It is therefore remarkable that the two term pairs (1 and 2)^2G and (1 and 2)^2F turn out to be rational in the F_k and that the cubic equation for the three ^2D turns out to have one root, here denoted by (1)^2D, which is also rational. Since the same phenomenon does not occur for any pair of terms in the configuration d^3 or d^4 one is justified in regarding it as a unique feature of d^5. In this connection one is reminded of another fact which simplifies d^5 in comparison with other d^z configurations, namely the vanishing of the spin-orbit interaction constant ζ for all terms. To be sure both results are true only in first approximation.

Comparison of the formulae with experimental values is best carried out by means of the following nomograph scheme. On transparent paper the experimental term distances are marked off along a vertical line. These points are then connected by means of straight lines to a fixed point. Thus on any line parallel to the original vertical line the convergent rays will mark off proportional distances. This transparent graph is then laid on top of Fig. 1 and so adjusted that the straight convergent lines and the curves of Fig. 1 intersect along a vertical line. The two parameters can then be read off. Figure 2 contains a comparison of the formulae with nine terms of d^5 in the spectrum of Cr II. The data were kindly supplied by Dr. C. C. Kiess. A preliminary fit was obtained within a very short time by the graphical method just described. The figure contains a plot of the formulae calculated by setting $F_2=1050$ and $F_4/F_2=0.0681$.

The author wishes to thank Mr. B. Vinograde for assistance in the numerical calculations. A grant from the Faculty Research Fund of the University of Michigan is gratefully acknowledged.

Degeneracies Among Terms of a Configuration of Equivalent Electrons

OTTO LAPORTE, *University of Michigan, Ann Arbor, Michigan*

AND

JOHN R. PLATT, *University of Minnesota, Minneapolis, Minnesota*

(Received January 19, 1942)

If the radial integrals occurring in the term formulae for a configuration l^z assume certain integer ratios given in Table III all elements of the energy matrix become low multiples of a common value. As a consequence high degeneracies are seen to occur. The reason for this behavior is proved to be the existence of an identity [Eq. (6)] concerning sums of products of three integrals of spherical harmonics. The regularity mentioned may serve in the approximate allocation of energy levels or as a check for exact energy formulae. Ostrofsky's formulae for d^4 were found to be incorrect in this way. The correct formulae are given in §2.

WITH the assumption of Russell-Saunders coupling the term energies due to electrostatic interaction for configuration l^z of z equivalent electrons may be written in the form:

$$E=\sum_{k=0,\,2,\,\cdots}^{l} A_k(z,l,L,S)F_k(n,l), \qquad (1)$$

where

$$A_0=\tfrac{1}{2}z(z-1)$$

and

$$F_k=F^k/D_k(l). \qquad (2)$$

For values of D_k see Table I, and for the definition of F^k see the preceding paper, formulae (1) and (2). As is seen from the upper limit of the sum, the relative term values depend on l parameters, *i.e.*, one for p^z, two d^z, etc. The single parameter for p^z simply defines the scale of the configuration, the distances between terms having a fixed interval ratio. This is different for d^z, where after one parameter, say F_2, has been used to fix the scale, the ratios of distances between terms yet depend on the values of F_4/F_2. As a consequence not even the order of the terms within a configuration is fixed.

In order to gain a clear picture of the term energies within a d^z configuration it therefore seems reasonable to plot reduced term values defined by

$$T_{\text{red}}=[E-E(L_{\max},S_{\max})]/F_2$$

as functions of the variable F_4/F_2. A similar graphical representation for f^z would be three-dimensional, for g^z four-dimensional. In Fig. 1 such plots are given for the configurations d^z. For the abscissa value 0.2, *i.e.*, for

$$F_2 : F_4=5 : 1, \qquad (3)$$

high degeneracies are seen to occur to which the following lines are devoted.

1. DEGENERACIES FOR CONFIGURATIONS d^z

The arrangement of terms at the point of degeneracy is best described by Table II which is reminiscent of early tables of Hund.[1] It contains all terms due to the configurations d^z, $z=0\cdots 5$. The arrangement is such that terms of a d^z which have occurred before, *i.e.*, for smaller z, are put into the same column as before while new terms are separated according to S values and put into new columns.

The order of the columns is determined by the numbers in the last row. These numbers indicate the term values at the point of degeneracy as taken from the right-hand side of each graph of Fig. 1. Since according to the definition of T_{red} the scale is arbitrary, the factor 7 has been

TABLE I. Table of numerical coefficients $[D_k(l)]^{\frac{1}{2}}$ defined by $c^k=c_k/[D_k(l)]^{\frac{1}{2}}$ and by $F^k=F_kD_k(l)$.

	$k=0$	2	4	6	8
$l=1$	1	5			
2	1	7	$3\cdot 7$		
3	1	$3\cdot 5$	$3\cdot 11$	$\frac{3\cdot 11\cdot 13}{5}$[1]	
4[2]	1	$7\cdot 11$	$\frac{7\cdot 11\cdot 13}{9}$	$11\cdot 13$	$\frac{11\cdot 13\cdot 17}{7}$

[1] Instead of this value Condon and Shortley gave 7361·64. This is an error.
[2] This row of values is due to Shortley and Fried, reference 4.

[1] F. Hund, Zeits. f. Physik **33**, 345 (1925).

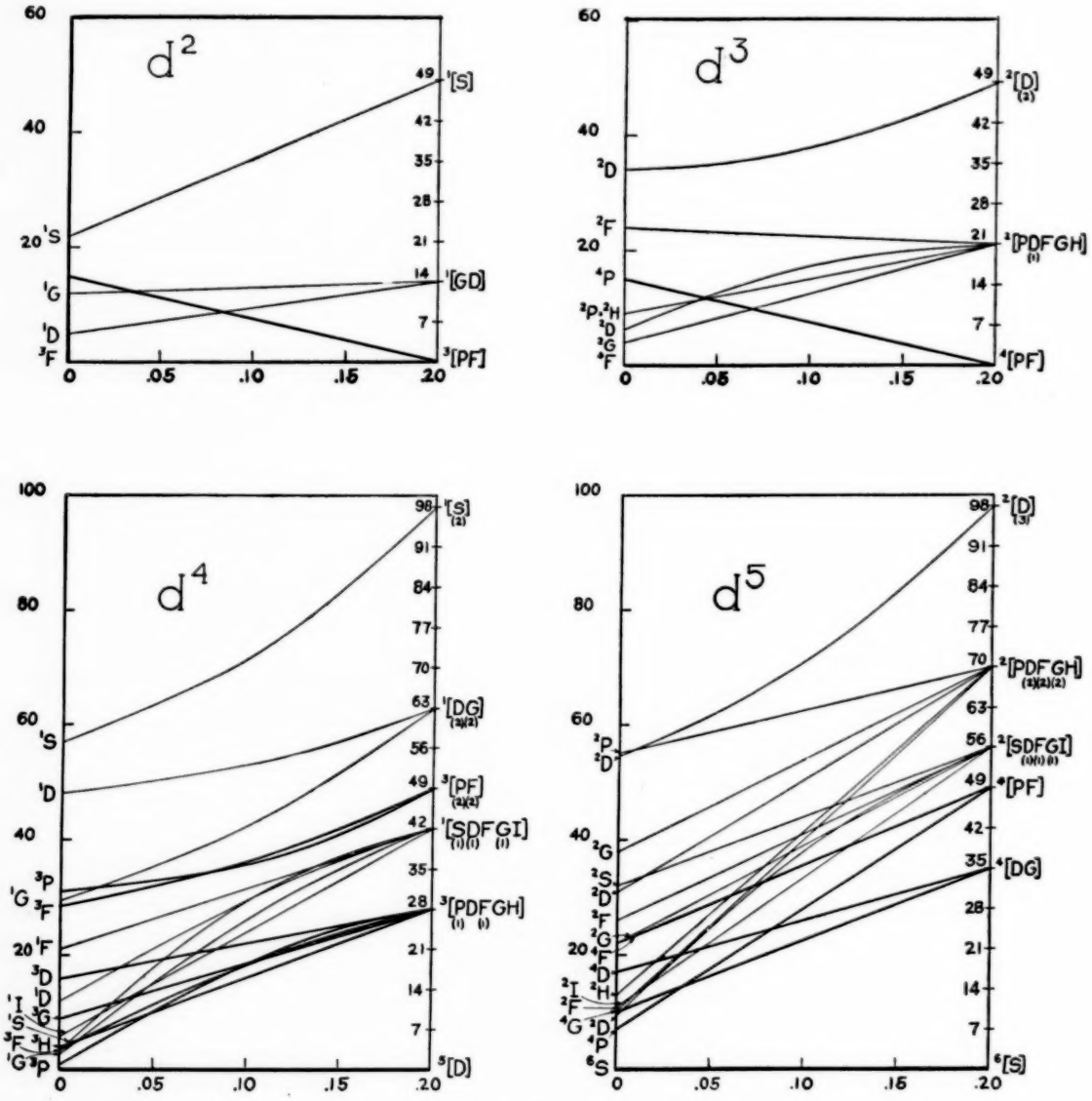

FIG. 1. Relative term values due to d^z for $z=2$, 3, 4, 5 referred to the term of maximum S and maximum L value as zero, considered as functions of F_4/F_2. The place of degeneracy is at the extreme right of each of the four diagrams. Since all observed data can be fitted to these curves with abscissa values between zero and 0.2 the above diagrams were not continued past the point of degeneracy. It may also be of interest to note that with any reasonable assumption for the radial eigenfunctions (like $\rho^a e^{-\rho}$) the ratio F_4/F_2 turned out to be <0.2.

suppressed and only the multiple is given. By referring the relative term values to the highest term instead of the lowest, it is possible to assign to each term group a number which will give its distance from the highest term in the configuration (^2D or ^1S) regardless of the value of z. Thus the term groups ^1S, $^1(DG)$, $^3(PF)$ have distance 5 : 2 not only in d^2 but also in d^4. Similarly the term groups of d^3 reoccur with the same distances in d^5.

There is still a further regularity contained in Table II. The occurring term groups are, for even configurations:

$$^2D\ ^2(PDFGH)\ ^2(SDFGI)\ ^4(PF)\ ^4(DG)\ ^6S,$$

for odd configurations, written in the opposite directions

$$^5D\ ^3(PDFGH)\ ^1(SDFGI)\ ^3(PF)\ ^1(DG)\ ^1S.$$

Since the numbers in the last row of Table II

TABLE II. Grouping of terms at the point of degeneracy.

Configuration	Term Groups								
d^0	^1S								
d^1	^2D								
d^2	^1S		$^1(DG)$		$^3(PF)$				
d^3	^2D	$^2(PDFGH)$				$^4(PF)$			
d^4	^1S		$^1(DG)$		$^3(PF)$				
d^5	^2D	$^2(PDFGH)$		$^2(SDFGI)$		$^4(PF)$	$^1(SDFGI)$	$^4(DG)$	$^3(PDFGH)$	^5D ^6S
relative term value	0	4	5	6	7		8	9	10	14

are symmetrical with respect to their middle, it is possible to associate d^5 with the inverted d^4 if one only changes S values according to the above juxtaposition.

2. CORRECTED FORMULAE FOR d^4

The term formulae for d^4, as published by Ostrofsky[2] do not all conform to the degeneracy at $F_2/F_4=5$. The entire configuration was therefore recomputed adopting a method essentially identical with that described in the previous paper and errors were found for the two term pairs $(1,2)^1S$ and $(1,2)^1G$. The correct formulae showing the expected degeneracy are given below.

$$
\begin{aligned}
^5D &= 6\,F_0 - 21\,F_2 - 189\,F_4,\\
^3H &= 6\,F_0 - 17\,F_2 - 69\,F_4,\\
^3G &= 6\,F_0 - 12\,F_2 - 94\,F_4,\\
(1,2)^3F &= 6\,F_0 - 5\,F_2 - 76.5\,F_4 \pm \tfrac{1}{2}(612\,F_2^2 - 4860\,F_2F_4 + 20025\,F_4^2)^{\frac{1}{2}},\\
^3D &= 6\,F_0 - 5\,F_2 - 129\,F_4,\\
(1,2)^3P &= 6\,F_0 - 5\,F_2 - 76.5\,F_4 \pm \tfrac{1}{2}(912\,F_2^2 - 9960\,F_2F_4 + 38025\,F_4^2)^{\frac{1}{2}},\\
^1I &= 6\,F_0 - 15\,F_2 - 9\,F_4,\\
(1,2)^1G &= 6\,F_0 - 5\,F_2 - 6.5\,F_4 \pm \tfrac{1}{2}(708\,F_2^2 - 7500\,F_2F_4 + 30825\,F_4^2)^{\frac{1}{2}},\\
^2F &= 6\,F_0 - 48\,F_4,\\
(1,2)^1D &= 6\,F_0 + 9\,F_2 - 76.5\,F_4 \pm \tfrac{1}{2}(1296\,F_2^2 - 10440\,F_2F_4 + 30825\,F_4^2)^{\frac{1}{2}},\\
(1,2)^1S &= 6\,F_0 + 10\,F_2 + 6\,F_4 \pm \tfrac{1}{2}(3088\,F_2^2 - 26400\,F_2F_4 + 133200\,F_4^2)^{\frac{1}{2}}.
\end{aligned}
$$

3. CONNECTION OF DEGENERACIES WITH AN IDENTITY CONTAINING THE CONDON-SHORTLEY $c^k(lmlm')$

In order to understand the degeneracy just discussed it is necessary to retrace somewhat the steps which lead to formula (1). The electrostatic energies are roots of the energy matrix whose elements are of the form:[3]

$$
\left(ab\left|\sum\frac{e^2}{r_{ij}}\right|cd\right)
$$

$$
= \delta(m_s^a m_s^c)\,\delta(m_s^b m_s^d)\,\delta(m_l^a + m_l^b,\ m_l^c + m_l^d)
$$

$$
\cdot \sum_{k=0,\,2\cdots}^{l} c^k(lm_l^a lm_l^c)\,c^k(lm_l^d lm_l^b)\,F^k(n,l). \quad (4)
$$

a, b, c, d are four sets of quantum numbers sharing however n and l. The c^k are defined as coefficients in the expansion of a product of spherical harmonics into a series of spherical harmonics:

$$
\theta(lm)\,\theta(lm') = \sum_k \left(\frac{2k+1}{2}\right)^{\frac{1}{2}} c^k(lmlm') \times \theta(k, m-m') \quad (5)
$$

and the F^k by Eq. (2) of the preceding paper. The book of Condon and Shortley contains complete tables of the c^k coefficients for $l \leqq 3$, while for $l=4$ they are given by Shortley and Fried.[4]

The theorem from which the degeneracies discussed above and similar ones for $l=3$ and 4

[2] M. Ostrofsky, Phys. Rev. **46**, 604 (1934).

[3] E. U. Condon and G. H. Shortley, *Theory of Atomic Spectra*, Eq. (869), p. 175.

[4] G. H. Shortley and B. Fried, Phys. Rev. **54**, 739 (1938).

TABLE III. Values of $f_k(l)$ occurring in Eq. (7).

	$f_k(l)$					
	$k=(0)$	2	4	6	8	N_l
$l=2$	(14)	5	1			35
3	(132)	11	6	1		462
4	(20020)	65	90	91	14	90090

arises is the following:

$$\sum_k \frac{2k+1}{2} \frac{c^k(lmlm')c^k(lm_1lm_1')}{c^k(l0l0)} = \delta(mm_1)\delta(m'm_1') \cdot (1+\delta(m,-m')\delta(m_1,-m_1'))\frac{2l+1}{4}, \quad (6)$$

where

$$m \geqq m', \quad m_1 \geqq m_1', \quad m-m'=m_1-m_1'.$$

The combination of Kronecker δ symbols on the right causes the sum over k to be 0, 1 or 2 times $(2l+1)/4$. For certain m and arbitrary l values this theorem has been proved by using Gaunt's formulae for c^k, transforming the k sum into a contour integral and deforming the path suitably. After inserting the values of $c^k(l0l0)$ from the tables and changing over to c_k by means of Table I we may write (6) in the following form:

$$\sum_k f_k(l)c_k(lmlm')c_k(lm_1lm_1') = (0, 1 \text{ or } 2)\cdot N_l. \quad (7)$$

The $f_k(l)$ and N_l are given in Table III. Comparison with (4) shows that for radial integrals whose ratio is that of Table III the matrix elements become small multiples of a common integer factor.

But if this is so for the matrix elements it must also be so for the eigenvalues. This is trivial for singly occurring terms for they can always be obtained by Slater's method solely from diagonal elements. But even for multiply occurring terms the eigenvalues will be integers because the energy matrix can always be reduced to one obtained when determining the distribution of a number of identical systems over two eigenvalues. Since such matrices have always rational roots they will in our case be integers.

4. DEGENERACIES FOR CONFIGURATIONS f^2 AND g^2

According to Table III similar degeneracies are expected for configurations of f electrons when the radial integrals F_k are in the ratio

$$F_2 : F_4 : F_6 = 11 : 6 : 1 \quad (8)$$

and for g configurations, if

$$F_2 : F_4 : F_6 : F_8 = 65 : 90 : 91 : 14. \quad (9)$$

These points of degeneracy should serve similarly in the higher shells for the approximate allocation of levels or as check on energy calculations as did the point $F_2 : F_4 = 5$ for d configurations.

As a case in point we mention that the term formulae given by Condon and Shortley[5] for ff were in this way discovered to be incorrect by error in sign; the formula for $^{1,3}F$ should be

$$^{1,3}F = F_0 - 10\,F_2 - 33\,F_4 - 286\,F_6 \pm (G_0 - 10\,G_2 - 33\,G_4 - 286\,G_6).$$

If we assume in f^2 the F_k to have the ratios (8), all triplet terms, namely $^3(PFH)$ coincide and the singlet terms $^1(DGI)$ coincide while ^1S lies alone above the latter group at a distance whose ratio to that between the other groups is as 7 : 1.

A similar result is obtained from Shortley and Fried's formulae for g^2 when assuming the parameter ratio (9) only that the ^1S term lies at a nine times greater distance above the other singlet terms than they themselves lie above the triplet terms.

[5] On page 207 of their book.

Electron Diffraction Studies on Thin Films

III. Powder Patterns Containing Anomalies Produced by Secondary Scattering[1]

L. H. GERMER
Bell Telephone Laboratories, New York, New York

(Received December 8, 1941)

As a consequence of considerable tolerance in glancing angle in the production of diffracted electron beams, each first-order beam can itself be diffracted a second time by the same set of planes, thus producing by this double process an apparent second-order beam. In patterns from polycrystalline substances this results in strengthening all second-order diffraction rings. The effect is appreciable only when the individual crystals are of considerable size, and it can be observed only when a *true* second-order diffraction ring is very weak. The phenomenon has been observed in diffraction patterns from CuCl, CuBr and CaF_2. One calculates that the true (222) ring is unobservably weak in these patterns; yet it is observed to be rather strong in many cases, varying in relative intensity with crystal size and being undetectable in patterns from small crystals.

SECONDARY scattering in polycrystalline films can account for certain sharp diffraction rings, the existence of which was, until recently, very puzzling. It is, of course, well known that multiple scattering in single crystals gives rise to interesting diffraction effects. The secondary scattering reported here to account for an anomalous ring in some Debye-Scherrer patterns is actually also a single crystal phenomenon; the individual crystals in the films, or at least many of the crystals, are so thick that some electrons are diffracted twice in the same crystal.[2]

It has been reported[3] that cuprous chloride (CuCl) produces electron diffraction patterns which correspond to the structure as determined by x-rays, except for the fact that the (222) ring is many times stronger than predicted. Examples of such anomalous patterns are reproduced as Figs. 1 and 2A. The former was obtained by scattering 47-kv electrons from a block of copper which had been exposed to chlorine, and the latter by passing 47-kv electrons through a Formvar foil upon which CuCl had been deposited by vaporization from a tungsten ribbon.[3] In each of these patterns the three smallest sharp rings are due to reflection from (111), (220) and (311) planes of CuCl crystals; the fourth and

FIG. 1. Reflection pattern of CuCl. The smallest rings (or arcs) in order of increasing radii are (111), (220), (311), and the anomalous (222).

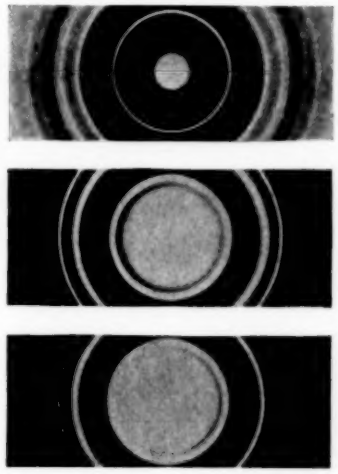

FIG. 2. Transmission patterns from films of CuCl on Formvar, arranged in order of decreasing film thickness which is also the order of decreasing mean crystal size and decreasing relative intensity of the (222) ring.

[1] The first two papers in this series, "I. Structure of very thin films" and "II. Anomalous powder patterns produced by small crystals," appeared in Phys. Rev. **56**, 58–71 (1939) and **60**, 447–454 (1941).

[2] Double diffraction in a single crystal has been reported, for example by H. Raether, Zeits. f. Physik **78**, 527 (1932). Figs. 11 and 13.

[3] L. H. Germer, Phys. Rev. **56**, 58–71 (1939). Table V and Fig. 10.

relatively weak ring is the (222) reflection with which this paper is concerned. The crystals which produced the pattern of Fig. 1 exhibit considerable preference for orientation with (111) planes parallel to the surface of the block, but a similarly anomalously strong (222) ring occurs in other reflection patterns in which there is no indication of preferential orientation.

The structure of cuprous chloride, designated in *Strukturbericht* as *B*3, can be described as a face-centered cubic arrangement of copper atoms and an identical arrangement of chlorine atoms, with atoms of the two sets located at (000) and at (1/4, 1/4, 1/4); the edge of the unit cube is $a_0=5.407$A.[4] If the atoms were all alike the structure would be similar to that of diamond. One expects the relative intensities of electron diffraction rings from CuCl crystals per unit length of ring to be proportional to S^2p/H^3 where $H=h^2+k^2+l^2$, p is the number of cooperating planes, and $S^2=(Z-F)_{Cu}{}^2+(Z-F)_{Cl}{}^2$ for (111) and (311) rings, $[(Z-F)_{Cu}-(Z-F)_{Cl}]^2$ for (200) and (222) rings, and $[(Z-F)_{Cu}+(Z-F)_{Cl}]^2$ for (220) and (400) rings; here $(Z-F)_{Cu}$ is the difference between the atomic number of copper and the x-ray structure factor, and $(Z-F)_{Cl}$ the corresponding difference for chlorine. Calculated intensities of Debye-Scherrer rings relative to that of the (111) ring taken as unity are written down in Table I, the quantities of the second column being obtained from the values of F given by Pauling and Sherman and those of the third column from the values given by James and Brindley.[5]

TABLE I. Comparison of calculated and experimental relative intensities.

	Calc. intensities (S^2p/H^3)		
hkl	Pauling and Sherman	James and Brindley	Experimental intensities*
111	1.	1.	1.
200	0.0027	0.014	—
220	0.56	0.41	0.42
311	0.30	0.21	0.30
222	0.0013	0.0039	0.10
400	0.069	0.043	0.07

* These are relative intensities from microphotometer trace of the diffraction pattern of Fig. 2A.

[4] T. Barth and G. Lunde, Norsk Geol. Tidsskr. **8**, 281 (1924–1925).

[5] L. Pauling and J. Sherman, Zeits. f. Krist. **81**, 1 (1932); R. W. James and G. W. Brindley, Phil. Mag. **12**, 81 (1932).

It is clear from inspection that, except for the (222) ring which is much too strong, the rings of Figs. 1 and 2A have relative intensities agreeing approximately with the values of Table I, and this conclusion has been confirmed quantitatively by intensities obtained from a microphotometer curve of a pattern similar to that of Fig. 2A. That the unexpected intensity of the (222) ring is a real anomaly is indicated by the fact that the (200) ring can be barely detected on the original plates and is very much too weak to appear on the reproductions, but the (222) ring is very clear on the reproductions although calculations indicate that it should be considerably weaker than the (200) ring. Furthermore, the (222) and (400) rings of Fig. 2A have about the same intensities. For points on the former the copper and chlorine atoms of the contributing crystals scatter exactly out of phase whereas on the latter all the atoms scatter in phase; it seems certain that the equal intensities of the adjacent (222) and (400) rings cannot be attributed to deviations of the atomic structure factors from the published values.

Electron diffraction patterns of single crystals consist in general of more than one spot, being unlike x-ray patterns in this particular. Corresponding to this effect, electron patterns from polycrystalline films are, in many cases at least, made up of pairs of spots giving a twofold axis of symmetry through the primary beam position. This characteristic is recognized when electrons are diffracted by polycrystalline films made up of so few crystals that the resulting rings are clearly resolved into spots.[6] The two spots of a pair are interpreted as (hkl) and $(\bar{h}\,\bar{k}\,\bar{l})$ reflections from the same set of crystallographic planes, the indicated tolerance in glancing angle upon the reflecting planes being attributed in some cases to crystal imperfection.

As an immediate consequence of this considerable tolerance in glancing angle it is clear that an (hkl) diffraction beam can *itself* produce another pair of (hkl) $(\bar{h}\,\bar{k}\,\bar{l})$ reflections within the same crystal; and these new beams will have directions coinciding respectively with the singly diffracted beam $(2h, 2k, 2l)$ from the crystal and with the primary beam (000). In the case of

[6] See, for example, H. Boersch, Zeits. f. Physik **116**, 469 (1940) Fig. 2e.

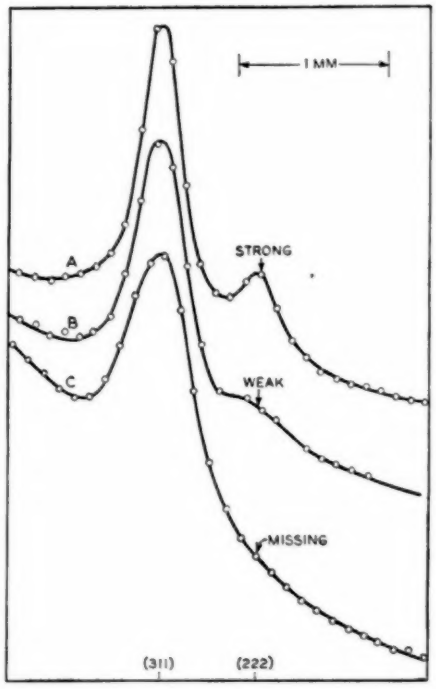

FIG. 3. Microphotometer curves through the (311) and (222) rings of the patterns of Fig. 2.

Debye-Scherrer patterns made up of continuous rings there will be strengthening of all second order rings due to this effect, the amount of the strengthening being determined chiefly by the dimensions of the individual crystals in the direction of the primary beam. Considerable strengthening can occur only when the crystals are so thick that an appreciable fraction of an (*hkl*) diffraction beam is diffracted a second time before leaving the crystal in which it was produced, and the effect can be noticeable only in patterns from crystals for which for single diffraction a ring would be strong in the first order and very weak in the second order. This latter condition is satisfied for CuCl; the data of the second and third columns of Table I indicate that the (111) ring is expected to be several hundred times as strong in the first order as in the second. It remains then to consider whether or not each of the spots which make up the (222) ring from CuCl is actually due to two *successive* first-order (111) reflections within the same crystal.

If this interpretation of the (222) ring from CuCl is correct, then we should find that the relative intensity of the ring varies in some simple way with the mean crystal size, and some estimate of the nature of this variation can be made. We assume crystals of cylindrical shape of length T with ends normal to the primary beam direction. Designate by i_0 the primary beam incident upon a crystal which is oriented to produce (111) reflections, and by x a variable location in the crystal measured from the plane at which the beam enters. The intensity $i_{111}(x)$ of the two (111) diffraction beams at the plane x will then be given by $di_{111}(x)/dx = Ki_0 \exp(-Cx) - Ci_{111}(x)$ which, with the condition $i_{111}(0)=0$, has the solution $i_{111}(x) = Ki_0 x \exp(-Cx)$; here C is the fractional decrease in intensity of a beam per unit length of path in the crystal, and K the fraction of the primary beam at any plane x which is diffracted into the (111) and $(\bar{1}\,\bar{1}\,\bar{1})$ beams per unit length of path. Similarly, for each of the apparent (222) beams produced by secondary diffraction of the (111) beam, $di_{222}(x)/dx = (K/2)i_{111}(x) - Ci_{222}(x)$ which has the solution $i_{222}(x) = (K^2/4)i_0 x^2 \exp(-Cx)$; the constant K in the differential equation is divided by 2 because in the case of the secondary diffraction only one of the beams appears as an apparent (222) reflection, the other returning to the primary beam. The relative intensities of these two diffraction rings *per unit length of ring*, which is the way we measure with the microphotometer, is

$$I_{222/111} = i_{222}(T)/2i_{111}(T) = KT/8. \qquad (1)$$

An attempt has been made to test Eq. (1) by obtaining diffraction patterns from films of CuCl of various thicknesses, and by correlating the ratio of intensities of the (222) and (111) rings with estimates of crystal size obtained from breadths of rings. In these tests patterns were obtained from 9 different films, each prepared by vaporizing highly purified CuCl in vacuum upon a Formvar supporting foil. (See reference 3 for

TABLE II. Intensity ratios and breadths at half maximum from microphotometer curves of Fig. 3.

Film	$I_{222/111}$	$I_{222/111}$	ΔR^* (mm)	Mean crystal size, C (A)	$\frac{8I_{222/111}}{C}$ (A^{-1})
A	0.22	0.066	0.36	150	0.0035
B	0.08	0.024	0.46	90	0.0021
C	0.00	0.00	0.60	60	0.000

* From (311) peaks of Fig. 3.

the method.) Diffraction patterns from three typical films are reproduced in Fig. 2, and corresponding microphotometer curves through the (311) and (222) rings in Fig. 3. The patterns and curves, designated as A, B and C, are in the order of decreasing film thickness. In the second column of Table II are given values of the ratio $I_{222/311}$ of intensities of the (222) and (311) rings obtained from Fig. 3, and in the third column values of $I_{222/111}$ calculated from these by multiplying by 0.3 which is the ratio $I_{311/111}$ given in the last column of Table I. In Table II are also given the breadths at half maximum ΔR of the (311) peaks on Fig. 3 and mean crystal dimensions C estimated from these breadths by means of the Scherrer formula in the form $C=L\lambda/\Delta R$, each value of ΔR being first corrected for the primary beam size by subtracting 0.2 mm.

These patterns and data are typical of those from all of the films. They indicate that the (222) ring is very weak or unobservable in the thinnest films, and increases in intensity with increasing thickness reaching a maximum of about 7 percent of the intensity of the (111) ring. The crystal size C, as estimated from breadths of rings, varies in the same way with thickness, but much less rapidly, so that there is not a linear relation between $I_{222/111}$ and C. There is, furthermore, considerable scattering of the data, and they have not been plotted for this reason. It seems altogether probable that the failure of Eq. (1) to be satisfied if we substitute C for T is due to the fact that the crystals are not strictly equi-axed and that, as film thickness is increased, the mean dimension of crystals measured normal to the film, T, is increased more rapidly than the dimension in the plane of the film, C, which we are able to estimate. It seems clear that at some film thickness T and C will be approximately equal and for this thickness the constant K will be given by Eq. (1) after replacing T by C. Thus one estimates that for 47-kv electrons in a CuCl crystal, K is of the order of 0.002A^{-1}. (See the last column of Table II.) This seems a reasonable value.

From 5 of the 9 films of CuCl diffraction patterns were obtained with electrons of 27 kv, as well as with electrons of 47 kv. In each case the relative intensity of the apparent (222) ring was greater in the pattern produced by the slower electrons, the average estimate of the difference being about 30 percent. Thus, we conclude that for 27-kv electrons K is of the order of magnitude of 0.003A^{-1}.

Observation of the occurrence of second-order rings which are due to secondary diffraction must be fairly rare, because in diffraction patterns from most materials the effect is masked by the considerable strength of the true second-order diffraction. The phenomenon has, however, been observed in patterns from cuprous bromide and calcium fluoride. The former has the same type of structure as cuprous chloride and, although copper and bromine have scattering powers which are more nearly the same than copper and chlorine and must therefore produce a true (222) ring of even lower relative intensity, it has been observed that the apparent (222) ring is clear and fairly strong in a number of patterns from CuBr. It has been reported (reference 3, Fig. 11 and Table V) that films of CaF_2 also produce patterns in which the apparent (222) ring is many times stronger than was expected. There are other types of structure in which this phenomenon could be detected and one could undoubtedly find a great many examples if the appropriate compounds were studied.

The Structure of Evaporated Films of Chromium and Aluminum on Glass

ANNE REBECCA OLIVER*
Cornell University, Ithaca, New York
(Received December 29, 1941)

The structure of evaporated films of aluminum on glass, and of aluminum on chromium deposited on glass, was investigated by electron diffraction. No evidence was found that would indicate the nature of the hardening produced in aluminum films by using a chromium base or by washing with water. The oxide film on aluminum, if present, is very thin and amorphous.

MIRRORS made by evaporating films of aluminum on glass are widely used in physics and astronomy. It has been claimed that such aluminum films are more resistant to scratching if deposited on an evaporated chromium film on glass than if deposited on glass directly, and also that the films are hardened if washed with water after preparation.[1] An electron diffraction study of these films was undertaken in order to determine their structure, with particular reference to the hardening effect of the chromium base and the treatment with water.

The electron diffraction camera was a modified form of the Thomson-Fraser camera,[2] with a hot filament electron source. The accelerating voltages were 25 to 30 kv. A plate magazine made it possible to take five photographs in succession without opening the camera. Thus the films, which were prepared in the camera, could be examined during preparation without exposing them to air.

The technique used in evaporating the films followed as closely as possible the methods used in the manufacture of aluminum mirrors. A piece of glass about 1 cm square was cleaned by washing with potassium hydroxide, hydrochloric acid, and rinsing with distilled water. When dry it was placed in the camera, care being taken to avoid contaminating it in handling. Opposite the specimen holder were electrical leads to which were fastened spirals of 15-mil tungsten wire, one containing chromium, the other containing aluminum. The camera was evacuated and after the pressure had been reduced to 5×10^{-5} mm of Hg or less, the filaments were heated by a small current to drive off impurities. The filament containing chromium was then heated by a current of 15 amperes and the chromium evaporated. The progress of the evaporation could be watched through a window in the apparatus. After the chromium was deposited a photograph of the diffraction pattern produced by the film was obtained. Aluminum was then evaporated on the chromium. Two photographs of the diffraction pattern were taken, one after a small quantity of aluminum had been evaporated, the other after a thick film was deposited. The camera was then opened and the specimen exposed to air, after which another photograph was taken to determine whether any change in the diffraction pattern could be detected after such exposure. Still another record of the diffraction pattern produced by the film was made after the film had been rinsed with water.

The diffraction pattern produced by the chromium film could be explained completely in terms of the body-centered cubic structure of chromium as determined by x-rays ($a=2.88$A). In most of the films there was preferred orientation, with the (111) plane parallel to the surface of the glass. None of the films showed any trace of the presence of an oxide of chromium. Beeching,[3] who has also investigated the properties of chromium films on glass, found that with thin films he obtained a pattern containing oxide rings. This may have been because the films he studied had been produced by evaporation at a higher pressure (10^{-4} mm of Hg) than in the present case.

The thick films of aluminum on chromium

* Now at Connecticut College, New London, Connecticut.

[1] G. B. Sabine, Phys. Rev. **55**, 1064 (1939).

[2] G. P. Thomson and C. G. Fraser, Proc. Roy. Soc. **A128**, 641 (1930).

[3] R. Beeching, Phil. Mag. **22**, 938 (1936).

gave the pattern to be expected from the face-centered structure of aluminum. No rings were present which could be attributed to aluminum oxide. The aluminum showed preferred orientation on the chromium, with the cube face parallel to the surface of the glass. It was noted that the distance between adjacent atoms in the (111) plane of chromium ($\sqrt{2}\times 2.88 = 4.07$A) was almost the same as the distance between alternate atoms in the cube face of aluminum ($a = 4.04$A). It was thought that the orientation of the aluminum might be determined by that of the chromium. To test this the orientation was determined for aluminum evaporated directly on glass, and was found to be the same as for aluminum on chromium. Apparently the relation between the distances is an accidental one.

The orientation of aluminum on various substrates has been investigated by Dixit[4] and Bruck.[5] They found that the temperature of the base seemed to be the most important factor in determining which plane was oriented parallel to it. Beeching[3] found that the direction of evaporation was also a factor influencing orientation.

The patterns from the thin layers of aluminum were not significantly different from those produced by the thick layers. The rings were possibly somewhat more diffuse in the case of the thinner layers, a fact which might indicate smaller crystals.

The pattern obtained from the aluminum films was unchanged after exposure to air and after washing with water. Beeching[3] has reported that he investigated the effect of washing with methyl alcohol, which he was told had a hardening action on a film of aluminum on chromium. He found no change in the diffraction pattern produced by the film after this treatment.

Since aluminum at room temperature is believed to be covered with a protective oxide film, the fact that no evidence of the presence of any oxide was found in any of the patterns, even after exposure to air, is of some interest. There have been many attempts to detect this oxide film and to study its properties by electron diffraction. However, there seems to be little agreement as to the structure or thickness of the film. Although Dixit,[4] Preston and Bircumshaw,[6] Belwe,[7] Steinheil,[8] Bound and Richards,[9] and Yamaguchi[10] have studied reflection specimens of aluminum, only Beeching and Yamaguchi have obtained patterns which could be attributed to a form of aluminum oxide. The nature of the evidence Beeching found led him to the conclusion that the oxide he detected was formed when the specimens were evaporated, probably because of an oxygen layer on the surface of the glass. Yamaguchi, using an aluminum block, has found two faint rings which he attributed to aluminum oxide. In general the evidence would seem to show that the oxide film on aluminum is very thin and probably is amorphous, since only thus can the general absence of oxide rings in the diffraction patterns be explained. This conclusion is, however, not in agreement with the work of Tronstad and Höverstad.[11] They investigated the thickness of the oxide film on aluminum by an optical method and found that the film was 100 to 150A thick.

In conclusion, the author wishes to express her appreciation to Professor C. C. Murdock and Professor R. C. Gibbs for the helpful suggestions and criticism received during the course of the work.

[4] K. R. Dixit, Phil. Mag. **16**, 1049 (1933).
[5] L. Bruck, Ann. d. Physik **26**, 233 (1936).
[6] G. D. Preston and L. L. Bircumshaw, Phil. Mag. **20**, 706 (1935).
[7] E. Belwe, Zeits. f. Physik **100**, 192 (1936).
[8] A. Steinheil, Ann. d. Physik **19**, 465 (1934).
[9] M. Bound and D. A. Richards, Proc. Phys. Soc. **51**, 256 (1939).
[10] S. Yamaguchi, Inst. Phys. Chem. Res., Tokyo, Sci. Papers No. 942, pp. 463–470.
[11] L. Tronstad and T. Höverstad, Trans. Faraday Soc. **30**, 362 (1934).

Mechanism for Self-Diffusion in Metallic Copper

H. B. HUNTINGTON* AND FREDERICK SEITZ
Randal Morgan Laboratory of Physics, University of Pennsylvania, Philadelphia, Pennsylvania
(Received December 6, 1941)

The problem of the mechanism of diffusion in metallic copper is discussed from the standpoint of the modern theory of metals. Three competing processes are considered in detail, namely the mechanism of direct interchange of atoms, the mechanism of interstitial diffusion, and the mechanism of vacancy diffusion. The energies of the equilibrium and saddle-point configurations for the processes are determined first in an approximation in which the electronic charge distribution is assumed to be uniform throughout the lattice, and second in a further approximation in which polarization is taken into account by a simple variational method based on the one-electron scheme. The results indicate that the vacancy mechanism is strongly preferred and yield a value of the activation energy for diffusion in reasonable agreement with the observed one. The vacancy process is considered in greater accuracy in a paper by Huntington following this.

I. INTRODUCTION

THERE are three reasonable mechanisms of atomic diffusion in the interior of solids, namely diffusion by direct interchange of neighboring atoms in a perfect lattice, diffusion by means of interstitial atoms, and diffusion by means of vacancies. The likelihood of each of these processes has been examined[1] most completely for ionic crystals since the computational techniques for this type of solid are most widely known and easiest to apply. As a result of this work, it seems to be generally agreed that diffusion by means of holes is the most probable in all ionic crystals in which the ions have rare gas configurations and the coordination number is high. This includes, for example, the alkali halides possessing sodium chloride and cesium chloride structures and such divalent salts as magnesium oxide. On the other hand, it seems likely that interstitial atoms play an important role both in crystals of low coordination number, such as oxides and sulfides having zincblende and wurtzite lattices, and in highly coordinated crystals, such as the silver halides, in which the metal ion contains a newly closed d shell. A large amount of supporting evidence concerning the crystals of low coordination number has been obtained by Wagner[2] and his associates on experimental grounds, whereas the evidence for salts such as the silver halides is still mainly theoretical.

The purpose of this paper is to examine the diffusion mechanism in metals more closely than has been done hitherto. Naturally, it would be most convenient from the purely theoretical side to carry out computations for the alkali metals, since their cohesive properties are most fully understood. Unfortunately there is not available at the present time experimental information on diffusion in these metals and it seems unlikely that such information will become available in the immediate future. For this reason, we have decided as a compromise to work with copper, in which self-diffusion has been measured by radioactive tracer methods.[3] The theory of copper has been investigated extensively by Fuchs[4] and the results of his work, which will now be described briefly, are summarized in

TABLE I. Copper data.

	Fuchs	Observed
Cube edge distance	4.2A	3.609A
Sphere radius r_s		2.64a
Atomic ionization energy		7.7 ev
Cohesive energy	33 kg cal./mole	81 kg cal./mole
Compressibility	0.69×10^{-6} cm²/kg	0.70×10^{-6} cm²/kg
$c_{11}-c_{12}$	5.10×10^{11} dy/cm²	5.1×10^{11} dy/cm²
c_{44}	8.9×10^{11} dy/cm²	8.2×10^{11} dy/cm²

* Now at Washington University, Saint Louis, Missouri.

[1] W. Jost and C. Nehlep, Zeits. f. physik. Chemie **B32**, 1 (1936). See also the book by W. Jost, *Diffusion und Chemische Reaktiones in festen Stoffen* (J. Steinkopf, 1937). N. F. Mott and M. J. Littleton, Trans. Faraday Soc. **34**, 485 (1938).

[2] C. Wagner, Zeits. f. physik. Chemie **B22**, 181 ff. (1933).

[3] J. Steigman, W. Shockley, and F. Nix, Phys. Rev. **56**, 13 (1939); B. D. Rollin, Phys. Rev. **55**, 231 (1939).

[4] K. Fuchs, Proc. Roy. Soc. **151**, 585 (1935); **153**, 622 (1936); **157**, 444 (1936).

Table I. It should be mentioned at this point that the inherent accuracy of Fuchs' computations for copper is considerably less than that for lithium and sodium. It seemed worthwhile to proceed with copper in spite of this fact, for, as will be shown, the results in which we are particularly interested turn out to be relatively insensitive to the weaker points of Fuchs' work.

Fuchs determined approximate wave functions for copper by the cellular method and concluded that the electrons are very nearly free, as in sodium. We shall accept this approximate result as a basic assumption in deriving the Fermi energy, exchange energy and correlation energy for the metal. In this approximation, the electronic energy of the valence electrons in the metal is[5]

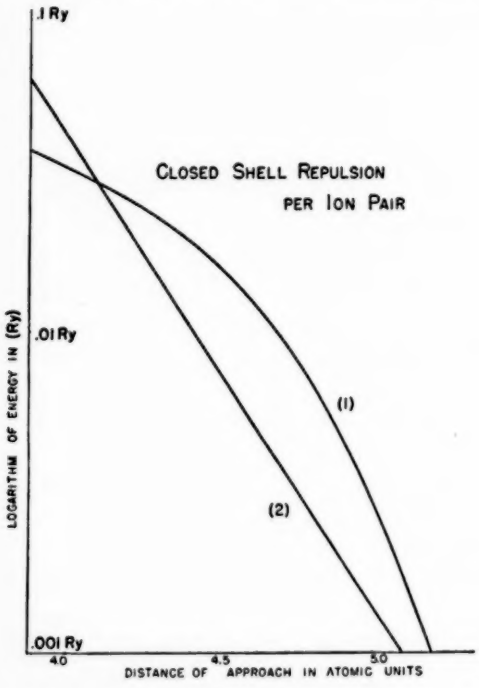

FIG. 1. Comparison of the two alternative curves for the closed-shell repulsive force, (1) the displaced Fuchs model and (2) the exponential force law. The equilibrium distance of nearest neighbors is 4.77 a_0.

$$E=N\left(\epsilon_0+\frac{\hbar^2}{2m}\frac{2.21}{r_s^2}+\frac{e^2}{2N}\int\rho(\mathbf{r}_1)\int\frac{\rho(\mathbf{r}_2)}{r_{12}}dV_1dV_2\right.$$
$$\left.+\sum_a{}'\int_c\rho(\mathbf{r}_1)\frac{e^2}{r_{1a}}dV-\frac{0.458e^2}{r_s}-\frac{0.288e^2}{r+5.1a_0}\right), \quad (1)$$

in which N is the number of unit cells in the lattice, r_s is the radius of the sphere whose volume is equal to that of the unit cell, ϵ_0 is the energy of the lowest electron in the field of the nearest ion core, and $\rho(\mathbf{r})$is the valence electron charge distribution function. The terms in the right-hand side of Eq. (1) have the following interpretation. The first is the combined potential and kinetic energy of the lowest energy electron, exclusive of its potential energy of interaction with other valence electrons and with ions other than that in the unit cell in which it is temporarily located. These two energy terms are given, respectively, by the third and fourth terms in (1), the integration in the fourth being over a single cell and the sum extending over all ions in the lattice except that in the given cell. The integration in the third term extends over the entire crystal. The second term in (1) is the mean kinetic energy of all electrons relative to the kinetic energy of the lowest, and is the same as the expression for the mean kinetic energy of a set of perfectly free electrons in a Fermi distribution. If the effective electron mass were not unity, as Fuchs' work indicates to be nearly the case, the m in the denominator would be replaced by the effective electron mass m^*. The fifth term in the expression is the mean exchange energy of one of the valence electrons and the last is the correlation energy.

Fuchs computed the ion-ion repulsive interaction with the aid of an interaction potential derived by a modified Fermi-Thomas method. We shall call this interaction the "Fuchs potential" in the following discussion. Now the ion-ion interaction is of fundamental importance for determining the elastic constants in a metal of the type of copper, so that the merits of a particular interaction can be evaluated by examining the elastic constants computed with it. Fuchs found that his interaction gave excellent results for the theoretical equilibrium spacing of the lattice, which, unfortunately, is about 17 percent larger than the actual spacing (Table I). We may conclude from this that his potential is too large at the actual spacing.

As a result of this difficulty it was decided to use two alternative ion-ion interaction functions. One of these was a curve derived from Fuchs' by displacing his to shorter distances by 17

[5] See for example, *The Modern Theory of Solids*, Chapter X (McGraw-Hill Book Company, 1940).

percent, and the other was a two-parameter exponential function of the type used by Born and Mayer[6] in their treatment of ionic crystals, where the parameters were chosen to yield the best least square determination of the three elastic constants. If the Born-Mayer function is taken in the form $Ae^{-(r/\rho)}$, the best values of A and ρ are $A=5.64$ Rydberg units per ion pair and $\rho=0.284$A. As may be seen from Fig. 1, the two types of curve differ appreciably. It was hoped that by considering both a good idea could be obtained of the importance of the ion-ion interaction in two rather extreme cases. Actually we have every reason to expect that the Born-Mayer type of curve is the more accurate of the two for, not only does it yield reasonable results in the case of ionic crystals, but in addition, it would lead to a compressibility that would steadily decrease as the crystal is compressed, whereas the displaced Fuchs curve would lead to a compressibility nearly independent of the volume in the neighborhood of the equilibrium spacing, in contradiction with experiment.

In addition to the exchange repulsion energy between ions, we are interested in the van der Waals attraction between ions. This has been discussed by Mayer and Levy[7] in connection with computations of the stability of the copper halides. They employed a function of the form

$$4.1\times10^{-60}/r^6 \text{ erg}$$

for the van der Waals energy of two copper ions, r being the distance of separation in cm. The contributions arising from this term are practically negligible compared with other quantities for the values of r with which we shall be concerned.

We shall now proceed with the computation of the activation energy for the three diffusion processes described above. In each of the cases this activation energy may be divided into two parts, namely, (1) the energy required to form the lattice defect in an equilibrium state, and (2) the additional activation energy required to pass from one equilibrium position to another. The first of these is of course zero for the mechanism of direct atomic interchange. As we shall see, the two energies may be evaluated individually in two successive stages of approximation, namely, a first approximation in which the electronic charge distribution is regarded as uniform throughout the crystal, and a later approximation in which the redistribution of charge in the immediate neighborhood of the diffusing atom is taken into account. Steigman, Shockley, and Nix give 2.6 ev as the experimental value for the activation energy for self-diffusion in copper.

II. ACTIVATION ENERGIES IN APPROXIMATION IN WHICH ELECTRONIC REDISTRIBUTION ABOUT DIFFUSING ATOMS IS NEGLECTED

The equilibrium and saddle-point configurations for the three types of diffusion to be considered are shown in Fig. 2. In the case of direct interchange, the equilibrium configuration is, of course, that for the perfect lattice, whereas the saddle-point configuration is shown in Fig. 2A. In this arrangement two nearest neighbors, namely those indicated by squares at the face-center positions, have rotated through 90° about a (100) axis bisecting perpendicularly their line of centers. The spacing of these neigh-

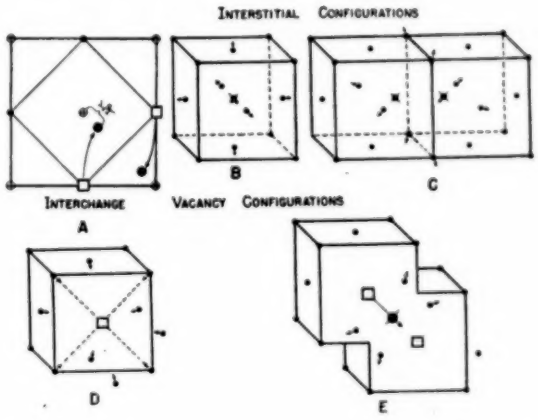

FIG. 2. Configurations involved in the various mechanisms for diffusion. ● denotes an atom at an ordinary lattice site. ✳ denotes an interstitial atom. □ denotes a vacancy. Small arrows indicate displacements under the influence of the closed-shell repulsive force. Configuration A shows the plane of interchange (100). Atoms in planes directly above and below are indicated by ⊕.

[6] M. Born and J. E. Mayer, Zeits. f. Physik **75**, 1 (1932) *et seq.*

[7] J. E. Mayer and R. B. Levy, J. Chem. Phys. **1**, 647 (1933).

bors will of course change in general during the process. Figure 2B shows the probable equilibrium position for the interstitial atom at the center of the unit cube, whereas Fig. 2C shows the saddle-point configuration in which the interstitial atom and one of its six nearest neighbors have become symmetrically disposed relative to one of the cube faces. The neighboring atoms are shifted from normal sites in both of these cases in the manner suggested by the arrows. It evidently is not clear at this stage of our reasoning which of the two configurations has the lower energy, but subsequent work will show that the assignment probably is as given. Figure 2D shows the equilibrium vacancy configuration whereas E shows the transition configuration during diffusion.

1. Direct Interchange

For investigation of the saddle-point for direct interchange, consider the two diffusing ions to be taken from their equilibrium positions and placed near adjoining "interstitial sites," i.e., body centers and edge centers. If we designate their distance from the respective neighboring interstitial sites by $\sqrt{2}\lambda a/2$, where λ is a parameter and a is half the cube-edge distance, their mutual distance of separation is $(1-2\lambda)\sqrt{2}a$. Similarly, we shall designate the distance by which the nearest neighbors in the plane of motion move in the (100)-type directions by $\mu a/2$, and shall designate the displacement vectors of neighbors to the interstitial sites lying in other planes by $(\nu a/2, 0, 0)$, etc. The total change in repulsive energy is then given by

$$\Delta E(\lambda,\mu,\nu)=\left[R\left\{\frac{\sqrt{2}a}{2}(1-2\lambda)\right\}+4R\left\{\frac{a}{2}((1+\nu)^2+2\lambda^2)^{\frac{1}{2}}\right\}+4R\left\{\frac{a}{2}((1+\lambda+\mu)^2+\lambda^2)^{\frac{1}{2}}\right\}\right.$$
$$-23R\left\{\frac{\sqrt{2}a}{2}\right\}+16R\left\{\frac{a}{2}((1-\nu)^2+1)^{\frac{1}{2}}\right\}+16R\left\{\frac{a}{2}((1-\mu)^2+1)^{\frac{1}{2}}\right\}$$
$$\left.+8R\left\{\frac{a}{2}((1+\mu)^2+(1+\nu)^2)^{\frac{1}{2}}\right\}-40R\left\{\frac{\sqrt{2}a}{2}\right\}\right], \quad (2)$$

where $R(x)$ is the energy of repulsion per ion pair at an interatomic distance x. When the two diffusing atoms are taken from their equilibrium positions, 23 repulsive contacts are broken since these atoms had one contact in common. The first three terms in Eq. (2) represent the new contacts established in this configuration. Each of the four atoms in the plane in which the interchanging atoms move, which are displaced by an amount determined by the μ parameter, alters its contacts with other atoms behind it. These changes account for the coefficient 16 in the sixth term. The situation for the atoms whose displacements are determined by the ν parameter is similar. By evaluating this expression numerically for suitable ranges of the parameters the minimum value was determined. Since the interesting ranges of the parameters turn out to be small, it was found permissible to disregard all but the linear terms in the expansion of the arguments of the functions.

With the use of the exponential repulsive curve, it was found that the energy minimum occurred at about 6.2 ev for $\lambda=0.11$, $\mu=0.2$, and $\nu=0.08$. The displaced-Fuchs type of repulsive function, on the other hand, leads to meaningless results in the present case because of the fact that it varies comparatively slowly with interionic distance, as we remarked in the previous section.

In addition to the energy arising from ion-ion repulsion, it is also necessary to take into account the change in electrostatic energy resulting from the motion of the ions through the electron cloud. Assuming that the electronic cloud remains uniform, we found that the electrostatic energy increased by more than 11 ev in going from the normal to the saddle-point configuration. This gain would be diminished somewhat by including the effect of polarization of the valence electron distribution, perhaps to a third or half of its original value.

2. Interstitial Configurations

In order to find the energy required to form an interstitial atom under the assumption that the electron distribution remains neutral, it is necessary to consider the situation in which an ion is taken from the surface and placed in an interstitial site and the electronic charge which previously surrounded the ion is distributed in a thin, uniform layer throughout the crystal. Consider the change in kinetic and electrostatic energy of the system. If we regard the lattice from the standpoint of the "s sphere approximation,"[5] we see that the interstitial ion is very near to the peripheries of the s spheres of the surrounding atoms, so that its *net* electrostatic interaction with the electrons and remaining ions lattice is small. Thus the increase in electrostatic energy may be obtained in first approximation by considering the remaining system alone. Each of the electrons is still in the electrostatic field of an ion, so that there is no change in ϵ_0 [see Eq. (1)]. On the other hand, the electron gas is compressed, so that the other terms are altered. The changes in Fermi, exchange, and correlation energies may easily be derived by noting that the effective sphere radius is changed from r_s to $r_s(1-1/3N)$. Similarly, the change in the electrostatic self-energy of the electrons may be derived by noting that the new electron density is $(1+1/N)$ and that it extends over $N-1$ cells instead of N. Hence the total change in electrostatic energy is

$$\frac{2}{3}\times\frac{2.21}{r_s^2}\frac{\hbar^2}{2m}-\frac{1}{3}\times\frac{0.458e^2}{r_s}-\frac{0.288r_se^2}{3(r_s+5.1)^2}+\frac{e^2}{2}\int\rho(\mathbf{r}_1)\int\frac{\rho(\mathbf{r}_2)}{r_{12}}dV_2dV_1. \quad (3)$$

For the uniform electron distribution, the self-energy of the electrons in a cell is $0.6e^2/r_s$. Taking r_s equal to 2.64 a_0 for copper, we obtain 7.34 ev for (3).

A value of this energy could also be obtained from experiment by considering a process in which an atom is evaporated from the surface, ionized, and the electron is replaced in the metal at the top of the Fermi band. If the dipole layer at the surface of the metal is small, the net energy required should be nearly equal to (3), since the isolated ion at infinity, like the interstitial ion in the present approximation, would not interact electrostatically with the rest of the metal. A computation of this energy, based on the measured quantities leads to a value of 7.19 ev, in remarkably close agreement with the foregoing value. Since it is reasonable to suppose that the surface dipole moment of pure copper is not larger than 1 ev, this agreement suggests that the free electron approximation is reliable.

The nearest neighbors of the interstitial ion will retreat from it under the influence of the short-range repulsive forces discussed in Section 1. This motion will, of course, influence the electrostatic energy of the interstitial ion, but it seems unwise to compute this effect at present since it should be considered along with the energy resulting from polarization of the electron cloud by the ion. The change in the short-range energy may be evaluated approximately as follows. In taking an ion from the surface and placing it at an interstitial site, six surface repulsive bonds at the ordinary interatomic distance $(\sqrt{2}a/2)$ are broken and six new repulsive bonds are formed at a distance $(1+\lambda)a/2$. If the six neighbors remained at their normal sites, the parameter λ evidently would vanish. If we neglect the displacements of next nearest neighbors, the change in repulsive energy can then be written

$$\Delta E_{\text{rep}}=6\left[R\left\{\frac{a}{2}(1+\lambda)\right\}+2R\left\{\frac{\sqrt{2}a}{2}(1+\lambda)\right\}+4R\left\{\frac{a}{2}((1-\lambda)^2+1)^{\frac{1}{2}}\right\}-7R\left\{\frac{\sqrt{2}a}{2}\right\}\right] \quad (4)$$

in analogy with (2). This has a minimum of 5.5 ev at $\lambda=0.2$ for the exponential repulsive function and a minimum of 3.85 ev at $\lambda=0.1$ for the displaced Fuchs repulsion. Addition of the 7.34-ev term derived from Eq. (3) leads, respectively, to values of 12.84 ev and 11.19 ev for the energy of configuration B (Fig. 2) in the present approximation.

Using the repulsive force, we have estimated that the additional repulsive energy required to go from the B configuration to the C configuration is about 0.5 ev.

TABLE II. Ion-core contributions for "E" configuration.

	Exponential	Displaced Fuchs
Broken repulsive contacts	−0.69 ev	−1.65 ev
Energy of mutual neighbors	0.51 ev	1.59 ev
Energy of 14 other neighbors	−0.19 ev	−0.40 ev
	−0.37 ev	−0.46 ev
Value for λ-parameter	0.125	0

3. Vacancy Configuration

In the vacancy case, those terms which appeared in Section 2 as a result of compressing the electron gas now appear with reversed sign since the electron gas expands by an amount equal to the volume of a single cell when an ion is taken from an interior site and placed on the surface. However, this gain of 7.34 ev [see Eq. (3)] is counterbalanced by the fact that in the present approximation the vacancy is occupied uniformly by an electronic cloud uncompensated by a positive charge. Thus in the sphere approximation this electron distribution has an energy equal to $-\epsilon_0$, the energy of the lowest electron in the filled band. One may estimate $-\epsilon_0$ from the sum of the ionization energy, the heat of sublimation, and the mean Fermi energy to be about 15.5 ev. As a result, the increase of electron energy needed to form a hole can be taken as 8.2 ev for a basis of comparison at this stage.

The change in repulsive energy may be computed next following the same general procedure. For the simple vacancy distribution D, the number of ordinary repulsions will be decreased by 6 in taking the ion to the surface, but a further decrease results from the motion of the atoms neighboring the vacancy toward it. This change is

$$\Delta E_{\text{rep}}=12R\left\{\frac{\sqrt{2}a}{2}(1+\lambda)\right\}+48R\left\{\frac{\sqrt{2}a}{2}(1+\lambda+\lambda^2)^{\frac{1}{2}}\right\}+24R\left\{\frac{\sqrt{2}a}{2}(1-\lambda)\right\}-90R\left\{\frac{\sqrt{2}a}{2}\right\}, \quad (5)$$

in which the displacement of nearest neighbors is given by $\lambda\sqrt{2}a/2$. The decrease is about 0.4 ev for the exponential repulsion with $\lambda=0.025$ and about 1.0 ev for the displaced Fuchs function with $\lambda=0.038$.

The configuration E of Fig. 2 is the saddle-point arrangement for the process since its energy is higher than that of the configuration just discussed. In the new arrangement, two ions are taken from adjacent positions in the interior and one is placed at the surface with a net decrease of 17 repulsions (12+11−6). Next, the other ion is placed at the center of the rectangle formed by the four ions that are mutually adjacent to both vacancies. These ions retreat, as a result, and the displacement vectors may be represented in the form $(\lambda a/2, \lambda a/4, \lambda a/4)$. The part of the change in repulsive energy arising from the variation in λ is

$$\Delta E_{\text{rep}}=4\left[R\left\{\frac{6^{\frac{1}{2}}a}{4}(1+\lambda)\right\}+R\left\{\frac{10^{\frac{1}{2}}a}{4}\right\}+3R\left\{\frac{a}{2}(2-\lambda)^{\frac{1}{2}}\right\}+\tfrac{1}{2}R\left\{\frac{a}{2}(2+2\lambda)^{\frac{1}{2}}\right\}+2R\left\{\frac{a}{2}(2-3\lambda)^{\frac{1}{2}}\right\}+2R\left\{\frac{a}{2}(2+\lambda)^{\frac{1}{2}}\right\}-7\tfrac{1}{2}R\left\{\frac{\sqrt{2}a}{2}\right\}\right], \quad (6)$$

in which terms in λ^2 have been omitted in the expansion of the arguments. Using the exponential repulsion function we obtained a net energy increase of 0.51 ev relative to the normal lattice for $\lambda=0.125$, whereas the increase was 1.59 ev for $\lambda\backsimeq 0$ when the displaced Fuchs function was used. Now each of the two "half vacancies" in the E configuration have seven neighbors whose environment is indirectly affected as a result of the presence of the vacancies. For an order of magnitude estimate, their change in energy was taken to be the same as the decrease found in the case of Fig. 2D for the neighbors of the simple vacancy. Adding together the three results (see Table II), we obtain as the repulsive energy for the E configuration −0.37 ev when the exponential curve is used and −0.48 ev when the displaced Fuchs curve is employed.

III. COMPUTATION OF THE ELECTRONIC REDISTRIBUTION BY A VARIATIONAL SCHEME

An easy method for estimating the lowering of the energy which results from electronic redistribution is a variational procedure based on the use of one-electron functions of the form

$$\psi_k(1+f(r)). \tag{7}$$

The ψ_k are the normalized, free-electron functions $V^{-\frac{1}{2}}\exp[2\pi i\mathbf{k}\cdot\mathbf{r}]$, for the case in which the charge is uniformly distributed, and $f(r)$ is a function equal practically to zero everywhere except in the immediate vicinity of the interstitial atom or vacancy, where its value is to be determined by variation. We shall assume that it is radially symmetric about the lattice defect. The functions (7) may be readily normalized by the use of the condition

$$\int(1+f(r))^2dV=V, \tag{8}$$

in which the integration extends over the entire lattice and V is the volume of the lattice. The function f is not exactly zero at large distances, because the redistribution affects the density of electronic charge infinitesimally throughout the crystal. It is convenient to introduce at this point for later use a function, $g(r)$, which is exactly zero except in the neighborhood of the lattice defect and is defined by setting $(N/V)[1+g(r)]$ equal to the electronic density in the lattice. The density can also be expressed in terms of $f(r)$, as

$$\frac{N\pm1}{V}[1+f(r)]^2. \tag{9}$$

The plus or minus sign applies according to whether we are dealing with an interstitial or vacancy defect respectively. It follows that

$$g(r)=[2f(r)+f^2(r)]\pm1/N. \tag{10}$$

The functions (7) are not, however, mutually orthogonal and therein lies the chief weakness of the present method. It is simple only if the functions are treated as though they were orthogonal. Fortunately the results obtained here by assuming orthogonality are in reasonable agreement with those obtained by a more exact procedure employed in the following paper. This indicates that the lack of orthogonality does not prevent the method from giving sensible answers to problems concerning energy.

The total energy of the system is then[8]

$$E_T=\sum_k\epsilon'_k-\frac{e^2}{2}\sum_k\sum_{k'}\int\int\frac{|\psi_k(r_1)(1+f(r_1))|^2|\psi_{k'}(r_2)(1+f(r_2))|^2}{|\mathbf{r}_1-\mathbf{r}_2|}dV_1dV_2$$
$$+\tfrac{1}{2}\sum_{\alpha,\beta}{}'\frac{e^2}{r_{\alpha\beta}}-\sum_\alpha V_d(r_\alpha)+E_e+E_c+E_r, \tag{11}$$

in which E_e and E_c are the total exchange and correlation energies for the electrons and E_r is the ion-ion repulsive energy. The third term is the mutual electrostatic interaction of the ions of the lattice, and the fourth term gives their interaction with the lattice defect. The energy parameter ϵ_k' is the mean value of the Hamiltonian for the kth electron wave function,

$$\epsilon'_k=\int\psi_k(1+f)H\psi_k(1+f)dV. \tag{12}$$

For this problem the Hartree Hamiltonian operator for the system of wave functions (7) becomes

$$H=-\frac{\hbar^2}{2m}\Delta+V_l(r)+V_d(r)+e^2\sum_k\left\{\int\frac{|\psi_k(r_1)(1+f(r_1))|^2}{|\mathbf{r}-\mathbf{r}_1|}dV_1-\int\frac{|\psi_k(r_1)|^2}{|\mathbf{r}-\mathbf{r}_1|}dV_1\right\}, \tag{13}$$

[8] See, for example, reference 5, Chapter VI.

in which $V_l(r)$ is the potential of the lattice for a uniform charge distribution, $V_d(r)$ is the radial symmetric potential of the lattice defect, either interstitial atom or vacancy, and finally the term in braces is the difference in potential resulting from redistribution.

Now we can write

$$\sum_k \epsilon'_k = \sum_k \int \psi^*_k(1+f)\left(-\frac{h^2}{2m}\Delta + V_l + V_d\right)\psi_k(1+f)dV$$

$$+\sum_{k,k'} e^2 \int |\psi_k(r_1)(1+f(r_1))|^2 \left[\int \frac{|\psi_{k'}(r_2)|^2(2f(r_2)+f^2(r_2))}{|\mathbf{r}_1-\mathbf{r}_2|}dV_2\right]dV_1. \quad (14)$$

The summand in the first term of this expression can be transformed to

$$\int \psi^*_k(1+f)^2\left(-\frac{h^2}{2m}\Delta + V_l\right)\psi_k dV - \int |\psi_k|^2(1+f)\left(-\frac{h^2\Delta}{2m} + V_d\right)(1+f)dV$$

$$-\frac{h^2}{m}\int \psi^*_k(1+f)\,\text{grad}\,\psi_k \cdot \text{grad}\, f dV. \quad (15)$$

The first term in (15) is evidently equal to ϵ_k, the energy parameter for the uniform distribution, whereas the third term is

$$-\frac{1}{V}\frac{h^2}{m}\int 2\pi i\mathbf{k}\cdot\text{grad}\, f(1+f)dV,$$

which vanishes when summed over the range of k values occurring in a uniformly filled band. Hence the sum of terms arising from (15) becomes as a result of the plane-wave character of the ψ_k,

$$\sum_k \epsilon_k - \frac{h^2}{2m}\frac{N}{V}\int (1+f)\Delta(1+f)dV + \frac{N}{V}\int (1+f)^2 V_d dV. \quad (16)$$

The second term in (14) may be expanded to give

$$\frac{N^2}{V^2}e^2\int\int \frac{2f(r_2)+f^2(r_2)}{r_{12}}dV_1dV_2 + \frac{N^2e^2}{V^2}\int 2f(r_1)+f^2(r_1)dV_1\int \frac{2f(r_2)+f^2(r_2)}{r_{12}}dV_2. \quad (17)$$

If the second term in (11) is expanded in a similar way and added to (17), we obtain

$$-\frac{N^2}{V^2}\frac{e^2}{2}\int\int \frac{1}{r_{12}}dV_1dV_2 + \frac{N^2}{V^2}\frac{e^2}{2}\int g(r_1)dV_1\int \frac{g(r_2)}{r_{12}}dV. \quad (18)$$

The quantities involving $1/N$ which appeared in the last term can be easily shown to be negligible.

Combining all these results, we find

$$E_T = \left\{\sum_k \epsilon_k - \frac{N^2}{V^2}\frac{e^2}{2}\int\int \frac{1}{r_{12}}dV_1dV_2 + \tfrac{1}{2}\sum_{\alpha,\beta}\frac{e^2}{r_{\alpha\beta}} + E_e + E_c + E_r\right\} - \sum_\alpha V_d(r_\alpha)$$

$$+\frac{N}{V}\int (1+f)^2 V_d dV - \frac{N}{V}\frac{h^2}{2m}\int (1+f)\Delta(1+f)dV + \frac{N^2}{V^2}\frac{e^2}{2}\int g(r_1)dV_1\int \frac{g(r_2)}{r_{12}}dV_2. \quad (19)$$

If we assume that E_e and E_c are changed by relatively small amounts during the redistribution of charge, the expression in brackets gives the energy of the lattice before redistribution, except for terms involving the potential of the lattice defect.

1. The Interstitial Case

From the terms in (19) not in the bracket one can set aside

$$-\sum_a V_d(r_a)+\frac{N}{V}\int V_d dV. \tag{20}$$

They represent the interaction of the interstitial atom with the lattice in the state of uniform electronic distribution. We have previously shown by the s sphere argument that this quantity is small. The remaining terms in (19) give then the lowering of the energy with the polarization of the electronic charge.

By an application of Green's theorem,

$$\int(1+f)\Delta(1+f)dV=\int(1+f)\Delta f dV=\int(2+f)\Delta f dV, \tag{21}$$

we can express this polarization energy in the form

$$\frac{N}{V}\int(2+f)\left(-\frac{\hbar^2}{2m}\Delta+V_d\right)f dV+\frac{N^2}{V^2}e^2\int g(r_1)dV_1\int\frac{g(r_2)}{r_{12}}dV_2. \tag{22}$$

Though the integration indicated in the first term is over the whole lattice, it can be shown that the only non-negligible contribution arises from the region in the vicinity of the interstitial atom. A convenient estimate of the size of this term can be made by taking $f(r)$ to be the eigenfunction of the valence electron in a free copper atom, and, with this choice, the energy becomes

$$\epsilon_{Cu}\frac{N}{V}\int(2f+f^2)dv+\frac{N^2e^2}{V^2}\int g(r_1)\int\frac{g(r_2)}{r_{12}}dV_1dV_2, \tag{23}$$

in which $-\epsilon_{Cu}$ is the ionization energy of copper, namely 7.7 ev. For the limited region of integration, indicated by dv, $(2f+f^2)$ is equivalent to g. It is obviously necessary to assume that the interstitial ion polarizes the electronic charge distribution by one electronic unit since this is just sufficient to neutralize its charge at large distances. This means that $(N/V)\int g(r)dv=1$. If the second integral of (22) is evaluated for the copper functions with the use of the same normalization for $g(r)$, it is found to have the value 5.0 ev. Thus the polarization energy is found to be about 2.5 ev in the present approximation. This indicates that the polarization energy is not sufficient to reduce the 13 ev of activation energy computed in the previous section for the unpolarized system to a value comparable with the observed value of 2.6 ev. As a result we may conclude that the interstitial mechanism is highly improbable in copper.

2. The Vacancy Case

We can make use of Eq. (19) also in computing the energy needed to form a vacancy. That part of the energy of the lattice before redistribution, which is represented by the expression in the brackets, excluding E_r, has already been discussed at length and shown to lie 7.34 ev below E_n, the energy of a normal lattice containing the same number of copper ions.

TABLE III. Summary of results.

	Direct Interchange A	Interstitial B	Interstitial C	Vacancy D	Vacancy E
Electronic energy in uniform distribution	11 ev	7.34 ev		8.2 ev	
After polarization		~4 ev		1.4 ev	
Repulsive energy (Fuchs)		3.85 ev		−1.0 ev	−.46 ev
Total energy (Fuchs)		~8 ev		.4 ev	
Repulsive energy (exponential)	6.6 ev	5.5 ev	6 ev	− .4 ev	−.37 ev
Total energy (exponential)	over 8 ev	~9.5 ev		1.0 ev	

The first term which follows the bracket in (19) gives the electrostatic, ion-ion interactions which must be subtracted when a vacancy is formed. According to the sphere approximation this is equivalent to

$$-\frac{N}{V}\int(1+g_s)\,V_d dV, \tag{24}$$

in which g_s is a "step function" which is zero everywhere but in the vacant cell where it has the value minus one, and V_d is no longer the potential field of a copper ion, as it was in the case of the interstitial defect, but this field with a reversed sign, since the defect is now a vacancy. In the next term one may replace $(2f+f^2)$ by g. The combination of these two terms gives then

$$\frac{N}{V}\int(g-g_s)\,V_d dV. \tag{25}$$

The total energy can now be expressed,

$$E_T=E_n-7.34\text{ ev}+\Delta E_r+\frac{N}{V}\int(g-g_s)\,V_d(r)dV + \frac{N^2}{V^2}\frac{e^2}{2}\int g(r_1)\int\frac{g(r_2)}{r_{12}}dV_1dV_2+\frac{\hbar^2}{2m}\frac{N}{V}\int|\text{grad } f|^2dV. \tag{26}$$

We evaluated the last three terms with the use of the function

$$f(r)=\begin{cases}\alpha r-1 & r<1/\alpha\\ 0 & r>1/\alpha,\end{cases} \tag{27}$$

in which $\alpha^3=2/5r_s^3$, and obtained the result

$$\frac{0.12e^2}{r_s}+\frac{\hbar^2}{2m}\left(\frac{5}{2}\right)^{\frac{1}{3}}\frac{1}{r_s^2}+\frac{0.53e^2}{r_s}. \tag{28}$$

The first term was evaluated by determining the potential arising from the distribution $(N/V)e^2(g-g_s)$ and assuming that the ionic charge is localized within the region near the origin where this potential is nearly constant. Numerical evaluation of (28) gives $E_t-E_n=1.9$ ev $+\Delta E_r$. This result is not very sensitive to the analytic form chosen for (27). A function which avoids the discontinuity in derivative is a Gauss error function,

$$f(r)=-e^{-(r/d)^2}, \tag{29}$$

in which normalization determines d to be $0.775\,r_s$. The corresponding energy needed to form a vacancy turns out to be 1.4 ev.

These results, like those found in the interstitial case, do not include the change in exchange and correlation energies that occurs in polarizing the distribution, nor does it include the change in ion

repulsion. The former will be discussed in detail in the paper by Huntington, whereas the latter was found in the preceding section to be -0.4 ev when the exponential-type function was used for the equilibrium configuration. The variational procedure then indicates about 1.0 ev as the complete energy needed to form a vacancy. For the saddle-point configuration, the change in the repulsive energy, when the exponential function is used, is found nearly the same, -0.37 ev, but the polarization of the electronic distribution is far less effective in lowering the energy for this configuration because of the more complicated density modulation that is involved.

IV. CONCLUSION

The results of these computations are summarized in Table III, and seem to show beyond a reasonable doubt that the vacancy mechanism of diffusion is greatly preferred over the other two types considered here for copper. A more careful treatment of the vacancy case, presented in the paper by Huntington, supports this conclusion further.

MARCH 1 AND 15, 1942 PHYSICAL REVIEW VOLUME 61

Self-Consistent Treatment of the Vacancy Mechanism for Metallic Diffusion*

H. B. HUNTINGTON†
Randal Morgan Laboratory of Physics, University of Pennsylvania, Philadelphia, Pennsylvania
(Received December 6, 1941)

Previous calculations have indicated the predominance of the vacancy mechanism in metallic self-diffusion. Here a more detailed calculation of the energy needed to form a vacancy has been carried out. A self-consistent solution to the Hartree-Fock equation was used with a free-electron model corresponding to the copper lattice. The result agreed essentially with the value predicted by Huntington and Seitz. In addition a rough upper limit was established for the energy required to move a vacancy. This value compares satisfactorily with the observed energy of activation for copper self-diffusion. The anisotropy recently observed in zinc self-diffusion can also be qualitatively explained to some extent on the basis of a vacancy process. In the case of the alkali metals present considerations are insufficient to decide between the interstitial and vacancy mechanisms.

INTRODUCTION

LATTICE vacancies are physically important in metallic diffusion. In the preceding paper[1] by Huntington and Seitz we investigated three possible mechanisms which might be responsible for diffusion in a typical metal, copper. Energetic considerations indicated definitely that vacancy diffusion plays the dominant role, as against interstitial diffusion and diffusion by direct interchange. The calculation for the energy needed to form a vacancy had, however, two shortcomings. In the first place, the wave functions used in the variational procedure were not a mutually orthogonal set, though the simplified treatment there employed necessarily used them as though they were. Secondly, no account was taken of the change in the exchange potential which must accompany any modulation of the electron distribution. Therefore it was decided to undertake a self-consistent solution of the problem in the Hartree-Fock approximation.

I. SELF-CONSISTENT SOLUTION FOR THE VACANCY PROBLEM

1. Potential Field near the Vacancy

To handle the problem at all it was necessary to use throughout the free-electron model with

* Part of a Dissertation presented to Princeton University for the degree of Doctor of Philosophy.
† Now at Washington University, Saint Louis, Missouri.
[1] Frederick Seitz and H. B. Huntington, Phys. Rev. **61**, 315 (1942); preceding paper. Equations, figures, and tables of this paper will be designated by primed references.

TABLE I. Wave function formulae.

		For r large	For r small	Density at small r
Uniform distribution	S	$\frac{\sin(kr)}{kr}$	$1-\frac{(kr)^2}{6}$	$\frac{k_m^3}{3}-\frac{k_m^5 r^2}{15}$
	P	$\frac{\sin(kr)-kr\cos(kr)}{(kr)^2}$	$\frac{kr}{3}\left[1-\frac{(kr)^2}{10}\right]$	$\frac{k_m^5 r^2}{45}$
Barrier distribution	S	$\frac{\sin(kr-\alpha_S)}{kr}$	$\frac{\sin(kR-\alpha_S)}{\sinh(KR)}\frac{\sinh(Kr)}{kr}$	$\int_0^{k_m}\left[\frac{K\sin(kR-\alpha_S)}{\sinh(KR)}\right]^2 dk$
	P	$\frac{d}{dr}\frac{\sin(kr-\alpha_P)}{k^2 r}$	$\frac{\sin(kR-\alpha_P)}{\sinh(KR)}\times\frac{Kr\cosh(Kr)-\sinh(Kr)}{(Kr)^2}$	$\int_0^{k_m}\left[\frac{Kkr\sin(kR-\alpha_P)}{3\sinh(KR)}\right]^2 dk$

uniform distribution to represent the original state of the copper lattice. Any lattice defect, such as a vacancy at a lattice site, would bring about a disturbance in the electron distribution, which would nearly possess spherical symmetry. The solution to the problem is then most simply expressed in a series of spherical harmonics which reduce at large distances to the well-known expansion of plane waves. Since the vacancy cell is a region of high potential, the electronic density is there necessarily reduced. The situation is closely analogous to a scattering problem in which electrons of various energies impinge from every direction upon a spherical barrier.

The form of this potential barrier is, to some extent, dependent upon the assumption made in setting up the problem. Since one wishes the solutions to reduce to plane waves at large distances, it is not practical to use the actual lattice potential, but rather to replace it everywhere by a constant value. The withdrawal of an ion to form a vacancy involves the introduction of a potential peak $-V(r)$, where $V(r)$ is the potential field of the ion, upon the uniform potential plane. As a consequence our potential field near the vacancy goes infinite as $r\rightarrow 0$, in contradiction to what one knows must be the case. This error is unimportant, however, because the region concerned is small and because it is the very region in which the uniform-distribution model breaks down. Since this potential infinity had no physical meaning, it was a great help in the work of numerical solution to consider the potential as being flat from $r=0.8a_0$ into $r=0$.

Besides the potential $-V(r)$ of the missing, or pseudo-"negative," ion at the vacancy site, there is also an electrostatic contribution from the electronic charge displaced from this region. This displaced charge is assumed equivalent to one electron, so that the vacancy region may be neutral at large distances.

2. Exchange Potential

In addition to these electrostatic forces some account was taken of the change in the "exchange potential" in the neighborhood of the vacancy as a result of the decrease in the electronic distribution. In general such an "exchange potential," $A_k(x)$, is written

$$A_k(x)=\frac{e}{2\chi_k(x)}\int\frac{\chi_k(x_1)\sum^{k'}\chi_{k'}(x_1)\chi_{k'}(x)}{|r-r_1|}dV_1 \quad (1)$$

and so varies with k. The χ_k are the wave functions of the metal. The summation over k' includes all the electrons of both spins. The use of such a set of A_k in solving for the self-consistent χ_k would lead to non-orthogonal functions. To avoid this it was decided to replace the $A_k(x)$ by a suitable average over k, $A(x)$. The procedure for averaging is determined only to the extent that $A(x)$ must reduce to $0.916e/r_s$ for plane wave functions, the eigenvalue for the exchange operator in that representation. Therefore in the interest of simplicity the following average was chosen,

$$A(x)\cdot\rho(x,x)=\frac{e}{2}\int\frac{\rho(x,x_1)^2}{|r-r_1|}dV_1, \quad (2)$$

where

$$\rho(x_1,x_2)=\sum^{k}\chi^*_k(x_1)\chi_k(x_2).$$

The problem of finding the exchange potential in the neighborhood of the vacancy is, to some extent, the radial analogue of the one-dimensional

problem of the metal surface, which Bardeen[2] investigated when studying the influence of the double layer on the work function. (Bardeen used the $A_k(x)$ as he was concerned with the electronic densities rather than energies.) Since the problem involves spherical symmetry, it was convenient to expand the plane waves into spherical harmonics:

$$e^{ik\cdot r}=\sum^{n}(2n+1)i^n j_n(kr)P_n(\cos\theta). \quad (3)$$

Here the $j_n(x)$ are the spherical Bessel functions[3] and the P_n are the Legendre polynomials. It soon became evident that only the S, P, and D parts of the wave (i.e., $n=0$, 1, 2) would be appreciably affected by the disturbing potential at the vacancy.

It is to be emphasized that the exchange contributions to this disturbing potential are the differences between the exchange potentials for the vacancy wave functions and those for the free electrons. Moreover, the exchange contribution is different for each harmonic. To see this one expands the vacancy wave functions also into spherical harmonics:

$$S(kr)+3iP(kr)P_1(\cos\theta) -5D(kr)P_2(\cos\theta)+\text{etc.} \quad (4)$$

Then A_S and A_P, the respective exchange potentials for the S and P parts, are evaluated from the expressions:

$$\int|S(kr)|^2 dV_k\cdot A_S =\frac{e}{2}\int\int\frac{S^*(kr)S(kr_1)\rho(x,\,x_1)}{|r-r_1|}dV_k dV_1,$$
$$\int|P(kr)|^2 dV_k\cdot A_P =\frac{e}{2}\int\int\frac{P^*(kr)P(kr_1)\rho(x,\,x_1)}{|r-r_1|}dV_k dV_1, \quad (5)$$

where the summation over k states has been replaced by integration, not only as shown explicitly but also implicitly in the expression for $\rho(x, x_1)$. The k-volume element is $(2\pi)^{-3}2k^2dkd\omega_k$, where k is integrated from 0 to $k_m=1.92r_s$, and $d\omega_k$ is the solid angle in k-space. (The factor 2 is supplied by summation over spins.) This choice insures the normalization of electron density to unity over the unit cell.

Because of the complications involved, a general evaluation of the A's is very difficult. Instead one can expand about the center of the vacancy in powers of r (henceforth called ϵ) and investigate the size and curvature of A_S and the size of A_P, at this point. Since this point will give the largest values of the differences between vacancy and free-electron exchange potentials, a reasonable estimate can be deduced for the behavior

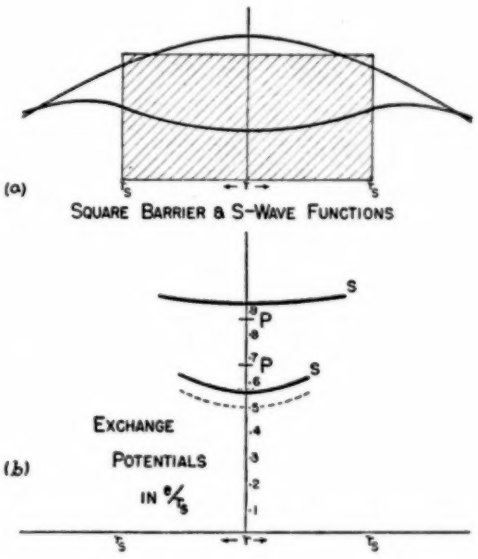

FIG. 1. (a) Comparison of $S(kr)$ for a square barrier with corresponding plane wave, $j_0(kr)$, for the free electron. The square-cut barrier is superimposed. (b) The exchange potentials for the harmonics in the neighborhood of the vacancy center. The upper full lines are for the free-electron functions, the lower full lines for the solutions of the square barrier, and the dotted lines for the self-consistent solutions.

throughout of this contribution to the disturbing potential. The factor $|\epsilon-r_1|^{-1}$ can be replaced by its expansion in harmonics:

$$1/|\epsilon-r_1| =\begin{cases}(1/r_1)\sum^{n}(\epsilon/r_1)^n P_n(\cos\theta) & \text{for } \epsilon<r_1,\\ 1/\epsilon & \text{for } \epsilon>r_1.\end{cases} \quad (6)$$

All three of the integrations over solid angle can

[2] J. Bardeen, Phys. Rev. **49**, 653 (1936).
[3] See P. Morse's *Vibration and Sound*, pp. 246, 335.

now be carried out, with the help of the relation,

$$\int P_n(\cos\theta)P_n(\cos\theta')d\omega = 4\pi(2n+1)P(\cos\theta''), \quad (7)$$

where θ and θ' are referred to poles which make an angle of θ'' with each other. By considering no terms of higher order than ϵ^2, i.e. no D terms, one obtains the following expressions for the A's:

$$S(\epsilon,\epsilon)\cdot A_S(\epsilon)=\frac{2e}{\pi}\left\{\int_0^\infty\left[\frac{|S(\epsilon,r)|^2}{r}+\frac{\epsilon}{r^2}S(\epsilon,r)P(\epsilon,r)+\cdots\right]r^2dr-|S(\epsilon,\epsilon)|^2\int_0^\epsilon\left(\frac{1}{r}-\frac{1}{\epsilon}\right)r^2dr\right\} \quad (8)$$

$$P(\epsilon,\epsilon)\cdot A_P(\epsilon)=\frac{2e}{\pi}\int_0^\infty\left[\frac{|P(\epsilon,r)|^2}{r}+\frac{\epsilon}{3r^2}S(\epsilon,r)P(\epsilon,r)+\cdots\right]r^2dr.$$

Here $S(x,y)$ is an abbreviation for $\int_0^{km}S(kx)\times S(ky)k^2dk$ and similarly for $P(x,y)$.

If we consider first the A's for the free-electron distribution, then $S(kr)=j_0(kr)=(\sin kr)/kr$ and $P(kr)=j_1(kr)=(\sin kr-kr\cos kr)/(kr)^2$. All integrations over k and r can be performed exactly and give:

$$\int_0^\infty|S(\epsilon,r)|^2rdr=\frac{k_m^4}{4}-\frac{5k_m^6\epsilon^2}{36},$$
$$\int_0^\infty|P(\epsilon,r)|^2rdr=\frac{k_m^6\epsilon^2}{108}, \quad (9)$$
$$\int_0^\infty S(\epsilon,r)P(\epsilon,r)dr=k_m^6\epsilon/54.$$

Solving for the $A_S(\epsilon)$ and the $A_P(\epsilon)$ we obtain [see Fig. 1b]

$$A_S(\epsilon)=\frac{3ek_m}{2\pi}\left[1+\frac{2(k_m\epsilon)^2}{135}\right],$$
$$A_P(\epsilon)=\frac{3ek_m}{2\pi}\frac{25}{27}. \quad (10)$$

The constant free-electron exchange, $0.916e/r_s$, is given by $3ek_m/2\pi$. Moreover, if we take the weighted sum $S(\epsilon,\epsilon)A_S+3P(\epsilon,\epsilon)A_P$, the terms quadratic in ϵ drop out, as one would expect, since A is a constant for free electrons.

To obtain values for the exchange potential with vacancy distribution, one must make some choice of starting functions from which to work towards self-consistency. It was decided to represent the potential in the neighborhood of the vacancy by a square-wall barrier in the first approximation with height H for $r<R$ and zero elsewhere. For this case the wave solutions can be found immediately by fitting at the barrier wall. In Table I are compiled the analytic expressions for the S and P functions of both uniform and square-barrier distributions inside and outside the barrier. The respective contribution of each function to the density at the origin is also given. The α_S and the α_P are the phase shifts which appear in the vacancy wave functions as a result of the repulsive potential. For the S waves the α_S are given exactly as a function of k by

$$\cot(kr-\alpha_S)=(K/k)\coth KR, \quad (11)$$

where $\frac{1}{2}(K^2+k^2)$ in atomic units is equal to H. Expressions for α_P and α_D proved to be more complex, but could be closely approximated by

$$\tan\alpha_P=(2/45)kR^3H\sin^2kR,$$
and
$$\tan\alpha_D=(2/1575)k^3R^5H\sin^2kR. \quad (12)$$

The greater sensitiveness of the higher harmonics to the extent of the potential barrier is shown by the presence of the R^{2n+1} factor. On the other hand the height of the barrier appears only to the first power in each expression for the wave shifts. An actual barrier was next chosen with R equal to r_s and H equal to $\frac{1}{2}k_m^2$, since this seemed about the size needed to displace one electron from the region of the vacancy. A comparison between a square-barrier function $S(kr)$ and the corresponding $j_0(kr)$ of the uniform distribution is shown by way of illustration in Fig. 1(a). The square-barrier potential has been schematically superimposed.

The integrations over k, indicated in the expressions for $S(x,y)$ and $P(x,y)$, were next approximated by summing appropriately over five evenly spaced values of k. Then the inte-

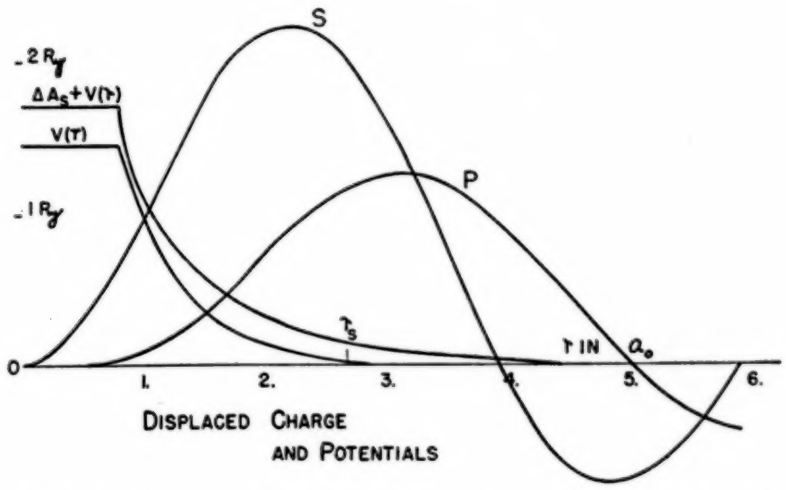

FIG. 2. The electrostatic potential for the first integration is shown here; also the potential used for the S functions formed by adding ΔA_S. The distribution of the displaced charge for the S and P functions are superimposed for comparison.

grations over r were carried out numerically with the following results:

$$S(\epsilon, \epsilon) = (0.357 - 0.044\epsilon^2) r_s^{-3},$$

$$P(\epsilon, \epsilon) = 0.155\epsilon^2 r_s^{-3},$$

$$\int_0^\infty |S(\epsilon, r)|^2 r dr = (0.164 + 0.081\epsilon^2) r_s^{-4}, \tag{13}$$

$$\int_0^\infty |P(\epsilon, r)|^2 r dr = (0.061\epsilon^2) r_s^{-4},$$

$$\int_0^\infty S(\epsilon, r) P(\epsilon, r) dr = 0.072\epsilon^2 r_s^{-5}.$$

Here ϵ is measured in units of r_s. Substituting these values in Eq. (8), one obtains

$$A_S(\epsilon) = (0.56 - 0.26\epsilon^2) e/r_s$$

and

$$A_P(\epsilon) = 0.67 e/r_s. \tag{14}$$

In Fig. 1(b) these data for the square-barrier exchange potentials are shown in full lines. The corresponding quantities for the uniform distribution, also in full lines, lie above them. By subtracting one set from the other, one obtains

$$\Delta A_S(\epsilon) = (0.35 - 0.20\epsilon^2) e/r_s$$

and

$$\Delta A_P(\epsilon) = 0.18 e/r_s. \tag{15}$$

These differences describe the contributions of the exchange terms to the disturbing potential of the vacancy in the region of its center. Moreover these contributions must become negligible at about that distance where the distribution regains its normal density, or near $1.8r_s$. This information was sufficient to determine A_S with accuracy sufficient for our purpose, since the exchange terms did not play the dominant role in displacing the electrons. The shape of ΔA_P was taken similar to ΔA_S.

3. Integration of the Self-Consistent Solution

The contributions of the exchange potentials were next added to the potential of the "negative ion" and of the initial distribution of the displaced charge, which has been previously discussed. The initial distribution, which determines the shape of the "hole" formed in the electronic fluid about the vacancy site, was composed of about 60 percent of an S electron, 30 percent of a P electron, and 10 percent of a D electron. In their respective potential fields S and P functions were next integrated numerically for five evenly spaced values of k. If one writes $N_0 R_{0,k}(r)$ for $krS(kr)$ and $N_1 R_{1,k}(r)$ for $krP(kr)$, etc., the wave equation becomes

$$d^2R_{n,k}(r)/dr^2 - \left[2V_n(r) - k^2 + \frac{n(n+1)}{r^2}\right] R_{n,k}(r) = 0, \tag{16}$$

for the radial part of the nth harmonic, where

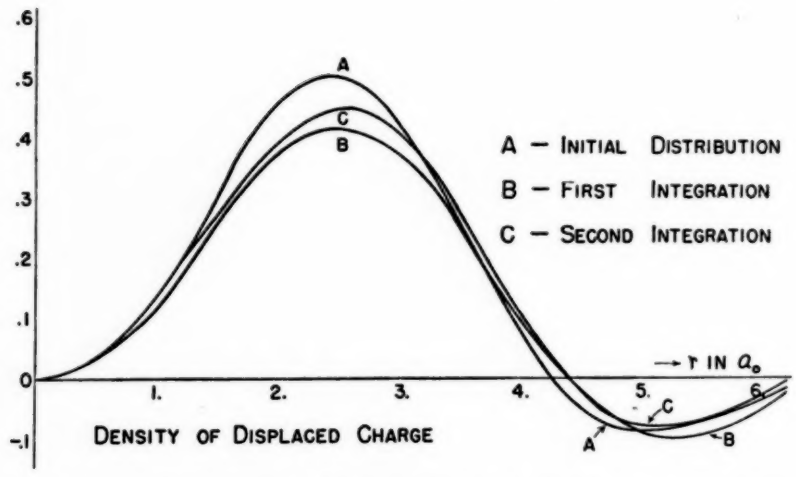

FIG. 3. Comparison of densities of displaced charge in units of ea_0^{-1} for the various distributions of each step in the self-consistent process.

atomic units have been used throughout. In the region from $r=0$ to $0.8a_0$ the V_n (the potentials appropriate to the harmonics in question) were taken to be constants, for reasons which have been previously discussed. Thus the starting conditions for the R_n were determined at $0.8a_0$ to fit with hyperbolic functions of the type used for the square barrier. Beyond the value $5a_0$, the $V_n(r)$ become nearly zero and one could identify N_0R_0 with $\sin(kr-\alpha_S)$ and N_1R_1 with $(1/kr)[\sin(kr-\alpha_P)-kr\cos(kr-\alpha_P)]$. The phase shifts α_n, could then be determined together with the normalizing constants, N_n.

After these functions were obtained, the next steps were to normalize them with multiplication by N_n, to square them, to average over k, and finally to subtract these densities from the corresponding quantities computed from the free-electron harmonics to get the distribution of displaced charge. In Fig. 2 the S and P contributions to this distribution are shown for this stage of the solution. What is plotted is the density of charge in a spherical shell of radius r as a function of r. The electrostatic potential and $V_{n=0}$ used in the integration are superimposed on the same graph. The results from this step give 0.49_0S electron and 0.35_8P electron. Little could be said about the D function with certainty, since the exchange potential was not known. Investigations of this potential in the region around $r=0$ would be necessarily laborious and give little information about this term at distances where the D function would be most sensitively affected. Certainly the effect of the exchange potential will decrease with increasing order of the harmonic. For the D function it may well be negligible. One integration was carried out by using the electrostatic potential alone. Comparing the phase shift so obtained with that of the corresponding square-barrier function, one could estimate, on the basis of an approximate treatment applied to the latter, that less than 3 percent of a D electron was displaced. In all this gives a total of nearly 88 percent electron displaced at this stage.

In the next step a new electrostatic potential was devised, essentially by treating the 88 percent electron as a whole. (It seemed reasonable to assume that the vacancy cell will be neutral at large distances.) New integrations gave 47 percent S electron and 44 percent P electron, whereas about four or five percent D electron was estimated. With the second step in the self-consistent process about 96 percent of an electron had been displaced. A new potential calculated from this distribution would differ but slightly from the previous one—it would show in fact a small increase. Adequate self-consistency, under the condition that one electron be displaced, seems assured to the accuracy with which it is feasible to determine the displaced D. The behavior of the initial distribution and of those from the two successive integrations is illustrated in Fig. 3.

With the final wave functions the exchange

calculations were repeated, both to check the previous work and to determine the sensitiveness of the A_n to the distribution used. The results gave:

$$\Delta A_S=(0.42_4-0.27_8\epsilon^2)e/r_s$$

and

$$\Delta A_P=0.27_5e/r_s. \quad (17)$$

The potentials from which these values are obtained are represented by dotted lines in Fig. 1, where they may be compared with the other exchange potentials.

4. Energy of the Vacancy

The procedure for setting up the expression for the energy of the vacancy is somewhat involved. Fortunately it resembles that followed in the preceding paper by Huntington and Seitz where the vacancy was treated by a variational method. Except for two important changes, the development is the same. In the first place the self-consistent wave functions are actually eigenfunctions of the vacancy problem in the expanded lattice. The mean value of the Hamiltonian for the kth electron, which was formerly written[4]

$$\int\psi_k(1+f)H\psi_k(1+f)dV$$
$$=\epsilon_k-\frac{h^2}{2mV}\int(1+f)\Delta(1+f)dV$$
$$+\frac{1}{V}\int[1+f(r_1)]^2$$
$$\times\left[V(r_1)+\frac{e^2}{V}\int\frac{2f(r_2)+f(r_2)^2}{|r_1-r_2|}dV_2\right]dV, \quad (18)$$

now nearly corresponds with the energy parameter, ϵ'_k, of our self-consistent solution. The correspondence is not exact because in this paper we have been dealing with the Hartree-Fock equation, whereas in the other no attempt was made to take into account any change in the exchange energy. This marks the second important difference between the two procedures.

Let us investigate the ϵ'_k of the self-consistent solution. They differ from $(hk)^2/2m$ of the free electrons because of the wave shifts introduced by the vacancy barrier. The new wave functions must satisfy the same boundary conditions as the eigenfunctions of the expanded lattice. At large distances the principal difference between the two sets of functions arises from the wave shifts, $\alpha(n, k)$. If we consider our copper specimen to be a sphere of radius R, then the wave number k' of the self-consistent solutions must be related to the k of the expanded lattice by the equation,

$$(k'R-\alpha)=kR, \quad \text{or} \quad k'=k+(\alpha/R). \quad (19)$$

There is then a small change in k, inversely proportional to the linear dimensions of the copper crystal. The change in energy parameter of a given electron wave is given by $2k\alpha/R$ in Ry. The number of wave functions belonging to the same harmonic but to different values of k is given by $N=k_mR/\pi$. For a given harmonic it follows that the increase in the energy parameters is given by

$$\Delta E_n=\frac{2(2n+1)}{\pi}\sum_0^{k_m}k\alpha(n, k) \text{ in Ry.} \quad (20)$$

The value of the summation was approximated by taking k_m times the evenly weighted average of the five values for $k\alpha$ obtained from the five integrations for S and P harmonics. Results gave $\Delta E_0=0.103$ Ry for S and $\Delta E_1=0.048$ Ry for P.

In the final expression for the energy in the variational scheme, Eq. (19′), the term involving the Laplacian of f appears. It measures the difference in the kinetic energies of the modified wave functions and the free-electron waves of the "expanded lattice." Since the left-hand side of Eq. (18) can be evaluated as the sum of the ϵ'_k of the self-consistent solution, one can solve this equation for the kinetic term and obtain the expression

$$\Delta E_0+\Delta E_1-\int\rho_s(r_1)$$
$$\times\left[V(r_1)+e^2\int\frac{\rho_s(r_2)-\rho_u(r_2)}{|r_1-r_2|}dV_2\right]dV_1. \quad (21)$$

Here the subscripts u and s on the density functions refer to the uniform and self-consistent functions, respectively.

There is still to be treated the second point of difference between the two procedures. When the

[4] Compare with Eq. (12′) and (13′).

variational attack was used, no attempt was made to take into account any change in the exchange potential. Now that the recent method has incorporated into it a term of this nature in the potential field used in solution, one must finally subtract away one-half of the average exchange potential, in accordance with the standard procedure for obtaining the total energy in the Hartree-Fock approximation. The quantity to be included can be written as follows:

$$-\tfrac{1}{2}\int (A_s\rho_s - A_u\rho_u)dV =$$

$$-\tfrac{1}{2}\int (A_s - A_u)\rho_s dV + \tfrac{1}{2}\int A_u(\rho_u - \rho_s)dV. \quad (22)$$

The exchange operator for plane waves, A_u, is a constant, and consequently the second term on the right vanishes. The first term can be treated by breaking it up into S and P parts.

A compilation of the terms which enter into the energy of the formation of a vacancy follows here. It contains the energy of the "extended lattice" and the potential terms analogous to those appearing in the earlier treatment, the kinetic energy expressed in its new form, and finally the exchange terms just discussed above.

TABLE II. Energy contributions from neighbors for "D" configuration.

	Exponential	Displaced Fuchs
Lattice potential term	0.00 ev	0.02 ev
Dipole interactions	0.00 ev	0.03 ev
Shielded vacancy ion potential	0.84 ev	0.90 ev
Ion-core repulsions	−0.24 ev	−0.68 ev
	0.60 ev	0.27 ev
Value for λ-parameter	0.00	0.01

Energy of the "extended lattice"	−0.544 Ry
Self-energy of the displaced charge	0.393
$\int\left[\rho_u-\rho_s-\frac{N}{V}g_s\right]V(r)$ (see Eq. (31'))	0.168
Change in the energy parameters for the S functions	0.103
Change in the energy parameters of the P functions	0.048
$-\int\rho_s(r_1)\left[V(r_1)+e^2\int\frac{\rho_s(r_2)-\rho_u(r_2)}{\lvert r_1-r_2\rvert}dV_2\right]dV_1$	−0.017
Exchange term for the S function	−0.051
Exchange term for the P function	−0.009
	1.23 ev = 0.091 Ry

This result is surprisingly close to the 1.4 ev found by the variational method with the use of a function of the Gauss error type in the neighborhood of the vacancy. Evidently the decrease in energy, which one would expect in a numerical solution, has been compensated in part by the inclusion of the change in the exchange potential.

The radial distributions plotted in Fig. 3 show that the density is *greater* than its normal value at distances of $5a_0$ and $6a_0$. Apparently the electrostatic potential of the vacancy is actually positive at a radius equal to the interatomic distance. Some electrostatic considerations can now be used in conjunction with the results already obtained for the repulsions of closed shells to redetermine the positions of next neighbors. There are first the potentials of the vacancy and of the lattice,

$$12\left[E\left(\frac{\lambda a}{2},\frac{\lambda a}{2},0\right)-E(0)+\left\{-V(r_1)\right.\right.$$

$$\left.\left.-e^2\int\frac{\rho_s(r_2)-\rho_u(r_2)}{\lvert r_1-r_2\rvert}dV_2\right\}_{r_1=a\sqrt{2}(1-\lambda)/2}\right]. \quad (23)$$

The potential of the lattice for an ion in its own cell, $E(x)$, can be accurately calculated by some method such as Ewald's, but for these purposes it will be adequately represented by the quadratic term of central symmetry, r^2/r_s^3 Ry. The displacement of nearest neighbors toward the vacancy is given by $\lambda\sqrt{2}a/2$. There are, in addition to (23), the interactions of the displacements of the various neighbors, which may be calculated by the standard formula for dipole-dipole energy. The results after including these quantities are shown in Table II. The exponential repulsion gives the energy of neighbors as 0.6 ev, the Fuchs repulsion as 0.3 ev with λ equal to 0.01. In each case the positive contribution from the electrostatic interactions has overbalanced the decrease in the repulsive energy. Final values for the energy needed to form a vacancy are 1.8 ev and 1.5 ev, according to the exponential and Fuchs repulsion, respectively.

The large increase in the electrostatic energy just considered is to some extent a spurious effect, which arises because the spherical modulation of the wave function alone is inadequate at large distances from the vacancy center. This situation

with the next neighbors contributes the largest uncertainty in the value for the energy of vacancy formation. The next largest causes for error arise from the use of the free-electron model and from the limited degree of accuracy to which the self-consistent solution has been carried.

II. UPPER LIMIT TO THE ENERGY OF THE SADDLE-POINT

Unfortunately the saddle-point for vacancy diffusion, configuration E,[5] cannot be treated as rigorously as the situation in the preceding section. Here the problem is more complicated because only symmetry about the direction of diffusion remains. A direct attack by the variational method would give a reasonably good answer, since the variational and Hartree-Fock methods have shown substantial agreement in the preceding case. Unfortunately the integrations involved in the self-potential and kinetic terms would be extremely awkward. I have chosen instead a rather makeshift approach, which nevertheless can give considerable information. There follows a discussion of the model employed and the assumptions which are necessarily made in treating it.

1. Description of the Assumed Electronic Distribution

As before, we start from a uniform distribution in the "expanded" lattice with its energy of -7.34 ev. Next in the region of diffusion two vacancy cells are placed at adjoining sites, and a diffusing ion is put halfway between them. Suppose this ion brings with it its atomic cell and that this cell is deformed to include the region about the diffusing ion which is not part of the polyhedron cells of its four nearest neighbors.[5] Then the deformed atomic cell will fill up one-half of each of the vacancy cells on either side. The rest of these vacancy cells will be henceforth referred to as the "regions outside atomic cells," and they may be taken to be hemispherical in shape, as shown by the cross-hatched areas in Fig. 4(a). These regions have a high potential energy as compared with the rest of the lattice. In line with previous treatment one must introduce some modification of the electronic distribution to decrease the density of charge at these places. The only kind of distribution which can be dealt with simply, i.e., without introducing extremely complicated spatial integrations for the kinetic and potential terms, must possess spherical symmetry. Accordingly a model was chosen in which there were removed two spherical distributions, each of charge $\frac{1}{2}e$, one from each hemisphere. The center of each distribution was placed at the centroid of the respective hemisphere, and its radial behavior was taken to be the same as that of the self-consistent solution in Part I for the single vacancy, except that the radial scale was reduced by the factor $1/\sqrt[3]{2}$ (see Fig. 4(b)).

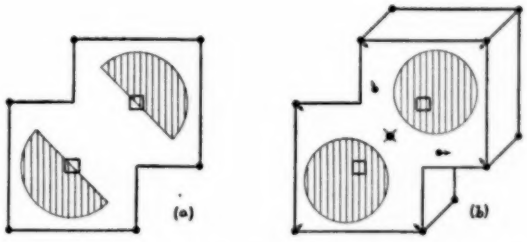

FIG. 4. (a) A model for the two-vacancy configuration, where the "regions outside atomic cells" are shown as two hemispheres separated by the cell of the diffusing atom. (b) Here the spherical holes of charge $\frac{1}{2}e$ have been made in the electronic distributions, as represented by the cross-hatched, circular areas. The centers of these charge holes coincide with the centroids of the hemispheres shown in (a).

There are several apparent defects in this model and it is well to examine them critically before proceeding. In the first place no account has been taken of the change in form of the self-consistent solution when applied to the smaller "region outside atomic cells." Such a charge hole will be relatively more shallow, as a rigorous solution would show. To obtain an upper limit for the energies involved, however, the present procedure will suffice. A far more serious shortcoming, I believe, is the fact that the charge taken from the hemispherical "regions outside atomic cells" has been assumed to have a spherical arrangement. This is very different from what is actually the case, but one must remember that, even for the exact solution of the problem of the hemispherical potential barrier, the surfaces of equal electronic density will have a more nearly spherical form than the equipotentials of the barrier itself. This reduces modulation of the

[5] See Fig. 2 in preceding paper.

wave functions and resulting kinetic energy. At a later point an estimate of the involved error will be made by calculating the increase in kinetic energy which would accompany the deformation of our charge holes from spherical form into oblate spheroids of the same volume. Finally the assumed electronic distribution of the two charge holes leaves the density of charge about the diffusing ion at its uniform value, whereas we know that this cell is at a higher potential than the rest of the crystal and consequently collects some extra charge within it. This latter is, however, a minor defect and probably causes only a small error in the final energy value for this model.

2. The Ion-Ion Electrostatic Interaction

Before proceeding with the charge holes, one considers the increase in the ion-ion electrostatic interaction which comes about when the diffusing atom moves to the saddle-point position. If one starts with a vacancy and the uniform distribution of the "extended" lattice, then the increase in energy of the lattice as a whole, when one of the neighboring ions moves halfway in to fill up the vacancy, is given by

$$E(\tfrac{1}{4}a, \tfrac{1}{4}a, 0) - E(0) - \sqrt{2}e^2/a. \qquad (24)$$

The last term comes from the change in the Coulomb interaction of the diffusing ion with the "vacancy ion" (negative). Actually the expression (24) gives a negative result. The reason for this is that, while the diffusing cell moves to a higher potential, the self-potential energy of the charge outside atomic cells has decreased from that of a uniformly charged sphere to that of two uniformly charged hemispheres at a distance L apart, where L, the distance between the centroids of the two hemispheres, is $\frac{1}{2}\sqrt{2}a + \frac{3}{4}r_s$. The classical problem of the self-potential of a uniformly charged hemisphere cannot be solved in closed form but estimates (as obtained in Appendix I) place the size of this energy at approximately nine-tenths of that for a sphere of the same charge density and total charge. For a uniformly charged sphere the self-potential is $0.6C^2/R$, where C is the total charge and R is the radius. Then the change in the energy of the charge outside atomic cells is given by

$$0.6\left[\frac{e^2}{r_s} - 2(0.9)\left(\frac{e}{2}\right)^2 \frac{\sqrt[3]{2}}{r_s}\right] - \frac{e^2}{4L} \qquad (25)$$

and this term must be added to (24) to give the increase in the electrostatic ion-ion interaction for the diffusing ion.

3. Consideration of the Charge Holes

At this point one introduces "vacancy ions" of charge $-\frac{1}{2}e$, placed at the centroids of the hemispheres. The uniform distribution is replaced by the modulated distribution containing the two charge holes, as has already been postulated. The terms which occur in the expression for the energy for the one-vacancy "D" configuration can now be taken over into this calculation, after they have been multiplied by the appropriate factor, as determined by dimensional analysis. For the "D" configuration the kinetic energy in Eq. (21) was obtained from the difference between the change in the energy parameters of the electron waves and the integral of the final distribution in the final vacancy field. Within vacancy cells, whose linear dimensions are reduced by the factor $2^{-\frac{1}{3}}$, this term is accordingly multiplied by $2^{\frac{1}{3}}$. In considering the potential terms the relatively less important exchange potentials were combined with the corresponding electrostatic terms. The self-energy quantities were multiplied by $2^{-\frac{1}{3}}$, as obtained from reasoning exactly analogous to that applied above to the uniformly charged spheres. In addition the interaction of the two charge holes gives $e^2/4L$, which cancels a similar term of the opposite sign in Eq. (25) of the preceding paragraph. A factor $2^{-\frac{1}{3}}$ multiplies also the quantity

$$\int\left[\rho_u - \rho_s - \frac{N}{V}g_s\right]V(r)\,dV. \qquad (26)$$

These considerations do not give the complete energy for the formation of the two charge holes, since there has been omitted any account of the error introduced by replacing the high potential hemispheres with "vacancy ions" of charge $-\frac{1}{2}e$. There seems, however, no convenient way to compute simply and directly this effect.

4. Behavior of Nearest Neighbors

Some revision of those quantities, as given in Table II′, which relate to atoms adjacent to the site of the diffusion jump, can now be made by including electrostatic forces with the ion-ion repulsions. In our procedure we have added to the regular lattice potential, two negative "vacancy ions," one positive diffusing ion, and two holes in the negative electron charge. For the four nearest neighbors of the diffusing ion, the following electrostatic terms are to be considered in addition to the previously calculated ion-core repulsions:

(a) The potential of the lattice for the ion in its cell, which can be conveniently approximated as before by r^2/r_s^3 Ry.

(b) The energy gained by allowing each ion to retreat from the diffusing ion a fraction, λ, of its equilibrium distance, which is given per ion by

$$\frac{2\sqrt{2}e^2}{\sqrt{3}a}\left[\frac{1}{1+\lambda}-1\right].$$

(c) Finally, the Coulombic interactions with the "negative ions" and the charge holes. Here the λ displacement can be treated as a dipole of moment $-\frac{1}{4}6^{\frac{1}{2}}\lambda ae$. The distance between the diffusing ion and a charge hole is nearly $\frac{1}{2}a$. The

TABLE III. Energy contributions from neighbors to "E" configuration.

	Exponential	Displaced Fuchs
17 broken repulsive contacts	−0.69 ev	−1.65 ev
Energy of 14 "D"-type neighbors	0.98 ev	0.99 ev
Energy of 4 neighbors of diffusing ion	0.89 ev	1.56 ev
	1.18 ev	0.90 ev
Value of λ-parameter for 4 neighbors	0.08	0.025

distances from the displaced neighbor to the negative ions and to the charge holes are, respectively, $\frac{1}{2}\sqrt{2}a$ and $\frac{1}{4}10^{\frac{1}{2}}a$. Accordingly these terms give

$$-\frac{6^{\frac{1}{2}}}{4}\lambda ae\left[-2e\cdot\frac{\sqrt{3}}{2}\cdot\frac{2}{a^2}+e\cdot\left(\frac{3}{5}\right)^{\frac{1}{2}}\cdot\frac{8}{5a^2}\right]. \quad (27)$$

The combination of these three contributions with the curves for ion-core repulsion has a minimum of about 0.89 ev with λ equal to 0.08—exponential repulsion, and a minimum of 1.56 ev with λ equal to 0.025—Fuchs repulsion.

As before the fourteen neighbors, which adjoin only one or the other of the two vacancies, can be treated as though they were simply neighbors of a "D"-type vacancy. This is not strictly true, but a detailed consideration would hardly be consistent with the other approximations involved. The energy of such a neighbor of a "D"-type vacancy has already been treated in the preceding section. All the terms for the saddle-point, which depend upon neighboring ions, are compiled in Table III. The energy for exponential repulsion is given as 1.18; for the Fuchs repulsion, 0.90 ev.

5. Compilation of Terms

From the terms so far considered some idea can be gained of the energy for the E configuration as follows:

$E(\frac{1}{2}a, \frac{1}{2}a, 0)-E(0)$	$1.177\ e^2/a$	
$-\sqrt{2}e^2/a$	$-1.414\ e^2/a$	
$0.6\ e^2/r_s[1-(2)^{-\frac{1}{2}}(0.9)]$	$0.663\ e^2/a$	
Ion-ion electrostatic energy	$0.426\ e^2/a =$	1.698 ev
Kinetic energy term		2.94 ev
Self-energy of charge in electronic distribution		2.84 ev
$\int[\rho_u-\rho_s-(N/V)g_s]V(r)dV$		1.43 ev
Expanded lattice term		−7.34 ev
		1.55 ev

	Exponential		Displaced Fuchs
With the inclusion of neighbor terms	2.73 ev	or	2.45 ev

6. Estimate of an Upper Limit

Because an important potential term has been omitted in obtaining these values for the energy with the two spherical charge holes, the results cannot be considered to represent an upper limit to the activation energy for diffusion. It is possible to estimate the error by the following argument.

The potential term which has been neglected in the preceding treatment would have been unimportant if the shape of the charge distribution had been chosen to minimize its interaction with the hemispheres of high potential. A nonspherical distribution would have also a lower self-energy but its kinetic energy would be increased. One can estimate the increase by this device: Suppose $F(r)$ is a spherically symmetric

wave function for which the associated kinetic energy is known. By a volume-conserving transformation of coordinates one obtains a new wave function $F\{[(x^2/\lambda^2)+\lambda y^2+\lambda z^2]^{\frac{1}{2}}\}$. It can be shown (see Appendix II) that the kinetic energy resulting from the Laplacian of the new function is $\frac{1}{3}(\lambda^{-2}+2\lambda)$ times that of the old. Let the x axis coincide with the direction of the diffusion and set λ equal to the ratio of the radius of the hemisphere to the diameter of the equivalent sphere, namely 0.628. Consequently the kinetic energy associated with the new wave function is higher by 27 percent than that of the spherically symmetric one. This increase, or 0.79 ev for our case, is a measure of the inaccuracy of the two-vacancy procedure. If it is added to the other results, it gives for *upper limits* to the energy of the saddle-point, 3.52 ev on the exponential basis, and 3.24 ev with the displaced Fuchs curve.

The experimental value for the energy of activation for copper is 2.6 ev, as given by Steigman, Shockley, and Nix.[6] This lies in the region where the present results indicate that the energy for configuration E is also located. The approximations throughout have the effect of putting the energy values too high with a probable error of roughly 35 percent. Within such limits the agreement is satisfactory. On the other hand Fuchs made use of a modified free-electron model in his work on copper. His result for the binding energy is less than half the experimental value, as can be seen from Table I′ in the preceding paper. That such a discrepancy has not been encountered here in calculating the activation energy for diffusion indicates that the computed energies for vacancy configurations are not greatly sensitive to the inadequacies of the models assumed for the normal state of the metal.

The ion-core repulsion term is relatively unimportant for the vacancy configurations. It is fortunate that the uncertainty of its behavior did not prevent the determination of the favored mechanism for diffusion. In this regard it may be emphasized that these results definitely complete the case for vacancy diffusion from the theoretical standpoint. It has been shown that the energy of the saddle-point for this process lies below those required in either interstitial or direct-interchange diffusions.

III. EXTENSION TO OTHER METALS

It is natural to inquire to what extent these results for copper may be applied to other metals. It should be pointed out that it is the ion-core repulsion which plays the dominant role in eliminating from consideration the interstitial and direct interchange processes. There is reason to believe that the same forces would be important for metals near copper in the periodic table.

The self-diffusion of zinc, both in single crystals and in polycrystalline specimens, has been studied by Banks and Miller.[7] Their results indicate that diffusion in this substance is strongly anisotropic. From preliminary work they give that the energy of activation is about 0.85 ev along the c axis and about 1.24 ev in the basal plane. It is customary to set the diffusion constant equal to $D_0e^{-Q/RT}$, where Q is the activation energy for diffusion and D_0 is the temperature independent factor. It is also found that the D_0 for the diffusion constant for the basal rate is larger by a factor of about 10^3 than for the corresponding quantity for diffusion along the hexagonal axis.

Because zinc is very far from a free-electron metal, such calculations as we have applied to copper are out of the question here. Nevertheless some qualitative remarks, based on consideration of a simple, central-force law, can be made concerning the relative probabilities that a vacancy is filled by an atom in the same basal plane, or by a neighboring atom in an adjoining plane. For a close-packed hexagonal lattice the atom which makes the jump to fill the vacancy, whether it stays in the same basal plane or not, must pass through an activation point where it is equidistant from four of its neighbors. The shortest distance of approach is $(\sqrt{3}/2)$ times the normal interatomic distance. For such a close-packed lattice one would expect nearly isotropic diffusion. Actually zinc departs from close-packing by a 14 percent elongation along the hexagonal axis. In

[6] J. Steigman, W. Shockley, and F. Nix, Phys. Rev. **56**, 13 (1939).

[7] Floyd R. Banks, Phys. Rev. **59**, 376 (1941); F. R. Banks and P. H. Miller, Phys. Rev. **59**, 943A (1941).

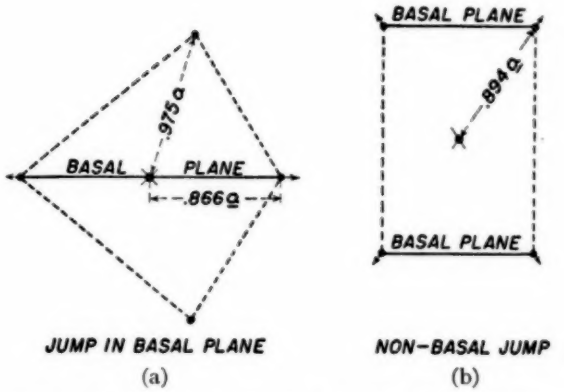

FIG. 5. Positions for diffusing atom in a zinc lattice. ✳ Diffusing atom. ● Neighboring atom. a Normal interatomic distance in the basal plane. In each case there are indicated the positions of the diffusing atom and its four nearest neighbors at the instant when the diffusing atom is halfway between vacancies. The plane section presented is that perpendicular to the path of the jump.

Fig. 5(a) the diffusing atom and its four nearest neighbors are shown in a cross section, perpendicular to the direction of diffusion, at the midpoint of a jump in the basal plane. The corresponding configuration for a jump from one basal plane to another is shown in Fig. 5(b).

If one calculates the activation energy for each case, the results turn out to be sensitive to the type of repulsive law chosen to represent the action of the ion-cores at close distances. For the exponential type, under certain conditions, the basal diffusion has a slightly higher activation energy than the non-basal diffusion. A curve of repulsion like Fuchs' would reverse the situation. Even with the exponential repulsion it seems hardly possible to account for the observed difference in activation energies, but there can be no doubt that such a treatment is far too simplified for the problem. This investigation does, however, throw some light on the reason for the larger D_0 for basal diffusion. In this case only the two neighbors in the same basal plane are near enough to obstruct the diffusing atom. For a jump from one adjoining plane to a vacancy in another, the moving atom is obstructed equally by four neighbors. It is evident that occasions propitious for a *basal* jump occur when *two* neighbors are favorably displaced from their equilibrium positions. On the other hand the *non-basal* jump is a more highly cooperative process since it depends on the favorable displacement of *four* neighboring atoms. One would expect that opportunities for the latter process would occur much more rarely.

To summarize the argument, then, one can remark the following: Self-diffusion rates in zinc appear to be markedly anisotropic. Were zinc strictly close-packed hexagonal, such a behavior would be difficult to explain on any model of diffusion. Taking into account the observed departure from close-packing and a rapidly increasing, close-range repulsive potential, one is able to show that the mechanism of vacancy diffusion predicts qualitatively at least the observed anisotropic behavior of the temperature-independent factor in the expression for the diffusion constant.

For the alkali metals the situation is to some extent reversed, in that they adhere quite closely to the free-electron model in their behavior, which greatly simplifies the theoretical problem. On the other hand no experiments have been performed to measure self-diffusion and there is little prospect that such experiments can be devised for some time to come.

When the results of the copper calculation are extrapolated to the alkalis with their larger lattice constants, the various kinetic and potential terms are decreased in size accordingly as their dependence on r_s indicates. The energy for the "extended lattice" can be taken from the analytic expression derived from free-electron consideration, or still better, from the sum of the ionization potential and heat of sublimation minus the work function, since Wigner and Bardeen[8] have shown that the two agree closely. The repulsions of the ion-cores can be treated with some assurance since the Born-Mayer formula has been well tested for its validity in dealing with these elements. The energies are, however, much smaller, of the order of 0.1 ev for an interstitial position, as contrasted to 6 ev for copper. In this way one can obtain crude values for the energies needed to form an interstitial atom, or a vacancy. Two clear deductions can be made. First, these energies range around one or two ev. Second, the interstitial and vacancy mechanisms are in much closer competition for the alkali metals than for copper, because here

[8] E. P. Wigner and J. Bardeen, Phys. Rev. **48**, 84 (1935), see Fig. 1.

the ion-core repulsion is nearly negligible. A more detailed attack, perhaps along the lines of the foregoing self-consistent solution, is required, before one can state with definiteness which is the important mechanism for diffusion in the case of any given alkali.

The author wishes to express his very sincere thanks to Professor Frederick Seitz for suggesting this problem to him and for his many helpful suggestions and criticisms in the course of its development.

APPENDIX I. ESTIMATE OF THE SELF-ENERGY OF A HEMISPHERE

An estimate for the self-energy of a uniformly charged hemisphere was obtained by the two following simple lines of investigation. In each case it turned out to be about ten percent lower than the self-energy of the sphere with the same charge density and total charge.

Along the axis of the hemisphere the potential can be found directly by a simple integration in polar coordinates. For that part of the axis which lies inside the hemisphere the potential is given by

$$P_i(\alpha)=\frac{e}{2r_s}\left\{\frac{3}{2}+\frac{(1+\alpha^2)^{\frac{1}{2}}-1}{\alpha}-2\alpha^2\right\}, \tag{28}$$

where $\frac{1}{2}e$ is the total charge, r_s is the radius of the hemisphere and α is the ratio R/r_s. The distance between the field point and the center of the polar system of coordinates is measured by R, with the positive direction on the same side as the hemisphere. This potential has a maximum near the centroid of the hemisphere at $\alpha=\frac{3}{8}$. On substitution one gets $P(\frac{3}{8})=1.795$ in $e/2r_s$. The potential at the center of the equivalent sphere is $1.5e(2)^{\frac{1}{2}}/2r_s$, or 1.892 in $e/2r_s$. This shows that the potential plateau is five percent lower for the hemisphere than for the sphere. We may assume that the self-energy of the two bodies will differ by twice as much, or ten percent.

A more convincing line of argument is to consider a complete sphere sliced into two hemispheres. Since the self-energy of the sphere is known, the problem reduces to finding the potential interaction of one hemisphere with the other. We approximate this by the potential of one hemisphere at the centroid of the other. Along the negative direction of the axis of the hemisphere we have

$$P_-(\alpha)=\frac{e}{2r_s}\left\{\frac{3}{2}-\frac{(1+\alpha^2)^{\frac{1}{2}}-1}{\alpha}+\alpha^2\right\}. \tag{29}$$

Since $P_-(\frac{3}{8})=1.067\,e/2r_s$, the interaction of the hemispheres is approximated by $0.267\,e^2/r_s$. The self-energy for the sphere is $0.6\,e^2/r_s$, and there is left then for each hemisphere $0.167\,e^2/r_s$. For the equivalent sphere the self-energy is $0.6\,e^2(2)^{\frac{1}{2}}/4r_s$, or $0.189\,e^2/r_s$. The value for the hemisphere is about 12 percent below the corresponding self-energy for the sphere.

APPENDIX II. KINETIC ENERGY OF A SPHEROIDAL DISTRIBUTION

The kinetic energy associated with a wave function possessing spherical symmetry, say $F(r)$, is proportional to the integral,

$$\int F(r)\nabla^2F(r)\,dV=\int F(r)\left[F''(r)+\frac{2}{r}F'(r)\right]dV. \tag{30}$$

If a new wave function is obtained by a volume-conserving transformation, the normalization will be unaltered. The Laplacian of $F([x^2/\lambda^2+\lambda y^2+\lambda z^2]^{\frac{1}{2}})$ is, when developed in Cartesian coordinates,

$$\left[\left(\frac{x}{\lambda^2\rho}\right)^2+\frac{\lambda^2}{\rho^2}(y^2+z^2)\right]F''(\rho)+\left[\left(\frac{1}{\lambda^2}+2\lambda\right)-\frac{1}{\rho^2}\left\{\left(\frac{x}{\lambda^2}\right)^2+\lambda^2y^2+\lambda^2z^2\right\}\right]\frac{F'(\rho)}{\rho}, \tag{31}$$

where ρ has been written for the argument of F. If this expression is substituted in (30) and the inverse transformation, $x=\lambda\bar{x}$, $y=\lambda^{-\frac{1}{2}}\bar{y}$, $z=\lambda^{-\frac{1}{2}}\bar{z}$, and $\rho=\bar{r}$, is employed, then the integral becomes

$$\int F(\bar{r})\left[\frac{F''(\bar{r})}{(\bar{r})^2}\left\{\left(\frac{\bar{x}}{\lambda}\right)^2+\lambda(\bar{y}^2+\bar{z}^2)\right\}+\frac{F'(\bar{r})}{\bar{r}}\left\{\frac{1}{\lambda^2}+2\lambda-\frac{1}{\bar{r}^2}\left(\frac{\bar{x}^2}{\lambda^2}+\lambda\bar{y}^2+\lambda\bar{z}^2\right)\right\}\right]dV. \tag{32}$$

The form of the integration is unaltered, because the transformation has left the size of the volume element unchanged and because the limits extend to infinity. If one now averages over angle, replacing $\bar{x}^2/\bar{r}^2$, etc. by $\frac{1}{3}$, the resulting expression is $\frac{1}{3}[(1/\lambda^2)+2\lambda]$ times the kinetic energy expression associated with the original, spherically symmetric wave function.

Electron Emission of Metals in Electric Fields

III. The Transition from Thermionic to Cold Emission*

EUGENE GUTH AND CHARLES J. MULLIN†
University of Notre Dame, Notre Dame, Indiana

(Received October 14, 1941)

The theory of Schottky emission is extended to include in the current those electrons which tunnel through the top of the potential barrier at the metal surface when rather strong electric fields are used. It is found that these tunnelling electrons contribute to the periodic deviations from the Schottky line, increasing the amplitude of the deviations. This increase leads to a better agreement with experiment, especially for large fields. This agreement requires that the Nottingham reflection coefficient be very small for fields greater than 10^4 volts per cm. Expressions are developed for the electron current emitted by a metal for various field intensities ranging from the small fields of thermionic work to the large fields used in cold emission. Results are obtained to indicate the temperature and field dependence of the electron current for all fields and temperatures of interest. Of particular interest is the expression developed for the current in the "transition region," i.e., $T\sim 500$–$1200°$K and $F\sim 10^7$–10^8 volts per cm. The modifications which must be made in the theory to take account of the polycrystalline nature of the emitting surface have no effect on the periodic deviations from the Schottky line, and very little effect on the fluctuations observed in field photo-currents.

I. INTRODUCTION

IT is possible to obtain electron currents emitted from metals under widely varying experimental conditions. For example: the electrons may be ejected from a hot cathode and collected by fields with a rather wide range of intensities; or the electrons may be pulled from a cold cathode by the application of very intense electric fields. Despite the different experimental conditions employed in these cases, a single general expression which is valid (under the usual assumptions of the free electron theory of metals) for all electron energies, fields, and temperatures may be given:

$$i=\int_0^\infty N(W)D(W,F)dW, \qquad (1)$$

where W is the energy which the electron has in the velocity component normal to the emitting surface, $N(W)$ is the number of electrons in the metal with this energy which strike unit area per second, and $D(W, F)$ is the probability that one of these electrons will escape through the metal surface under the influence of the applied field, F. Unfortunately, an evaluation of (1) valid for all energies cannot be given in an analytical form; however, some special cases of interest and importance can be fully treated. The familiar work on thermionic and Schottky emission has given a theory which holds for high temperatures and low fields [high values of W in Eq. (1)], and the well-known papers of Fowler and Nordheim[1] and of Nordheim[2] treat the case of very low temperatures and high fields [lower values of W in Eq. (1)]. In the present work an attempt is made to extend these theories and to bridge the gap between the two theories. In line with this,

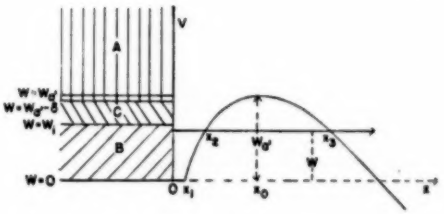

FIG. 1. Energy diagram for electrons in and out of the metal. W_a' is the total height of the barrier at the metal surface. Electrons from region A contribute to Schottky emission, those from region B to cold emission. x_2 and x_3 are the points at which $\phi=W-V=0$.

* This work is a section of a dissertation presented to the Faculty of the Graduate School of the University of Notre Dame, 1942, in partial fulfillment of the requirements for the degree of Doctor of Philosophy.

† Now at St. Louis University, St. Louis, Missouri.

[1] R. H. Fowler and L. W. Nordheim, Proc. Roy. Soc. **119**, 173 (1928).

[2] L. W. Nordheim, Proc. Roy. Soc. **121**, 626 (1928).

the recent theory[3] of the periodic deviations from the Schottky line is also extended to include the effect of the electrons which penetrate the top of the potential barrier at the metal surface (Fig. 1); this penetration effect is found to increase the amplitude of the deviations so as to improve somewhat the agreement between theory and experiment at the higher field intensities used. It is found that the improved agreement between the theoretical and experimental deviations requires that the reflection coefficient proposed by Nottingham[4] decrease with the applied field in such a way as to become nearly zero for fields of the intensities used to obtain the periodic deviations. An interesting result is also found for the current emitted when rather high fields and intermediate temperatures are used. In Part II of the present paper, the results which can be obtained from Eq. (1) for the case of an ideal surface with a single "effective" work function, or for a single crystal face, are discussed; in Part III the effects of the polycrystalline nature of the emitting surface on these results are considered; and in Part IV a brief derivation for the currents obtained under the various conditions discussed in II is given.

II. DISCUSSION OF THE RESULTS FOR AN IDEAL "SINGLE WORK FUNCTION SURFACE" OR FOR A SINGLE CRYSTAL

In order to evaluate (1) it is convenient to split the integral up into parts corresponding to various ranges of the energy W. If only values of W greater than W_a' (Fig. 1) are considered, that is, if the field applied is not strong enough to cause an appreciable number of electrons with energies below W_a' to be emitted, Eq. (1) leads to an expression for thermionic or Schottky emission; if only values of W less than W_i are considered, that is, if the filament temperature is so low that only a negligible number of electrons have energies greater than W_i, Eq. (1) leads to an expression for cold emission. For values of W ranging from W_i up to W_a', the current gradually takes on a stronger temperature dependence and weaker field dependence, passing from cold emission to thermionic emission; however, an analytical expression for the current valid in the entire region $W_i \leq W \leq W_a'$ has not yet been given. In the following work some limiting cases are treated.

(a) Low Fields, High Temperatures

In this case only electrons with energies above a certain value $W_a' - \delta$ contribute to the current, the others being reflected back into the metal when they strike the surface; the contributing electrons are those from region A in Fig. 1. The current from this region is

$$i = B(kT)^2 e^{-\chi'/kT}\left\{\sum_{n=0}^{\infty}(-1)^n \frac{(2n+1)\mu}{n(n+1)\mu^2+\mu-1} - \frac{W_a^{\frac{1}{2}}}{2kT}\left(1-\frac{1}{4x_0^2}W_a^2\right)\left[\frac{\cos v_a}{\{[\pi\alpha+(1/kT)]^2+\beta^2\alpha^2\}^{\frac{1}{2}}} + \frac{\cos v_b}{\{[2\pi\alpha-(1/kT)]^2+\beta^2\alpha^2\}^{\frac{1}{2}}}\right]\right\}, \quad (2)$$

where atomic units of length ($a=\hbar^2/me^2=0.527$A) and energy (unit $=e^2/2a=13.67$ ev) are used, and $\alpha=(\frac{1}{2}x_0^3)^{\frac{1}{2}}$; $\mu=2\pi\alpha kT$; $x_0=$char. Schottky distance (Fig. 1): $x_0=[(300e)^{\frac{1}{2}}/(2\times 0.527)](10^8/F^{\frac{1}{2}})$; $F=$volts/cm; $\chi=$work function for zero field, χ' for field F: $\chi'=\chi-(1/x_0)$; $W_a'=W_i+\chi'$; $\beta=\gamma+2\ln 2$; $\gamma=$Euler's const. $=0.5772$; $B=160\pi^6 m^3 e^9/ch^7$

$$v_a=\frac{4\sqrt{2}}{3}x_0^{\frac{1}{2}}-\frac{2}{W_a^{\frac{1}{2}}}+\tan^{-1}\frac{W_a^{\frac{1}{2}}}{4}-\tan^{-1}\frac{\beta\alpha}{\pi\alpha+(1/kT)},$$

$$v_b=\frac{4\sqrt{2}}{3}x_0^{\frac{1}{2}}-\frac{2}{W_a^{\frac{1}{2}}}+\tan^{-1}\frac{W_a^{\frac{1}{2}}}{4}+\tan^{-1}\frac{\beta\alpha}{\pi\alpha-(1/kT)}.$$

If the relatively small periodic term is neglected

$$i = B(kT)^2 e^{-\chi'/kT}\sum_{n=0}^{\infty}(-1)^n\frac{(2n+1)\mu}{n(n+1)\mu^2+\mu-1}. \quad (3)$$

If only the first term of the summation is taken, this result reduces to one obtained by Bethe[5]

$$i = B\frac{\mu}{\mu-1}(kT)^2 e^{-\chi'/kT}. \quad (4)$$

If $\mu \gg 1$, which means that high temperatures and

[3] E. Guth and C. J. Mullin, Phys. Rev. **59**, 575 (1941).
[4] W. B. Nottingham, Phys. Rev. **49**, 78 (1936).
[5] A. Sommerfeld and H. Bethe, *Handbuch der Physik* (1933), Vol. 24/2, p. 442.

low fields are employed, Eqs. (3) and (4) reduce to the familiar equation for Schottky emission, in which the mean transmission coefficient $\bar{D}\sim 1$,

$$i = B(kT)^2 e^{-\chi'/kT}. \tag{5}$$

It is seen that (5) and (3) differ in that (5) effectively considers only those electrons which have energies greater than W_a', i.e., which surmount the potential barrier of Fig. 1, while (3) also takes account of those electrons which tunnel through the barrier in the region $W_a' - \delta \leq W \leq W_a'$. This tunnelling occurs even for rather weak fields because even then the transmission coefficient is not zero at the top of the barrier of Fig. 1. A comparison of Eq. (2) with the equation obtained for the current by neglecting the tunnel effect shows that the second periodic term ($\cos v_b$) of (2) arises from the electrons penetrating the potential barrier at the metal surface. An interesting fact about the periodic term in (2) is that it becomes small both for low and high fields; for sufficiently high fields $x_0 \to x_1 \sim 1/2W_a$, so that the coefficient $(1-1/4x_0^2W_a^2)$ becomes smaller as the field becomes very high. The contribution of the second periodic term due to the tunnel effect gives a better agreement between the theoretical and experimental[6-8] amplitudes of the deviations at the high end of the field range used.

With all electrons accounted for in Eq. (2), the periodic deviations have an amplitude in good agreement with observation. This agreement affords a good opportunity to observe whether or not the electrons reaching the metal surface are suffering, at these rather high field intensities, a reflection of the type suggested by Nottingham.[4] In order to explain the non-Maxwellian distribution of the slow electrons in thermionic emission, Nottingham proposed that the electrons suffered a reflection

$$R_N = e^{-(W-W_a')/\omega}, \quad \omega \sim 0.2 \text{ ev}. \tag{6}$$

However, as Dr. Nottingham pointed out to the authors, the velocity distribution experiments require only that $\omega \sim 0.2$ ev for the very low fields used in those experiments. A transmission coefficient which meets the conditions imposed by R_N and at the same time introduces some of the influence of the barrier of Fig. 1 is given by

$$D = D_c(1 - R_N), \tag{7}$$

where D_c is the transmission coefficient for the barrier of Fig. 1. With this transmission, the current from the region A becomes

$$i = B(kT)^2 e^{-\chi'/kT}\left\{\sum_{n=0}^{\infty}(-1)^n\left(\frac{1}{n\mu+1}-\frac{1}{n\mu+1+(kT/\omega)}\right)\right.$$
$$\left.-\frac{W_a^{\frac{1}{2}}}{2kT}\left(1-\frac{1}{4x_0^2W_a^2}\right)\left[\frac{\cos u_1}{\{[\pi\alpha+(1/kT)]^2+\beta^2\alpha^2\}^{\frac{1}{2}}}-\frac{\cos u_2}{\{[2\pi\alpha+(1/kT)+(1/\omega)]^2+\beta^2\alpha^2\}^{\frac{1}{2}}}\right]\right\}, \tag{8}$$

where

$$u_1 = \frac{4\sqrt{2}}{3}x_0^{\frac{3}{2}} - \frac{2}{W_a^{\frac{1}{2}}} + \tan^{-1}\frac{W_a^{\frac{1}{2}}}{4} - \tan^{-1}\frac{\beta\alpha}{\pi\alpha+(1/kT)},$$

$$u_2 = \frac{4\sqrt{2}}{3}x_0^{\frac{3}{2}} - \frac{2}{W_a^{\frac{1}{2}}} + \tan^{-1}\frac{W_a^{\frac{1}{2}}}{4} - \tan^{-1}\frac{\beta\alpha}{\pi\alpha+(1/kT)+(1/\omega)}.$$

To keep the amplitude of the deviations appreciable would require that

$$\pi\alpha \sim 1/\omega, \text{ or } \omega \sim 1/2000 \text{ atomic units}, \omega \sim 1/200 \text{ ev}.$$

Thus, ω must depend upon the field in such a way that $\omega \sim 0.2$ ev when $F \sim 0$, and $\omega \to 0$ as F takes on the rather large values needed to obtain the periodic deviations. Practically, Eq. (8) shows that the Nottingham reflection does not operate at these relatively high fields. A discussion of the Nottingham reflection *versus* the theory of emission from "patches" is given by Nichols.[9]

[6] R. L. E. Seifert and T. E. Phipps, Phys. Rev. **56**, 652 (1939).
[7] D. Turnbull and T. E. Phipps, Phys. Rev. **56**, 663 (1939).
[8] W. B. Nottingham, Phys. Rev. **57**, 935 (1940).
[9] M. H. Nichols, to be submitted for publication.

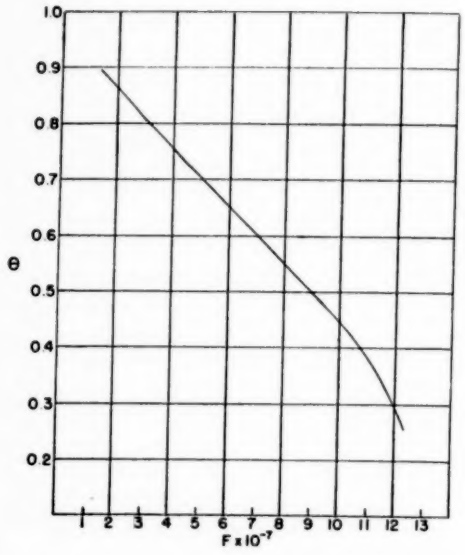

FIG. 2. The Nordheim function θ plotted against the accelerating field F.

It may be noted that the value $\omega=0.2$ ev leads to a mean transmission coefficient $\bar{D}=\frac{1}{3}$, while the value $\omega\sim 1/200$ ev leads to a $\bar{D}\sim 0.95$.

In the case of photoelectric emission under the influence of fields high enough to cause penetration of the topmost part of the barrier, the penetrating current plays a much less important role than in the above cited case of Schottky emission; the reason for this is immediately clear: In the photoelectric case the transmission decreases exponentially as the electron energy decreases from W_a', but the number of electrons available remains almost constant (since these electrons have energies less than W_i); hence, the current, which again depends upon the product $D(W, F)N(W)$, decreases very rapidly as W becomes progressively less than W_a'; this quick decrease makes the contribution to both nonperiodic and periodic parts of the current unimportant.

(b) High Fields, Low Temperatures

At low temperatures there are very few electrons with energy greater than W_i. However, with sufficiently high values of the applied field, electrons with energies less than W_i are pulled from the metal. The electrons contributing to this cold emission are from the region B of Fig. 1, most of them coming from the uppermost part of region B, since the transmission coefficient for this region decreases exponentially with decreasing energy. The current from this region is then,

$$i=B\exp\left[-\frac{8x_0^2}{3}\theta\chi^{\frac{1}{2}}\right]\left\{\frac{1}{16\theta^2x_0^4\chi}+\sum_{n=1}^{\infty}\frac{(-1)^{n+1}}{n}\frac{(kT)^2}{(n+4x_0^2\theta\chi^{\frac{1}{2}}kT}\right\} \quad (9)$$

or, if we express χ in electron volts and F in volts per cm,

$$i=\left\{1.55\times10^{-6}\frac{F^2}{\theta^2\chi}+120.5T^2\sum_{n=1}^{\infty}\frac{(-1)^{n+1}}{n}\times\frac{1}{n+8.81\times10^{+3}\theta\chi^{\frac{1}{2}}T/F}\right\}\cdot\exp\left(-6.838\times10^7\theta\chi^{\frac{3}{2}}/F\right)\text{ amp./cm}^2 \quad (10)$$

where θ is a slowly varying function[10] of F which varies from 1 to 0 as F varies from 0 to ∞. θ is plotted as a function of F in Fig. 2. If the summation term is neglected completely (This corresponds to taking only the first term in the expansion of the Fermi distribution function, a valid approximation for low temperatures), Eq. (10) reduces to

$$i=1.55\times10^{-6}\frac{F^2}{\theta^2\chi}\cdot\exp\left(-6.838\times10^7\theta\chi^{\frac{3}{2}}/F\right)\text{ amp cm}^2. \quad (11)$$

This formula has been recently checked experimentally by Haefer.[11] By taking the sum into consideration one obtains the temperature dependence of the current from region B of Fig. (1);

[10] This function was introduced by L. W. Nordheim, reference 1, to determine the effect of the image force on cold emission.

[11] R. Haefer, Zeits. f. Physik **116**, 604 (1940). This author determined the actual field strength acting on the point of the field emitting metal by obtaining the curvature of the point from electron microscope investigations. He found that field emission sets in at about 3×10^7 volts per cm as required by Eq. (11). Thus no "sensitive spots" need be introduced in order to explain the difference between the empirical and theoretical thresholds. Haefer accurately verified the dependence of the current on $\chi^{\frac{3}{2}}$ as given by (11).

if T is small so that $8.81\times10^{3}\chi^{\frac{1}{2}}VT/F\ll1$, Eq. (10) gives for the temperature dependence

$$\frac{i(T)}{i(0)}=1+7.77\times10^{7}\Theta^{2}\frac{\chi T^{2}}{F^{2}}\sum_{n=1}^{\infty}\frac{(-1)^{n+1}}{n^{2}}. \quad (12)$$

The first term of the series in Eq. (12) has been given by Bethe[12] who points out that this result is in agreement with the experimental data of Millikan and Eyring.[13] The temperature dependence is of the same type as that obtained for photo-emission for the simple reason that the electrons in each of these cases originate in the same region B.

For low temperatures the T^{2} term in (10) is unimportant, but it may become appreciable for higher temperatures; in any case, it seems that the inclusion of the temperature term in (10) is inconsistent unless this term is modified to include the contribution of those electrons which, because of the temperature dependence of the Fermi distribution function, have energies greater than W_i. However, field emission for which the temperature term is large (say for $T=800$–$1000°$K, $F=2-4\times10^{7}$ volts/cm) is not strictly cold emission, but rather may be classed as a transition case between cold and thermionic emission. The current obtained under these "transition conditions" is discussed in Section (c).

(c) Intermediate Fields and Temperatures

In this case the emission from region C of Fig. 1 must be considered. The current from this region should depend upon both the temperature and the field. An expression valid for all of region C is not easily obtained, but the contributions from the upper and lower parts may be given. A particularly important case involving the current from this region has been mentioned in the previous section. If the temperature and field are such that

$$4x_0^{2}\chi^{\frac{1}{2}}\Theta kT<1 \text{ (atomic units)},$$

i.e.,

$$8.813\times10^{3}\Theta\chi^{\frac{1}{2}}T/F<1 \text{ (ev and volt/cm)} \quad (13)$$

the current from region C is

$$i=Bk^{2}T^{2}\exp\left[-\frac{8x_0^{2}}{3}\Theta\chi^{\frac{1}{2}}\right]\sum_{n=1}^{\infty}\frac{(-1)^{n+1}}{n}\frac{1}{n-4x_0^{2}\Theta\chi^{\frac{1}{2}}kT}. \quad (14)$$

By adding this current to that from the region B, the total current for the fields and temperatures subject to the condition (12) is obtained

$$i=B\exp\left[-\frac{8x_0^{2}}{3}\Theta\chi^{\frac{1}{2}}\right]\left\{\frac{1}{16\Theta^{2}x_0^{4}\chi}+k^{2}T^{2}\sum\frac{(-1)^{n+1}}{n}\times\left(\frac{1}{n+4x_0^{2}\Theta\chi^{\frac{1}{2}}kT}+\frac{1}{n-4x_0^{2}\Theta\chi^{\frac{1}{2}}kT}\right)\right\}, \quad (15)$$

or, putting χ in ev and F in volt/cm

$$i=\left\{1.55\times10^{-6}\frac{F^{2}}{\Theta^{2}\chi}+120.5T^{2}\sum_{n=1}^{\infty}\frac{(-1)^{n+1}}{n}\times\left(\frac{1}{n+8.813\times10^{3}\Theta\chi^{\frac{1}{2}}T/F}+\frac{1}{n-8.813\times10^{3}\Theta\chi^{\frac{1}{2}}T/F}\right)\right\}\times\exp\left[-6.838\times10^{7}\Theta\chi^{\frac{3}{2}}/F\right]\text{amp/cm}^{2}. \quad (16)$$

Experimentally it should be possible to make a thorough study of currents under these "transition conditions." If $T=1000°$K, say, then by choosing $\chi=4.531$ ev (the value for tungsten) (16) is valid if $F\geqslant1.8\times10^{7}$ volts/cm. A plot of

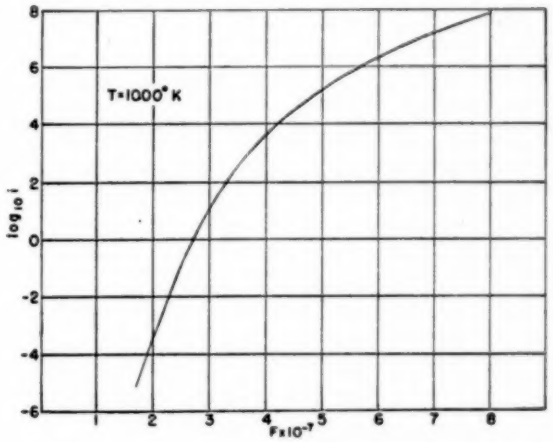

FIG. 3. A plot of the current given by Eq. (16).

[12] A. Sommerfeld and H. Bethe, *Handbuch der Physik* (1933), Vol. 24/2, p. 442.
[13] R. A. Millikan and C. F. Eyring, Phys. Rev. **27**, 51 (1926).

the current obtained from (16) is given in Fig. 3. It may be noted that for fields near the threshold for emission, Eq. (16) gives a current many times that expected from the simpler Nordheim expression given in Eq. (11). In particular, if $T=1000°\text{K}$ and $F=2\times10^7$ volt/cm, (16) gives a current about five times as large as that obtained from (11). If $F=3\times10^7$, (16) yields a value about 1.7 times as large as that given by (11). The larger current is due chiefly to those electrons coming from region C.

The expression (14) for the current from the lower part of C shows, as was expected, a larger temperature dependence and a smaller field dependence than was had for cold emission.

Photoelectric emission could be obtained from the region C by applying fields high enough to make the electrons struck with low frequency photons tunnel the barrier in the region adjacent to C. The photo-current from this region is

$$i=\exp\left[-6.838\times10^7\Theta(\chi-h\nu)^{\frac{1}{2}}/F\right]\left\{1.55\times10^{-6}\frac{F^2}{\Theta^2(\chi-h\nu)}+\sum_{n=1}^{\infty}\frac{(-1)^{n+1}}{n}\times\frac{k^2T^2}{n+8.81\times10^3\Theta(\chi-h\nu)^{\frac{1}{2}}T/F}\right\}. \quad (17)$$

This current is very similar to that for cold emission as given by Eq. (9). However, the photons have the effect of reducing the work function by an amount $h\nu$, so that really the electrons from region B are effectively raised to region C and tunnel through the barrier from this region.

III. THE EFFECT OF PATCHES ON THE EMISSION[14]

In all the above work the electrons are assumed to be emitted from a surface with one uniform "effective" work function. If, instead, the current is assumed to come from a number of crystal faces (hereafter called patches) with different work functions, the previous expressions for the current must be modified. If the applied fields used are high ($x_0\ll$patch diameter ~100A) as is generally true above, each patch may be assumed to emit independently, so that the resulting current is

$$i=\sum f_n i_n, \quad (18)$$

where i_n is the current from the nth crystal face, and f_n is the fractional area of this patch.

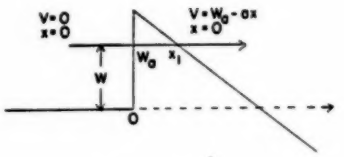

FIG. 4. The potential barrier at the metal surface if the image force is neglected.

(a) Thermionic Emission

If it is assumed that a certain number p of patches have work functions very nearly equal, the work function of the group being called χ, and if q patches have a work function $\chi+\delta$, the current from the first group is

$$i_1=\sum_{n=1}^{p} f_n i_n=\sum_{n=1}^{p} f_n A_0\bar{D}T^2e^{-(\chi-\Delta\chi)/kT} \quad (19)$$

and from the second

$$i_2=\sum_{n=1}^{q} f_n i_n=e^{-\delta/kT}\sum_{n=1}^{q} f_n A_0\bar{D}T^2e^{-(\chi-\Delta\chi)/kT}. \quad (20)$$

If $\delta>kT$, $i_2\ll i_1$ so that the principal contribution to the current comes from the patches of lowest work function. In this case the "ideal surface" emission constant $+A_0$ must be replaced by

$$A_0\sum_{n=1}^{p} f_n$$

which is always less or equal to A_0, the equality holding only if the entire surface has the same work function. For fields high enough that the patches emit independently, the Schottky line is the same as for an ideal surface, i.e.,

$$\ln i(F)-\ln i(0)\sim-\Delta\chi/kT=e^{\frac{3}{2}}F^{\frac{1}{2}}/kT. \quad (21)$$

If the various groups of crystal faces have work functions which differ by an amount $\delta>kT$, the current comes almost exclusively from the facets of lowest χ, and the periodic deviations found in Part II are unaffected. However, if there exists a δ for which the condition $\delta>kT$ is not fulfilled,

[14] For a complete discussion of the theory of patch emission see M. H. Nichols, reference 9; cf. also C. Herring, Phys. Rev. **59**, 889 (1941). We are indebted to Drs. Herring and Nichols for letting us have the manuscripts of their papers before publication.

then a current contribution from the corresponding group of patches must be considered. However, a δ this small would not affect the periodic deviations of Part II (which depend upon W_a), since their dependence upon χ is a rather insensitive one, and the only effect of this patch group is to increase the current. Thus, it is seen that the periodic deviations are never destroyed by "interference" between the emissions of different patches.

The arguments applied above about the effect of patches on thermionic emission may be applied also to cold emission (here there is no periodic term, of course) which, according to Eq. (9) depends exponentially upon $\chi^{\frac{1}{2}}$.

(b) Photoelectric Emission

In the case of photoelectric emission with rather high fields, neglecting the small periodic term we have

$$i_n \sim Bk^2T^2\left[\frac{\pi^2}{6}+\frac{1}{2}\delta^2-\sum_{n=1}^{\infty}\frac{(-1)^{n+1}}{n^2}e^{-n\delta}\right], \quad (22)$$

if

$$\delta=\frac{h\nu-\chi+\Delta\chi}{kT}>0,$$

or

$$i_n \sim Bk^2T^2\sum_{n=1}^{\infty}\frac{(-1)^{n+1}}{n^2}e^{n\delta} \quad \text{if } \delta<0.$$

It is seen that in this case the current does not fall off exponentially with increasing work function. Again suppose the two groups of patches with work functions χ and $\chi+\delta$ as above. Here it is possible to let δ have an appreciable value and yet to obtain an appreciable current contribution from the patches of work function $\chi+\delta$. Since the phase and amplitude of the periodic deviations found in the photo-current[15] emitted by a metal are dependent somewhat upon the work function of the metal, it is possible that the interference of the several currents from the crystal faces of different work functions might give deviations somewhat different in character from those calculated for an "ideal," single work function emitting surface. However, this interference effect must be small, for in order that two currents from patches with different work functions may have a large interference effect in their periodic terms, the two patches must have a rather large difference in their work functions; but a large difference in work function means that one current is small in comparison with the other, so that the interference effect will be small. This holds in spite of the fact, already pointed out by Nichols, that the Fowler plots are modified by patches. In the case of the Fowler plot a change of the work function by δ is of importance, while the periodic deviations, depending on $W_a(\sim 10$ ev) are rather insensitive to changes in χ of a few percent.

IV. DERIVATION OF THE RESULTS

(a) Low Fields, High Temperatures

In this case Eq. (1) is evaluated, (a) for $W_a' \leq W \leq \infty$, and (b) for $W_a'-\delta \leq W \leq W_a'$; these two contributions are then added to give the total current from region A.

(a) $W_a' \leq W \leq \infty$.

For this case the transmission coefficient and energy distribution are given by[16]

$$D(F,W)=\frac{1}{1+\exp\left[-2\pi\alpha(W-W_a')\right]}-\frac{W_a^{\frac{1}{2}}}{2}\left(1-\frac{1}{4x_0^2W_a^2}\right)\frac{\exp\left[-\pi\alpha(W-W_a')\right]\cos u_a}{\{1+\exp\left[-2\pi\alpha(W-W_a')\right]\}^{\frac{1}{2}}}, \quad (23)$$

$$u_a=\frac{4\sqrt{2}}{3}x_0^{\frac{1}{2}}-\frac{2}{W_a^{\frac{1}{2}}}+\tan^{-1}\frac{W_a^{\frac{1}{2}}}{4}-\beta\alpha(W-W_a')$$

$$N(W) \sim BkT\exp\left[-(W-W_i)/kT\right], \quad (24)$$

[15] E. Guth and C. J. Mullin, Phys. Rev. **59**, 867 (1941).

[16] For these results and the calculation of the corresponding current cf. E. Guth and C. J. Mullin, Phys. Rev. **59**, 575 (1941). The transmission coefficient given here is obtained by use of the W.K.B. solution to the wave equation.

$$i=\int_{W_a}^{\infty} D(F, W)N(W)dW=\int_0^{\infty} D(F, \epsilon)N(\epsilon)d\epsilon,$$

$$\epsilon=W-W'_a=W-W_a+1/x_0,$$

$$i=Bk^2T^2\exp(-\chi'/kT)\left\{\sum_{n=0}^{\infty}(-1)^n\frac{1}{2n\pi\alpha kT+1}-\frac{W_a^{\frac{1}{2}}}{2kT}\frac{[1-(1/4x_0^2W_a^2)]\cos v_a}{\{[\pi\alpha+(1/kT)]^2+\beta^2\alpha^2\}^{\frac{1}{2}}}\right\}, \tag{25}$$

$$v_a=\frac{4\sqrt{2}}{3}x_0^{\frac{1}{2}}-\frac{2}{W_a^{\frac{1}{2}}}+\tan^{-1}\frac{W_a^{\frac{1}{2}}}{4}-\tan^{-1}\frac{\beta\alpha}{\pi\alpha+(1/kT)}.$$

(b) $W_a'-\delta\leq W\leq W_a'$.

The fields in this region are presumed to be such that the electrons penetrate only the topmost part of the barrier of Fig. 1. Then proceeding as in (a)

$$D(F, W)=\frac{\exp[-2\pi\alpha(W_a'-W)]}{1+\exp[-2\pi\alpha(W_a'-W)]}-\frac{W_a^{\frac{1}{2}}}{2}\frac{[1-(1/4x_0^2W_a^2)]\exp[2\pi\alpha(W_a'-W)]}{\{1+\exp[-2\pi\alpha(W_a'-W)\}^{\frac{1}{2}}}\cos u_b, \tag{26}$$

$$u_b=\frac{4\sqrt{2}}{3}x_0^{\frac{1}{2}}-\frac{2}{W_a^{\frac{1}{2}}}+\tan^{-1}\frac{W_a^{\frac{1}{2}}}{4}+\beta\alpha(W_a'-W),$$

$$N(W)\sim BkTe^{-(W-W_i)/kT}, \tag{27}$$

$$i=\int_{W_a'-\delta}^{W_a'}N(W)D(W, F)dW=\int_0^{\infty}N(y)D(y, F)dy,$$

$$y=W_a'-W=W_a-W-1/x_0,$$

$$i=Bk^2T^2e^{-\chi'/kT}\left\{\sum_{n=0}^{\infty}(-1)^n\frac{1}{2(n+1)\pi\alpha kT-1}-\frac{W_a^{\frac{1}{2}}}{2kT}\frac{(1-1/4x_0^2W_a^2)}{\{[2\pi\alpha-(1/kT)]^2+\beta^2\alpha^2\}^{\frac{1}{2}}}\cos v_b\right., \tag{28}$$

$$v_b=\frac{4\sqrt{2}}{3}x_0^{\frac{1}{2}}-\frac{2}{W_a^{\frac{1}{2}}}+\tan^{-1}\frac{W_a^{\frac{1}{2}}}{4}+\tan^{-1}\frac{\beta\alpha}{2\pi\alpha-(1/kT)}.$$

The region of integration is taken as $0\leq y\leq\infty$ since it is assumed that the integral vanished at the upper limit. Actually, the integration range should be $0\leq y\leq\delta$ corresponding to $W_a'-\delta\leq W\leq W_a'$.

Adding the results of (a) and (b) gives for the current from the region A

$$i=Bk^2T^2e^{-\chi'/kT}\left\{\sum_{n=0}^{\infty}(-1)^n\frac{(2n+1)\mu}{n(n+1)\mu^2+\mu-1}\right.$$

$$\left.-\frac{W_a^{\frac{1}{2}}}{2kT}\left(1-\frac{1}{4x_0^2}W_a^2\right)\left[\frac{\cos v_a}{\{[\pi\alpha+(1/kT)]^2+\beta^2\alpha^2\}^{\frac{1}{2}}}+\frac{\cos v_b}{\{[2\pi\alpha-(1/kT)]^2+\beta^2\alpha^2\}^{\frac{1}{2}}}\right]\right\}. \tag{29}$$

If the transmission coefficient given by Eq. (7) is used and only electrons for which $W\geqslant W_a'$ are counted

$$i=BkTe^{-\chi'/kT}\int_0^{\infty}D_c(1-e^{-\epsilon/\omega})e^{-\epsilon/kT}d\epsilon$$

$$=BkTe^{-\chi'/kT}\int_0^{\infty}D_ce^{-\epsilon/kT}d\epsilon-\int_0^{\infty}D_ce^{-[(1/kT)+(1/\omega)]\epsilon}d\epsilon.$$

The first integral has been evaluated above, and the second integral may be obtained from the first by replacing $1/kT$ with $1/kT+1/\omega$. Hence

$$i=Bk^2T^2e^{-\chi'/kT}\left\{\sum_{n=0}^{\infty}(-1)^n\left(\frac{1}{n\mu+1}-\frac{1}{n\mu+1+(kT/\omega)}\right)\right.$$

$$\left.-\frac{W_a^{\frac{1}{2}}}{2kT}\left(1-\frac{1}{4x_0^2}W_a^2\right)\left[\frac{\cos u_1}{\{[\pi\alpha+(1/kT)]^2+\beta^2\alpha^2\}^{\frac{1}{2}}}-\frac{\cos u_2}{\{[\pi\alpha+(1/kT)+(1/\omega)]^2+\beta^2\alpha^2\}^{\frac{1}{2}}}\right]\right\}, \quad (30)$$

$$u_1=\frac{4\sqrt{2}}{3}x_0^{\frac{1}{2}}-\frac{2}{W_a^{\frac{1}{2}}}-\tan^{-1}\frac{W_a^{\frac{1}{2}}}{4}-\tan^{-1}\frac{\beta\alpha}{\pi\alpha+(1/kT)},$$

$$u_2=\frac{4\sqrt{2}}{3}x_0^{\frac{1}{2}}-\frac{2}{W_a^{\frac{1}{2}}}-\tan^{-1}\frac{W_a^{\frac{1}{2}}}{4}-\tan^{-1}\frac{\beta\alpha}{\pi\alpha+(1/kT)+(1/\omega)}.$$

(b) High Fields, Low Temperatures

For this case only electrons from region B need be considered. Here

$$D\sim\exp(-2Q);\quad Q=\int_{x_2}^{x_3}\left(W_a-W-\frac{1}{2x}-\frac{x}{2x_0^2}\right)^{\frac{1}{2}}dx. \quad (31)$$

The effect of the image force on electrons from region B is small. Hence, to evaluate Q it is legitimate to set $2Q=2\Theta Q_0$, where

$$2Q_0=2\int_{x_2}^{x_3}\left(W_a-W-\frac{x}{2x_0^2}\right)^{\frac{1}{2}}dx=\frac{8x_0^2}{3}(W_a-W)^{\frac{1}{2}}$$

is the exponent which is obtained in the transmission coefficient if the effect of the image force is neglected, and Θ is the correction function which has been used previously. The potential barrier used in the determination of Q_0 is shown in Fig. 4. Since the transmission coefficient decreases exponentially, the current vanishes when $\epsilon=W_i-W$ is large. Hence, Q_0 may be expanded in powers of ϵ:

$$Q_0\sim(4x_0^2/3)\chi^{\frac{1}{2}}+2x_0^2\chi^{\frac{1}{2}}\epsilon$$

and since

$$N(\epsilon)=B\left[\epsilon+kT\sum_{n=1}^{\infty}\frac{(-1)^{n+1}}{n}e^{-n\epsilon/kT}\right],$$

$$i=B\exp\left[-\frac{8x_0^2}{3}\Theta\chi^{\frac{1}{2}}\right]\left\{\int_0^{\infty}\epsilon\exp\left[-4\Theta x_0^2\chi^{\frac{1}{2}}\epsilon\right]d\epsilon+kT\sum_{n=1}^{\infty}\frac{(-1)^{n+1}}{n}\int_0^{\infty}\exp\left[-\left(4\Theta x_0^2\chi^{\frac{1}{2}}+\frac{n}{kT}\right)\epsilon\right]d\epsilon\right\}$$

$$=B\exp\left[-\frac{8x_0^2}{3}\Theta\chi^{\frac{1}{2}}\right]\left\{\frac{1}{16\Theta^2x_0^{\frac{1}{2}}\chi}+\sum_{n=1}^{\infty}\frac{(-1)^{n+1}}{n}\frac{k^2T^2}{n+4x_0^2\Theta\chi^{\frac{1}{2}}kT}\right\}, \quad (32)$$

or if χ is put in ev and F in volt/cm

$$i=\left\{1.55\times10^{-4}\frac{F^2}{\Theta^2\chi}+120.5T^2\sum_{n=1}^{\infty}\frac{(-1)^{n+1}}{n}\frac{1}{n+8.81\times10^3(\Theta\chi^{\frac{1}{2}}T/F)}\right\}$$

$$\times\exp\left[-6.838\times10^7\Theta\chi^{\frac{1}{2}}/F\right]\text{amp/cm}^2. \quad (33)$$

(c) Intermediate Fields and Temperatures

If the fields and temperatures are such that $4x_0^2\Theta\chi^{\frac{1}{2}}kT<1$, the current comes from the lower part of C. Again if we take

$$D\sim\exp\left[-(8x_0^2/3)\Theta\chi^{\frac{3}{2}}+4Vx_0^2\chi^{\frac{1}{2}}\beta\right],\quad \beta=W-W_i$$

as above, and use

$$N(\beta)=BkT\sum_{n=1}^{\infty}\frac{(-1)^{n+1}}{n}e^{-n\beta/kT}$$

there results

$$i=Bk^2T^2\exp\left[-\frac{8x_0^2}{3}\Theta\chi^{\frac{3}{2}}\right]\sum_{n=1}^{\infty}\frac{(-1)^{n+1}}{n}\cdot\int_0^{\infty}\exp-\left[4x_0^2\Theta\chi^{\frac{1}{2}}-(n/kT)\right]\beta d\beta$$

$$=Bk^2T^2\exp\left[-\frac{8x_0^2}{3}\Theta\chi^{\frac{3}{2}}\right]\sum_{n=1}^{\infty}\frac{(-1)^{n+1}}{n}\cdot\frac{1}{n-4\Theta x_0^2\chi^{\frac{1}{2}}kT}. \tag{34}$$

By adding this current to that from region B, the total current for the condition $4x_0^2\Theta\chi^{\frac{1}{2}}kT<1$ is obtained

$$i=B\exp\left[-\frac{8x_0^2}{3}\Theta\chi^{\frac{3}{2}}\right]\left\{\frac{1}{16\Theta^2x_0^4\chi}+k^2T^2\sum_{n=1}^{\infty}\frac{(-1)^{n+1}}{n}\left(\frac{1}{n+4\Theta x_0^2\chi^{\frac{1}{2}}kT}-\frac{1}{n-4\Theta x_0^2\chi^{\frac{1}{2}}kT}\right)\right\} \tag{35}$$

or putting χ in ev and F in volt/cm

$$i=\left\{1.55\times10^{-6}\frac{F^2}{\Theta^2\chi}+120.54T^2\sum_{n=1}^{\infty}\frac{(-1)^{n+1}}{n}\left(\frac{1}{n+8.81\times10^3(\Theta\chi^{\frac{1}{2}}T/F)}+\frac{1}{n-8.81\times10^3(\Theta\chi^{\frac{1}{2}}T/F)}\right)\right\}$$

$$\times\exp\left[-6.838\times10^7(\Theta\chi^{\frac{3}{2}}/F)\right]\text{amp/cm}^2. \tag{36}$$

The current penetrating the very top of the barrier has been given in Part IV (28).

The photoelectric emission from C consists of electrons for which

$$D(W+h\nu,\ F)\sim\exp\left[-\frac{8\Theta x_0^2}{3}(\chi-h\nu)^{\frac{3}{2}}\right]-4\Theta x_0^2(\chi-h\nu)^{\frac{1}{2}}/\epsilon,$$

$$N(W)=B\left[\epsilon+kT\sum_{n=1}^{\infty}\frac{(-1)^{n+1}}{n}e^{-n\epsilon/kT}\right].$$

Because of the large exponential in the transmission coefficient, the majority of the current comes from electrons for which $y=W_i-W$ is small; hence

$$i=B\exp\left[-\frac{8x_0^2\Theta}{3}(\chi-h\nu)^{\frac{3}{2}}\right]\left\{\frac{1}{16\Theta^2x_0^4\chi}+k^2T^2\sum_{n=1}^{\infty}\frac{(-1)^{n+1}}{n}\frac{1}{n+4\Theta x_0^2(\chi-h\nu)^{\frac{1}{2}}kT}\right\} \tag{37}$$

or, using ev and volts per cm,

$$i=\left\{1.55\times10^{-6}\frac{F^2}{\Theta^2(\chi-h\nu)}+120.5T^2\sum_{n=1}^{\infty}\frac{(-1)^{n+1}}{n}\frac{1}{n+8.81\times10^3[\Theta(\chi-h\nu)^{\frac{1}{2}}T/F]}\right\}$$

$$\cdot\exp\left[-6.838\times10^7\frac{\Theta(\chi-h\nu)^{\frac{3}{2}}}{F}\right]\text{amp/cm}^2. \tag{38}$$

Flow of Energy in Thermal Transpiration for a Bose-Einstein and a Fermi-Dirac Gas

D. V. GOGATE AND D. S. KOTHARI
University of Delhi, India

(Received October 13, 1941)

In the case of two chambers maintained at different temperatures containing an *ideal* gas (classical $\beta=0$, Fermi-Dirac $\beta=-1$, or Bose-Einstein $\beta=+1$) and intercommunicating through an effusion-orifice, there is, in the steady state brought about by thermal transpiration, no net flow of matter but a continuous flow of energy (due to effusion of particles) from the chamber at the higher temperature to the other one. This energy flow is determined for a completely relativistic and a completely non-relativistic gas. Three possible cases are discussed for each of them: (a) gas non-degenerate in both chambers, (b) gas degenerate in both chambers, and (c) gas non-degenerate in one chamber and degenerate in the other. Case (b) is possible for a F.-D. gas only. In case (c) the rate of flow of energy to a first order is the same as in case (a) but with the temperature of the chamber at the lower temperature (i.e., the chamber containing the degenerate gas) put equal to zero, which is in accord with the properties of a degenerate gas. In case (a) for a relativistic *classical* gas ($\beta=0$) the energy flow is proportional to the concentration n which is the same in both the chambers and to the difference of temperature between them. For a non-relativistic *classical* gas the energy flow varies as $n_1T_1^{\frac{1}{2}}(T_1-T_2)$, n_1 being the concentration in the chamber at temperature T_1. For a F.-D. gas the flow is slightly less and for a B.-E. gas slightly greater than that for the classical gas under the same conditions. In case (b) when there is F.-D. degenerate gas in the two chambers, the energy flow to a first order both for the relativistic and non-relativistic cases, varies as $n_1^{\frac{1}{3}}(T_1^2-T_2^2)$; in the relativistic case, of course, $n_1=n_2$. For fixed temperatures, the energy flow is always greater when the concentrations are such that the gas in the two chambers is degenerate than when the gas in both of them is non-degenerate.

IN a recent paper Srivastava[1] has considered the phenomena of thermal transpiration for a Fermi-Dirac and a Bose-Einstein gas, but the flow of energy, which takes place under the steady state conditions characterizing thermal transpiration, has not been discussed before, and this is taken up in the present paper.[2] Section I deals with the law of thermal transpiration. In Section II, the flow of energy for a relativistic (degenerate and non-degenerate) Fermi-Dirac and Bose-Einstein gas is discussed, and Section III deals with the non-relativistic case.

I

We shall first prove a theorem which is required in discussing thermal transpiration phenomena.

The flow, due to molecular effusion, of mass, energy or number per second per unit area in the case of a Bose-Einstein or Fermi-Dirac gas from a chamber at temperature T_1 into vacuum will be given by an expression of the form[3]

$$I_{10}=\int_0^\infty \frac{\varphi(\epsilon)d\epsilon}{(1/A_1)e^{\epsilon/kT_1}-\beta}, \tag{1}$$

where $\beta=0$ for *classical* statistics, $\beta=-1$ for F.-D. statistics, $\beta=+1$ for B.-E. statistics, and $\varphi(\epsilon)$ is a function appropriate for the particular flow considered. A_1 is called the absolute activity: $kT\log A_1$ is Gibb's free energy per particle. The flow from the chamber (1) into a chamber (2) containing the same gas but at temperature T_2 will be

$$I_{12}=\int_0^\infty \frac{\varphi(\epsilon)d\epsilon}{(1/A_1)e^{\epsilon/kT_1}-\beta}\left\{1+\frac{\beta n_2(\epsilon)}{a_2(\epsilon)}\right\}, \tag{2}$$

[1] Srivastava, Proc. Roy. Soc. **A171**, 469 (1939).

[2] When we have two chambers maintained at temperatures T_1 and T_2, respectively, and connected through a porous plug, then under steady state conditions, there is no net flow of matter from one chamber to the other, but there is a continuous flow of energy from the higher to the lower temperature side. This energy flow is intimately connected with the problem of thermal conduction in the Knudsen region. In two interesting papers, Kennard [Phys. Rev. **22**, 617 (1923); Proc. Nat. Acad. Sci. (U. S. A.) **18**, 237 (1932)] has discussed thermal transpiration for a *classical* gas from the point of view of a reversible process, and this can be easily extended to a B.-E. and a F.-D. gas by using the results given here.

[3] The suffixes 1 and 2 attached to a quantity refer to its value in the chambers (1) and (2), respectively.

where the factor within brackets is introduced to take account of the "already-occupiedness" of the phase-cells in the second chamber. $n_2(\epsilon)$ denotes the number of particles in the second chamber lying in the energy range ϵ to $\epsilon+d\epsilon$, and $a_2(\epsilon)$ the number of independent states or phase-cells available in this energy range. Using the distribution law

$$n_2(\epsilon)d\epsilon=\frac{a_2(\epsilon)d\epsilon}{(1/A_2)e^{\epsilon/kT_2}-\beta}, \tag{3}$$

we have

$$I_{12}=\int_0^\infty \frac{\varphi(\epsilon)d\epsilon\cdot 1/A_2\cdot e^{\epsilon/kT_2}}{[(1/A_1)e^{\epsilon/kT_1}-\beta][(1/A_2)e^{\epsilon/kT_2}-\beta]}. \tag{4}$$

The expression for I_{21} is obtained from (4) by interchanging the suffixes 1 and 2. Hence the net flow from chamber (1) to chamber (2) is

$$I_{12}-I_{21}=\int_0^\infty \varphi(\epsilon)d\epsilon\left\{\frac{1}{(1/A_1)e^{\epsilon/kT_1}-\beta}-\frac{1}{(1/A_2)e^{\epsilon/kT_2}-\beta}\right\}, \tag{5}$$

which shows that

$$I_{12}-I_{21}=I_{10}-I_{20}, \tag{6}$$

i.e., the net flow from chamber (1) to chamber (2), even when one takes into account the occupancy of the phase-cells, is equal to the difference between the flow from chamber (1) into vacuum and that from chamber (2) into vacuum. Therefore, in calculating the *net* flow, the factor which takes account of the occupiedness of the cells can be ignored without affecting the result. We shall now apply (6) to effusion of particles and derive the law of thermal transpiration.[4]

The number of particles effusing from chamber (1) into vacuum per unit area per unit time is

$$N_{10}=\int_0^\infty n(\epsilon)d\epsilon\cdot\tfrac{1}{4}\vartheta, \tag{7}$$

where

$$\vartheta=c\left\{1-\left(\frac{1}{1+\epsilon/mc^2}\right)^2\right\}^{\frac{1}{2}}, \tag{8}$$

m is the rest-mass of the particle, and c is the velocity of light.

Substituting for v and $n(\epsilon)d\epsilon$, and noting that

$$a(\epsilon)d\epsilon=(4\pi g/c^3h^3)(\epsilon^2+2mc^2\epsilon)^{\frac{1}{2}}(\epsilon+mc^2)d\epsilon, \tag{9}$$

we have

$$N_{10}=\frac{\pi g}{c^2h^3}(kT_1)^3\int_0^\infty \frac{(u^2+2uy_1)du}{(1/A_1)e^u-\beta}, \tag{10}$$

where $u=\epsilon/kT_1$, $y_1=mc^2/kT_1$, and g is the "weight factor" for the particle. If there is no net flow of matter between the chambers (1) and (2) then we have

$$N_{12}-N_{21}=N_{10}-N_{20}=0, \tag{11}$$

which gives the transpiration law in its general form,

$$T_1^3\int_0^\infty \frac{(u^2+2uy_1)du}{(1/A_1)e^u-\beta}=T_2^3\int_0^\infty \frac{(u^2+2uy_2)du}{(1/A_2)e^u-\beta}, \tag{12}$$

or

$$T^3\int_0^\infty \frac{(u^2+2uy)du}{(1/A)e^u-\beta}=\text{constant}. \tag{13}$$

[4] Some of the results of this section have been given by Srivastava, reference 1, but they are added here for the sake of completeness. The treatment followed is also somewhat different. Also see Gogate, Phil. Mag. **29**, 85 (1940).

It may be noted for ready reference that

$$n=\frac{N}{V}=\frac{4\pi g}{c^3h^3}(kT)^3\int_0^\infty \frac{(u^2+2umc^2)^{\frac{1}{2}}(u+mc^2)du}{(1/A)e^u-\beta}, \tag{14}$$

and

$$U=\frac{4\pi g(kT)^4}{c^3h^3}\int_0^\infty \frac{u(u^2+2umc^2)^{\frac{1}{2}}(u+mc^2)du}{(1/A)e^u-\beta}, \tag{15}$$

where n is the number of particles per unit volume of the assembly and U denotes the energy density. The relation (12) enables us to determine A_2 for every value of T_2, when T_1 and A_1 are considered as fixed.

As is usual in discussions of quantum statistics, we shall consider two limiting cases: (1) the *completely non-relativistic* case ($y\to\infty$) and (2) the *completely relativistic* case ($y\to 0$). The first case is characterized by the average kinetic energy of a particle being negligibly small compared to its rest-mass energy, and in the second case, it is just the opposite. We shall first take up the relativistic case since in this instance all the effusion phenomena become markedly simple because all particles have (almost) the velocity of light.

In the completely relativistic case, Eq. (12) becomes

$$T_1^3\int_0^\infty \frac{u^2du}{(1/A_1)e^u-\beta}=T_2^3\int_0^\infty \frac{u^2du}{(1/A_2)e^u-\beta}, \tag{16}$$

and as (14) reduces to

$$n=\frac{4\pi g(kT)^3}{c^3h^3}\int_0^\infty \frac{u^2du}{(1/A)e^u-\beta}, \tag{17}$$

the transpiration law becomes

$$n_1=n_2 \quad \text{or} \quad n=\text{constant}. \tag{18}$$

This result is physically obvious, because in the completely relativistic case all particles possess (almost) the velocity of light, and thus the condition of no net flow of particles would reduce to the constancy of n in the chambers concerned.

For the completely non-relativistic case, on the other hand, the law of transpiration is from (12)

$$T_1^2\int_0^\infty \frac{udu}{(1/A_1)e^u-\beta}=T_2^2\int_0^\infty \frac{udu}{(1/A_2)e^u-\beta}, \tag{19}$$

and for this case,

$$n=\frac{4\pi gm(2m)^{\frac{1}{2}}(kT)^{\frac{1}{2}}}{h^3}\int_0^\infty \frac{u^{\frac{1}{2}}du}{(1/A)e^u-\beta}. \tag{20}$$

Unlike the relativistic case, the integrals occurring in (19) and (20) are different and therefore the transpiration law can only be expressed in terms of n by expanding the integrals in series expansions. Thus it becomes necessary to consider separately the non-degenerate and degenerate approximations. We take first the non-degenerate case. The series expansion for the relevant integral is[5]

$$\frac{\beta}{\Gamma(2)}\int \frac{udu}{(1/A)e^u-\beta}=(\beta A_N{}^0)-(\beta A_N{}^0)^2(a_2-\tfrac{1}{4})-(\beta A_N{}^0)^3\left(a_3+\frac{a_2}{2}-\frac{1}{9}\right), \tag{21}$$

where $A_N{}^0$, called the degeneracy-discriminant, is defined by

$$A_N{}^0=\frac{nh^3}{g(2\pi mkT)^{\frac{1}{2}}}. \tag{22}$$

[5] The series expansions and the values of the numerical constants a_2, a_3, etc. are given in the appendix.

In the case of F.-D. statistics, for non-degeneracy $A_N{}^0 \ll 1$, and for the degenerate case $A_N{}^0 \gg 1$. In the case of B.-E. statistics, for the non-degenerate case $A_N{}^0 \leqq \zeta(\frac{3}{2})$ and for degeneracy $A_N{}^0 > \zeta(\frac{3}{2})$, where $\zeta(\frac{3}{2})$ is the Riemann zeta-function.

Since it will be required in the sequel we may note here that for the completely relativistic case, the degeneracy discriminant $A_R{}^0$ is defined by

$$A_R{}^0 = \frac{n}{8\pi g}\left(\frac{ch}{kT}\right)^3. \tag{23}$$

For F.-D. statistics $A_R{}^0 \gg 1$ for the degenerate case and $A_R{}^0 \ll 1$ for the non-degenerate case, and in the case of B.-E. statistics $A_R{}^0 \leqq \zeta(3)$ in non-degeneracy and $A_R{}^0 > \zeta(3)$ for degeneracy.

We shall use the suffix N to designate the non-relativistic case and R for the relativistic case, but when there is no likelihood of any ambiguity their use is suppressed.[6]

By using (21), one finds the transpiration law for the non-relativistic non-degenerate case reduces to (retaining the first three terms in the expansion)

$$T_2{}^2 A_2{}^0 = T_1{}^2 A_1{}^0\left[1+\beta(a_2-\tfrac{1}{4})A_1{}^0 T_1{}^2\left(\frac{1}{T_2{}^2}-\frac{1}{T_1{}^2}\right)+\beta^2\left(a_3+\frac{a_2}{2}-\frac{1}{9}\right)T_1{}^4 A_1{}^{02}\left(\frac{1}{T_2{}^4}-\frac{1}{T_1{}^4}\right)\right.$$
$$\left.+2\beta^2(a_2-\tfrac{1}{4})^2\frac{T_1{}^4 A_1{}^{02}}{T_2{}^2}\left(\frac{1}{T_2{}^2}-\frac{1}{T_1{}^2}\right)+\cdots\right]. \tag{24}$$

For the non-relativistic degenerate case (F.-D. statistics), the transpiration law becomes (we write for brevity $\zeta_1{}^0$, $\zeta_2{}^0$ instead of $\zeta_{N_1}{}^0$, $\zeta_{N_2}{}^0$ and retain up to the third term in the series),

$$(\zeta_1{}^0)^2\{1+2c_2(kT_1/\zeta_1{}^0)^2-\tfrac{1}{2}(c_2{}^2+3c_4)(kT_1/\zeta_1{}^0)^4\} = (\zeta_2{}^0)^2\{1+2c_2(kT_2/\zeta_2{}^0)^2-\tfrac{1}{2}(c_2{}^2+3c_4)(kT_2/\zeta_2{}^0)^4\}, \tag{25}$$

where

$$\zeta_1{}^0 = \frac{h^2}{2m}\left(\frac{3n_1}{4\pi g}\right)^{\frac{2}{3}} = \left(\frac{3\pi^{\frac{1}{2}}}{4}\right)^{\frac{2}{3}}(A_1{}^0)^{\frac{2}{3}}, \tag{26}$$

and

$$\zeta_2{}^0 = \frac{h^2}{2m}\left(\frac{3n_2}{4\pi g}\right)^{\frac{2}{3}} = \left(\frac{3\pi^{\frac{1}{2}}}{4}\right)^{\frac{2}{3}}(A_2{}^0)^{\frac{2}{3}}. \tag{27}$$

Using successive approximations, we have

$$\zeta_2{}^0 = \zeta_1{}^0\left\{1+\frac{c_2k^2}{(\zeta_1{}^0)^2}(T_1{}^2-T_2{}^2)-\frac{c^2k^4}{4(\zeta_1{}^0)^4}(T_1{}^2-T_2{}^2)(3T_1{}^2-T_2{}^2)-\frac{3}{4}c_4\frac{k^4}{(\zeta_0)^4}(T_1{}^4-T_2{}^4)\right\}. \tag{28}$$

II

We shall now determine the rate of flow of energy between the two chambers. In the steady state brought about by thermal transpiration there is no net flow of matter, but there is a continuous flow of energy from the chamber at the higher temperature to the other chamber. We shall investigate separately the *completely* relativistic and *completely* non-relativistic cases, treating under each of them the following three possible cases: (1) non-degenerate gas in both chambers, (2) degenerate gas in both chambers and (3) non-degenerate gas in one chamber and degenerate gas in the other. Cases (1) and (3) exist for a F.-D. as well as for a B.-E. gas, but the second case is not possible in a B.-E.gas. In the case of a degenerate B.-E. gas the rate of effusion of particles from a chamber into vacuum depends only on the temperature and is independent of the concentration for, by taking $A=1$ and $\beta=1$ in (10) we obtain

$$N_{10} = (2\pi g/c^2h^3)(kT_1)^3[\zeta(3)+(mc^2/kT)\zeta(2)]. \tag{29}$$

[6] $A_N{}^0$ is the same as A_0 used in previous papers [Kothari and Singh, Proc. Roy. Soc. (1941) (In press)].

We see, therefore, that when two chambers are maintained at different temperatures, in the steady state characterizing thermal transpiration ($N_{12}=N_{21}$, i.e. $N_{10}=N_{20}$), the B.-E. gas cannot be degenerate in both of them.

The rate of flow of energy from a chamber into vacuum per unit area of the effusion opening is

$$E_{10}=\int \epsilon n(\epsilon)d\epsilon\cdot\frac{\vartheta}{4}=\frac{\pi g}{c^2h^3}\int\frac{\epsilon(\epsilon^2+2\epsilon mc^2)d\epsilon}{(1/A_1)e^{\epsilon/kT_1}-\beta}, \tag{30}$$

where ϑ the velocity of a particle is given in terms of ϵ by (8). Therefore the net flow from chamber (1) into chamber (2) will be

$$E_{12}-E_{21}=(E_{10}-E_{20})=\frac{\pi g}{c^2h^3}\int_0^\infty\left\{\frac{\epsilon(\epsilon^2+2\epsilon mc^2)d\epsilon}{(1/A_1)e^{\epsilon/kT_1}-\beta}-\frac{\epsilon(\epsilon^2+2\epsilon mc^2)d\epsilon}{(1/A_2)e^{\epsilon/kT_2}-\beta}\right\}. \tag{31}$$

Equation (31) gives the general expression for the flow of energy. Let us first take the completely relativistic case, then we have

$$(E_{12}-E_{21})_R=\frac{\pi g}{c^2h^3}\int_0^\infty\left\{\frac{\epsilon^3d\epsilon}{(1/A_1)e^{\epsilon/kT_1}-\beta}-\frac{\epsilon^3d\epsilon}{(1/A_2)e^{\epsilon/kT_2}-\beta}\right\}, \tag{32}$$

and as (15) reduces to

$$U_R=\frac{4\pi g}{c^3h^3}\int_0^\infty\frac{\epsilon^3d\epsilon}{(1/A)e^{\epsilon/kT}-\beta}, \tag{33}$$

we obtain for the completely relativistic case,

$$(E_{12}-E_{21})_R=\tfrac{1}{4}c(U_1-U_2)_R, \tag{34}$$

a result which is physically obvious.

We shall now substitute in (34) series expansions for U for the degenerate and non-degenerate cases. For degeneracy we have[7]

$$U^-=\tfrac{3}{4}n\zeta^0[1+8c_2(kT/\zeta^0)^2-48(2c_2^2-c_4)(kT/\zeta^0)^4], \tag{35}$$

and for non-degeneracy

$$U^+=3nkT\left[1-\frac{\beta}{16}A^0-\frac{47\beta^2}{5184}(A^0)^2\right], \tag{36}$$

where as already mentioned

$$A^0=(n/8\pi g)(ch/kT)^3, \tag{37}$$

and

$$\zeta^0=ch(3n/4\pi g)^{\frac{1}{3}}=kT(6A^0)^{\frac{1}{3}},\quad c_2=\pi^2/12,\quad c_4=7\pi^4/720,\quad 48(2c_2^2-c_4)=\pi^4/5.$$

Thus we obtain for the completely-relativistic non-degenerate case (up to the third term)

$$(E_{12}-E_{21})^+=\tfrac{3}{4}nkc(T_1-T_2)\left[1+\frac{\beta A_1^0}{16}T_1\frac{(T_1+T_2)}{T_2^2}+\frac{47\beta^2}{5184}\frac{(A_1^0)^2T_1}{T_2^5}(T_1^4+T_1^3T_2+T_1^2T_2^2+T_1T_2^3+T_2^4)\right], \tag{38}$$

where $n=n_1=n_2$, and $\beta=0$ for *classical* statistics, $\beta=-1$ for F.-D. statistics and $\beta=+1$ for B.-E.

[7] Non-degeneracy approximation is denoted with $a+$suffix and degeneracy approximation with $a-$suffix.

statistics. In the completely-relativistic degenerate case (F.-D. statistics), we have

$$(E_{12}-E_{21})^{-}=\frac{c}{4}\frac{\pi^2}{2}\frac{nk^2}{\zeta^0}(T_1^2-T_2^2)\left[1-\frac{3\pi^2k^2}{10}\frac{(T_1^2+T_2^2)}{(\zeta^0)^2}\right]$$

$$=\frac{\pi^2}{8}\frac{nk^2}{h}\left(\frac{4\pi g}{3n}\right)^{\frac{1}{3}}(T_1^2-T_2^2)\left[1-\frac{3\pi^2k^2}{10}\frac{(T_1^2+T_2^2)}{(\zeta^0)^2}\right]. \tag{39}$$

We note that (considering only the first terms in the expansions), the ratio of energy flow in non-degeneracy to that in degeneracy is

$$\frac{(E_{12}-E_{21})_R^{+}}{(E_{12}-E_{21})_R^{-}}=\frac{6}{\pi^2}\frac{ch}{k(T_1+T_2)}\left(\frac{3n}{4\pi g}\right)^{\frac{1}{3}}=\frac{6}{\pi^2}\frac{(6A_R^0)^{\frac{1}{3}}}{(T_1+T_2)}. \tag{40}$$

It now remains to consider the third case, the gas non-degenerate in one chamber and degenerate in the other. Since in the relativistic case the transpiration law is $n_1=n_2$, the gas will be non-degenerate in the chamber at higher temperature and degenerate in the other chamber. We shall assume the chamber (1) to be at a higher temperature ($T_1\gg T_2$).

The net flow of energy from chamber (1) to chamber (2) is

$$(E_{12}-E_{21})=\frac{c}{4}(U_1^{+}-U_2^{-}). \tag{41}$$

Substituting the appropriate expressions for the energy density, we have considering the first terms only, for a F.-D. gas

$$(E_{12}-E_{21})=\frac{c}{4}\left[3nkT_1-\frac{3}{4}nch\left(\frac{3n}{4\pi g}\right)^{\frac{1}{3}}\right]=\frac{3}{4}nckT_1\left[1-\frac{6^{\frac{1}{3}}}{4}(A_1^0)^{\frac{1}{3}}\right]\doteq\frac{3nckT_1}{4}, \tag{42}$$

and for a B.-E. gas

$$(E_{12}-E_{21})=\frac{c}{4}\left[3nkT_1-\frac{4}{15}\frac{\pi^3g}{c^3h^3}(kT_2)^4\right]=\frac{3}{4}nckT_1\left\{1-\frac{\pi^2}{30}\frac{T_2}{T_1}\frac{1}{A_2^0}\right\}\doteq\frac{3}{4}nckT_1. \tag{43}$$

III

We now take up the completely non-relativistic case and determine the rate of energy flow for the three cases enumerated at the beginning of Section II.

The rate of flow of energy due to effusion of particles from chamber (1) into vacuum per unit area of the opening is

$$E_{10}=\frac{2\pi gm}{h^3}(kT_1)^3\int\frac{u^2du}{(1/A_1)e^u-\beta},$$

and hence the rate of net flow of energy from chamber (1) to (2) is

$$E_{12}-E_{21}=E_{10}-E_{20}=\frac{2\pi gm}{h^3}\left[(kT_1)^3\int_0^{\infty}\frac{u^2du}{(1/A_1)e^u-\beta}-(kT_2)\int_0^{\infty}\frac{u^2du}{(1/A_2)e^u-\beta}\right]. \tag{44}$$

We first consider the case when the gas is non-degenerate in both the chambers. Writing the relevant series expansions up to the second terms, we have

$$\frac{(E_{12}-E_{21})^{+}h^3}{4\pi gmk^3}=\frac{(E_{01}-E_{02})^{+}h^3}{4\pi gmk^3}=(T_1^3A_1^0-T_2^3A_2^0)-\beta(a_2-\tfrac{1}{8})(T_1^3A^{0}{}_1^2-T_2^3A^{0}{}_2^2). \tag{45}$$

Substituting from expression (24) for A_2^0 in terms of A_1^0 we obtain (putting $a_2=\frac{1}{2}$[1])

$$\frac{(E_{01}-E_{02})^+h^3}{4\pi gmk^3}=(T_1-T_2)T_1^2A_1^0\left[1-\beta A_1^0\left\{\frac{1}{2^{\frac{1}{2}}}-\frac{1}{4}-\frac{T_1}{8T_2}\right\}\right]$$

or

$$(E_{12}-E_{21})^+=n_1\left(\frac{2}{\pi m}\right)^{\frac{1}{2}}k^{\frac{1}{2}}T_1^{\frac{1}{2}}(T_1-T_2)\left[1+\beta A_1^0\left\{\frac{T_1}{8T_2}+\frac{1}{4}-\frac{1}{2^{\frac{1}{2}}}\right\}\right], \tag{46}$$

where $\beta=0$, -1 or $+1$ depending on whether the gas is classical, F.-D., or B.-E.

We shall now discuss the case when the gas is degenerate (F.-D. statistics) in both the chambers. After we introduce the approximate series expansion in powers of (kT/ζ^0), we find the net energy flow is given by

$$\frac{3(E_{12}-E_{21})^-h^3}{2\pi gm}=(\zeta_1^0)^3\left[1+9c_2\left(\frac{kT_1}{\zeta_1^0}\right)^2-\frac{9}{4}\left(\frac{kT_1}{\zeta_1^0}\right)^4(5c_2^2+c_4)\right]$$
$$-(\zeta_2^0)^3\left[1+9c_2\left(\frac{kT_2}{\zeta_2^0}\right)^2-\frac{9}{4}\left(\frac{kT_2}{\zeta_2^0}\right)^4(5c_2^2+c_4)\right]. \tag{47}$$

Substituting from (28) for ζ_2^0 in terms of ζ_1^0, we have after a little simplification

$$\frac{3(E_{12}-E_{21})^-h^3}{2\pi gm}=6c_2\zeta_1^0k^2(T_1^2-T_2^2)\left[1-\frac{c_2k^2}{(\zeta_1^0)^2}(2T_1^2+3T_2^2)\right],$$

or

$$(E_{12}-E_{21})^-=\frac{\pi^3}{6}\frac{k^2g}{h}\left(\frac{3n_1}{4\pi g}\right)^{\frac{2}{3}}(T_1^2-T_2^2)\left[1-\frac{\pi^2k^2(2T_1^2+3T_2^2)}{12(\zeta_1^0)^2}\right]. \tag{48}$$

The ratio in the non-relativistic case of the energy flow for non-degeneracy to that for degeneracy is (only the first terms are considered)

$$\frac{(E_{12}-E_{21})^+}{(E_{12}-E_{21})^-}=\frac{3^{1/3}\cdot4^{5/3}}{\pi^{7/3}}\frac{1}{1+(T_2/T_1)}(A_{N_1}^0)^{1/3}. \tag{49}$$

When the first terms only are considered, it will be noticed that the expression for the energy flow, when the gas is degenerate in both the chambers, is exactly the same for the *completely* relativistic and non-relativistic cases *viz.*,

$$(E_{12}-E_{21})^-=\frac{\pi^3}{6}\frac{k^2g}{h}\left(\frac{3n_1}{4\pi g}\right)^{\frac{2}{3}}(T_1^2-T_2^2). \tag{50}$$

This suggests that for the degenerate case, the first term in the expression for energy flow will be the same throughout the entire region from the *completely non-relativistic* at one end to the *completely relativistic* at the other end.[8]

It will be of interest, therefore, to consider the *completely* degenerate case and take account of relativistic mechanics and not restrict ourselves to the two extreme cases (completely non-relativistic and relativistic) only.

Equation (12) defining the law of thermal transpiration gives, on integration and retaining only the first two terms of the series,

$$(\zeta_1^3/3+\zeta_1^2mc^2)+4c_2(kT_1)^2(\zeta_1+mc^2)+\cdots=(\zeta_2^3/3+\zeta_2^2mc^2)+4c_2(kT_2)^2(\zeta_2+mc^2)+\cdots, \tag{51}$$

[8] The expression is independent of m or c, which is obviously necessary for it to be identical in the non-relativistic and relativistic cases, for, in a non-relativistic expression c would not occur, and m would not occur in a relativistic expression.

where $\zeta_1/kT_1=\log A_1$ and $\zeta_2/kT_2=\log A_2$. Substituting $\zeta_2=\zeta_1(1+z)$, we obtain

$$z=\frac{4c_2}{\zeta_1^2}\frac{(\zeta_1+mc^2)(T_1^2-T_2^2)}{(\zeta_1+2mc^2)}. \tag{52}$$

The rate of flow of energy from chamber (1) to (2) is after integrating (31)

$$\frac{(E_{12}-E_{21})^- c^2h^3}{\pi g}=\left[\frac{\zeta_1^2}{4}+\frac{2}{3}\zeta_1^2mc^2+2c_2(kT_1)^2(3\zeta_1^2+4mc^2\zeta_1)\right]$$
$$-\left[\frac{\zeta_2^2}{4}+\frac{2}{3}\zeta_2^3mc^2+2c_2(kT_2)^2(3\zeta_2^2+4mc^2\zeta_2)\right] \tag{53}$$

or to a first order in z we have

$$\frac{(E_{12}-E_{21})^- c^2h^3}{\pi g}=2c_2k^2(T_1^2-T_2^2)\zeta_1(\zeta_1+2mc^2). \tag{54}$$

Substituting for ζ_1 its value, (taking only the first term in its expansion), we have

$$\zeta_1=\zeta_1^0=mc^2[(1+x_1^2)^{\frac{1}{2}}-1], \quad x_1=\frac{h}{mc}\left(\frac{3n_1}{4\pi g}\right)^{\frac{1}{3}}. \tag{55}[9]$$

We obtain

$$(E_{12}-E_{21})^-=\frac{\pi^3 g}{6}\frac{k^2}{h}\left(\frac{3n_1}{4\pi g}\right)^{\frac{1}{3}}(T_1^2-T_2^2),$$

which is Eq. (50).

It now only remains to consider the case that the gas in chamber (1), with $T_1\gg T_2$, is non-degenerate and that in chamber (2) is degenerate. Let us first take the F.-D. gas. For the non-relativistic case that we are treating, the transpiration relation, after we integrate (19) and retain only the first terms becomes

$$(kT_1)^2A_1^0=(\zeta_2^0)^2/2. \tag{56}$$

The rate of flow of energy from chamber (1) to (2) will be from (44)

$$(E_{12}-E_{21})=\frac{2\pi gm}{h^3}\left[2(kT_1)^3A_1^0-\frac{(\zeta_2^0)^3}{3}\right]=\frac{4\pi gm}{h^3}(kT_1)^3A_1^0\left[1-\frac{2^{\frac{1}{2}}}{3}(A_1^0)^{\frac{1}{2}}\right]$$
$$=\left(\frac{2}{\pi m}\right)^{\frac{1}{2}}n_1(kT_1)^{\frac{1}{2}}\left[1-\frac{2^{\frac{1}{2}}}{3}(A_1^0)^{\frac{1}{2}}\right]\fallingdotseq\left(\frac{2}{\pi m}\right)^{\frac{1}{2}}n_1(kT_1)^{\frac{1}{2}}. \tag{57}$$

In the case of a B.-E. gas, instead of (56), the transpiration law will be from (19)

$$A_1^0=\zeta(2)(T_2/T_1)^2, \tag{58}$$

where $\zeta(2)$ is the Riemann zeta-function for the parameter 2, $\zeta(2)=\pi^2/6$. The energy flow from chamber (1) to (2) will be from (44)

$$E_{12}-E_{21}=\frac{2\pi gm}{h^3}[2(kT_1)^3A_1^0-2(kT_2)^3\zeta(3)], \tag{59}$$

[9] When $x_1\to\infty$, $\zeta_1^0\to\zeta_{R1}^0$, and when $x_1\to o_2\zeta_1^0\to\zeta_{N1}^0$. Except as used here, ζ_1^0 stands either for ζ_{N1}^0 or ζ_{R1}^0 depending on the content.

where $\zeta(3)=1.202$. Substituting (58) in (59) we have

$$E_{12}-E_{21}=\frac{4\pi gm(kT_1)^3}{h^3}A_1{}^0\left[1-\frac{\zeta(3)}{\zeta(2)}\left(\frac{T_2}{T_1}\right)\right]=\left(\frac{2}{\pi m}\right)^{\frac{1}{2}}n_1(kT_1)^{\frac{1}{2}}\left\{1-\frac{\zeta(3)(A_1{}^0)^{\frac{1}{2}}}{[\zeta(2)]^{\frac{1}{2}}}\right\}\doteq\left(\frac{2}{\pi m}\right)^{\frac{1}{2}}n_1(kT_1)^{\frac{1}{2}}. \quad (60)$$

These results—that is Eqs. (57) and (60)—are to be compared with the case of a non-degenerate gas in the two chambers. They are identical with the corresponding expression (if we consider only the first terms) for the non-degenerate case but with T_2 in it put equal to zero, and this is what would be expected from the physical properties of a degenerate gas.

APPENDIX

It is often convenient to have a series expansion expressed in powers of A_0 (or $1/A_0$ as the case may be) for the usually occurring integral

$$I_p=\int_0^\infty \frac{u^p du}{(1/A)e^u-\beta}. \quad (1A)$$

A_0 and (ζ_0/kT) are defined by

$$A_0=\frac{n}{C(kT)^q}\frac{1}{\Gamma(q)}=\frac{I_{q-1}}{\Gamma(q)}, \quad \text{and} \quad (\zeta_0/kT)^q=\Gamma(q+1)A_0=\frac{qn}{C(kT)^q}=qI_{q-1}, \quad (2A)$$

where n is the concentration and C is a constant. [See Eqs. (17) and (20).] The energy per particle (U/n) will be given by

$$U/n=(1/n)C(kT)^{q+1}I_q=q\zeta_0(kT/\zeta_0)^{q+1}I_q. \quad (3A)$$

[See Eqs. (14) and (15).]

For the non-degenerate case $(A<1)$, we have

$$\beta I_p=\int_0^\infty u^p\beta Ae^{-u}(1-\beta Ae^{-u})^{-1}du=\sum_{n=1}^\infty\int_0^\infty u^p(\beta A)^n e^{-nu}du$$

or

$$\beta I_p=\Gamma(p+1)\sum_{m=1}^\infty\frac{(\beta A)^m}{m^{p+1}}. \quad (4A)$$

Substituting $p=q-1$ in (4A), we have using (2A),

$$\beta A_0=\sum_{m=1}^\infty\frac{(\beta A)^m}{m^q}=(\beta A)+\frac{(\beta A)^2}{2^q}+\frac{(\beta A)^3}{3^q}+\cdots \quad (5A)$$

and inverting the series (5) we obtain

$$\beta A=\beta A_0-a_2(\beta A_0)^2-a_3(\beta A_0)^3-a_4(\beta A_0)^4-\cdots \quad (6A)$$

where

$$a_2=\frac{1}{2^q}, \quad a_3=\frac{1}{3^q}-\frac{2}{4^q}, \quad a_4=\frac{1}{4^q}-\frac{5}{6^q}+\frac{5}{8^q}. \quad (7A)$$

With the help of (6A), we obtain for the expansion of the integral I_p in terms of A_0,

$$\frac{\beta I_p}{\Gamma(p+1)}=(\beta A_0)-(\beta A_0)^2\left(a_2-\frac{1}{2^{p+1}}\right)-(\beta A_0)^3\left(a_3+\frac{a_2}{2^p}-\frac{1}{3^{p+1}}\right)$$
$$-(\beta A_0)^4\left(a_4+\frac{a_3}{2^p}+\frac{a_2}{3^p}-\frac{a_2{}^2}{2^{p+1}}-\frac{1}{4^{p+1}}\right). \quad (8A)$$

The values of the numerical coefficients are

$$\left.\begin{array}{ll} a_2= & 0.12500 \\ a_3= & 0.005787 \\ a_4= & 0.002243 \end{array}\right] \text{for the completely relativistic case } (q=3)$$

and

$$\left.\begin{array}{ll} a_2= & 0.3535 \\ a_3= & -0.05755 \\ a_4= & 0.005764 \end{array}\right] \text{for the completely non-relativistic case } (q=\tfrac{3}{2}). \tag{9A}$$

We now consider the degenerate case. Taking first the case of F.-D. statistics ($\beta=-1$, $A\gg 1$), we have,[10]

$$I_p=\int_0^\infty \frac{u^p du}{(1/A)e^u+1}=\frac{(\zeta/kT)^{p+1}}{p+1}+2c_2p(\zeta/kT)^{p-1}+2c_4p(p-1)(p-2)(\zeta/kT)^{p-3}+\cdots, \tag{10A}$$

where we write $\log A=\zeta/kT$ and $c_2=\pi^2/12$, $c_4=7\pi^4/720$. Substituting for I_{q-1} in (2A) from (10A), we have

$$(1/q)(\zeta_0/kT)^q=(1/q)(\zeta/kT)^q+2c_2(q-1)(\zeta/kT)^{q-2}+2c_4(q-1)(q-2)(q-3)(\zeta/kT)^{q-4}+\cdots$$

and inverting the series we obtain after a little algebra

$$\zeta=\zeta_0[1-2c_2(q-1)(kT/\zeta_0)^2-2(q-1)(q-3)\{c_4(q-2)-c_2^2(q-1)\}(kT/\zeta_0)^4]. \tag{11A}$$

Substituting from (11A) in (10A) we obtain for the integral I_p in powers of (kT/ζ_0) the series

$$\begin{aligned}(p+1)I_p=(\zeta_0/kT)^{p+1}[1&+2c_2(p+1)(p-q+1)(kT/\zeta_0)^2\\&+2p(p+1)(kT/\zeta_0)^4\{c_2^2(q-1)[q-2p+1+(q-1)(q-3)/p]\\&+c_4[(p-1)(p-2)-(q-1)(q-2)(q-3)/p]\}].\end{aligned} \tag{12A}$$

Writing $p=q$ in (12A) we have

$$\begin{aligned}(q+1)I_q=(\zeta_0/kT)^{q+1}[1&+2c_2(q+1)(kT/\zeta_0)^2\\&+6(q+1)(q-1)(kT/\zeta_0)^4\{c_4(q-2)-c_2^2(q-1)\}+\cdots],\end{aligned} \tag{13A}$$

and using (2A) we obtain for the energy per particle

$$\frac{U}{n}=\frac{q}{q+1}\zeta_0[1+2c_2(q+1)(kT/\zeta_0)^2+6(q+1)(q-1)(kT/\zeta_0)^4\{c_4(q-2)-c_2^2(q-1)\}+\cdots]. \tag{14A}$$

We have so far considered the degenerate case in Fermi statistics. In Bose degeneracy $A=1$, and therefore

$$I_p=\int_0^\infty \frac{u^p du}{e^u-1}=\Gamma(p+1)\zeta(p+1), \tag{15A}$$

where $\zeta(p+1)$ is the Riemann zeta-function.

[10] Sommerfeld, Zeits. f. Physik **47**, 1 (1928).

Elasticity and Creep of Pb Single Crystals

IRVIN H. SWIFT AND E. P. T. TYNDALL
Department of Physics, State University of Iowa, Iowa City, Iowa

(Received January 12, 1942)

The rigidity modulus and Young's modulus of lead single crystals have been measured by static methods as functions of crystal orientation. The elastic parameters so obtained are in agreement with the previous values determined dynamically by Goens and Weerts. The bending-torsion effect is large for certain orientations, and its effect upon the measurement of rigidity modulus by torsion has been studied. The elastic limit for lead under longitudinal stress occurred when the resolved shear stress on the most favorably placed octahedral plane was about 2×10^6 dynes per cm^2. Observations have been made of the transient creep under longitudinal stress. The creep strain velocity at any instant was found to be proportional to the difference between the final strain reached under that load and the strain present at the instant.

GOENS and Weerts[1] have measured the adiabatic elastic constants of lead from torsional and flexural oscillations of single crystal rods. The elastic region under steady stress has been studied by Deming[2] who measured Young's modulus by the bending beam method.[3] He found definite elastic behavior with a linear relation between stress and strain up to a resolved shear stress of about 2×10^6 dynes/cm^2, beyond which creep and permanent set (after removing the load) appeared. The values of Young's modulus for crystals with orientation functions near zero agreed fairly well with those of Goens and Weerts, but for other orientations the agreement was poor.[4]

In the following, the elasticity of lead under steady stress has been studied by determining the rigidity modulus for various crystal orientations with a torsion apparatus, and the Young's modulus by observing the increase in length under applied longitudinal stress. Some observations of creep have also been made with the latter method.

The lead was from the same lot used by Deming.[5] The preliminary castings were made in an iron tube[6] in the shape of cylinders about 15 cm long and 0.9 cm in diameter. After being sharpened to a point at one end, they were coated with Alundum cement, dried, rolled in moistened asbestos paper, and slipped into a brass tube. They were formed into single crystals by the Bridgman method of lowering through a furnace. The rate of growth was about 2 cm/hr. and the gradient was about 10°C/cm. The cement-asbestos paper coating was removed from the final crystal by soaking in water. This procedure was believed to be less likely to produce strains than other methods such as growing in a glass tube, etc. The orientation of each crystal was determined after etching[7] by the reflection of light from crystal planes by the procedure described by Webb.[3] The reflections were mainly from the {111} and {100} planes, although fainter reflections were also observed from the {110} and {113} planes.

RIGIDITY MODULUS

The elastic properties of a cubic crystal such as lead may be expressed in terms of three main parameters, s_{11}, s_{12} and s_{44}, when referred to the crystallographic axes. One may also use a set of axes, x', y', and z', not coinciding with the

[1] E. Goens and J. Weerts, Physik. Zeits. **37**, 321 (1936).
[2] A. Deming, M.S. thesis, State University of Iowa 1939, unpublished.
[3] Wayne Webb, Phys. Rev. **55**, 297 (1939), footnote 26.
[4] This is now believed to be due to the reciprocal bending-torsion effect, the influence of which could not be effectively estimated with the apparatus used by Deming.
[5] We are indebted to Professor H. F. Moore of the University of Illinois for the material. It has about 0.005 percent impurity, according to an analysis made by Baker, Betty, and Moore (Trans. Am. Inst. Min. and Met. Eng. **128**, 111 (1938), Inst. of Metals Div.).
[6] A spectrographic analysis showed no impurities were introduced.
[7] Two etch solutions were used; a stronger to remove oxide (for ½ hr.) and a weaker (for several hr.). The two solutions are composed of nitric acid, acetic acid and water in the proportions 1 : 1 : 2 and 2 : 3 : 20. This procedure was suggested by Deming and is a modification of the one used by B. B. M.

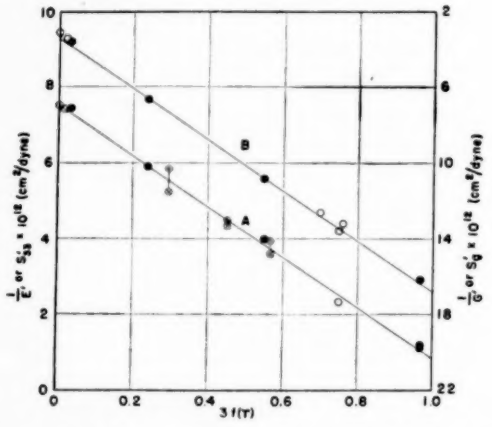

FIG. 1. Curve A, reciprocal of rigidity modulus; Curve B, reciprocal of Young's modulus, as functions of orientation. Lines and solid circles (●) are from Goens and Weerts. Other points are the writers' values. On Curve A, the symbols have the following significance: ○, no bending-torsion correction; ⊕, from "maximum slope" run; ⊗, from "minimum slope" run and correction factor ϕ.

crystallographic axes, and a set of "primed" parameters, s'_{ij}, which are, of course, functions of the main parameters and of the relative orientation of the two sets of axes. In general, a crystal either under axial torque or with an applied bending moment both twists and bends. With an appropriate choice of axes, the following equations[8] hold for a cylindrical crystal of length l and radius r:

$$\pi r^4\theta/2l = s'_g N - \bar{s}'_{34} M, \tag{1}$$

$$1/\rho = (2/\pi r^4)(\bar{s}'_{34} N - 2s'_{33} M), \tag{2}$$

in which θ is the angle of twist, N is the axial torque, ρ is the radius of curvature, and M is the component of the applied bending moment in the plane in which bending occurs. The parameters s'_g, s'_{33}, and $\bar{s}'_{34}$ are expressed in terms of the main parameters by the following:

$$s'_g = s_{44} + 4sf(\gamma), \tag{3}$$

$$s'_{33} = s_{11} - 2sf(\gamma), \tag{4}$$

$$\bar{s}'^2_{34} = 4s^2[(\gamma_1^6+\gamma_2^6+\gamma_3^6) - (\gamma_1^4+\gamma_2^4+\gamma_3^4)^2], \tag{5}$$

where

$$s = s_{11} - s_{12} - \tfrac{1}{2}s_{44}, \tag{6}$$

$$f(\gamma) = \gamma_1^2\gamma_2^2 + \gamma_1^2\gamma_3^2 + \gamma_2^2\gamma_3^2, \tag{7}$$

and the γ's are the direction cosines of the length of the crystal specimen with respect to the crystallographic axes. In the following, we shall define G' $(=1/s'_g)$ as the "free" rigidity modulus [N only; $M=0$ in Eq. (1)], and G as the modulus which is measured when bending is prevented [$1/\rho=0$ in Eq. (2)]. If the crystal is free to bend, the expression for G' reduces to $G'=2lN/\pi r^4\theta$, the usual "isotropic" formula. If the crystal is prevented from bending the reciprocal of the free modulus is given by[9] $1/G'=(1/G)\phi$ where $\phi=1/[1-(\bar{s}'^2_{34}/2s'_{33}s'_g)]$ and G is given now by the "isotropic" formula. The correction factor ϕ is 1.00 for orientations in which the length of the specimen is in the [100] ($f(\gamma)=0$), [110] ($f(\gamma)=0.25$), and [111] ($f(\gamma)=0.33$) directions. It has a maximum value of about 1.25 for lead.

The torsion apparatus was of the usual type having for the measurement of the twist, θ, an optical system with a minimum observable angle of about one second of arc. The fixed end of the crystal was set in Wood's metal, and the movable end was held in jaws on a torsion head which was free to rotate in ball bearings. An approximately pure torque, clockwise or counter-clockwise, was applied to the torsion head by a suitable arrangement of four springs.

Three crystals for which the bending-torsion coupling was absent were grown and measured. The stress-strain[10] plots for these crystals were all straight and the slopes consistent, within the experimental error of about one percent. The points indicated by open circles (○), curve A, Fig.

TABLE I. Summary of data.

Crystal No.	$f(\gamma)$	ϕ	$\frac{1}{G'}\times10^{12}$	$\frac{1}{E'}\times10^{12}$	Stress at elastic limit§ Longitudinal	Stress at elastic limit§ Resolved shear
1	0.000	1.00	6.91	(9.71)* 9.47	6.8	1.4
2	0.004[6]	1.02	7.11			
3	0.006			(9.61)* 9.31	4.1	1.8
4	0.099	1.21	11.50† 10.27‡			
5	0.151	1.19	13.3† 13.0‡			
6	0.189	1.12	14.8† 14.1‡			
7	0.233			4.70		
8	0.250	1.00	17.35	4.22		
9	0.254			4.41	4.3	1.8

* Before annealing.
† Computed from maximum slope.
‡ Computed from minimum slope and correction factor, ϕ.
§ In 10^8 dynes/cm².

[8] E. Goens, Ann. d. Physik **16**, 693 (1933).

[9] This may also be written in the equivalent form $1/G' = 1/G$ plus a "bending-torsion" correction. See W. A. Good, Phys. Rev. **60**, 605 (1941).

[10] More accurately—angle of twist *vs.* axial torque.

1, are the averages of a number of runs on these crystals and are in good agreement with the data of Goens and Weerts.[1]

For the crystals which had an appreciable bending-torsion correction ($\phi > 1$), the situation is more complicated. The ball bearings were not perfectly tight, but had a play estimated to be about 10^{-3} cm, which is actually about sufficient to allow free bending. Thus one might expect the stress-strain curve to have a slope corresponding to the free modulus (G'). If, however, the bearing reaction produced a partial restraint, the slope should correspond to something greater than G', i.e. nearer G. In the extreme case where the torsion head was initially definitely in contact with one side of the bearing torque in one sense would produce no bending while under the opposite torque very nearly free bending would occur. The stress-strain curve should then be two straight lines, one with a slope, for one sense of torque, corresponding to G, and the other to G'. These two cases are illustrated by curves C and D of Fig. 2, which are successive runs on crystal No. 5. In the first, only a pure torque was used, and the line is straight, with a slope fairly close to that corresponding to free bending. In curve D, a weight was hung on the torsion head sufficient to press it definitely against one side of the bearing. Since a constant bending moment (contrasted to a bending moment which is proportional to the torque) gives a line with a slope corresponding to G', a double slope line was expected and was actually obtained. The difference in the slopes of the two lines (14 percent) corresponds fairly well to the computed difference of 19 percent ($\phi = 1.19$) between G and G'. This experiment was repeated with another crystal with similar results. The same experiment with a crystal having no bending-torsion coupling gave a null result.

Of all the runs on the crystals having a bending-torsion coupling ($\phi > 1.00$), the results were about as follows: Either single straight lines were observed, with slopes corresponding fairly well to G', or they were of the double slope type. Examples of the latter are curves E and F, Fig. 2. From the various slopes observed for any one of these crystals (5 to 20 runs), the extreme values were picked out. The maximum was assumed to be that for free bending and G' was computed from it. The minimum value was assumed to give G and from it another value of G' ($1/G' = (1/G)\phi$) was computed. These two values are plotted in Fig. 1 with separate symbols and are given in Table I. The average of these two values should be and is reasonably close to the value of G'.

The diversity of slopes of the stress-strain relations for crystals with a large correction factor as compared with the constancy of slopes for crystals with no (or very small) bending-torsion correction is shown in Fig. 3.

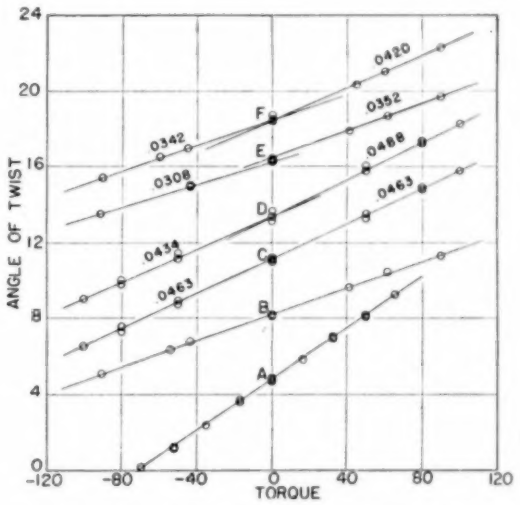

FIG. 2. Angle of twist against axial torque. Curve A is for a brass rod. Curves B to F are runs on lead single crystals. B and C are typical examples of straight line plots, while E and F are typical examples of runs of the double slope type. The slopes are shown by the numbers near the curves. The unit of torque is 1960 dyne cm and the unit of twist is 5.6×10^{-6} radian.

YOUNG'S MODULUS

The apparatus used for determining Young's modulus[11] and observing creep was developed particularly for measuring very small extensions of metal single crystals under longitudinal stress. It consists of an optical lever system attached to the specimen, a change in length of which causes the image of a scale to move past the cross hair in a low power microscope. The magnification of the device is about eight hundred. If one considers the smallest definite observable change in scale reading as 0.01 mm (one-tenth of the smallest scale division), the corresponding least observ-

[11] This is E' Eq. (4) and is $1/s'_{33}$.

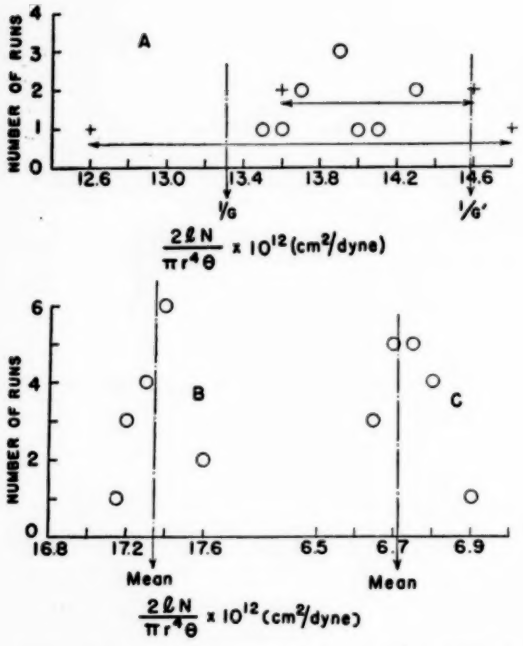

FIG. 3. The number of runs giving values of $2lN/\pi r^4\theta$ to the closest value plotted against these values. A is for a crystal (No. 6, $\phi = 1.12$) which has a large bending-torsion coupling and B and C are for crystals having zero and small coupling (No. 8 and No. 2), respectively. A value of $2lN/\pi r^4\theta$ obtained from a straight run is plotted as a circle (○) while the two values obtained from a double slope are plotted as plus signs connected by the arrow ↔.

able increment of strain on a specimen 7 cm long is 1.8×10^{-7}. A fairly accurate stress-strain curve can therefore be run with the upper limit of allowable strain as low as 4×10^{-6} above the strain caused by the initial, or zero, load. By the use of a photoelectric multiplying device very similar to, and suggested by, one used by McKeehan and Cioffi,[12] the accuracy of observation is increased and the lower limit of observable strain reduced. With it, in fact, a 1-cm scale deflection of a galvanometer corresponds to a strain increment of about 2×10^{-8} (on a 7 cm length), and a determination of Young's modulus can be made with a total strain not exceeding about 10^{-6} beyond the initial value. The initial load was made small enough to produce in a crystal of 0.65 cm² cross section a stress of 0.6×10^6 dynes[13] per cm².

Young's modulus was determined by the photoelectric method for five crystals with orientation functions near zero and near 0.25. The results are plotted as open circles (○), Curve *B*, Fig. 1, and are given in Table I. They agree well with the adiabatic[14] determination of Goens and Weerts. The load-extension curves for both increasing and decreasing loads were straight lines, with no observable hysteresis or permanent set. Two of the crystals (see Table I) gave somewhat high values for $1/E'$ when first run but yielded values in agreement with Goens and Weerts after an anneal of three hours at 200°C, followed by slow cooling. Crystals which gave the expected value on the initial determination were not annealed.[15]

ELASTIC LIMIT AND PLASTICITY

Three of the crystals were taken into the plastic region. This was done mainly by the visual observation method. The load was increased by steps of about 275 grams. In all cases the load which caused the first deviation from a linear relation between load and extension was accompanied by easily observable creep and by subsequent permanent set when the load was removed. This was taken to be the elastic limit. Elastic limits so determined are given in Table I both as longitudinal stress (column 6) and as

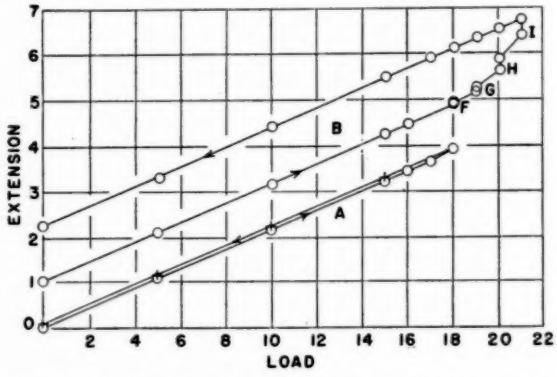

FIG. 4. Load against extension for crystal No. 1. Each unit of load produces a stress of 0.415×10^6 dynes/cm². The zero load is 0.67 dyne/cm². Each unit of extension corresponds to a longitudinal strain of 18×10^{-6}. Curve *B* was taken directly after curve *A* and the ascending branch coincides with the descending branch of curve *A*, but is offset to avoid confusion. The first elastic limit observed for this crystal was at 14 on the load scale.

[12] L. W. McKeehan and P. P. Cioffi, Phys. Rev. **28**, 146 (1926).

[13] For the orientation, $f(\gamma) = 0$, with the smallest modulus this is an initial strain of about 5×10^{-6}.

[14] The theoretical difference between the reciprocals of the adiabatic and isothermal modulus is 0.016×10^{-12} cm²/dyne and is too small to show in the graph.

[15] Crystal No. 9 was also high, but this was a crystal with a somewhat irregular cross section. It had also had considerable previous use.

resolved shear stress (column 7). The resolved shear stress was obtained as follows. The glide plane is known to be the most favorably situated of the octahedral planes and the component of longitudinal stress parallel to this plane was obtained and then resolved into the nearest glide direction [110]. This resolved shear stress, for any orientation, comes out fairly close to four-tenths of the longitudinal stress, except for the case where glide may take place on two equally favorably situated glide planes. In this case the resolved shear stress is half as great as for resolution on a single plane. Crystals Nos. 3 and 9 seemed to satisfy the former condition, while crystal No. 1 was so nearly oriented along a cube edge that the assumption of double glide appeared correct. Computing the resolved shear stress on this assumption we obtain the values in the table. If single glide for No. 1 is assumed, a value twice as high is obtained.

It must be realized that any specification of elastic limit, the presence of permanent set, presence or absence of hysteresis, etc., are inherently indefinite and conditioned by the particular observational method used. Thus, the writers feel safe in saying that the load-extension curve is linear and the same for increasing and decreasing loads up to a fairly well-defined point, corresponding to a resolved shear stress of not more than 2×10^6 dynes per cm^2. It is implied, however, that this is true within the limitations of the apparatus, namely, the ability to determine a change in strain of about 2×10^{-7} which may occur in, say, five or six minutes. The same change occurring in five or six hours is not considered observable.[16] Elastic curves were obtained whether the runs were made in ten minutes or in one hour, but a run which took a week could conceivably be different.

A decrease in the load after the specimen had been taken slightly beyond the elastic limit produced a load-extension curve parallel to the increasing load curve, but offset by the amount of the plastic deformation. Curve *A*, Fig. 4 is an example of this behavior. Curve *B*, taken directly after *A*, shows the effect of again increasing the load. The first, very small creep was observed at *F*, the maximum load of the previous curve. At *G*, *H*, and *I*, the lower point indicates the reading taken as soon as possible after reaching[17] the indicated load. The higher point indicates the extension reached after several minutes when the creep had practically stopped. The curve from *I* down is parallel to the increasing load curve. In general, after a specimen was left loaded until the creep seemed to stop, its subsequent behavior was elastic almost up to this point with no certain change in modulus (not more than 1 percent). The elastic limit of the crystal in Fig. 4 has been raised about 50 percent by other runs of this sort. No self-annealing at room temperature was observed, i.e., after the elastic limit was pushed up to a certain value, it stayed there.

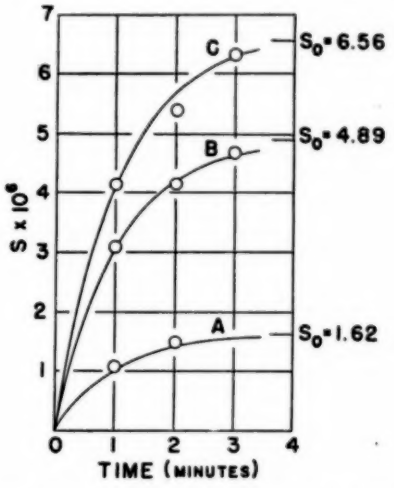

FIG. 5. Creep as function of time. Ordinate is longitudinal strain, *S*; abscissa, time in minutes.

The progress of creep with time at such points as *G*, *H*, and *I*, Fig. 4, is of some interest. Curves *A*, *B*, *C*, Fig. 5, depict this behavior. The strain existing at each of the lower points *G*, *H*, *I* in Fig. 4 is set equal to zero, with time equal to zero also, and the subsequent longitudinal strain ($S=\Delta l/l$) under the steady load is plotted as a function of time. The experimental points are

[16] The reason for this is that the apparatus is temperature sensitive, because of unequal expansion of crystal and measuring system. With the best compensation of this, good thermal insulation, etc., it is always probable that some small change taking place in several hours is due to temperature change. Long time observations were therefore precluded.

[17] The load was applied by gradually running mercury into a container hung from the lower end of the crystal. Adding the 275 gram increment took not more than twenty seconds.

indicated by circles and the curves are plotted from the equation:

$$S=S_0(1-e^{-at}) \tag{8}$$

with a equal to unity and the values of S_0 shown on the curves. The constant a was found from suitable pairs of experimental points. The values actually found were: from points on A, 1.14; from B, 1.04, 0.87, 0.97; from C, 1.18, 0.70, 1.00. Another set of three similar curves, taken previously on this same crystal at somewhat lower loads, were also fitted quite well with a equal to unity. After several intervening runs, which pushed the elastic limit higher yet, a set of two curves taken beyond I, Fig. 4 (at 22.3 and 22.6 on the arbitrary load scale) was fitted by $S=7.00(1-e^{-0.36t})$ and $S=7.29(1-e^{-0.36t})$. It is to be noted that the a is definitely less. Although the fitting of such a curve to three points is not very sensitive to changes in a, a value of unity for a produced no fit at all.

The strain velocity, during creep, is given by

$$dS/dt=S_0ae^{-at}=a(S_0-S), \tag{9}$$

that is, the velocity is proportional to the creep (strain) still to be accomplished. If F, curve B, Fig. 4, is taken as the elastic limit, G, H, and I are 1, 2, and 3 load units, respectively, beyond this. The values of S_0 on curves A, B, and C, Fig. 5, are 1.98, 9.06, and 20.96×10^{-6} strain unit, respectively above the extrapolated elastic curve. These numbers are roughly in the ratio of $1:4:9$, or proportional to the square of the load added above the elastic limit. Thus, if it is valid to extrapolate the strain velocity relation, Eq. (9), back to this point, such loads if applied suddenly would produce initial creep rates proportional to the square of the load above the then existing elastic limit. These initial strain velocities are, of course, equal to 1.98, 9.06, and 20.96×10^{-6} per minute. Chalmers[18] has found very similar results for tin, although he found a linear relation between strain velocity and stress in this region of "transient creep," and found that the previous history of the specimen had no effect.

The data on creep presented here are not very extensive but it seems that results of this type should throw useful light on the general problem of plasticity in metals and particularly the validity of Taylor's dislocation theory.[19] Thus the relations of Eqs. (8) and (9) may imply that under a given load there are a certain number of dislocations which are capable of moving (or disappearing) in such a way as to change the specimen length by a certain amount, and that the number of these which move (or disappear) per unit time is proportional to the number present at that time. A further increase in load then makes an additional number of dislocations effective, and so on throughout the region of transient creep. In this way one might, with more extensive data, arrive at quantitative results for density of dislocations, energy to move them, etc.

Finally, the writers do not believe that their data on elasticity warrant any change in the elastic parameters s_{11}, s_{12} and s_{44} from those recommended by Goens and Weerts. The isothermal parameters are, then, in cm²/dynes: $s_{11}=9.28$, $s_{12}=-4.24$, $s_{44}=6.94$, all $\times10^{-12}$, and the compressibility, computed from these is 2.40×10^{-12} cm²/dyne.

---

[18] B. Chalmers, Proc. Roy. Soc. **156**, 427 (1936).

[19] See Frederick Seitz and T. A. Read, J. App. Phys. **12**, 470 (1941), particularly Figs. 43 and 44.

Theory of Electrical Contact Between Solids

H. Y. Fan
Radio Research Laboratory, National Tsing Hua University, Kunming, China
(Received November 6, 1941)

The phenomena of electrical contact are examined in detail. The difference between the behaviors of metals and semi-conductors is pointed out. It is shown that the density of conduction electrons in a semi-conductor can be expected to change appreciably from its normal value which may be important for the explanation of certain phenomena.

INTRODUCTION

THE theory of electrical contact between two metals gives the well-known relation between the contact potential and the work functions of the metals. A theory has also been developed for the contact between a metal and a semi-conductor.[1] The theories are necessarily very crude as the subject concerns the surface phenomena. Since the surface is a region of discontinuity, the phenomena taking place there are much more difficult to handle than those inside the body and rigorous treatment would be very difficult. However, by examining the problem more closely we can get a clearer picture, bring out explicitly the assumptions and limitations of the existing theories and derive some additional information about the problem. This is the purpose of the present paper.

To simplify the problem we shall assume that the electron energy states are not affected by the surface. Various investigators[2] have shown that the surface gives rise to energy states within the forbidden band and other changes. To take such effects into consideration would greatly complicate the problem. As the number of surface states is small compared with the number of normal states we shall make the approximation of neglecting them.

SURFACE POTENTIAL BARRIER

The potential of an electron inside a solid is periodic with the period of the lattice, going through deep depressions in the neighborhood of each atomic nucleus. It rises sharply at the surface forming a potential barrier which keeps the electrons confined to the body. The potential energy is lowered inside a solid owing to the actions of the positive charges of the atomic nuclei and of the negative charges of the rest of the electrons. (Determining factors in the latter action are the exchange forces between electrons of the same spin and the electrostatic repulsive forces between pairs of electrons.) These actions of the charges continue outside the body. In the case of metals these actions reduce to the image force at sufficient distances from the surface. The above cause of the lowering of the potential energy inside a solid is a volume effect. In addition the potential barrier is affected by surface phenomena. The electron distribution around the surface ions is not symmetrical because of the fact that the charge about these ions on the inner side of the surface is different from that on the outside. This unsymmetrical distribution of negative electrons around positive ions results in a double layer which produces a potential difference across the surface. It has been shown by Bardeen[3] that for pure metals the surface double layer plays only a minor part.

Let us consider the relation between the potentials inside two solids in contact. When the bodies are far apart the relation is indicated by Fig. 1a. As they approach each other closer and closer the two parts of Fig. 1a simply shift toward each other (Fig. 1b) until at sufficiently

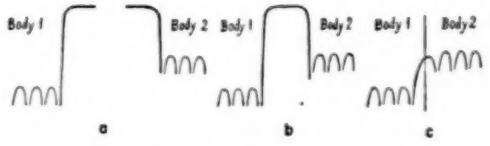

FIG. 1. (a) Potential barrier bodies far apart; (b) bodies near each other; (c) bodies in contact.

[1] A. H. Wilson, Proc. Roy. Soc. **A136**, 487 (1932).
[2] E. T. Goodwin, Proc. Camb. Phil. Soc. **35**, 205 (1939).
[3] E. Wigner and J. Bardeen, Phys. Rev. **48**, 84 (1935); J. Bardeen, Phys. Rev. **49**, 653 (1936).

close distances the distributions of electrons near the surfaces of the two bodies begin to change under mutual interaction of the charges of the two bodies. The potential barriers will then be changed. As a result we cannot simply shift the two parts closer to each other at such close ranges. If we neglect, however, the change of potential barriers owing to changes of charge distribution near the surface then the relation will be given by Fig. 1c. Actually such a picture does not correspond to equilibrium, which requires that the number of electrons entering one body from the other must be just balanced by the flow in the opposite direction. (Of course the energies carried by the electrons flowing in opposite directions must also balance each other.) This condition has not yet been taken into consideration.

CONTACT BETWEEN TWO METALS

The energy levels of solids are grouped into bands separated by gaps of forbidden energy. The lower bands are filled with electrons, each level having its full quota of two electrons. In metals there is a band only partially filled above the full bands. This is the conduction band, only electrons of this band participating in conduction. Upon coming into contact with another metal the full bands having their full quota of electrons cannot receive any more from the latter, and under equilibrium conditions no electrons should go over to the other metal from these bands. Therefore these bands can be disregarded in considering the exchange of electrons between the two metals and only the conduction bands need be considered. The electrons are distributed among the energy levels according to Fermi-Dirac statistics:

$$n=\frac{2}{e^{(E-\zeta)/KT}+1}. \tag{1}$$

The parameter ζ is the thermodynamic potential per electron and is determined by the total number of electrons which should be equal to the summation of n over all energy states. The choice of energy zero is arbitrary and it is convenient to choose the bottom of the conduction band. Figure 2a shows the potential barriers and conduction bands for two metals and Fig. 2b shows the two metals in contact. We have disregarded the condition for equilibrium. The bottom of the conduction band should actually not be at the same level clear up to the surface as indicated by horizontal line O_1 or O_2, since the potential near the surface is not the same as that inside the body. But this takes place near the very surface and we neglect it to simplify the picture and bring out the points we want to emphasize.

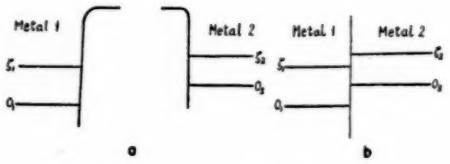

FIG. 2. (a) Potential barriers and conduction bands; (b) metals in contact.

Let us now consider the equilibrium condition. Frenkel[4] gave a good discussion using the free electron model. Bethe[5] gave substantially the same treatment, but he used a wave-mechanical treatment. We shall give Bethe's derivation with a few additions for clearer understanding. The wave function of an electron in a periodic field inside a solid is of the form:

$$\psi=e^{ikr}u, \tag{2}$$

where u is a periodic function with period of the lattice. The velocity of the electron in the direction x is

$$v_x=(2\pi/h)(\partial E/\partial k_x), \tag{3}$$

the electron energy being a function of $k(k_x, k_y, k_z)$. The number of electrons in body 1 arriving at the boundary surface (YZ plane) with a velocity component toward body 2 is

$$\frac{2}{(2\pi)^3}\int dk_x^1\int_{-\infty}^{\infty}dk_y^1\int_{-\infty}^{\infty}dk_z^1 \times\frac{2\pi}{h}\frac{\partial E_1}{\partial k_x^1}\frac{1}{e^{(E_1-\zeta_1)/KT}+1}. \tag{4}$$

The integration with respect to k_x^1 is over all values for positive v_x. This integral can be re-

[4] J. Frenkel, *Wave Mechanics, Elementary Theory.*
[5] A. Sommerfeld and H. Bethe, *Handbuch der Physik*, Vol. 24/2.

written by changing the variable from k_x^1 to E_1

$$\frac{2}{(2\pi)^3}\int_{-\infty}^{\infty}dk_y^1\int_{-\infty}^{\infty}dk_z^1\int_{(E_1)}^{\infty}\frac{dE_1}{e^{(E_1-\zeta_1)/KT}+1}, \quad (5)$$

where (E_1) is the minimum value of E_1 for the set values of k_y^1 and k_z^1. Similarly the number of electrons arriving at the contact surface from body 2 heading for body 1 is

$$\frac{2}{(2\pi)^3}\int_{-\infty}^{\infty}dk_y^2\int_{-\infty}^{\infty}dk_z^2\int_{(E_2)}^{\infty}\frac{dE_2}{e^{(E_2-\zeta_2)/KT}+1}. \quad (5a)$$

Let the wave number (k_x^1, k_y^1, k_z^1) of an electron in body 1 change to (k_x^2, k_y^2, k_z^2) upon crossing the contact surface. To insure the same relation along the contact surface between the wave functions on both sides we must have $k_y^1=k_y^2$ and $k_z^1=k_z^2$. Since the electron energy should remain the same we have the following relation:

$$E_2(k_x^2, k_y^2, k_z^2)=E_1(k_x^1, k_y^1, k_z^1)-P, \quad (6)$$

where P is the difference between the energy zeros adopted for the two bodies. Whether an electron may enter a body or not depends in the first place upon the occupation of the particular energy level by electrons. The probability can be written in the form:

$$1-\frac{\alpha}{e^{(E_2+P-\zeta_1)/KT}+1} \quad (7)$$

for electrons of energy E_2 in body 2 to enter body 1, and correspondingly

$$1-\frac{\alpha}{e^{(E_1-P-\zeta_2)/KT}+1} \quad (7a)$$

for electrons of energy E_1 in body 1 to enter body 2. Furthermore electrons may suffer reflection at the boundary surface where two different periodic fields join together. We have to introduce a transmission coefficient which is a function of the wave numbers: $D(k_x, k_y, k_z)$ or $D(E, k_y, k_z)$. The number of electrons entering body 2 is

$$\frac{2}{h(2\pi)^2}\int_{-\infty}^{\infty}dk_y^1\int_{-\infty}^{\infty}dk_z^1\int_{(E_1)}^{\infty}D_{12}(E_1, k_y^1, k_z^1)$$
$$\times\frac{1}{e^{(E_1-\zeta_1)/KT}+1}\left(1-\frac{1}{e^{(E_1-P-\zeta_2)/KT}+1}\right)dE_1. \quad (8)$$

The number of electrons entering body 1 is

$$\frac{2}{h(2\pi)^2}\int_{-\infty}^{\infty}dk_y^2\int_{-\infty}^{\infty}dk_z^2\int_{(E_2)}^{\infty}D_{21}(E_2, k_y^2, k_z^2)$$
$$\times\frac{dE_2}{e^{(E_2-\zeta_2)/KT}+1}\left(1-\frac{1}{e^{(E_2+P-\zeta_1)/KT}+1}\right)$$
$$=\frac{2}{h(2\pi)^2}\int_{-\infty}^{\infty}dk_y^1\int_{-\infty}^{\infty}dk_z^1$$
$$\times\int_{(E_2)+P}^{\infty}D_{21}(E_1-P, k_y^1, k_z^1)$$
$$\times\frac{dE_1}{e^{(E_1-P-\zeta_2)/KT}+1}\left(1-\frac{1}{e^{(E_1-\zeta_1)/KT}+1}\right). \quad (8a)$$

The lower limit of integration for E_1 in (8) and (8a) should be the same. Let $(E_1)<(E_2)+P$. The electrons with energies $E_1<(E_2)+P$ cannot, however, enter body 2 in which no electrons can have energy less than (E_2). These electrons must be reflected. The transmission coefficient obeys a general theorem which states in terms of our notation: $D_{12}(k_x^1, k_y^1, k_z^1)=D_{21}(k_x^2, k_y^2, k_z^2)$; it follows: $D_{12}(E_1, k_y^1, k_z^1)=D_{21}(E_1-P, k_y^2, k_z^2)$. Thus we have

$$\int_{-\infty}^{\infty}dk_y^1\int_{-\infty}^{\infty}dk_z^1\int_{E_1^0}^{\infty}D_{12}(E_1, k_y^1, k_z^1)$$
$$\times\frac{dE}{e^{(E_1-\zeta_1)/KT}+1}\left(1-\frac{1}{e^{(E_1-P-\zeta_2)/KT}+1}\right)$$
$$=\int_{-\infty}^{\infty}dk_y^2\int_{-\infty}^{\infty}dk_z^2\int_{E_1^0}^{\infty}D_{12}(E_1, k_y^1, k_z^1)$$
$$\times\frac{dE_1}{e^{(E_1-P-\zeta_2)/KT}+1}\left(1-\frac{1}{e^{(E_1-\zeta_1)/KT}+1}\right), \quad (9)$$

where E_1^0 is the common lower limit of integration. This reduces to

$$\int_{-\infty}^{\infty}dk_y^1\int_{-\infty}^{\infty}dk_z^1\int_{E_1^0}^{\infty}D_{12}(E_1, k_y^1, k_z^1)$$
$$\times\left(\frac{1}{e^{(E_1-\zeta_1)/KT}+1}-\frac{1}{e^{(E_1-P-\zeta_2)/KT}+1}\right)dE_1=0. \quad (10)$$

This equation can be satisfied only with

$$E_1-\zeta_1=E_1-P-\zeta_2$$

or

$$P=\zeta_1-\zeta_2. \tag{11}$$

This means that the energy zero for body 2 (chosen at the bottom of its conduction band) should be higher than that chosen for body 1 by the amount $(\zeta_1-\zeta_2)$, therefore the levels ζ_1 and ζ_2 must be the same energy level when a

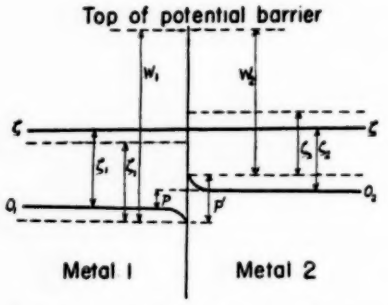

FIG. 3. Energy relations for metals in contact.

common energy scale is taken for the two bodies. This is the condition for equilibrium.

The same result is obtained directly from a general consideration of statistical equilibrium. When groups of electrons are in equilibrium their thermodynamic potentials must be equal. For the conduction electrons of the two bodies to be in equilibrium we must have

$$\zeta_1=\zeta_2=\zeta,$$

when a common energy zero is used for the two bodies. Difference between ζ_1 and ζ_2 must be due to the difference in the chosen energy zeros:

$$P=\zeta_1-\zeta_2.$$

Thus the same result as given by (11) is obtained. The first derivation is given because it shows the physical process more clearly.

Such condition as shown by Fig. 2b does not therefore correspond to equilibrium. More electrons will flow from body 2 to body 1. The former will be charged positively and the latter—negatively. We can look into the problem more closely by using the free electron model and consider the space distribution of the excess or deficiency of electrons and the average potential inside the two bodies. According to Fermi-Dirac statistics the density of electrons in space is given approximately by[6]

$$n=\frac{8\pi}{3h^3}[2m(\zeta-V)]^{\frac{3}{2}}, \tag{12}$$

where V is the potential energy of the electron at the point under consideration. The force driving the electrons from a point of higher to a point of lower potential is compensated by the force resulting from the difference in the electron densities at the two points. In metals the density of conduction electrons is very high and a space charge (excess or deficiency of electrons) enough to produce an appreciable potential field makes little change in the electron density. The action due to the difference of electron densities is, therefore, unimportant in metals. The space distribution of electrons is predominantly governed by electrostatics a fact which shows that charges on metals must be all on the surface (actually—near the surface). At the contact a sort of double layer will be formed. The electron potential inside metal 1 which is negatively charged will be raised and that of metal 2 will be lowered. The energy difference between the level ζ and the bottom of the band, being a measure of the electron density, remains the same inside each metal. At the contact surface we have $\zeta_1'>\zeta_1$ and $\zeta_2'<\zeta_2$ due to the excess of electrons in metal 1 and deficiency in metal 2. The energy difference at the contact between the bottoms of the conduction bands is approximately given by (see Fig. 3):

$$P'=W_1-W_2,$$

in which we have neglected the effects of the proximity of the two metals and of the charges resulting from electron flow on W_1 and W_2.[7] ζ_1' and ζ_2' adjust themselves by the metals' losing or gaining electrons near the surface until the condition for equilibrium (11) is satisfied. The electron potential and consequently the bottom of the conduction band of metal 1 have a convex form near the surface due to the negative charge of excess electrons and those of metal 2, concave. The detailed examination of

[6] J. Frenkel, *Wave Mechanics, Elementary Theory*.
[7] Actually these effects may be very important.

electron exchange at the surface gives in fact only

$$P' = \zeta_1' - \zeta_2', \tag{13}$$

whereas from the general consideration of statistical equilibrium it follows that we should also have

$$P = \zeta_1 - \zeta_2.$$

The work function is defined as the energy difference between an electron at rest outside of the surface and an electron at energy level ζ. The space charge near the surface due to excess or deficiency of electrons causes an additional potential difference between the interior of the metal and the outside. The work function will thus be changed by the contact. Actually such effect should be very small everywhere except at the contact. This can be made clear by the following consideration. The charges at the contact surface are responsible for producing the shift of potential

$$\begin{aligned} P' - P &= W_1 - W_2 - (\zeta_1 - \zeta_2) \\ &= (W_1 - \zeta_1) - (W_2 - \zeta_2) = \varphi_1 - \varphi_2. \end{aligned} \tag{14}$$

These charges are distributed over a very narrow region near the contact surface, this shift having to be produced within a very short distance, therefore the density of charges must be very high. A uniform layer of positive charge density ρ_1 of thickness a joining a uniform layer of negative charge density $-\rho_2$ of thickness b produces a potential difference between the two ends

$$\Delta V = \rho_1 a^2/2 + \rho_2 b^2/2. \tag{15}$$

To make $dv/dx = 0$ at the two ends the following relation has to hold

$$\rho_1 a = \rho_2 b.$$

Therefore

$$\Delta V/4\pi = \tfrac{1}{2}\rho_1 a(a+b) = \tfrac{1}{2}\sigma(a+b). \tag{16}$$

σ is the charge of each sign per unit area. Such a rough picture shows that the charge near the contact per unit area is

$$\sigma_c = \frac{P' - P}{\tfrac{1}{2}(a+b)} = \frac{\varphi_1 - \varphi_2}{\tfrac{1}{2}(a+b)}. \tag{17}$$

Consider on the other hand the charges at the surfaces A and B of Fig. 4. The potential difference between two points each immediately outside the surface of one metal is defined as contact potential and is given by the difference between the work functions of the two metals:

$$V_C = \varphi_1 - \varphi_2. \tag{18}$$

The potential difference between the surfaces A and B is

$$4\pi\sigma d = \varphi_1 - \varphi_2,$$

therefore

$$\sigma_A = \sigma_B = (\varphi_1 - \varphi_2)/4\pi d. \tag{19}$$

Since for metals charges must be nearly on the surface, the values of a and b of (17) must be very small. σ_C and σ_A will be of different orders of magnitude. The effect of σ_A on the potential between a point inside and a point immediately outside the metal must be negligible compared with such effect of σ_C which is measured by $(\varphi_1 - \varphi_2)$. It follows that the work functions of the metals are not changed appreciably by their coming into contact. The contact potential is quite accurately given by the difference between the original work functions of the metals.

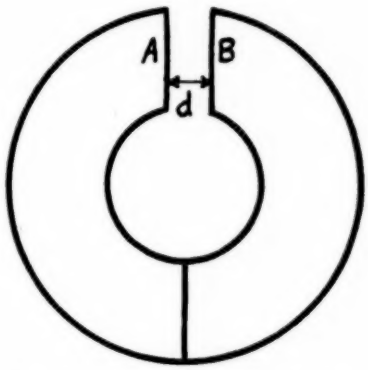

FIG. 4. Arrangement of two metals.

CONTACT BETWEEN METALS AND SEMI-CONDUCTORS (OR INSULATORS)

In an insulator the highest occupied band is completely full of electrons at 0°K and the next higher band is empty. At higher temperatures a small number of electrons will go over to the higher band. Depending upon whether the number of electrons going over to the higher band is large or small the substance is classified as insulator or semi-conductor. A semi-conductor has usually another source of electrons. Such

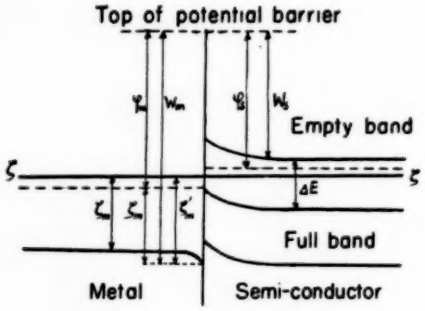

FIG. 5. Energy relations for a metal and semi-conductor in contact.

substance usually has impurity atoms with localized electron energy levels. These atoms may supply electrons to the empty band by being ionized or absorb electrons from a full band in case of electronegative atoms. Besides, their energy levels may provide a sort of stepping stone for the electrons of a full band to go over to the higher empty band.[8] For each kind of substance we have a definite relation between the numbers of electrons in the different bands and impurity levels. The numbers of electrons are all functions of the thermodynamic potential ζ. The latter can therefore be determined from this relation. Fowler[9] gives expressions of ζ for different types of semi-conductors in terms of the density of impurity atoms and the energy gaps between the different bands and the impurity levels. It is shown that as first approximation ζ lies half way between the two sets of energy levels, one full and one empty. The contact between a semi-conductor and a metal is usually treated by simply putting ζ's of the two substances on the same level.

As we have seen, in order to bring about equilibrium an initial unbalanced flow of electrons is required, resulting in the bodies becoming charged. The electron density in the semi-conductor will therefore be changed upon coming into contact with the metal. The normal relation between the number of electrons in the different bands will be upset and ζ will not be given by the usual expression. But it can be shown by a rough estimation that such effect is ordinarily small. For an intrinsic semi-conductor (no impurity) ζ obtained by equating the number of electrons in the conduction band and the number of holes in the next lower band is given by:[9]

$$\zeta=\tfrac{1}{2}\Delta E+KT\log C, \tag{20}$$

where C is a constant and ΔE is the energy gap between the two bands. If the number of electrons in the conduction band should be increased to N times the number of holes in the lower band the increase in ζ will be:

$$\Delta\zeta=KT\log\sqrt{N}. \tag{21}$$

With $N=10$ and at $T=300°$K this amounts to only 0.03 electron volt. This is small compared with the order of magnitude of ΔE (0.72 ev for Cu_2O).[10]

Although the effect of the contact on ζ itself is small the electron density in the conduction band which is normally small can be changed appreciably. Therefore the change in ζ should not be neglected when the electron density is being considered and it is not proper simply to equate ζ of the metal with the original ζ of the semi-conductor. Since there are only a few electrons in the conduction band of a semi-conductor their distribution is Maxwellian. For simplicity of treatment it is usually assumed that these electrons behave like free electrons with an effective mass. While this is not strictly correct[11] rigorous treatment would be too complicated. With this approximation the density of electrons is given by the usual formula for an electron gas:

$$n=2\frac{(2\pi mkT)^{\frac{3}{2}}}{h^3}e^{\zeta/KT}, \tag{22}$$

the potential energy of the electrons or the bottom of the conduction band being taken as zero. When the semi-conductor is in contact with a metal ζ is changed due to the gain or loss of electrons. By entering the expression for n in the exponential factor it is found a small change in ζ will cause considerable change in n, in agreement with the statement made above. The energy difference between the bottoms of the conduction bands is given by (W_m-W_s), there-

[8] B. Gudden, Ergebnisse d. exakten Naturwiss., Vol. 13.
[9] R. H. Fowler, *Statistical Mechanics*, second edition.
[10] W. Juse and B. W. Kurtschatow, Physik. Zeits. de Sowjetumon **2**, 453 (1932).
[11] N. F. Mott and H. Jones, *Theory of Properties of Metals and Alloys*, p. 83.

fore as shown by Fig. 5:

$$\zeta = \zeta_m' - W_m + W_s. \tag{23}$$

The semi-conductor is charged positively or negatively depending upon whether $\varphi_m > \varphi_s$ or $\varphi_m < \varphi_s$. (Figure 5 shows the semi-conductor positively charged.) In the first case the electron density in the conduction band will be less than normal and the reverse is true for the second case. The excess of deficiency in electrons will not be concentrated near the surface as in metals. Because the numbers of electrons in the conduction band and holes in the lower band are small a semi-conductor can support a space charge and appreciable potential difference. The density of conduction electrons at the contact surface is given by (22). The space charge (conduction electrons and holes in the lower band) inside the body is determined jointly by Poisson's equation and Boltzmann's distribution law. With the additional condition of equilibrium between the electrons in the two bands the density of conduction electrons and the density of the holes in the lower band can be determined separately.

The space variation of the density of conduction electrons to be expected in semi-conductors may be important in the explanation of certain phenomena. Upon this is based Schottky's theory[12] of semi-conductor rectifiers which assumes the semi-conductor to be charged positively with region of low electron density at the contact.

[12] W. Schottky, Zeits. f. Physik **113**, 367 (1939).

MARCH 1 AND 15, 1942 PHYSICAL REVIEW VOLUME 61

Distribution in Angle of Protons from the D-D Reaction

H. P. MANNING, R. D. HUNTOON,* F. E. MYERS,† AND V. J. YOUNG
Department of Physics, New York University, New York, New York

(Received December 5, 1941)

The angular distribution of the disintegration protons from the D–D reaction has been investigated as a function of energy from 60 kev to 390 kev. The distribution was found to be well represented by $I(\theta) = 1 + A \cos^2\theta$ at any one energy. The value of A increases smoothly with bombarding energy over the range investigated.

INTRODUCTION

MEASUREMENTS of the relative yield of protons from the reaction

$$H^2 + H^2 = H^3 + H^1$$

as a function of the angle of the emitted proton with the line of approach of the deuterons have shown an anisotropy of the form

$$I(\theta) = 1 + A \cos^2\theta$$

in the center of mass system of coordinates. Previous investigators[1,2] have disagreed markedly on the value of A and its dependence upon energy.

The desired condition for angular distribution measurements where the anisotropy is energy dependent is that all observed disintegrations be due to impinging particles having the same energy at the time of impact. This condition is most nearly realized in a gas target. Without using foils thick enough to invalidate the use of a gas target, permanent gases require the use of a very small capillary and high speed pumping at high vacuum and at an intermediate pressure. Vapors can be handled with a larger capillary and a cold trap, refrigerated with liquid air. This allows higher counting rates and a great reduction in statistical error without loss in angular resolution. Thus, since the deuteron reaction with oxygen is highly improbable below

* Now at National Bureau of Standards, Washington, D. C.
† Now at Frankford Arsenal, Philadelphia, Pennsylvania.
[1] Huntoon, Ellett, Bayley and Van Allen, Phys. Rev. **58**, 97 (1940).
[2] Kempton, Browne, and Maasdorp, Proc. Roy. Soc. **A157**, 386 (1936); Haxby, Allen, and Williams, Phys. Rev. **55**, 1940 (1939); H. Neuert, Ann. d. Physik **36**, 437 (1939).

300 kev, we have been led to the choice of heavy water for the target.

APPARATUS

Accelerating potentials were obtained from a Cockcroft-Walton voltage quadrupler and measured by a resistance voltmeter. The voltmeter was calibrated and periodically checked by measuring the voltage-current characteristics of the resistor. The beam was magnetically analyzed before entering the target assembly. This allowed a check for linearity of the voltmeter by setting the analyzing magnet and changing the voltage to bring the various m/e components of the beam into the target chamber and showed the voltmeter to be linear within 2 percent over the energies used.

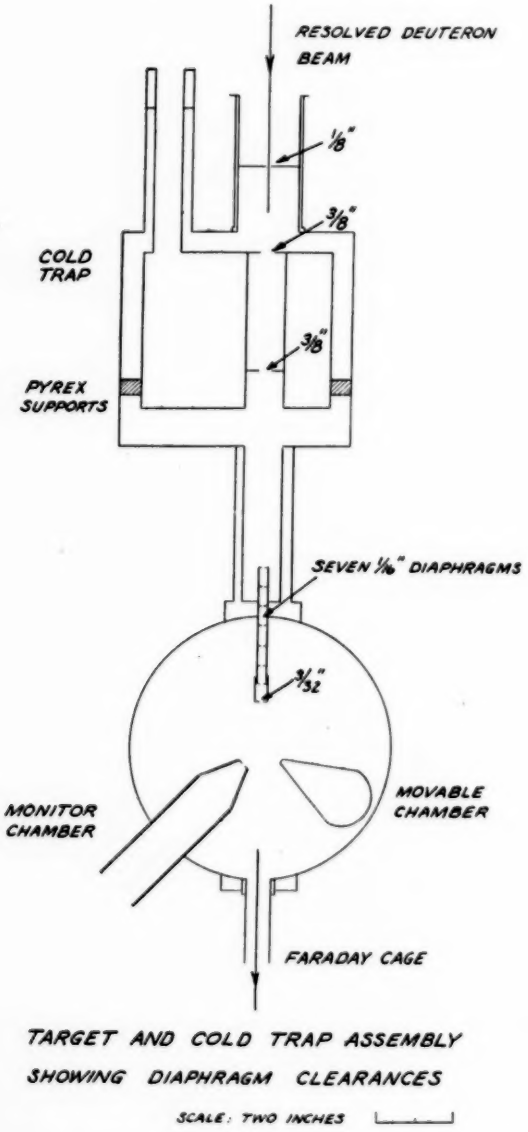

FIG. 1. Target and cold trap assembly showing the path of the beam and all diaphragm clearances beyond the analyzing magnet.

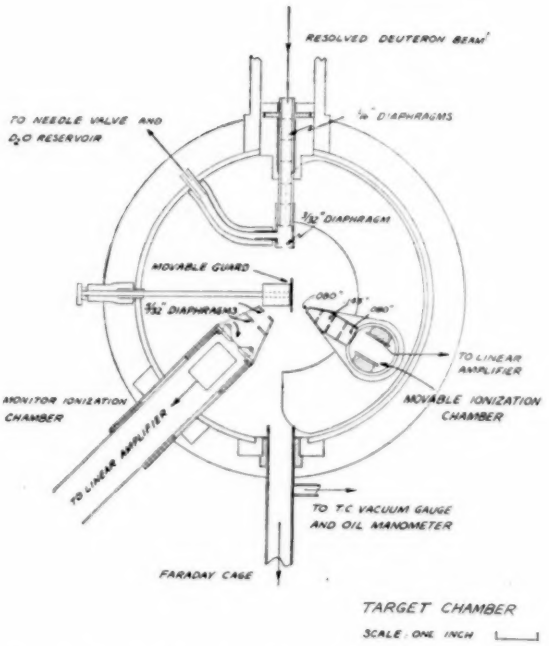

FIG. 2. Detailed drawing of target chamber. The guard, used to measure background of the counters, is shown in a position to block the movable ionization chamber.

In connection with a separate experiment, performed in this laboratory by Mr. C. M. Crenshaw, the loss of energy of the beam in traversing heavy water vapor was determined. The loss of energy in getting to the observation volume varied from 7 kev at 250 kev to 13 kev at 100 kev. The change in energy of the beam along the part viewed by the ionization chambers was 0.85 kev at 100 kev and 0.45 kev at 250 kev. This latter is the uncertainty in energy due to the thickness of the target.

The disintegration particles were observed by means of two ionization chambers, each one cm deep, and associated amplifiers. The signal to noise ratio of these amplifiers was never less than 10–1 for any of the data taken.

TARGET ASSEMBLY

Figure 1 shows a sketch of the entire assembly below the analyzing magnet. The diaphragms

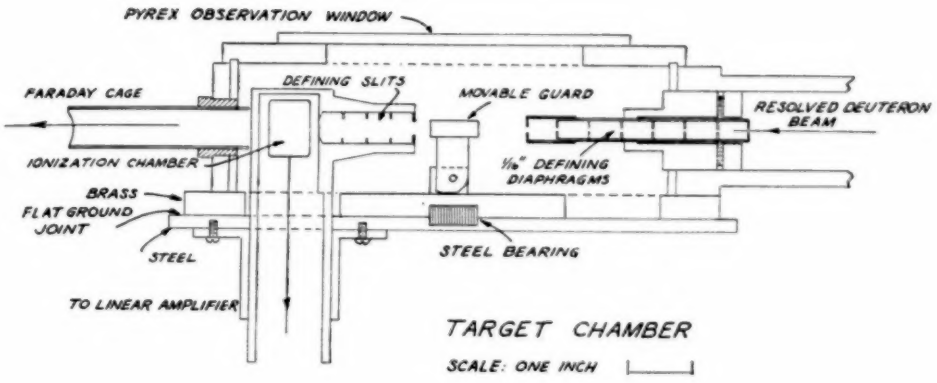

FIG. 3. Edgewise view of the target chamber.

through which the beam entered the target chamber were aligned optically. The seven $\frac{1}{16}$-inch diaphragms forming the entrance capillary to the target chamber, used in conjunction with the cold trap, permitted a pressure of water vapor of more than 1 cm Hg without affecting the pressure in the accelerating tube, although all the data were taken with a pressure of $1\frac{1}{2}$ mm.

Figures 2 and 3 show detailed views of the target chamber. The resolved deuteron beam entered through the diaphragm capillary and struck no solid material until completely out of the target chamber into the Faraday cage. The water vapor was admitted at the base of the entrance capillary to reduce flow through the observation volume. The monitor ionization chamber which was fixed at an angle of 45° to the incoming beam served to measure the relative beam intensity. The movable ionization chamber protruded through a semi-circular slot

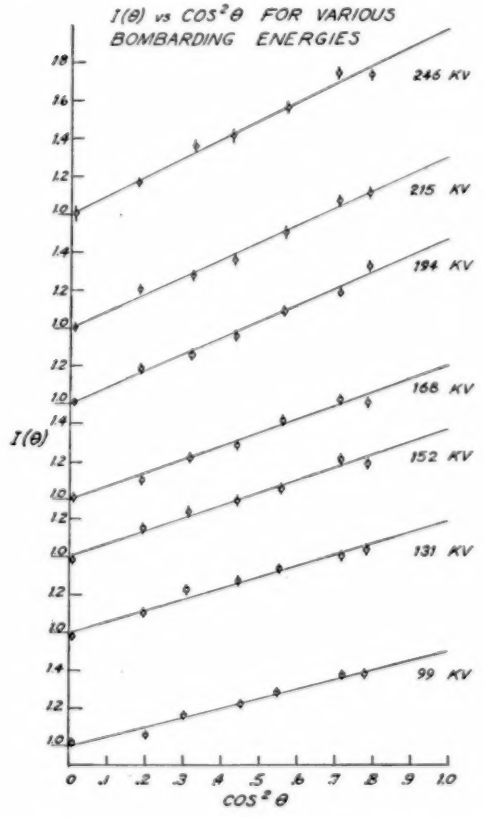

FIG. 4. Data from representative runs showing intensity as a function of $\cos^2\theta$ at various energies.

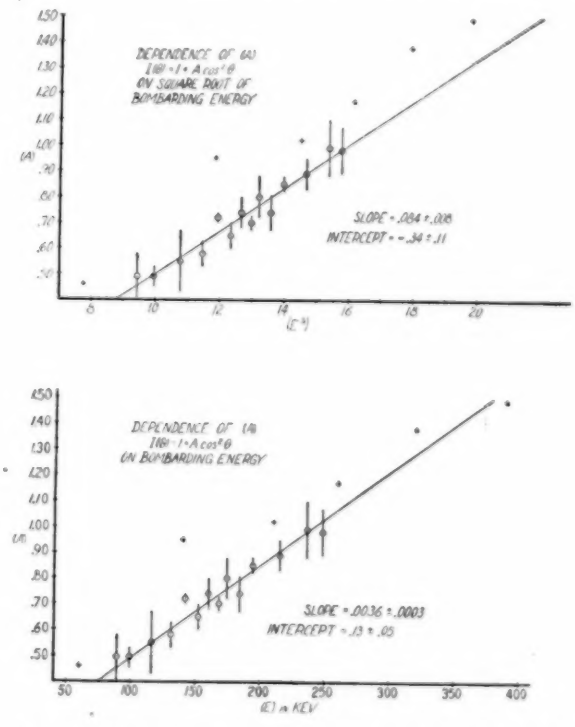
DEPENDENCE OF (A) I(θ)=1+A cos²θ ON SQUARE ROOT OF BOMBARDING ENERGY
SLOPE = .084 ± .008
INTERCEPT = -.34 ± .11
DEPENDENCE OF (A) I(θ)=1+A cos²θ ON BOMBARDING ENERGY
SLOPE = .0036 ± .0003
INTERCEPT = .13 ± .05
E in KEV

FIG. 5. Final results, showing A in $I(\theta)=1+A\cos^2\theta$ as a function of energy. Crosses indicate points taken from Iowa data.

in the back of the target chamber and was externally fastened to a steel plate. The steel plate was ground to the back plate of the assembly and a vacuum seal made with heavy stopcock grease. This type of vacuum seal has proven to be very satisfactory and requires no attention other than occasional greasing. The angular position of the movable chamber was read with an error of less than 5 minutes and was continuously variable from 20° to 160° to the direction of the beam. The entrance capillary and the two ionization chambers were aligned so that their three axes intersected within 0.001 inch of a point on the axis of rotation of the movable chamber.

The background of the movable chamber was found to be appreciable and the installation of a guard, which could be used to block the view of that chamber to the target volume, was necessary. At all times the guard was completely out of the line of the beam, and when not blocking the chamber was completely out of the cross fires of the chamber. When in position, the guard completely shielded the chamber from view of the beam at all positions of the chamber. The background of the monitor chamber was also checked but turned out to be proportional to the strength of the beam, so that it did not alter the results.

COUNTING PROCEDURE

Simultaneous counts were taken in the monitor and movable chambers at each energy for each angle investigated. The ratio of the number of counts in the movable chamber to the number in the monitor was taken and a background ratio subtracted from the total to give the net ratio at each angle. The net ratio was then corrected for geometrical changes from one angle to another and transformed into the center of mass coordinate system. The corrected ratio as a function of $\cos^2\theta$ was then analyzed by least squares and normalized to unity at $\cos^2\theta = 0$.

TABLE I. Values of A obtained for the energies investigated. Probable errors are indicated.

kev	A	p.e.±	kev	A	p.e.±
89	0.49	0.09	168	0.70	0.03
99	0.49	0.04	174	0.80	0.08
116	0.55	0.12	184	0.74	0.07
131	0.58	0.05	194	0.85	0.03
142	0.72	0.02	215	0.89	0.06
152	0.65	0.05	236	0.99	0.11
160	0.74	0.06	246	0.98	0.09

The values of A all conform to certain requirements. Each angle has been observed at least twice, each observation including a background bracketed by two total counts. The total number of counts in the movable chamber for each angle of the run was more than four thousand. Because of its position in the forward direction and sensitivity to a larger solid angle, the number of counts in the monitor chamber always exceeded that in the movable one.

RESULTS

Figures 4 and 5 and Table I show the results obtained. These results are in fair agreement with those of Huntoon, Ellett, Bayley, and Van Allen,[1] whose data are indicated by crosses in Fig. 5. A comparison of Fig. 4 of this paper with Fig. 3 of theirs shows the decreased statistical error obtained by the use of a vapor target. The difference in the results obtained in the two laboratories can probably be ascribed largely to a difference in the two voltage scales. On this assumption, the combined data show that the coefficient A increases smoothly with bombarding energy over the range from 60 kev to 390 kev.

We are pleased to acknowledge the generous assistance of Mr. C. M. Crenshaw, not only for the measurements cited earlier, but also throughout the course of the experiment.

Diffuse Reflection of X-Rays by Anisotropic and Isotropic Solids

H. A. JAHN AND K. LONSDALE
The Royal Institution, London, England

(Received January 5, 1942)

THE elastic vibrations of a single crystal cause an extension of reflecting power around each reciprocal lattice point, the intensity of reflection along a given direction depending essentially upon the frequencies of the vibrations propagated in that direction and upon the angular relation of the directions of oscillation to the directions of reciprocal lattice vectors. The expression for the frequencies introduces the elastic constants of the crystal, as has been shown by Waller in his dissertation;[1] and one of us has shown[2] that for a monatomic cubic crystal the general Waller expression can be used to obtain the shapes of the isodiffusion surfaces in the close neighborhood of the reciprocal lattice points (L, M, N) in the following form:

$$\begin{aligned} r^2(l,m,n) = [&L^2\{c_{44}^2+c_{44}(c_{11}-c_{44})(m^2+n^2)+(c_{11}+c_{12})(c_{11}-c_{12}-2c_{44})m^2n^2\} \\ &+M^2\{c_{44}^2+c_{44}(c_{11}-c_{44})(n^2+l^2)+(c_{11}+c_{12})(c_{11}-c_{12}-2c_{44})n^2l^2\} \\ &+N^2\{c_{44}^2+c_{44}(c_{11}-c_{44})(l^2+m^2)+(c_{11}+c_{12})(c_{11}-c_{12}-2c_{44})l^2m^2\} \\ &-2MNmn(c_{12}+c_{44})\{c_{44}+(c_{11}-c_{12}-2c_{44})l^2\}-2NLnl(c_{12}+c_{44})\{c_{44}+(c_{11}-c_{12}-2c_{44})m^2\} \\ &-2LMlm(c_{12}+c_{44})\{c_{44}+(c_{11}-c_{12}-2c_{44})n^2\}] \\ \div [&c_{11}c_{44}^2+c_{44}(c_{11}+c_{12})(c_{11}-c_{12}-2c_{44})(m^2n^2+n^2l^2+l^2m^2) \\ &+(c_{11}+2c_{12}+c_{44})(c_{11}-c_{12}-2c_{44})^2l^2m^2n^2], \end{aligned}$$

where r is the radius of the isodiffusion surface measured from the reciprocal lattice point along the direction (l, m, n); L, M, N, l, m, n being direction cosines. For particular values of $(L, M, N)(l, m, n)$ this expression is readily simplified; a useful way of expressing the results graphically for any particular crystal (that is, for any particular relative values of c_{11}, c_{12}, c_{44}) is to do so by means of a stereographic projection of the isodiffusion surface for each lattice point (L, M, N), a method which reveals very sharply the differences between the reciprocal lattice points of a given anisotropic solid.[3]

Measurement of the diffuse reflecting regions for various planes of sodium single crystals (for which $c_{11}=0.52, c_{12}=0.40, c_{44}=0.41\times10^{11}$ dynes/cm^2)[4] are found to be in excellent agreement with the above formula. The observations were made, with radiation from a copper target, on a succession of Laue photographs taken at small angular intervals in various crystal orientations, over ranges covering the observable regions of reflecting power for all possible planes.[5] Similar photographs of lithium single crystals, which are isomorphous with those of sodium (body-centered cubic structure), indicated that the relative values of the elastic constants of this very light metal are similar to those of sodium. The formula given above applies to all cubic lattices, and in proof of this it has been found that lead single crystals, which are face-centered cubic in structure, but elastically anisotropic in the same sense as sodium $(c_{11}-c_{12}<2c_{44})$ give photographs leading to similar reflecting regions.

For all cubic crystals so far examined $c_{11}>c_{44}$; for some ionic compounds, such as KCl, NaCl, the Cauchy relation $c_{12}=c_{44}$ is fulfilled and $c_{11}\gg c_{44}$. This implies a very small extension of reflecting power along the reciprocal lattice vector itself, for all values of (L, M, N). This and other more detailed consequences of the theory are confirmed by the observations and measurements of Knaggs, Lonsdale and Smith upon single crystals of KCl and NaCl, using the radiation from molybdenum and silver targets.[6]

[1] Waller, Dissertation, Uppsala (1925).
[2] H. A. Jahn, Nature **147**, 511 (1941); Proc. Roy. Soc. London **A179**, 326 (1941).
[3] H. A. Jahn, Proc. Roy. Soc. London (in the press).
[4] S. L. Quimby and S. Siegel, Phys. Rev. **54**, 299 (1938); values extrapolated to room temperatures. See also Fuchs, Proc. Roy. Soc. London **A157**, 444 (1936).
[5] K. Lonsdale and H. Smith, Nature **148**, 628 (1941).
[6] K. Lonsdale and H. Smith, Proc. Roy. Soc. London **A179**, 8 (1941); see also W. H. Zachariasen, Phys. Rev. **59**, 207 (1941) and other papers in the same volume.

One way of simplifying the general formula given above is to use solids for which the condition of isotropy $c_{11}-c_{12}=2c_{44}$ is fulfilled. The expression then becomes

$$r^2(l, m, n; L, M, N)$$

$$=\frac{1}{c_{11}}+\left(\frac{1}{c_{44}}-\frac{1}{c_{11}}\right)[1-(Ll+Mm+Nn)^2]$$

$$=\frac{\cos^2\theta}{c_{11}}+\frac{\sin^2\theta}{c_{44}},$$

where θ is the angle between the directions l, m, n) and (L, M, N). For pure transverse waves (the case originally considered by Faxén) this reduces to $r^2=(1/c_{44})\sin^2\theta$, and the isodiffusion surfaces have the shape of an anchor ring of vanishing internal diameter, obtained by rotating about the reciprocal lattice vector (L, M, N) two equal circles touching at the reciprocal lattice point, their line of centers being *perpendicular* to the reciprocal lattice vector. The surfaces corresponding to pure longitudinal waves alone, given by $r^2=\cos^2\theta/c_{11}$, would be pairs of equal spheres touching at the reciprocal lattice point, the line of centers being *along* (L, M, N). It is to be noted that even for isotropic solids the formula

$$r^2=(1/c_{11})\cos^2\theta+(1/c_{44})\sin^2\theta$$

leads to a whole series of possible shapes according to the ratio $c_{11}:c_{44}$. Tungsten, for which $c_{11}=51.3$, $c_{12}=20.6$, $c_{44}=15.3\times10^{11}$ dynes/cm²,[7] is an example of a hard, isotropic, body-centered cubic structure. It gives small, elliptical diffuse spot reflections which fade out quickly as the orientation changes, quite unlike the detailed, persistent diffuse spots and streaks obtained for the soft, anisotropic alkali metals and lead.

While Faxén[8] gave a correct formula for the scattering by the longitudinal and transverse waves of an isotropic solid, he also gave an approximate formula $a(\sin\theta+\cos\theta\tan\theta_1)=\lambda$, to which much reference has been made and which has been obtained in various forms by various theoretical processes. This formula is in fact a very poor approximation to the truth. It implies that in the neighborhood of the reciprocal lattice points the isodiffusion surfaces are spheres concentric with those points. This can never really be the case, according to the above theory. For r^2 to be independent of θ, c_{11} must be equal to c_{44}. Since $c_{11}-c_{12}=2c_{44}$, that would mean $c_{12}=-c_{11}=-c_{44}$. Either the compressibility $(c_{11}+2c_{12})$ or the shear coefficient (c_{44}) would thus have to be negative, which is clearly impossible. In fact, for positive compressibility and positive shear coefficient, c_{12} can never have a negative value which is numerically greater than $c_{11}/2$, or a positive value which is greater than c_{11}, and therefore the maximum value of c_{44} which fulfills the isotropy condition $c_{11}-c_{12}=2c_{44}$ is $3c_{11}/4$. This sets an upper limit to the extension of the surfaces of isodiffusion, along the direction of the radius vector for each reciprocal lattice point. It can never be more than $\frac{3}{4}$ of the extension in a perpendicular direction, and is usually considerably less.

[7] P. Bridgman, Proc. Am. Acad. Sci. **60**, 305 (1925); see also Wright, Proc. Roy. Soc. London **A126**, 613 (1930).

[8] Faxén, Zeits. f. Physik **17**, 266 (1923).

On the Theory of Temperature Diffuse Scattering

M. BORN
Department of Mathematical Physics, University of Edinburgh, Scotland
(Received December 19, 1941)

W. H. ZACHARIASEN[1] has published a note under the same title as the present one in which he shows that his results[2] and those obtained by Miss Sarginson and me[3] are in complete agreement (though ours are more general). I wish to emphasize that we have expressed no doubt about the correctness of Zachariasen's formula. Our criticism was directed against the method of derivation, which has been used not only by him but by several authors (quoted in our paper). He remarks that we do not seem to be aware of the fact that our general intensity formula is based on the same approximation as that used by himself. This remark is erroneous and compels me to reply. For although Zachariasen and we are in complete agreement about the fundamental assumptions of the theory of background scattering, and although we have obtained the same results and share the critical attitude against other theories (Preston-Bragg, Raman-Nilakantan), I must insist that Zachariasen's method lacks rigor at the deciding point. It was just this point alone which induced us to reconsider the problem studied already by so many excellent authors. We have tried to explain the situation in the introduction of our paper, but as it seems that it has been misunderstood, I shall try to do it again using Zachariasen's own notation.

The main factor in his expression (5) for the scattered intensity[2] is given by his formula (6), p. 548:

$$\langle \exp\left[i2\pi(\mathbf{k}-\mathbf{k}_0)\cdot(\boldsymbol{\Delta}_l-\boldsymbol{\Delta}_{l'})\right]\rangle_{Av}$$
$$=\exp\{-s^2[\langle(\mathbf{u}\cdot\boldsymbol{\Delta}_l)^2\rangle_{Av}-\langle(\mathbf{u}\cdot\boldsymbol{\Delta}_l)\cdot(\mathbf{u}\cdot\boldsymbol{\Delta}_{l'})\rangle_{Av}]\}, \quad (1)$$

where $s=2\pi|\mathbf{k}-\mathbf{k}_0|=4\pi\sin\vartheta/\lambda$, while $\mathbf{u}$ is a unit vector along $\mathbf{k}-\mathbf{k}_0$. The formula is introduced with the words "One finds readily . . ." As a matter of fact, the transformation expressed by this equation is first given in Debye's original paper[4] and has therefore the weight of authority and age; but it is nevertheless wrong, and this is exactly the point against which my criticism is directed. The procedure leading from the left-hand term to the right-hand term is this: develop

$$\exp\left[2\pi i(\mathbf{k}-\mathbf{k}_0)(\boldsymbol{\Delta}_l-\boldsymbol{\Delta}_{l'})\right]$$
$$=\exp\left[is\mathbf{u}\cdot(\boldsymbol{\Delta}_l-\boldsymbol{\Delta}_{l'})\right]=1+is\mathbf{u}\cdot(\boldsymbol{\Delta}_l-\boldsymbol{\Delta}_{l'})$$
$$-\frac{s^2}{2}[\mathbf{u}\cdot(\boldsymbol{\Delta}_l-\boldsymbol{\Delta}_{l'})]^2+\cdots, \quad (2)$$

average over the atomic displacements $\boldsymbol{\Delta}_l$ and observe that this destroys the linear terms, then replace the first two terms

$$1-\tfrac{1}{2}s^2\langle[\mathbf{u}\cdot(\boldsymbol{\Delta}_l-\boldsymbol{\Delta}_{l'})]^2\rangle_{Av}=1-s^2[\langle(\mathbf{u}\cdot\boldsymbol{\Delta}_l)^2\rangle_{Av}$$
$$-\langle(\mathbf{u}\cdot\boldsymbol{\Delta}_l)\cdot(\mathbf{u}\cdot\boldsymbol{\Delta}_{l'})\rangle_{Av}] \quad (3)$$

by

$$\exp\{-s^2[\langle(\mathbf{u}\cdot\boldsymbol{\Delta}_l)^2\rangle_{Av}-\langle(\mathbf{u}\cdot\boldsymbol{\Delta}_l)\cdot(\mathbf{u}\cdot\boldsymbol{\Delta}_{l'})\rangle_{Av}]\}. \quad (4)$$

This procedure would be justified if the quadratic terms in the expansion (2) were small for all values of the $\boldsymbol{\Delta}_l$ which are used in the averaging. But this is not the case.

For the atomic displacements $\boldsymbol{\Delta}_l$ are superpositions of the normal vibrations ξ, and the average of the second-order terms reduces to a sum of terms of the form $\mu\langle\xi^2\rangle_{Av}$. The equiportion law gives for the potential energy of an oscillator of frequency

$$\tfrac{1}{2}\omega^2\langle\xi^2\rangle_{Av}=\tfrac{1}{2}kT, \quad \text{or} \quad \langle\xi^2\rangle_{Av}=kT/\omega^2. \quad (5)$$

Now the frequency spectrum of any crystal lattice has three branches (the acoustical branches) which contain the value $\omega=0$. Hence there are regions in the phase space where $\langle\xi^2\rangle$ is very large for any temperature; the same holds for $\langle\boldsymbol{\Delta}_l\rangle_{Av}$. The $\boldsymbol{\Delta}_l$ are therefore not small throughout, and there is no justification for breaking off the expansion (2) at the second-order terms.

Debye has used this unsatisfactory reasoning in his pioneer work, but Waller already was

[1] W. H. Zachariasen, Phys. Rev. **60**, 691 (1941).
[2] W. H. Zachariasen, Phys. Rev. **57**, 597 (1940).
[3] M. Born and K. Sarginson, Proc. Roy. Soc. **A179**, 69 (1941).
[4] P. Debye, Ann. d. Physik **43**, 49 (1914).

clearly aware of its faultiness. He has devoted a special appendix (Anhang, pp. 54–58) of the first part of his dissertation[5] to an attempt at improving Debye's method, and he has succeeded for the case of high temperatures; but he had to be content with an estimate of the order of magnitude for low temperatures. His careful consideration shows that he considered Debye's result as not at all obvious. Our own paper shows how by rearranging the argument the problem can be reduced to a theorem expressed by the formula

$$\langle \exp(i\mu\xi)\rangle_{Av} = \exp\left[-(\mu^2/2\omega^2)\langle\epsilon\rangle_{Av}\right], \qquad (6)$$

where ξ is the amplitude and ϵ the energy of a harmonic oscillator and the averaging has to be taken over an assembly of quantized oscillators in statistical equilibrium.

The first proof of this theorem was given by Ott,[6] and the whole scattering problem is in principle settled by his paper; in praxis, however, this is not the case as Ott's work is extremely complicated and has a very abstract aim (to show that a correct quantum treatment of all electronic levels of the crystal atoms leads in the end to the same formula as Waller's method which considers only the quantized vibrational levels). Our aim was to give a simple treatment on Waller's lines, but by making use of Ott's formula for which we gave a new and much simpler proof.

After having thus obtained the correct average of the exponential function representing the interference of the scattered x-rays we have, of course, expanded this average with respect to kT/ω_0^2, where ω_0 is a characteristic frequency (for instance the maximum frequency) of the spectrum, and as this ω_0 is not a variable but a constant, this expansion is valid indeed except for very low temperatures (that is very narrow surroundings of a Laue spot). Zachariasen's remark that we have used the same approximation as he is therefore based on a misunderstanding.

I take this opportunity to comment on another paper of Zachariasen[7] in which he applies his scattering formula for cubic lattices and shows that it is possible to express the intensity in terms of the elasticity constants by using a model of the kind suggested by von Kármán and myself, in which forces between the nearest neighbor atoms are introduced. A more satisfactory treatment of this problem is again to be found in Waller's dissertation[5] (Part I, Sections 3, 4), where it is shown that the expression of the scattering intensity in terms of the elasticity constants can be obtained (for the vicinity of a Laue spot) from general properties of lattice vibrations without using a special model. This method of Waller has been applied by Miss Sarginson,[8] and independently by Jahn[9] for calculating the scattering power of cubic crystals, and Mrs. Lonsdale and Smith[10] have shown that Jahn's results are in excellent agreement with the observations. I have further developed Waller's idea[11] and shown that it provides a method (at least in principle) to determine experimentally the complete matrix, which represents the coefficients of the quadratic terms in the potential energy. If this could be done, one could say that the background scattering permits photographing the dynamics of a lattice in the same way as the Laue-Bragg scattering determines its geometry.

[5] T. Waller, Diss. Uppsala (1925).
[6] H. Ott, Ann. de Physique **23**, 169 (1935).
[7] W. H. Zachariasen, Phys. Rev. **59**, 860 (1941).
[8] K. Sarginson, Proc. Roy. Soc. (in press).
[9] H. A. Jahn, Nature **147**, 511 (1941); Proc. Roy. Soc. (in press).
[10] K. Lonsdale and H. Smith, Nature **148**, 628 (1941).
[11] M. Born, Proc. Roy. Soc. (in press).

Letters to the Editor

PROMPT publication of brief reports of important discoveries in physics may be secured by addressing them to this department. The closing date for this department is the third of the month. Because of the late closing date for the section no proof can be shown to authors. The Board of Editors does not hold itself responsible for the opinions expressed by the correspondents. Communications should not in general exceed 600 words in length.

Nuclear Levels of the Compound Li_5

G. BECK AND SAN-TSIANG TSIEN
Laboratorio de Fisica da Universidade de Coimbra, Portugal, and Institut de Physique Générale de la Faculté des Sciences, Lyon, France
February 10, 1942

THE experimental analysis of the angular and velocity distribution of protons projected by incident α-particles[1] has led one of us to the conclusion that the compound nucleus Li_5 has, in the examined energy range, six levels corresponding to the energies

0.56 0.64 0.74 0.83 0.91 1.00 mev.

Spacing and breadth of these levels are of the order of 0.1 mev.

We have applied to these measurements the criteria which had been developed by P. Wenzel,[2] taking into account the fact, that one of the two colliding particles has a spin $\frac{1}{2}$. In this case the scattered resonance wave will be a mixture of two partial waves, e.g., if the resonance level has the angular momentum $\frac{1}{2}$, a mixture of the waves $s_{\frac{1}{2}}$ and $p_{\frac{1}{2}}$. Wenzel's maxima curves depend, in this case, not only on the value of the angular momentum of the resonance level, but also on the ratio of mixture of the two partial waves involved. If we determine this ratio in a way to make the maxima curve fit the observed maximum scattering values at $\vartheta=\pi$, we can check its value with the data on the angular dependence of the scattering. We find in this way excellent agreement, if we assume, that the angular momentum of the six levels indicated above is equal to $\frac{1}{2}$. The mixture ratio varies only very slightly for the six investigated levels.

Since the mixture ratio of the $s_{\frac{1}{2}}$ and the $p_{\frac{1}{2}}$ wave is a complex quantity, the argument of which is not known, the experimental values permit one to determine only limits for its absolute value q

$$14 \text{ percent} \leqslant q \leqslant 86 \text{ percent}.$$

The value of q shows that, contrary to what happens if an electron collides with an atom, a proton entering a compound nucleus has a considerable probability of leaving the compound with its original spin direction changed. According to current ideas on nuclear forces a change of spin direction may even occur with considerable probability in a single collision between two elementary nuclear particles. Our result could be, however, also explained by assuming that the probability for a change of spin direction in an elementary collision is of the order $(v/c)^2 \sim 1$ percent, since the total probability for a change of spin direction of the proton is owing, in our case, to a great number of elementary collisions in the compound state.

[1] San-Tsiang Tsien, J. d. Phys. 1, 1,103 (1940).
[2] P. Wenzel, Zeits. f. Physik 90, 754 (1934).

Quenching and Depolarization of Resonance Radiation by Collisions with Molecules of a Foreign Gas. Remarks on papers by Ellett, Olsen, and Petersen* and by Olsen†

S. MROZOWSKI
Ryerson Physical Laboratory, University of Chicago, Chicago, Illinois
December 6, 1941

MITCHELL and Murphy[1] showed that from a study of the influence of a weak magnetic field on the polarization of the resonance radiation in the presence of a foreign gas one obtains, not τ_0 the lifetime of the unperturbed excited state, but the lifetime

$$\tau_1 = 1/(1/\tau_0 + \alpha p)$$

determined by the emission of radiation (probability $1/\tau_0$) and by quenching collisions (probability $\alpha\mathbf{p}$, $\mathbf{p}$ is the pressure of a foreign gas). The argument of Mitchell and Murphy has to be extended to include the depolarizing collisions. The number N of atoms excited by the absorption of light and remaining in a state from which they can emit polarized light decreases in time not only because of radiation and quenching, but also because of depolarization (probability $\alpha'\mathbf{p}$). The lifetime τ obtained represents not the average lifetime of all the excited atoms but only of those having the orientation in space defined by the direction of polarization of the exciting light ($1/\tau = 1/\tau_0 + \alpha\mathbf{p} + \alpha'\mathbf{p}$). It follows that the quenching cross section reported by Mitchell and Murphy for nitrogen really represents the sum of the cross sections for quenching and depolarization. The situation in the case of such measurements shows great similarity to the case of the measurements of the lifetimes with a fluorometer discussed some years ago by Jablonski.[2]

All depolarizing collisions whose duration is not longer than the lifetime τ are contributing to $\alpha'\mathbf{p}$. Only interactions caused by long range forces, which slowly change the polarization of the excited atoms, could contribute to the depolarization without affecting the value of τ determined from the field dependence. The range of such forces should be very large, at least of the order

$$v \cdot \tau_0 \geqq 100 \text{ } m/\text{sec.} \cdot 10^{-7} \text{ sec.} = 0.01 \text{ mm},$$

where $\mathbf{v}$ is the average velocity of a foreign gas molecule relative to a mercury atom. The probability of such depolarization $\gamma(\mathbf{p})$ would be increasing much slower than proportional to the pressure of the foreign gas. For such long range forces, the number of perturbing molecules surrounding a given excited atom is very large and the resultant perturbation for a uniform distribution would

vanish. Hence the depolarization would depend on the fluctuations in density in the neighborhood of the excited atom (proportional to $\sqrt{\mathbf{p}}$).[4] Naturally for such type of depolarization the calculation of cross section would be meaningless. In addition, the existence of forces of such large range seems very doubtful.

Ellett, Olsen, and Petersen* and recently Olsen† studied the resonance radiation of mercury vapor and obtained for several gases from the field dependence of polarization values for $\alpha+\alpha'$ which are smaller than the sum of the values α and α' determined from the dependence of the polarization on the pressure of a foreign gas with no field present. Therefore, Ellett, Olsen, and Petersen introduced in their theory besides the previously generally accepted kind of non-adiabatic depolarizing collisions leading to non-coherent excited states (probability $\alpha'\mathbf{p}$) a new type of depolarizing collisions, which according to their statement depolarize adiabatically leading to no loss of coherence (probability $\alpha''\mathbf{p}$). Collisions of the latter type should not contribute to τ. From the field dependence one then should obtain only $\alpha+\alpha'$; from the depolarization *versus* pressure with no field present the quenching α and the total depolarization coefficient $\alpha'+\alpha''$. The writer would like to emphasize, that the character of the collisions of the new type ($\alpha''\mathbf{p}$) seems very obscure and that Ellett, Olsen, and Petersen apparently used some different meaning from the commonly adopted meaning of the word "coherence," since a collision occurs *ex definitione* only when the phase of the oscillator has undergone a change (owing to the interaction of the particles). Moreover their exclusion of $\alpha''\mathbf{p}$ from the formula for τ is not justified, since as shown above all depolarizing collisions with a probability proportional to pressure (short and medium range forces) must be included in that formula. On the other hand for such collisions the transitions are not adiabatical. The only way to explain the disagreement of the two sets of experimental data seems to be by introduction of the long range forces (the only kind of adiabatical depolarization) or by taking into account the formation of $^3P_1$ excited atoms from metastable $^3P_0$ states by collisions (the probability $\alpha'\mathbf{p}+\gamma(\mathbf{p})$ would be obtained from the polarization *versus* pressure dependence in the first, $\alpha'\mathbf{p}+\delta(\mathbf{p})$ in the second case).

The question arises if the deviations found by the mentioned authors are real. The discrepancy between the results of Ellett, Olsen, and Petersen in the case of hydrogen and deuterium with results previously obtained by Evans[4] and Suppe[5] (who obtained practically identical curves for both gases, both for quenching and for depolarization) shows that at least some of the investigators overestimated the limits of accuracy of their measurements. The existence and the possible sources of this discrepancy have not been discussed by Ellett, Olsen, and Petersen. In spite of this discrepancy a consideration of their data makes the writer think that in fact the deviations found by them may be real. If so, new considerations must be made, since their explanation has been shown above to be inadequate. The deviations are certainly not caused by the long range forces ($\gamma(\mathbf{p})$), since α'' was found different from zero for rare gases (which certainly cannot exert long range magnetic forces) and $\alpha''=0$ for a paramagnetic molecule O_2. But in the case of N_2, the value of α'' relatively to α' was found to be several times greater than for the rare gases, i.e., α'' has an appreciable value only when metastable $^3P_0$ mercury atoms are known to be present in the vapor. It would be, therefore, worth while to calculate for the temperature given the rate of transfer of metastable atoms into the $^3P_1$ state and to see if by introduction of such a correction term $\delta(\mathbf{p})$ instead of $\alpha''\mathbf{p}$ ($\delta(\mathbf{p})$ for small $\mathbf{p}$ is $\leqq\mathbf{p}^2$, for higher $\mathbf{p}$ the increase is slower due to the slower than $\leqq\mathbf{p}$ increase of the concentration of metastable atoms) a substantially better agreement between theory and experiment could be obtained.

* A. Ellett, L. O. Olsen, and R. Petersen, Phys. Rev. **60**, 107 (1941).
† L. O. Olsen, Phys. Rev. **60**, 739 (1941).
[1] A. C. G. Mitchell and E. J. Murphy, Phys. Rev. **46**, 53 (1934).
[2] A. Jablonski, Zeits. f. Physik **95**, 53 (1935).
[3] R. C. Tolman, *The Principles of Statistical Mechanics* (Oxford, 1938), formulas (141.57) and (141.60) on pp. 646–647.
[4] M. G. Evans, J. Chem. Phys. **2**, 445 (1934).
[5] F. Suppe, Zeits. f. Physik **113**, 141 (1939).

Cloud-Chamber Track of a Mesotron Stopped by Gas

T. H. Johnson and R. P. Shutt
Bartol Research Foundation of the Franklin Institute, Swarthmore, Pennsylvania
February 13, 1942

In the cloud chamber arrangement previously described[1,2] the picture (Fig. 1) has been obtained which shows a mesotron track ending in argon of 1.3 atmospheres. The track, curved by a magnetic field of 1150 oersteds, shows the particle entering a lead plate of 1-cm thickness from which it emerges heavily ionizing. It undergoes 2 single scatterings of about 3° each at A and at B, and it ceases to ionize at C. The approximate mass of the particle has been determined in two ways. First, the radius of curvature of the track above the lead plate is 150 ± 50 cm. Combining this with the fact that its range is approximately 1 cm of lead we find a value of $m=100\pm50$ electron masses. Below the lead plate the radius of curvature between A and B is $\rho_1=23$ cm, and between B and C it is $\rho_2=17$ cm. The total ranges at the corresponding positions are, respectively, $R_1=12.0$ cm and $R_2=6.4$ cm, from which we find $m_1=80$, and $m_2=70$. For the computations of m the energy-momentum curves published recently by Rossi and Greisen[3] have been used.

The rather large curvatures in the second compartment can be measured with considerable accuracy, but errors are introduced by the multiple scattering which produces additional curvatures superimposed upon those caused by the magnetic field. Williams[4] has deduced the *average* radius of curvature ρ_s owing to the multiple scattering near the end of a track and finds

$$\rho_s\approx R\times1.3(m/Z)^{\frac{1}{2}},$$

where R is range of the particle, m is its mass, and Z is the atomic number of the scattering gas. As ρ_s may be either positive or negative one has to write

$$1/\rho-1/\rho_s<1/\rho_p<1/\rho+1/\rho_s,$$

where ρ_p stands for all probable values of the radius of

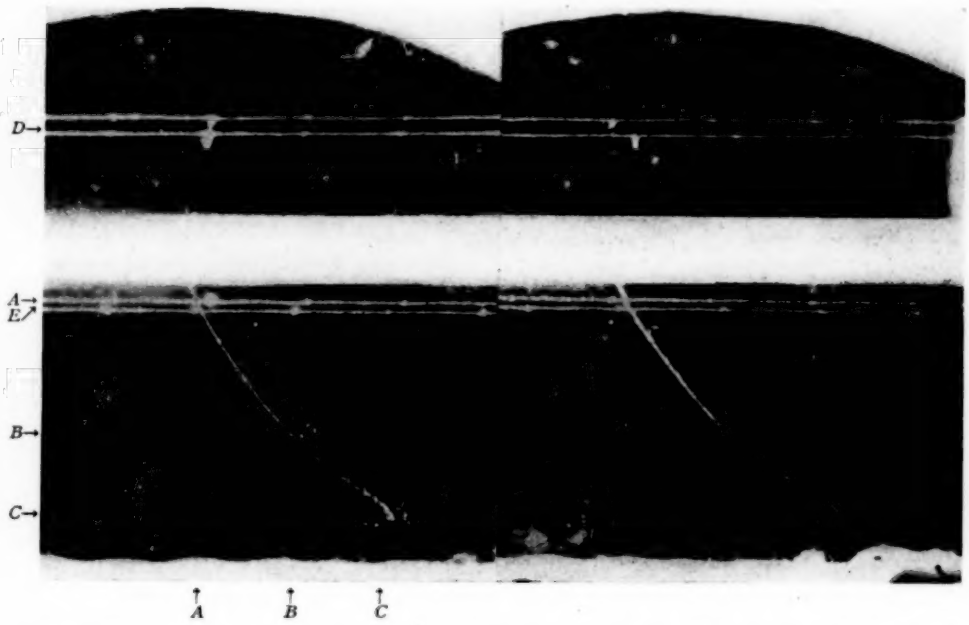

FIG. 1. Stereoscopic photographs of negatively charged mesotron stopping in the gas of the cloud chamber. Between the two compartments there is a lead plate 1 cm thick. *D* and *E* indicate scales aiding in the exact determination of geometrical positions.

curvature caused by the magnetic field alone. In our case one finds 11 cm $< \rho_{p1} <$ 42 cm and 6 cm $< \rho_{p2} <$ 39 cm. These give $m_{p1}=80$ with an uncertainty of $(+105, -55)$ and $m_{p2}=70(+150, -55)$. Averaging over m_1 and m_2, we have $m=75(+90, -40)$. This value is lower than that usually found, but this may arise from the inaccuracy introduced by the multiple scattering.

The direction of curvature is that of a negatively charged particle. It is also noted that no disintegration electron appears near *C*. The track ends at a distance of 1.4 cm in front of the background velvet. Near *B* it goes out of the directly illuminated part of the chamber and receives its light only from numerous mirrors placed around and inside the chamber, but by comparison with other pictures taken in the same arrangement a track of low density such as that of a fast electron would still be visible as close as 0.5 cm to the velvet. A mesotron at the point where it stops ionizing still has an energy of between 10^3 and 10^4 ev or a velocity of about 5×10^8 cm per sec. Since the particle appears not to disintegrate within a sphere of 0.9-cm radius around the end of the track, its lifetime after it had ceased to ionize must have been greater than 10^{-8} sec., with allowance made for a considerable increase of its path by scattering. Because of the high residual velocity of a mesotron after it stops losing energy by ionization, one cannot expect to find a disintegration electron near the end of every mesotron track. Table I shows a record of all published photographs of mesotrons stopping in the gas of a cloud chamber. Reviewing the records it appears that disintegration electrons have only been found from positive mesotrons.

TABLE I. Data on mesotrons stopped in gas of cloud chambers.

Reference	Number of electron masses	Charge	Electron track appearing near end of mesotron track	Remarks
a	220±35	+	slight indication	good, stereoscopic pictures
b	170±9	−	no	doubtful, nonster. pict.
c	20?	+		very doubtful,
	100±30	+		stereosc. pictures
	120±30	−	no	
	55±35	−		
	170±100	+		
d	250±70	+	yes	good, stereosc. pict.
e	not determined		yes(?)	somewhat doubtful, stereosc. pict
	not determined		yes(??)	
This article	75(+90, −40)	−	no	stereoscopic pictures

Concerning the frequency of ends of mesotron tracks occurring in the gas of a cloud chamber we should expect according to Williams[5] to find 8×10^{-7} particles per cm. With one such track found among 42,000 pictures in a cloud chamber containing 50 cm of gaseous path we actually find 5×10^{-7} track ends per cm.

The authors are indebted to the Carnegie Institution of Washington for extensive support given to these researches. They also wish to thank Mr. M. H. Hornstine and Mr. W. C. Sheppard for their assistance in operating the cloud chamber.

[a] S. H. Neddermeyer and C. D. Anderson, Phys. Rev. **54**, 88 (1938); Rev. Mod. Phys. **11**, 191 (1939).
[b] Y. Nishina, M. Takeuchi, and T. Ichimiya, Phys. Rev. **55**, 585 (1939).
[c] H. Maier-Leibnitz, Zeits. f. Physik **112**, 569 (1939).
[d] E. J. Williams and G. E. Roberts, Nature **145**, 102 (1940).
[e] E. J. Williams and G. R. Evans, Nature **145**, 818 (1940).

[1] T. H. Johnson, J. G. Barry, and R. P. Shutt, Phys. Rev. **59**, 470 (1941).
[2] R. P. Shutt, Phys. Rev. **61**, 6 (1942).
[3] B. Rossi and K. Greisen, Rev. Mod. Phys. **13**, 240 (1941).
[4] E. J. Williams, Phys. Rev. **58**, 292 (1940).
[5] E. J. Williams, Proc. Roy. Soc. **A172**, 194 (1939).

On the Validity of the Langevin Theory of Orientation and the Possibility of Distinguishing Between Inherent and Photoelastic Anisotropy

WILFRIED HELLER, *School of Chemistry, University of Minnesota, Minneapolis, Minnesota*

AND

GERMAINE QUIMFE, *Laboratoire des Recherches Physiques, Sorbonne, Paris, France*

February 13, 1942

The linear magneto-optical anisotropy of homogeneous and dispersed systems can be explained as the result of orientation of anisotropic elements, e.g., of molecules or crystals. This explanation is supported by experimental regularities, but no direct proof has been given. Such a proof may be based on the concept that orientation alone should not change the optical properties of the individual elements. A simple calculation[1,2] shows that for uniaxial particles

$$(f_{\parallel}-f_i)/(f_i-f_{\perp})=R=2.0, \qquad (1)$$

in which f_i is an optical constant, refraction index, absorption coefficient, etc., of the statistically isotropic system in zero magnetic field and $f_{\parallel}$ and $f_{\perp}$ represent the same constant in directions parallel and perpendicular to a magnetic field. No experimental test of the relation except the inconclusive one of Cotton and Mouton[1] has been made. At the suggestion of A. Cotton we used apparatus constructed for special colloid-optical work[3] which gave direct value of the absorption coefficients k_i, $k_{\parallel}$, and $k_{\perp}$. Its principle is shown in Fig. 1.

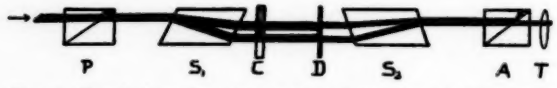

FIG. 1. *P*, polarizer; S_1, calcite prism; *C*, trough with two compartments (shaded part for colloidal solution, blank part for water); *D*, double-diaphragm; S_2, calcite prism; *A*, analyzer; *T*, telescope; light beam (unsplit and split) drawn in black; magnetic field: at *C*, parallel to paper plan and perpendicular to light beam.

TABLE I. Value of $R=(k_{\parallel}-k_i)/(k_i-k_{\perp})$ for an iron oxide sol. Temperature 20°, $\lambda=5400$A.

H(gauss)	3750	5200	7470	9510	11000	12150	13300
R	1.5	1.5	1.78	1.88	1.88	1.88	1.90

Table I gives a selection of data on an iron oxide sol that contained plate-like α-FeOOH crystals. At fields above 10,000 gauss, the value of R is nearly that given by (1). The deviation at lower fields is probably due to the strong heterodispersion of the sol used and the dependence of optical constants on size of particles in regions near an absorption band.[4] In order to obtain $R=2$, strong fields in which few particles, large or small, escape orientation must be used. In any case, the satisfactory result at high fields indicates that the linear magnetic dichroism (and implicitly, magnetic double refraction) is an effect of orientation of anisotropic particles.

A different situation is expected in the anisotropy of optical properties in electric fields or under hydrodynamical orientation. Here relation (1) may become valuable for detecting anisotropies not due to orientation alone, such as photoelasticity. In hydrodynamical orientation, a shear at sufficiently high velocity gradients may lead to a reversible or irreversible deformation of the elements if their internal elasticity is much lower (or plasticity higher) than that of crystals. Protein molecules and particle aggregates in which individual elements assume lone range equilibrium distances (isotropic geloids and tactoids) may be subject to photoelastic effects. Evidence for the deformation of tactoids in fairly weak electric fields and at small velocity gradients has been given by Zocher and Jacobsohn.[5] Since tactoids are known to increase in concentration as the colloid concentration increases,[6] the electrical and hydrodynamic optical effects dependent on orientation may change into complex orientation-deformation effects as the colloid concentration increases. A number of anomalies observed in variation of hydrodynamic double refraction with concentration can be thus explained although this possibility is being discounted at present.[7] If the hydrodynamic double refraction is partly a photoelastic effect, the value of R should deviate, with increasing velocity gradient, from the value 2.0.

The new technique may permit quantitative information on the elasticity and plasticity of colloidal particles. It may also improve the interpretation of double refraction created in isotropic materials by stretching or otherwise loading. This effect may *a priori* be due (1) to an orientaton of pre-existing anisotropic elements, or (2) to their deformation, or (3) to anisotropic distance-variations between the elements ("Newmann-effect"). A test of relation (1) in such cases will make it possible to decide whether and to what extent mere orientation is responsible for the effect observed, provided no biaxial particles are present. The test requires that, instead of phase differences or path differences, which can give only the magnitude of the double refraction ($n_{\parallel}-n_{\perp}$), the magnitudes of $n_{\parallel}$ and $n_{\perp}$ themselves are determined. The new method of measuring dichroism (Fig. 1) can easily be adapted to double refraction measurements of this type by an introduction into the set-up of an interferometer.

[1] A. Cotton and H. Mouton, Ann. Chim. Phys. [8] **11**, 145 (1907).
[2] P. Langevin, Le Radium **7**, 249 (1910).
[3] W. Heller and G. Quimfe, Comptes rendus **205**, 857, 1394 (1937); **206**, 64 (1938).
[4] W. Heller, Comptes rendus **205**, 971 (1937).
[5] H. Zocher and K. Jacobsohn, Kolloid-Beihefte **28**, 1 (1929).
[6] W. Heller, Comptes rendus **202**, 61 (1936); **204**, 43 (1937); J. Phys. Chem. (in press).
[7] J. T. Edsall, *Advances in Colloid Science* (Interscience Publishers, 1942); J. W. Mehl, Cold Spring Harbor Symposium on Quantitative Biology **6**, 218 (1938).

Dallas Meeting of Section B, A.A.A.S., and the American Association of Physics Teachers

SECTION B, American Association for the Advancement of Science, and the American Association of Physics Teachers met jointly at Dallas, Texas, on December 29 and 30, 1941.

Invited Papers

Sessions on Monday afternoon, December 29, and on Tuesday morning and afternoon, December 30, were devoted to the following invited papers:

Applications of Electron Scattering. Address of the Retiring Vice President for the Section on Physics (B). A. L. Hughes, *Washington University.*

Stereo-Microscopy with the Electron Microscope. V. K. Zworykin and J. Hillier, *RCA Manufacturing Company, Inc.*

Electron Micrograph Studies of Insect Structures. A. Glenn Richards, Jr., *University of Pennsylvania* and Thomas F. Anderson, *RCA Fellow of the National Research Council.*

Seismology. Cecil H. Green, *Geophysical Service, Inc.*

Electrical Methods in Prospecting. Dart Wantland, *Colorado School of Mines.*

The Gravimeter. D. H. Clewell, *Magnolia Petroleum Company.*

The Theory of Hydrocarbon Reactions. Everett Gorin, *Magnolia Petroleum Company.*

Applications of Spectroscopy to the Oil Industry. J. Rud Nielsen, *University of Oklahoma.*

Geophysical Exploration and Its Part in National Defense. C. A. Heiland, *Colorado School of Mines.*

Training of Physicists for Work in Geophysics. J. C. Karcher, *Coronado Company.*

Training of Students for Work in the Petroleum Industry. E. A. Stephenson, *University of Kansas.*

Contributed Papers, with Abstracts

The morning session on Monday, December 29, was devoted to ten contributed papers. The abstracts for papers No. 6 to 10, which pertain to instruction, will be found in the February, 1942 issue of the *American Journal of Physics.*

1. Mechanical Means for the Graphical Representation and Solution of Transcendental Functions. Lisle L. Wheeler and S. Leroy Brown, *University of Texas.*—A 30-element harmonic synthesizer is used to graph and to solve certain transcendental functions. Polar equations are graphed by the machine after the radius vector has been resolved into its two rectangular components. Trigonometric equations are solved by direct summation of the component terms. Certain trigonometric functions may be graphed and the value of the function determined for any angle. Legendre polynomials, associated Legendre polynomials and certain types of functions used to determine parameters in crystal structure are examples wherein the machine method of graphing is applicable. The machine method of solution may also be used to solve certain transcendental equations involving logarithmic, hyperbolic, or trigonometric functions. In these cases, the functions are expanded in a power series and the equations transformed to harmonic form by trigonometric substitution. However, the machine restricts to 30 the number of terms of the power series used to represent the function; therefore, a practical requirement is that the series converge rapidly within the interval of convergence.

2. Vibration-Rotation Energies of Planar ZXY_2 Molecules. Samuel Silver, *University of Oklahoma.*—The methods of Wilson and Howard[1] and of Shaffer, Nielsen, and Thomas[2] are used to develop the vibration-rotation energies of the planar ZXY_2 molecular model to the second order of approximation to include the cubic and quartic anharmonic terms in the potential energy, the dependence of the moments of inertia on the vibrational state, the centrifugal expansion effects, and interactions between the vibrational angular momentums and the total angular momentum. Owing to the low symmetry (C_{2v}), there are no inherent degeneracies. Under these conditions the interactions between the internal and total angular momentums contribute only in the second order of approximation. However, if an accidental degeneracy occurs between a pair of fundamental vibrations, the interaction between their angular momentums and the total angular momentum becomes large and produces a Coriolis splitting of the rotational levels. An approximate accidental degeneracy between a parallel and a perpendicular vibration is considered, and the dependence of the splitting upon the "closeness" of the degeneracy is evaluated. This latter problem finds application in the study of the formaldehyde molecule.

[1] E. B. Wilson, Jr. and J. B. Howard, J. Chem. Phys. **4**, 262 (1936).
[2] W. H. Shaffer, H. H. Nielsen, and L. H. Thomas, Phys. Rev. **56**, 895 (1939).

3. Raman Spectra of Compounds in the Gaseous and Liquid States. J. Rud Nielsen, *University of Oklahoma,* and Newton E. Ward, *Magnolia Petroleum Company.*—An apparatus for exciting the Raman spectra of gases and liquids at temperatures up to 300°C is described. For phosphorus trichloride, methyl chloride, methyl bromide, methyl alcohol, methylene chloride, methylene bromide, chloroform, and carbon tetrachloride, the Raman spectra of the gas and the liquid at the same temperature have been photographed in juxtaposition with a liquid-prism spectrograph of speed F : 2.9 and linear dispersion 27A/mm at 4400A. The Raman spectra of

gaseous *n*-pentane, *n*-hexane, and deuterium oxide have been photographed with 2537A-excitation. The change in the Raman frequencies with the state of aggregation is different for different vibrations and varies greatly from compound to compound. In the absence of an adequate theory for this phenomenon, a search has been made for empirical regularities. The perpendicular bands of the symmetrical-top-molecules are much less diffuse in the liquid than in the gas, showing that the intermolecular forces are effective in quenching the rotation of the molecules in the liquid. The other bands are about equally sharp in gas and liquid.

4. Vibrational Analysis of the 3200A Band System of CS_2. GENE T. PELSOR,* *University of Oklahoma.*—Experimental conditions were so chosen that the variation of band intensities with temperature could be determined. From these data—assuming a much smaller separation of rotational energy levels than of vibrational levels—the initial vibrational energy level for each of the more intense bands of the system was deduced, although with some uncertainty because of the overlapping of neighboring bands. In applying the general vibrational selection rules developed by Herzberg and Teller it was found that, for a "forbidden" type of transition which is indicated by the relative weakness of the system: (*a*) in case the molecule is linear and symmetric in the upper electronic state as it is in the ground state, the vibrational selection rules for infra-red absorption apply; (*b*) in case the upper state is not linear, Δv_3 must be odd. On the assumption of a linear upper state, a fairly plausible level scheme was constructed in which $\nu_2' = 172$ cm^{-1}, $\nu_3' = 707$ cm^{-1}, and $\nu_1' \leq 310$ cm^{-1}. If the upper state is bent, as indicated by Liebermann's results,[1] a rotational selection rule is required to explain the absence of pairs of bands terminating in the same level, one originating in the rotationless vibrationless level and the other in the rotationless level, $v_1 v_2 v_3 = 010$.

* Now at the University of New Mexico.
[1] L. N. Liebermann, Phys. Rev. **58**, 183 (1940); **59**, 106 (1941).

5. The Parabolic and Logarithmic Oxidation of Copper. A. L. DIGHTON AND H. A. MILEY, *Oklahoma Agricultural and Mechanical College.*—A recent study of the growth of oxide films on abraded copper surfaces, made from measurements obtained by the electrolytic reduction method, shows that copper may oxidize parabolically over a limited thickness range and then change to a logarithmic rate of growth. The parabolic growth is expressed by the equation $y^2 = Kt + A$, where y is the film thickness, t is the time, and K and A are constants. After the rate of growth becomes logarithmic, it is expressed by $y = k \log[a(t+t')+1]$, where k, a and t' are constants. Thus it appears that copper, which has been quoted often as a metal that is typical of parabolic oxidation, may also oxidize logarithmically. An electrochemical interpretation of Wagner's ionic theory of the oxidation and tarnishing of metals provides conditions that may permit a parabolic oxidation rate for ordinary thickness ranges and require a logarithmic rate for the more advanced ranges. The ionic theory postulates the movement of cations and electrons outwards and of anions inwards across the film. The growing film may be compared with a current-producing cell, the requirements for changing from a parabolic growth-rate to a logarithmic rate being provided by polarization. The critical film thickness, beyond which polarization may be expected, is influenced by all the factors that affect the perviousness of the films.

6. Production of Electric Charges in Water Spray. C. W. HEAPS, *Rice Institute.*

7. Units in Mechanics. E. A. SCHUCHARD, *Amarillo College.*

8. Up-to-date Experiments for the Laboratory. LOUIS R. WEBER, *Colorado State College of Agriculture and Mechanical Arts.*

9. The m.k.s. System, its Justification and Use. R. E. BEAM, *Southern Methodist University.*

10. Aviation Problems in Elementary Physics. EARL W. THOMSON, *United States Naval Academy.*

Proceedings of the American Physical Society

Meeting at Princeton, December 29–31, 1941

THE 246th meeting (the 43rd annual meeting) of the American Physical Society was held in the buildings of Princeton University and of the Institute for Advanced Study in Princeton, New Jersey, on December 29, 30, and 31, 1941. The American Association of Physics Teachers met on the same days, and some of the sessions were held in common. The gratitude of the societies was abundantly earned by the Local Committee, headed by Professor H. D. Smyth. Despite the circumstances of the times, upwards of four hundred people (as evinced by the list of registrants) were in attendance on these meetings, which are thus to be counted among the best of those that have occurred at this season during recent years. Professor A. Einstein and Dr. W. Pauli addressed a session held on Monday evening at the Institute, their topics being "On Solutions of Finite Mass of the Gravitational Equations" and "Problems of the Quantum Theory of Fields," respectively. On Tuesday afternoon the two societies listened to Professor G. W. Stewart giving his retiring presidential address, "Liquid Structure"; to Professor A. H. Compton, delivering the first Richtmyer Memorial Lecture of the American Association of Physics Teachers, "War Problems of the Physics Teacher"; and to Professor H. N. Russell, who graciously consented to replace a speaker hindered by illness, and gave us reminiscences of physics and astronomy at Princeton. There were five sessions for contributed papers; the abstracts of these are reproduced below (those numbered 35, 39, 45, and 46 correspond to papers not presented on the floor).

The dinner was held under the chairmanship of Professor G. W. Stewart on Tuesday evening, December 30, at the Nassau Tavern, and was attended by as many as the room could contain —some two hundred and twenty-five. President Stewart presided, and Dean Eisenhart in the first after-dinner speech welcomed the societies to Princeton. Our meetings had been signalized by the presence of the senior ex-president (Professor Henry Crew, president 1909–10) and the first secretary (Professor Ernest Merritt, secretary 1899–1921, president 1914–15) of the Physical Society; and these gentlemen made after-dinner speeches, as also did Professor P. W. Bridgman, Dr. E. U. Condon, Dean G. B. Pegram, and Professor R. M. Sutton.

At the business meeting of the Physical Society, formal announcement was made of the results of the election of officers for the year 1942. The elected officers are: *President*, P. W. Bridgman; *Vice President*, Albert W. Hull; *Secretary*, Karl K. Darrow; *Treasurer*, George B. Pegram; *Members of the Council*, Lee A. DuBridge and J. Stuart Foster; *Members of the Board of Editors*, Luis Alvarez, W. H. Furry, and E. M. McMillan.

Announcement was also made that the Council had conferred the title of "Acting Editor" on Professor J. W. Buchta, designating Dean J. T. Tate as "Editor on Leave" for the duration of the war or until further notice. It was further announced that the Council had appointed Professor R. T. Birge to the office of Local Secretary for the Pacific Coast. The roster of the Society as of December 23, 1941, was composed as follows: 5 Honorary Members, 891 Fellows, and 2976 Members.

The Council held protracted meetings on Monday and Tuesday. Word was received of the death of one Member, Rollin L. Charles. There were four resignations, twenty-four elections to Membership, fifteen elevations from Membership to Fellowship and one additional election to Fellowship. *Elected to Membership:* Charles E. Applegate, Elliot T. Benedikt, Fitzhugh W. Boggs, Otis L. Boothby, Kent H. Bracewell, William F. Brucksch, Jr., J. Robert Doig, Jr., Robert H. Esling, David Feldman, John K. Galt, Robert W. Hull, M. Eugene Merchant, Richard B. Nelson, Ed Ney, John J. O'Connor, Nathaniel Rochester, Elizabeth Rona, Louis Rosen, Kenneth B. Shiffert, Cyril S. Smith, Henry A. Strauss, Fred C. Von der Lage, Franklin E. Waterfall, Kurt E. Wilhelm. *Transferred from Membership to Fellowship:* Paul C. Aebersold, Stanley S. Ballard, Gerhard Herzog, Norman Hilberry, Robert E. Marshak,

Warren P. Mason, Marcel Schein, Glenn T. Seaborg, Wave H. Shaffer, George C. Southworth, Richard M. Sutton, Gerald W. Willard, Norman Wright, John Wulff, Robert T. Young, Jr. *Elected to Fellowship:* Charles T. Zahn.

KARL K. DARROW, *Secretary*
Columbia University, New York, New York

ABSTRACTS OF CONTRIBUTED PAPERS

1. Association Effects in the Raman Spectra of Thiophenol Solutions. FORREST F. CLEVELAND, M. J. MURRAY, AND ROBERT H. SAUNDERS, *Illinois Institute of Technology.*—Since the S−H vibration gives a sharp, intense line in the Raman spectrum, as contrasted to the broad, diffuse bands arising from the O−H vibration, it seemed quite suitable for use in an investigation of association effects. Consequently, Raman spectra were obtained, using solutions of one cm^3 of thiophenol in three cm^3 of the solvents, benzene, dioxane, pyridine, acetophenone and di-isobutyl ketone, with equal exposure times and comparable development. With benzene solution, the S−H line at 2570(9) cm^{-1} was sharp and appeared at the same frequency and intensity (if allowance is made for the smaller concentration) as in pure thiophenol. With acetophenone, di-isobutyl ketone and pyridine solutions the line still appears at the same frequency, but is now broader and has intensities of *5*, *5* and *4*, respectively, while with the dioxane solution two maxima were observed at 2569(3) and 2542(2). The results for the pyridine solution are in direct contrast with infra-red data[1] in which the S−H band was found to be shifted 114 cm^{-1} to lower frequencies, while the intensity *increased* several fold.

[1] Gordy and Stanford, J. Am. Chem. Soc. **62**, 500 (1940).

2. The Near Ultraviolet Absorption Spectrum of Monodeuterobenzene. C. A. BECK, *The Catholic University of America*, AND H. SPONER, *Duke University.*—The near ultraviolet absorption spectrum of monodeuterobenzene from 2270–2680A has been photographed in the first order of a 5-meter grating spectrograph. The spectrum resembles closely that of light benzene. The bands at 38640.8 ($A°_0$) and 37520.8 ($B°_0$) are assigned to the 0−1 and 1−0 transitions of the $603\epsilon^+_g$ vibration. This yields 517 cm^{-1} for the value of this ϵ^+_g vibration in the upper state. The 0,0 band is calculated to be 38123.8 and it occurs very faintly. Compared to light benzene, the $A°_0$ is shifted by 30 cm^{-1}, and the 0,0 band by 34.4 cm^{-1} from the calculated 0,0, both to the violet. As compared to heavy benzene, $A°_0$ is shifted by 149.4 cm^{-1}, and the 0,0 band by 167.8 cm^{-1} from the calculated 0,0, both to the red. Similar to benzene, bands appear displaced to the red from the main bands $603-517=86$ cm^{-1}. The frequency difference of 160 cm^{-1} found in light benzene remains unchanged. The totally symmetrical carbon vibration appears in progressions with separations of 912 cm^{-1} as compared to 923 cm^{-1} in light and 879 cm^{-1} in heavy benzene. Other bands were explained corresponding to assignments in light and heavy benzene.

3. Fine Structure of the Infra-Red Bands of C_2H_6. LINCOLN G. SMITH AND W. M. WOODWARD, *Princeton University.*—The bands of C_2H_6 have been studied under higher resolutions than previously[1] in the temperature range from 175°K to 300°K. From the structure of the fundamental $\parallel$ band at 1379.0 cm^{-1} (which structure is clear only at low temperatures), and that of harmonic $\parallel$ bands at 2753.3 cm^{-1} and 2369.3 cm^{-1} a value of $(42.25\pm0.05)\times10^{-40}$ gm cm^2 has been obtained for the large moment of inertia A. A single $\perp$ band with an anomalous decrease of both intensity and line spacing in the center (about 1484) has been observed in the 1480 cm^{-1} region. In the $\perp$ band at 827 cm^{-1} a peak of lower intensity about midway between each of the main peaks has been resolved. The intensities of these minor peaks decrease toward the center of the band and apparently increase relative to the major peaks as the temperature is lowered. $C=11.06\times10^{-40}$ gm cm^2 is calculated from the three active $\perp$ fundamentals by taking for the 1484 cm^{-1} band $\Delta\nu=5.20$ cm^{-1} which is the regular spacing of the lines at the sides of the band. This, together with $C-C=1.54\times10^{-8}$ cm,[2] gives $C-H=1.11\times10^{-8}$ cm and the tetrahedral value for all angles. The harmonic bands have all been studied but no new definite evidence has yet been obtained concerning the assignment of the degenerate fundamental frequencies. A complete report on this work will be published in the near future.

[1] Levin and Meyer, J. Opt. Soc. Am. **16**, 137 (1928); Bartholomé and Karweil, Zeits. f. physik. Chemie **B39**, 1 (1938).
[2] Pauling and Huggins, Zeits. f. Krist. **A87**, 205 (1934); Pauling and Brockaway, J. Am. Chem. Soc. **59**, 1223 (1937).

4. Pressure Effects on Spectral Lines. H. M. FOLEY* AND D. M. DENNISON, *University of Michigan.*—The intensity distribution in a spectral line due to interactions with neighboring atoms or molecules has been derived from the expressions for the growth of states, as in the quantum theory of radiation. The translational motion was treated classically, and the atomic interactions were introduced as time dependent perturbations. The adiabatic solution gives the well-known Fourier integral expression of Lorentz and Weisskopf. To the approximation that the duration of the collisions is small compared with the time interval between collisions (low density), the treatment of the interaction may be limited to the phase shifts appearing in the Fourier integral. With this approximation the line shape has been calculated, and it is shown that the phase changes alone will produce a shift of position as well as a broadening of the spectral line. The ratio of shift to broadening depends on the force law of the atomic interaction, and in particular upon the presence or absence of resonance interaction. The duration of the collisions has been taken into account as a next approximation, and the calculated line form shows typical asymmetry. Applications have been made to the self broadening and foreign gas broadening in molecular spectra.

* Chas. A. Coffin Fellow 1941–42.

5. The Calculation of the Magnetic Susceptibility of H_2, HD, and D_2 by Quantum Mechanics. ENOS E. WITMER, *University of Pennsylvania.*—The molar magnetic susceptibility χ_M of H_2, HD, and D_2 is given by a formula which may be written briefly as $\chi_M = -A + B$, where A is the diamagnetic term. Using the eleven-term wave functions of James and Coolidge, together with a Morse wave function for vibration, the value of A comes out to be 4.115×10^{-6} for H_2, 4.099×10^{-6} for HD, and 4.080×10^{-6} for D_2. Although B was calculated from wave functions also, the best value of B appears to be the value 0.093×10^{-6}, which was obtained by N. F. Ramsey from experimental data. Using this value, χ_M is -4.022×10^{-6} for H_2, -4.006×10^{-6} for HD, and -3.887×10^{-6} for D_2. Due to an approximation in the process of averaging by the Morse wave function, the values of A and therefore of χ_M are good to only three significant figures, but the differences are good to the third decimal places as written here. Summing up the experimental results, E. C. Stoner in his book gives χ_M for H_2 as $-4.00 \pm 0.05 \times 10^{-6}$. The calculated results above have a higher degree of accuracy, the uncertainty being less than $\pm 0.035 \times 10^{-6}$.

6. On the Heisenberg Theory of Ferromagnetism. P. R. WEISS, *Harvard University.*—The second of the Heisenberg approximations, based on the assumption of a Gaussian distribution of the energy levels belonging to a given value of the spin of the crystal about the mean value, leads to serious difficulties. As pointed out by Van Vleck, there is an error in Heisenberg's calculations of the mean square energy which makes his results invalid except in the case where the spin per atom is one-half. Moreover, it is found in this case that the second approximation leads to a low temperature critical point so that it predicts zero magnetization at very low temperatures. In this paper, the third and fourth moments of the energy are calculated for the general lattice assuming the spin per atom to be one-half. An expression for the critical temperature is obtained in the form of a series in descending powers of the coordination number. It is found that the values of the critical temperature and of the discontinuity in specific heat at the critical point obtained by including the successive moments converge satisfactorily. The calculations are also made for the case where the spin per atom is one and comparisons are made with the experimental results for iron and cobalt.

7. Strong Coupling Mesotron Theory of Nuclear Interactions. S. M. DANCOFF AND W. PAULI, *Institute for Advanced Study.*—We consider the results of the assumption of a strong coupling between nuclear particles and mesotrons of spin zero, treating the heavy particles as fixed sources of finite radius. Previous investigations* have indicated that this theory can account for the small scattering of cosmic-ray particles. They have also resulted in the prediction of excited states, or isobars, of the proton-neutron, differing in charge from the fundamental states. We here extend the treatment to the case of charged pseudo-scalar mesotrons; the appearance of the heavy particle spin in the formalism in this case gives ground for hope that nuclear forces may be properly described. This theory again results in heavy particle isobars; in this case, however, the isobars differ with respect to spin as well as charge, and the energy separation depends quadratically on spin and charge excesses.

* See, particularly, J. R. Oppenheimer and J. Schwinger, Phys. Rev. 60, 150 (1941).

8. On a Field Theory of Nuclear Forces. JULIAN SCHWINGER, *Purdue University.*—Mesotron theories of nuclear forces based on perturbation methods have suffered from the grave defect that the tensor forces which they predict possess inadmissible $1/r^3$ singularities. Although the concept of strong coupling, applied to the pseudo-scalar theory, is remarkably successful in accounting for cosmic-ray phenomena, it does not remove the objectionable singularities. If, however, in addition, a vector mesotron field is postulated which possesses the same nuclear coupling constant as the pseudo-scalar field, but whose particles differ in mass from the pseudo-scalar mesotrons observed in cosmic-rays, the inadmissible singularities are removed. The sign and magnitude of the resultant tensor interaction, which behaves as $1/r$ at small distances, is determined by the mass difference of the two mesotrons. It is satisfactory that the positive quadripole moment of the deuteron corresponds to the vector mesotron being more massive than the pseudo-scalar mesotron, for such particles will be highly unstable against disintegration into a pseudo-scalar mesotron and a γ-ray; and thus would not have been observed. However, the spontaneous disintegration of the vector mesotrons formed at the top of the atmosphere will provide a source of soft component to be added to the soft component production by the β decay of the pseudo-scalar mesotrons.

9. Theory of Nuclear Coulomb Energy. EUGENE FEENBERG, *New York University.*—A symmetry argument, similar to that applied by Wigner to the problem of nuclear mass defects, yields the following expressions for the Coulomb energy:

$$E_c = \frac{Z}{8}\{4(Z-1)L_c + 3L'_c\}$$

for even values of Z, and

$$E_c = \frac{Z-1}{8}\{4ZL_c + 3L'_c\}$$

for odd values of Z. The quantities L_c and L'_c are matrix elements involving the Coulomb interaction, the space coordinate exchange operator and the isotopic spin operators. It is assumed that L_c and L'_c are constant in an isobaric series and vary smoothly with n, the total number of particles. These assumptions make possible the determination of L_c and L'_c as functions of n. Numerical results and applications will be presented.

10. Theoretical Half-Lives of Beta-Transitions. C. L. CRITCHFIELD, *Harvard University.*—The results of Konopinski and Uhlenbeck[1] on the energy distribution of beta-particles in forbidden transitions have been integrated in

order to determine the relation between half-life and maximum energy in such transitions. It is assumed that $Z \ll 137$. Estimates of the matrix elements which appear in the five different interactions are made for intramultiplet transitions and compared with the experimental results on Na^{22}, Sc^{42}, P^{30}, Cl^{34} and K^{38}. It appears that all of these radioactivities may be first forbidden and that the interaction between the field of the nuclear particles and that of electron and neutrino must contain the product of tensor operators (tensor-interaction) or of pseudo-scalar operators or of both. Thus, possible assumptions for an interaction between the fields include the tensor and the antisymmetric interaction.[2]

[1] E. J. Konopinski and G. E. Uhlenbeck, Phys. Rev. **60**, 308 (1941).
[2] C. L. Critchfield and E. Wigner, Phys. Rev. **60**, 412 (1941).

11. Lifetimes for Forbidden Transitions in β-Decay and Orbital Electron Capture and Spins of Nuclei. R. E. MARSHAK, *University of Rochester.*—A general formula giving minimum lifetimes for forbidden β-transitions of arbitrary order or forbidden orbital electron capture is derived. Exact Coulomb wave functions are used for the electron. It is shown that the observed electron emission of K^{40} requires Gamow-Teller selection rules. Combined with the Konopinski-Uhlenbeck[1] result that only the tensor and vector interactions are compatible with the energy spectra of the β-rays from Na^{24}, P^{32} and RaE, it follows that the tensor interaction alone can explain both the lifetimes and energy spectra of forbidden β-transitions. The application of the tensor interaction to K^{40} and to the other long-lived β-emitters, Rb^{87}, Lu^{176}, Be^{10}, C^{14}, and to existing data on orbital electron capture, leads to certain spin and parity predictions about parent and product nuclei—e.g., neither Be^{10} nor C^{14} can have a spin greater than $3\hbar$, the 2 Mev γ-ray from K^{40} is associated with k-electron capture to an excited state of A^{40} having even parity, etc. The stability of the known neighboring isobars and the conditions under which L-electron capture becomes more probable than s-electron capture will also be discussed.

[1] E. J. Konopinski and G. E. Uhlenbeck, Phys. Rev. **60**, 308 (1941).

12. Elementary Explanation of Thermal Diffusion. W. H. FURRY, *Harvard University.*—A successful elementary explanation of thermal diffusion was first given quite recently by Frankel,[1] who accounted for the existence of the phenomenon for molecules which differ in mass, and for its dependence on the intermolecular force law. Frankel's idea may readily be extended to explain the appearance of the effect for molecules which differ only in radius, and also gives a result similar to that of the mathematical theory for the effect of the quantum-mechanical difference in cross-section for collisions between identical and non-identical molecules.[2] It may also be extended to explain the appearance of transport due to thermal diffusion, as well as the stationary case considered by Frankel. Simple considerations can be used to give a correct estimate of the value of the thermal diffusion constant.

[1] S. P. Frankel, Phys. Rev. **57**, 661L (1940).
[2] Effect first suggested by H. M. Mott-Smith.

13. Isotope Separation Factor of a Thermal Diffusion Column. RALPH SIMON, *Yale University.*—A hot wire type of Clusius and Dickel column was operated at various pressures for wire temperatures of 1100°K and 1500°K. In each case, after equilibrium had been obtained, the separation factor was measured by taking off samples of the gas (argon) at the top and bottom of the column and analyzing them with a Nier type mass spectrometer. The theoretical variation of the separation factor with pressure was verified and experimental values of the constants in the thermal diffusion theory of Furry, Jones, and Onsager were obtained. Running the column under conditions of turbulent flow produced only a slight, if any, decrease in the separation factor determined by extrapolation from the data obtained under conditions of lamellar flow.

14. Difference in Loss of Energy of Deuterons in D_2 and H_2. C. M. CRENSHAW, V. J. YOUNG, H. P. MANNING, *New York University.*—The energy loss of deuterons in D_2 and H_2 has been measured as a function of energy from 60 kev to 340 kev. A path length of 18.4 cm at 2 mm Hg pressure of gas was used for these measurements. Preliminary work indicates the loss to be linear with respect to pressure up to 3 mm Hg.

Incident energy	Loss in H_2	Loss in D_2	Difference
60 kev	18 kev	15 kev	3 kev
120	17	14	3
180	15	12	3
240	13	10	3
300	11	9	2
340	9	8	1

15. Evidence for p-Wave Proton-Proton Scattering. EDWARD C. CREUTZ AND ROBERT R. WILSON, *Princeton University.*—The accuracy in the measurement of the angular distribution of 8 Mev protons scattered from the hydrogen in cellophane foils has been improved. The yield appears to be somewhat greater at small angles than would be expected for a pure s scattering anomaly. This suggests the presence of some repulsive scattering of the p-wave. Thus the cross-section per unit solid angle is independent of angle from 20° to 45° with an accuracy of 2½ percent. At 45° where the effect of the p-wave vanishes,[1] the observed cross-section in the laboratory system is $1.7 \pm 0.1 \times 10^{-25}$ cm², in good agreement with the value 1.75×10^{-25} cm² calculated by BTE[2] on the assumption of a square potential well of depth 10.5 Mev and width e^2/mc^2. The largest source of error in the measurement of the absolute yield is the uncertainty in the composition of cellophane. This difficulty will be discussed.

[1] True on the assumption of a central field. See Breit, Kittel, and Thaxton, Phys. Rev. **57**, 255 (1940).
[2] Breit, Thaxton, and Eisenbud, Phys. Rev. **55**, 1018 (1939).

16. On the Relative Probability of the D,2n and the D,n Reactions in Ni and Zn. J. M. CORK, L. N. HADLEY, JR., AND C. V. KENT, *University of Michigan.*—Only a very few elements offer any possibility for studying the relative probability of the D,2n and the D,n reactions.

One of these elements is copper in which a 7.9 min. activity has been ascribed to Cu (60) and a 3.4 hr. activity to Cu (61). Since nickel (60) has an abundance of 27.2 percent and nickel (61) only 0.1 percent, the yield of these two copper radioactivities should tell the relative probability for the D,2*n* and the D,*n* reactions. Now by reducing the energy of the incident beam a change in the relative yield would be expected. Actually, the relative yield was found to be independent of the bombarding energy and hence indicates that the previous assignment is incorrect. A similar result is obtained in bombarding zinc and observing the radioactivity in gallium. Gallium (66) and (67) had been considered as radioactive isotopes of half-lives 9.4 hr. and 83 hr., respectively, and hence could both be made from Zn (66). Actually the relative yield of each was found to be independent of the bombarding energy, indicating that they are probably isomers. The gamma-radiations from the 83-hr. zinc have been studied in the magnetic spectrometer, giving energies of 94, 174, 187, 301 kev.

17. Radioactive Selenium from Arsenic. C. V. KENT, J. M. CORK, AND W. G. WADEY, *University of Michigan.*—Arsenic has a single stable isotope of mass 75. When bombarded with deuterons this can form selenium 75 by a (D,2*n*) reaction or selenium 76 by the (D,*n*) process. A single activity whose half-life is 160 days is observed in the selenium from this bombardment. When studied in a magnetic beta-ray spectrometer of high resolution, many electron groups, corresponding to internally converted gamma-rays, are observed. For energies below 300 kev, at least 8 gamma-rays are observed and for several of them, the $K-L$ difference and the relative conversion coefficients are given.

18. Radioactive Isotopes of Lanthanum. KATHERINE E. MOUNCE, M. L. POOL, AND J. D. KURBATOV, *Ohio State University.*—A radioactive isotope of lanthanum with a half-life of 19 ± 2 hr. is produced by bombardment of barium with 10 Mev deuterons. The radiation consists almost entirely of x-rays which were found by critical absorption measurements to be the characteristic x-rays of barium. Thus nearly all of the active lanthanum decays by the process of *K*-electron capture. Bombardments of cesium with 20 Mev alpha-particles and of lanthanum with fast neutrons do not reproduce the activity which therefore seems best assigned to La^{137}. Hilger H. S. lanthanum has been bombarded with deuterons and with slow neutrons for the purpose of investigating the discrepancies of previous reports[1,2,3] on the period of La^{140}. The activity produced in the lanthanum fraction by deuterons was followed through 11 half-lives, giving a period of 40 hrs. This same period was produced by the slow neutron bombardment. The radiation consists of beta-rays and gamma-rays of approximately 2 Mev as determined by absorption methods.

[1] J. K. Marsh and S. Sugden, Nature **136**, 102 (1935).
[2] M. L. Pool and L. L. Quill, Phys. Rev. **53**, 437 (1938).
[3] O. Hahn and F. Strassmann, Naturwiss. **28**, 543 (1940).

19. A Study of the Radiations from the Disintegration of I^{130} and I^{131}. J. R. DOWNING, M. DEUTSCH, AND A. ROBERTS, *Massachusetts Institute of Technology.*—The radiations from I^{130} (12.6 hr.) and I^{131} (8*d*) have been studied by spectrometer and coincidence techniques. The disintegration of I^{131} consists of a beta-ray spectrum of energy 0.595 Mev[1] which is now shown to be simple, followed by a 367 kev gamma-ray.[2] A gamma-ray of 80 ± 1 kev has been shown to be present by critical absorption of gamma-gamma coincidences. The beta-ray spectrum of I^{130} is found to be complex, consisting of two groups whose endpoints are 0.55 and 1.07 Mev. Four gamma-rays of energies 0.417, 0.535, 0.670, and 0.740 Mev are known.[2] Coincidence methods confirm the complexity of the beta-ray spectrum, and show also that all the gamma-rays are in cascade. The results are consistent with the assignment of the 0.535 Mev gamma-ray to the transition between the levels on which the beta transitions end. The higher energy spectrum includes 40 percent of all the beta-rays.

[1] M. Deutsch, Phys. Rev. **59**, 940A (1941).
[2] M. Deutsch and A. Roberts, Phys. Rev. **60**, 362 (1941).

20. Gamma-Rays from Long Period Activities. M. DEUTSCH, A. ROBERTS, AND L. G. ELLIOTT, *Massachusetts Institute of Technology.*—Gamma-ray spectrometer studies[1] have been extended to several long lived activities. Accuracy of the energy determinations (about ±3 percent, or better) and the energy range investigated (above 0.18 Mev) are generally about the same as in the previous report.[1]

Gamma-ray Energies

Isotope	Period	Gamma-rays (Mev)	Remarks
Ag^{106}	8 d.	0.505, 1.06, 1.63, 0.72(?)	2, 3
Ag^{105}?	45 d.	0.282, 0.345, 0.430, 0.650, >1.0	3
$Ag^{105 \text{ or } 110}$	225 d.	0.650, 0.925, 1.51	
In^{116}	54 min.	0.428, 1.12, 1.31, 2.32	4
Zn^{65}	250 d.	1.14	5
$Fe^{59 \text{ and } 55}$	>47 d.	1.10, 1.30	
Co (Fe+*d*)	long	0.119, 0.131, 0.847, 1.26, 1.75(?), 3.42	

[1] M. Deutsch and A. Roberts, Phys. Rev. **60**, 362 (1941).
[2] The 0.5 Mev ray may be annihilation radiation.
[3] In fair agreement with Enns, Phys. Rev. **56**, 872 (1939).
[4] Compare Curtis and Richardson, Phys. Rev. **53**, 942 (1938).
[5] Only a trace of annihilation radiation.

21. Isomeric States in Indium[112]. R. N. SMITH, *Purdue University.*—Silver bombarded with alpha-particles and indium by fast neutrons yield a pair of isomeric activities for which the growth of the lower activity resulting from the decay of the upper can be directly observed. Chemical identification assigns both states to indium[112]. Application of the formula for growth of one radioactive state from another gave half-lives of 16.5 ± 2 minutes for the upper and 17.5 ∓ 2 minutes for the lower level. The soft conversion electrons from the gamma transition between states were detected with a thin window electroscope and their energy estimated, giving a gamma-ray energy of 120 ± 15 kev. Both positrons and electrons were detected from the decay of the lower state, the positrons with a maximum energy of 1.3 ± 0.1 Mev and the electrons 0.47 ± 0.1 Mev. Another group of particles assumed to be conversion

electrons from a 95 ± 10 kev gamma-ray was associated with the lower state. This pair of activities replaces the 20-minute period previously obtained from alpha-particle bombardment of silver and assigned to indium^{110} or indium^{111}, but is distinct from the 23-minute period obtained from deuterons on cadmium.[1]

[1] J. L. Lawson and J. M. Cork, Phys. Rev. **57**, 982 (1940).

22. The Temperature Dependence of Slow Neutron Resonance Absorption in Silver. T. M. SNYDER, J. W. KEUFFEL,* J. J. GILVARRY, AND K. WAY,† *Princeton University.*—The width and cross section at resonance of the 2.5-volt neutron capture level of silver are obtained from its slow neutron "self-absorption" cross sections at 25°C and −72°C. The self-absorption cross section is determined by a comparison of the activities induced in detectors of two thicknesses. By averaging the activity of a detector over various positions inside a large paraffin block which contains the neutron source, the activity due to an isotropic distribution of neutrons is obtained. These activities are corrected for β-absorption in the silver and are now being corrected for activities induced by capture into higher levels. For accurate interpretation of results, a theory of the resonance activation of thick detectors is given which takes into account self-reversal with Döppler broadening. The shape of a resonance absorption level and the activities produced by both collimated and isotropic neutrons are given. These calculations permit a more accurate analysis of the slow neutron measurements of previous workers as well as our own.

* Now at California Institute of Technology.
† University of Tennessee.

23. Absorption of Thorium on Tungsten Single Crystals. MYRON H. NICHOLS, *Princeton University.*—Electron projection tube studies of the emission from single crystal tungsten wires onto which thorium has been evaporated from a thoriated tungsten source have shown that thorium is absorbed mainly on the (111) and (001) surfaces—i.e., on the surfaces closely surrounding the normal emergence of the (111) and (001) crystal directions. Emission patterns from large single crystals grown in specially doped thoriated tungsten show the same absorption properties as the pure tungsten onto which thorium has been evaporated. These observations agree with those obtained by Daniel[1] from a study of field emission patterns from thoriated tungsten single crystal points and from pure tungsten single crystal points onto which thorium was evaporated.

[1] J. H. Daniel, M.I.T. Doctor's thesis, June, 1940.

24. The Ferromagnetic Anisotropy of an Fe-Al Alloy. SIDNEY SIEGEL, *Westinghouse Research Laboratories.*—Single crystal bars of an Fe-Al alloy containing 4.1 percent Al were prepared by slow solidification of the melt in a vacuum furnace inductively heated. The crystals are cylinders 3 cm in diameter, up to 10 cm long. The orientation of the crystal is determined by x-rays. Disks about 2 cm in diameter, 0.1 cm thick were prepared with their planes parallel to either (100) or (110) crystallographic planes. The ferromagnetic anisotropy constant K_1 was determined by placing the disk in the gap of an electromagnet producing fields up to 3300 oersteds, and measuring the component of magnetization in the disk, J_n, perpendicular to the direction of the applied field H, as a function of the angle θ between a ⟨100⟩ direction in the disk and H. The value for K_1 for this alloy was found to be 3.9×10^5 ergs/cm^3. Several Fe-Si crystal disks, of Si content between 3 and 4 percent, were measured in the same apparatus and gave results in agreement with previous data. It appears that the rate of decrease of K_1 with increasing Al content is smaller than that for Si.

25. A Calculation of the Increase in Electrical Resistance Produced by Cold-Work. JAMES S. KOEHLER, *Westinghouse Research Laboratories,* AND FREDERICK SEITZ, *University of Pennsylvania.*—A calculation of the increase of the specific electrical resistance produced by cold-work has been made using Taylor's dislocation theory. It was assumed that the total specific electrical resistance can be written as

$$\rho=\rho_{\text{thermal}}+\rho_{\text{plastic}}$$

where ρ_{thermal} is the resistance resulting from thermal oscillations of the atoms and ρ_{plastic} is the resistance produced by the internal strains in a cold-worked material. It was also assumed that ρ_{thermal} is proportional to the mean square of the thermal atomic displacements and that ρ_{plastic} is proportional to the mean square of the atomic displacements resulting from the presence of dislocations in a cold-worked metal. It was further assumed that the two constants of proportionality are the same. The results of the calculation for severely cold-worked polycrystalline materials are given below:

	Cu	Ni	W
$\left[\frac{\rho_{\text{plastic}}}{\rho_{\text{thermal}}}\right]_{\text{calc.}}$	0.9%	1.0%	3.3%
$\left[\frac{\rho_{\text{plastic}}}{\rho_{\text{thermal}}}\right]_{\text{obs.}}$	3%	8%	34%*

It is found that the resistance produced by cold-work increases approximately linearly with the density of dislocations.

* See Schmidt and Boas, *Kristallplastizität*, p. 214 (1935).

26. Electronic Structure and Polymorphism of Iron Alloys. R. SMOLUCHOWSKI, *General Electric Company.*—Purest obtainable iron has up to the melting point a cubic body-centered crystal lattice with the exception of a short range of temperatures where it is cubic face-centered. It is well known that additions of various elements forming binary solid solutions with iron influence the range of existence of these two crystal lattices in various ways. This influence appears to be connected with the position of the elements in the periodic system. An explanation of this phenomenon is suggested on the basis of the structure of electron bands. Substitution of other atoms in the place of iron atoms in the lattice changes the electron density at the top of the Fermi distribution, affecting the specific heat, the energy and stability of both crystal forms. In the case of interstitial alloys with carbon, nitrogen, etc.,

the mechanism is somewhat different. This model helps also to understand the polymorphism in ternary solid solutions where the influence of various elements follows a simple additive law. Various facts can be explained qualitatively on the basis of the suggested model.

27. Hall Effect in Cuprous Oxide. S. J. ANGELLO, *University of Pennsylvania.*—Measurements of the Hall effect and conductivity of cuprous oxide have been made on samples prepared as follows: Copper of known purity was oxidized completely in air at 1000°C. The oxide was annealed 2 hours at a lower temperature, and quenched in water immediately. It is found that the Hall constant and conductivity do not obey the exponential laws of temperature dependence for temperatures above about 80°C. The precise value of this temperature depends on the annealing conditions. The deviation from the exponential law of the Hall constant is related to the disappearance of lattice defects. The rate of diffusion of defects can be increased by an electric field when the temperature is 100°C. The deviation of the conductivity from the exponential law is due not only to diffusion of lattice defects, but also to a rapid decrease of the mean free path with increasing temperature. The measurements have been carried to approximately 100°C.

28. Resistivity of Antimony-Tin Single Crystals at Low Temperature. C. T. LANE AND W. A. DODD, *Yale University.*—The electrical resistivity of pure antimony and alloys of antimony and tin in the form of single crystals has been investigated from room temperature down to the temperature of liquid helium. All measurements were made with the direction of the current perpendicular to the principal crystal axis, and for various amounts of tin up to about 3 atomic percent. It is found that the average temperature coefficient of resistance between 4.2°K and 77.3°K decreases sharply with increasing tin content assuming a small constant value at 3 atomic percent. While the addition of tin at room temperature changes the resistivity very little, the effect at 4.2°K is very large. This "residual" resistivity is approximately a parabolic function of the tin concentration. Comparison of these results with the Bloch theory of metals is made.

29. Remark Concerning Liquid Specific Heats. GREGORY H. WANNIER, *University of Iowa.*—The wave type of normal mode analysis has been extended recently from the solid to the liquid.[1] Because of disorder, liquid modes possess a stronger coupling and equipartition is not maintained. Lucas tried to estimate this effect assuming by the correctness of the viscosity concept for all waves. This makes the specific heat much too small, because viscous resistance becomes paramount for all transverse and the shorter longitudinal waves. It is more natural to assume that the liquid possesses instantaneously solid rigidity, but that the stress decays with a half-period computable from viscosity data. The liquid is then quasi-solid for wave-lengths shorter than 10^{-7} cm. For mercury, one finds the specific heat 10 percent below $3R$, tending to decrease with temperature. This agrees with observation. The treatment cannot apply in its present form near the critical point. However, Lenz[2] has shown that even gases may be treated by vibrational analysis if the change in nature of the sound velocity is observed. Thus it is probable that a unified theory of specific heats applicable to all three phases can be developed.

[1] René Lucas, Jour. de Phys. **10**, 60 (1939).
[2] Arnold Sommerfeld, Probleme der freien Weglänge. From *Vorträge über die kinetische Theorie*, Teubner, 1914.

30. Atomic Images with the Electron Microscope. L. I. SCHIFF, *University of Pennsylvania.*—Some of the conditions that must be satisfied in order to obtain an electron microscope image of the arrangement of the atoms in a molecule are discussed. It is shown that in typical cases the minimum aperture angle of the objective lens is not much less than the angle at which elastic scattering begins to fall off rapidly and is about equal to the greatest angle at which inelastic scattering is appreciable, independently of the velocity of the electron. In the usual transmission microscope many of the unscattered electrons will enter the objective lens and the image will show poor contrast. This difficulty can be overcome by inclining the axis of the condenser lens with respect to that of the rest of the microscope, so that the undeviated beam just misses the objective aperture. Then only scattered electrons enter the objective, and the problem of obtaining sufficient contrast is replaced by the more straightforward one of obtaining sufficient intensity. This method of "dark field" illumination appears to be superior to that which employs annular stops in the condenser system, since the necessarily very small objective aperture angle and scattering angle require the use of exceedingly well collimated condenser beams.

31. Nerve Fiber Impedance. KENNETH S. COLE, *Columbia University.*—A nerve fiber is similar to a submarine cable in that it has a low resistance interior with a high resistance capacitative membrane at the surface. The impedance characteristics of the membrane may be calculated by cable theory from measurements made between well-separated long electrodes surrounding each end of a single fiber. Such measurements have been made on the giant nerve fiber of the squid over the frequency range from 10 cycles to 200 kilocycles. The reactance is capacitative, as expected, at the higher frequencies, but it may become zero between 200 and 300 cycles and be inductive for lower frequencies. An approximate equivalent circuit for a cm^2 of this nerve membrane is found to be a capacity of $1\mu f$ shunted by a resistance of 400 ohms and an inductance of 0.2 henry in series. However preliminary experiments with various external electrolytes show that this circuit is over-simplified.

32. A Comparison of Optical and Electromechanical Methods of Studying Ultrasonic Fields.—WILLIAM GARTEN, *The Johns Hopkins University.*—Statements made regarding the accuracy to be obtained in measurements of ultrasonic velocity and absorption by various methods are not always borne out by the consistency of the results

themselves. This is particularly true in the case of liquids in which measurements have often been made with little attention paid to the effects of high intensity, and the accompanying possibility of distortion of measurements produced by heating effects. Such effects produce temperature gradients and give rise to large apparent decrements introducing errors both in velocity and absorption measurements.[1] Observation of ultrasonic fields in liquids by optical methods in the ultrasonic frequency region of 3 megacycles shows that intensities greater than those necessary to produce first order Debye-Lears spectra produce important distortions of the field. Measurements are possible by methods of acoustic interferometry with intensities from one to two orders less than those necessary for the optical methods, and at these low intensities distortions of field due to a possible temperature gradient have not been detected.

[1] J. C. Hubbard, Am. J. Phys. 8, 219 (1940); Phys. Rev. 59, 935 (1941).

33. Diffusion of Heat Through a Rectangular Bar and the Cooling Effect of Fins. I. The Steady State. MELVIN AVRAMI, *Columbia University*, AND J. B. LITTLE, *Bell Telephone Laboratories*.—Exact solutions for temperature distribution and heat flow through a rectangular fin are rederived in more general and simple form than previously given. These are studied numerically and graphically, and shown to yield new results not contained in the approximate formulas hitherto used. Except for the factor of thermal conductivity of the fin material, the cooling effect is a function only of the height-width ratio β of the fin, and of a dimensionless "relative boundary resistivity" μ governing the heat loss to the environment. It is shown that, for any value of this boundary resistivity, there is a fairly sharp optimum value of the height-width ratio beyond which further increase in height will not lead to much improvement in cooling effect. This optimum β decreases with decreasing μ until, at a certain critical value μ^* in the neighborhood of 1, it becomes zero. At the critical μ^*, the cooling effect is altogether independent of β, and the presence of the fin is a matter of indifference. Below μ^*, the cooling effect decreases with increasing β, so that the presence of the fin serves merely to insulate the hot plate. This analysis of a single fin is the basis upon which a study of the conditions for optimal cooling by an array of fins will be carried out in a subsequent publication.

34. The Consumption of the Positive Arc Carbon. H. G. MACPHERSON, *National Carbon Company*.—The consumption of the positive electrode of an arc between solid carbons in air results partly from evaporation and partly from oxidation. The oxidation is operative chiefly on the sides of the carbon, tapering the end of the electrode and thus producing a tip with a diameter $\frac{1}{2}$ to $\frac{2}{3}$ that of the original carbon. The consumption of the flat tip, or crater, however, is due almost entirely to evaporation. The evaporation rate is controlled by the pressure of carbon vapor at the crater surface and the mechanism of diffusion away from it. This diffusion was computed on the assumption that it is similar to that occurring in the evaporation from liquid drops of the same diameter as that of the carbon crater, and it was shown that the linear electrode consumption should be inversely proportional to the crater diameter. This was borne out approximately by measurements of consumption rates made near the overload current. The absolute values of the consumption rates are consistent with the hypothesis that the surface temperature of the positive crater is at or near the sublimation temperature of carbon.

35. Ionization by Neutral Atoms in the 2000- to 8000-ev Energy Range. H. W. BERRY, *Washington University*. (*Introduced by A. L. Hughes.*)—Using the space charge ion detector, ionization by collision of He and N_2 atoms by their own fast neutrals has been studied for energies up to 8000 electron volts. A beam of ions is first formed and accelerated to the desired velocity. After being homogenized by a velocity selector, the beam is neutralized by charge exchange in passing through its own gas. A retarding potential removes any ions remaining unneutralized, leaving a beam of neutral atoms with the velocity of the ions from which it was formed. The neutral beam then enters a space charge ion detector where the ionization takes place. Finally on striking a nickel plate, secondary electrons are released which serve as a measure of the intensity of the beam. The curves obtained are considered in relation to the method of measurement and interpreted in terms of a relative cross section.

36. Self-Quenching Geiger-Mueller Counters. PAUL WEISZ, *Bartol Research Foundation of the Franklin Institute*.—The investigations of Montgomery, Ramsay, Rose, Korff and other authors have yielded a very satisfactory picture of the discharge mechanism in counter tubes, and it is found that the difference in action of the "self-quenching" and the classical counter can be explained in terms of the same picture. In experiments with argon/ethyl-ether mixtures of successively greater ether concentration, the transition from the classical to the self-quenching counter mechanism was observed to take place in exactly the manner predicted by the picture arrived at, invoking emission and absorption of ultraviolet photons, and the electron capture phenomena. The nature of the "plateau" should largely be a probability question concerning the absorption of these photons by the polyatomic gas. In agreement with the consequences of this concept, the plateau of the self-quenching counter is found to be somewhat smaller than that of the classical counter, but with suitable mixing ratios plateaus of around 200 volts were obtained without difficulty. With proper care taken especially regarding the completion of the mixing process before filling the counters, very satisfactory tubes can be constructed with great reliability, and complete reproducibility.

37. The Ionization of Individual Cosmic Rays. W. F. G. SWANN AND PAUL WEISZ, *Bartol Research Foundation of the Franklin Institute*.—Previously, the results of an experiment employing a proportional counter in connection with

a telescopic counter arrangement of high resolution power to define the path length of the rays in the proportional counter were communicated. Plotting the number of particles against relative ionization, two distinct primary maxima were found confirming earlier findings of W. F. G. Swann and W. E. Ramsay, and E. Stuhlinger, the second maximum corresponding to about 1.5 times the ionization of the first. By measuring the distribution in ionization values with and without lead absorber, we have identified the first maximum as belonging to the penetrating rays, the second maximum as being created by the electron component. The same measurements were carried out at two greatly different gas pressures in the proportional counter to ascertain whether the density of the individual "electron avalanches" in the proportional counter may be of influence on the results supplied by the tube. However, identical results were obtained in both cases. Accepting the Bethe-Bloch ionization formula, we find difficulty in interpreting the two so distinct values of ionization for mesotrons and electrons of energies of the usually assumed order of magnitude, as well as the lack of a sharp cut-off of the distribution in ionization which this formula predicts.

38. The Penetrating Power of Extensive Cosmic-Ray Shower Particles at Sea Levels. NORMAN HILBERRY* AND ANN HEPBURN HILBERRY, *University of Chicago.*—To obtain information concerning the nature of the extensive cosmic-ray shower particles at sea level an experiment has been performed determining the variation in the number of such showers observed per unit time as a function of the thickness of a lead shield placed above the counters. Identical shields were placed over each counter unit; the units were shielded from the sides; and, so that they could be tripped only by air showers, the units were placed on the laboratory roof. Two series of measurements were taken, one with an over-all extension of 110 cm, the other of 40 cm. The shower-frequency curves come to a maximum at a shield thickness of 1.25 cm of lead as would be expected and then drop off with increasing thickness. With 10 cm of lead above each unit of a threefold coincidence set the counting rate is cut to about five percent of the zero shield value. This corresponds to a decrease to about thirty-five percent of the initial counting rate for each counter unit, indicating that about one-third of the extensive cosmic-ray shower particles at sea level can penetrate 10 cm of lead.

* On sabbatical leave from New York University.

39. Cloud Chamber Tracks of Heavy Particles at High Altitude. DONALD J. HUGHES,* *University of Chicago.*—During July of this year a series of 5000 cloud-chamber expansions were photographed at an altitude of 15,500 ft. in Peru. The results show a number of tracks with heavier ionization than electrons and with range greater than that of α-particles. The present paper deals only with these more obviously interesting cases, since detailed measurements and analysis of all the data have been delayed. About 15 of the heavy tracks show a measurable curvature in the magnetic field of 1165 gauss, hence allow a more or less accurate mass determination. It is found that approximately half of these slow, heavily ionizing particles are mesotrons, and half protons. One photograph shows a positive-negative pair of slow mesotrons, created in the material of the chamber. Several cases of knock-on electrons supply additional data for mass calculations. The rate of occurrence and range of the slow mesotrons can be compared with that of fast mesotrons to give an estimate of the mean energy at this altitude; the resulting value is markedly less than that at sea level. Complete curvature measurements of the tracks of the fast particles will furnish an interesting check on this estimate.

* Now at Naval Ordnance Laboratory, Washington, D. C.

40. Neutrons Produced by the Cosmic Radiation at 14,170 Feet Altitude. S. A. KORFF,* *Bartol Research Foundation of the Franklin Institute.*—A series of measurements on the neutrons produced by the cosmic radiation was carried out on Mt. Evans. The neutrons were detected by proportional counters filled with BF_3. The counters were surrounded by water, so that the neutrons detected should almost all be slow, and also, so that the neutrons detected should mostly have been produced in the water, very few of those generated outside the water reaching the counter. With this arrangement, counting rates were obtained as a function of pulse size, with and without a thin cadmium shield. Next, the neutron counter was operated in coincidence with a shower detecting unit, the geometry and the water being unchanged. This experiment was conducted with and without cadmium. The number of large showers tripping the arrangement was evaluated by causing the neutron counter alone, and then the neutron-shower coincidence, to control a cloud chamber. The results indicate that neutrons are present in some abundance, and their number increases with altitude by a factor of about two per meter of water, and that some of them appear to be generated by a process connected with the soft component, possibly a nuclear photo-effect.

* Now at New York University.

41. The Effect of Changes of Height of Air Mass on Mesotron Intensity. VICTOR F. HESS AND GEORGE O. ALTMANN, *Fordham University.*—The correlation of mesotron ground intensity with upper "air mass temperature" gives a coefficient of -0.4 percent per °C and is almost constant for all layers. This corroborates the view that the temperature effect of cosmic-rays is primarily an effect of atmospheric mass distribution variations.[1] Likewise the height of the position of the center of gravity $\bar{h}$ gives a good correlation (0.7) with mesotron intensity. A coefficient β was computed $=-\partial I/I\partial\bar{h}=17.5$ percent/km change of altitude. Since $\alpha=\partial I/I\partial T_m$ we have $\beta=-\alpha\partial T_m/\partial\bar{h}$. Thus the mean life range of a mesotron $\bar{L}=c\tau_0\gamma=\partial\bar{h}/\alpha\partial T_m=1/\beta$, if we use Blackett's relation $\alpha=\partial\bar{h}/L\partial T$ or $L=\partial h/\alpha\partial T$. Therefore $\bar{L}=1/0.175=5.7\pm0.4$ km, $\tau_0\gamma=1.9\times10^{-5}$ sec. and the mesotron life time at rest $\tau_0=1.5\times10^{-6}$ sec. assuming $\gamma=12.5$ corresponding to mesotrons of 1 Bev mean energy. From $\partial\bar{h}/\partial T_m=-\alpha/\beta$ we also obtain an independent determination of the change of the position of the center of gravity of the air mass with the lower mass temperature which is numerically 22.5 meters/°C.

[1] V. F. Hess and F. A. Benedetto, Phys. Rev. **60**, 610 (1941).

42. Cosmic-Ray Measurements between New York and Valparaiso. EDWARD B. BERRY, S.J., *Fordham University.* (*Introduced by Victor F. Hess.*)—A Compton Model C cosmic-ray meter, aboard the steamship *Santa Ana*, has been in continuous operation since January 10, 1941 between geomagnetic latitude 52° 00′ N and 22° 10′ S. Hourly intensities were averaged over a Greenwich meridian day and the corresponding mean position of the ship determined in geomagnetic coordinates. The daily means were corrected to a standard of 30.00 inches Hg, using as barometer coefficient Gill's[1] value. To correct for mean atmospheric temperature, the data were divided into those obtained at geomagnetic latitudes lower than 17.5°N and S and those at higher latitudes. Departures from five degree mean values were correlated with atmospheric temperature. For high latitudes $\alpha=\partial I/I\partial T=-0.12\pm0.01$ percent per C°, for low latitudes $\alpha=-0.08\pm0.01$, in good agreement with some values obtained by Compton and Turner and by Gill[1] on the Pacific. All corrected data, compared to an arbitrary absolute value of ionization, show a magnetic latitude effect in the Northern Hemisphere of 7 percent and a temperature latitude effect of 1.5 percent.

[1] P. S. Gill, Phys. Rev. **55**, 1151 (1939).

43. Nuclear Forces in the Strong Coupling Theory.** S. M. DANCOFF* AND R. SERBER, *University of Illinois.*—Although cosmic-ray evidence proves the existence of a strong interaction between mesotrons and nuclear particles, the calculations of mesotron scattering and of nuclear forces made on the basis of mesotron field theories have not given satisfactory results. These calculations have been made on the supposition that the coupling between heavy particles and mesotrons could be regarded as small, a supposition contradicted by the results of the calculations themselves. It has therefore been hoped that the fault lay, not in the structure of the theory, but in the approximations made in its application. The development of the theory for large, rather than small, couplings was begun by Wentzel,[1] and extended by Oppenheimer and Schwinger, who showed that on this basis the small observed mesotron scattering could be understood. However, the nuclear forces resulting from such a strong coupling turn out to be, over most of their range, ordinary forces (non-exchange, non-spin dependent) which are unacceptable since they do not lead to saturation. This can be understood in a general way; for strong interactions the quantum field theory approaches the classical one, and all effects of the exclusion principle consequently drop out. The calculations have been carried out for charged scalar and for neutral and charged psuedo-scalar mesotron fields. However, the argument is of such a general nature that it seems unlikely that any strong coupling theory can lead to suitable forces.

* Now National Research Fellow, Institute for Advanced Study.
[1] G. Wentzel, Helv. Phys. Acta **13**, 269 (1940).
** To be called for after Paper No. 11, Session A.

44. Application of an Electric Model to the Study of Two-Dimensional Heat Flow.* MELVIN AVRAMI AND VICTOR PASCHKIS, *Columbia University.*—The experimental electric model method of solving problems in heat flow, previously described by one of the authors, is here reviewed and applied to the diffusion of heat through a long rectangular bar placed with a long side on a hot plate. The general mathematical solution for this problem has been worked out by the other author in a previous paper.† The model consists of a network of lumped resistances and capacitances so arranged as to simulate the distribution of resistance and heat capacity in the analogous thermal situation. The results on the model are compared with the mathematical solutions for the steady state, heat flow, and transient state. The agreement, even with fairly crude lumping (i.e., representing the body by a network with a small number of sections), is remarkably good, generally within two percent. An important result is that it is possible, using a representative network with non-uniform sections, to concentrate investigation on the flow in one part of the body without appreciable sacrifice of accuracy.

* To be called for after Paper No. 33, Session C.
† See Abstract no. 33.

PAPERS TO BE READ BY TITLE

45. Energy Distribution of Mesotrons. M. E. ROSE, *Bartol Research Foundation.*—Taking into account decay and energy loss according to the Bethe-Bloch ionization formula the energy distribution of vertically incident mesotrons has been calculated for various elevations and under Pb. Assuming mesotron production in a layer 10 percent from the top of the homogeneous atmosphere and with a $E^{-2.9}$ primary energy distribution, the distributions at sea level for various proper lifetimes, τ_0, are compared with observations. A lifetime of 2×10^{-6} sec. gives good agreement with measurements (Blackett, Wilson) although the experimental error and the insensitivity of shape of the distribution to τ_0 do not exclude a τ_0 as much as 3×10^{-6} sec. The distribution and total number of mesotrons at sea level and under Pb thicknesses up to 2 meters have been calculated. The linear decrease of intensity and the calculated absorption coefficient, 3.0×10^{-3} cm^{-1} Pb, are in excellent agreement with the measurements of Wilson and of Pomerantz. The total number of slow mesotrons ($E<E_0$, $E_0<\sim10^7$ ev) as a function of Pb thickness increases rapidly for small thicknesses but at 45 cm Pb a flat maximum is attained. This optimum Pb thickness is virtually independent of the definition of a "slow" mesotron (of E_0). The decline in number of slow mesotrons for large Pb thickness is in accord with cloud-chamber data obtained in this laboratory.

46. On Photometry with the Photoelectric Cell. F. T. ROGERS, JR.,* *The University of Houston, Houston, Texas.*—Over a usefully wide range of steady cathode-illumination values (L) and steady cathode-to-anode potentials (V), the steady current passed by a photoelectric cell may conveniently be expressed as

$$i=L[\alpha(1-e^{-\beta V})+\gamma(e^{\delta V^2}-1)], \qquad (1)$$

where α, β, γ, and δ are suitable constants for a particular photocell and quality of illumination. This expression is

especially suited to gas-filled photo-cells; for vacuum photo-cells, the γ, δ-term is often negligible. For example, for a certain set-up with a type 921 photo-cell, the values $\alpha=14$, $\beta=0.35$, $\gamma=43$, and $\delta=0.00015$ were used in Eq. (1) to give i in microamperes when L was in lumens and V in volts. For $L\leq 0.06$ lumen and $30\text{ v}\leq V\leq 90\text{ v}$, these yielded i/L values within a very few percent (the amount of experimental uncertainty) of the measured values. This precision is adequate for many photometric purposes, and probably does not represent the ultimate of which Eq. (1) is capable.

* With The University of California (1941–1942), on leave of absence.

Author Index to Abstracts of the Princeton Meeting

Altmann, George O.—see Hess, Victor F.
Angello, S. J.—No. 27
Avrami, Melvin and J. B. Little—No. 33
Avrami, Melvin and Victor Paschkis—No. 44

Beck, C. A. and H. Sponer—No. 2
Berry, Edward B.—No. 42
Berry, H. W.—No. 35

Cleveland, Forrest F., M. J. Murray, and Robert H. Saunders—No. 1
Cole, Kenneth S.—No. 31
Cork, J. M., L. N. Hadley, Jr., and C. V. Kent—No. 16
Cork, J. M.—see Kent, C. V.
Crenshaw, C. M., V. J. Young, and H. P. Manning—No. 14
Creutz, Edward C. and Robert R. Wilson—No. 15
Critchfield, C. L.—No. 10

Dancoff, S. M. and W. Pauli—No. 7
—— **and R. Serber**—No. 43
Dennison, D. M.—see Foley, H. M.
Deutsch, M., A. Roberts, and L. G. Elliott—No. 20
—— see Downing, J. R.
Dodd, W. A.—see Lane, C. T.
Downing, J. R., M. Deutsch, and A. Roberts—No. 19

Elliott, L. G.—see Deutsch, M.

Feenberg, Eugene—No. 9
Foley, H. M. and D. M. Dennison—No. 4
Furry, W. H.—No. 12

Garten, William—No. 32
Gilvarry, J. J.—see Snyder, T. M.

Hadley, L. N., Jr.—see Cork, J. M.
Hess, Victor F. and George O. Altmann—No. 41
Hilberry, Norman and Ann Hepburn Hilberry—No. 38
Hilberry, Ann Hepburn—see Hilberry, Norman
Hughes, Donald J.—No. 39

Kent, C. V., J. M. Cork, and W. G. Wadey—No. 17
—— see Cork, J. M.
Keuffel, J. W.—see Snyder, T. M.
Koehler, James S. and Frederick Seitz—No. 25
Korff, S. A.—No. 40
Kurbatov, J. D.—see Mounce, Katherine E.

Lane, C. T. and W. A. Dodd—No. 28
Little, J. B.—see Avrami, Melvin

MacPherson, H. G.—No. 34
Manning, H. P.—see Crenshaw, C. M.
Marshak, R. E.—No. 11
Mounce, Katherine E., M. L. Pool, and J. D. Kurbatov—No. 18
Murray, M. J.—see Cleveland, Forrest F.

Nichols, Myron H.—No. 23

Paschkis, Victor—see Avrami, Melvin
Pauli, W.—see Dancoff, S. M.
Pool, M. L.—see Mounce, Katherine E.

Roberts, A.—see Deutsch, M.
—— see Downing, J. R.
Rogers, F. T., Jr.—No. 46
Rose, M. E.—No. 45

Saunders, Robert H.—see Cleveland, Forrest F.
Schiff, L. I.—No. 30
Schwinger, Julian—No. 8
Seitz, Frederick—see Koehler, James S.
Serber, R.—see Dancoff, S. M.
Siegel, Sidney—No. 24
Simon, Ralph—No. 13
Smith, Lincoln G. and W. M. Woodward—No. 3
Smith, R. N.—No. 21
Smoluchowski, R.—No. 26
Snyder, T. M., J. W. Keuffel, J. J. Gilvarry, and K. Way—No. 22
Sponer, H.—see Beck, C. A.
Swann, W. F. G. and Paul Weisz—No. 37

Wadey, W. G.—see Kent, C. V.
Wannier, Gregory H.—No. 29
Way, K.—see Snyder, T. M.
Weiss, P. R.—No. 6
Weisz, Paul—No. 36
—— see Swann, W. F. G.
Wilson, Robert R.—see Creutz, Edward C.
Witmer, Enos E.—No. 5
Woodward, W. M.—see Smith, Lincoln G.

Young, V. J.—see Crenshaw, C. M.